Autophagy and mitophagy flux disruption in cellular models of MERRF syndrome

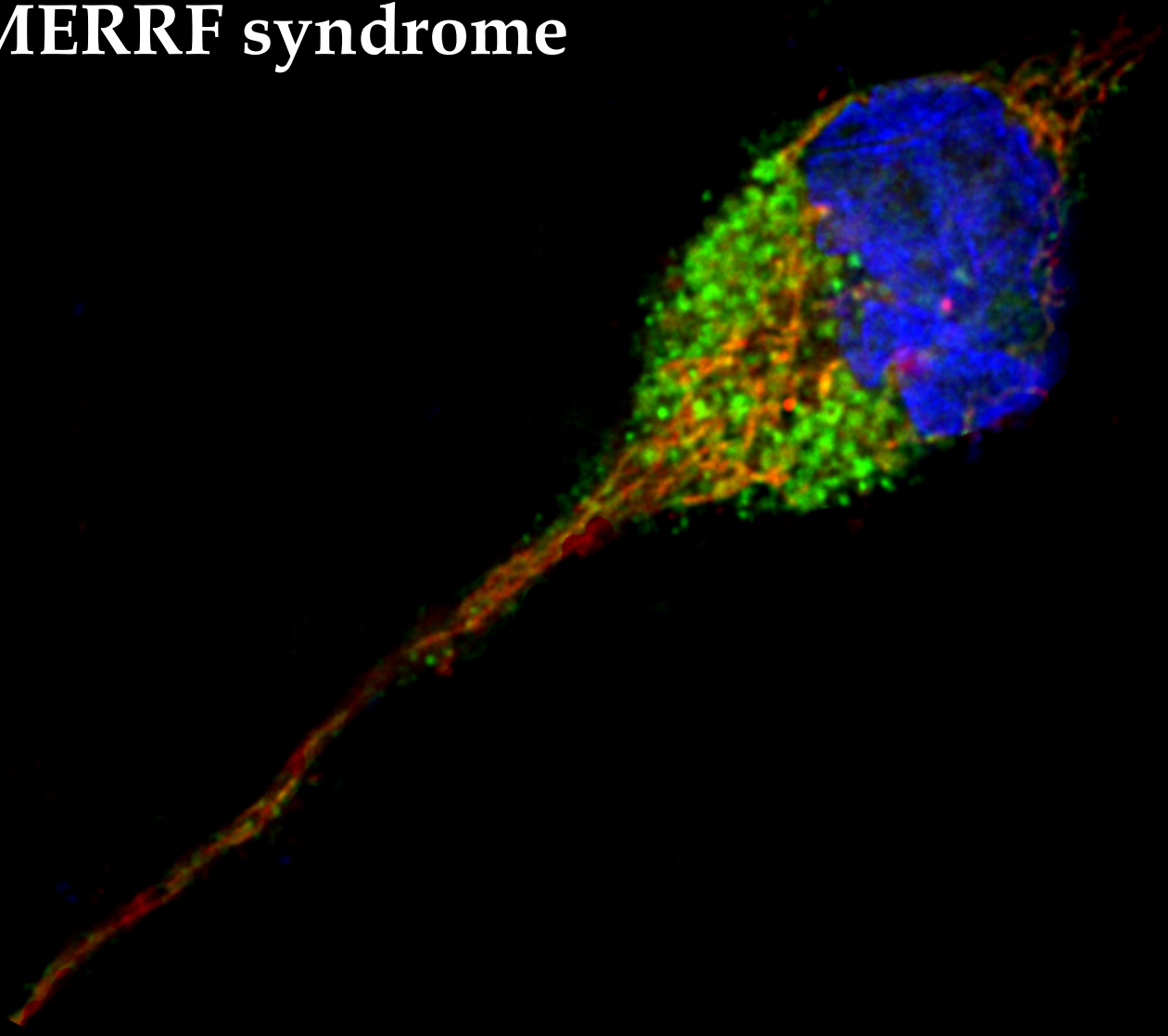

Tesis Doctoral

Marina Villanueva Paz

Sevilla, 2019

Autophagy and mitophagy flux disruption in cellular models of MERRF syndrome

Tesis doctoral

Marina Villanueva Paz

Sevilla, 2019

Centro Andaluz de Biología del Desarrollo
CSIC
JUNTA DE ANDALUCIA
GOBIERNO DE ESPAÑA
MINISTERIO DE EDUCACIÓN, CULTURA Y DEPORTE

Autophagy and mitophagy flux disruption in cellular models of MERRF syndrome

Tesis doctoral

Memoria de tesis doctoral presentada por MARINA VILLANUEVA PAZ, licenciada en Biotecnología, para optar al título de Doctor enmarcado en el programa de Doctorado en Biotecnología, Ingeniería y Tecnología Química. Esta tesis doctoral ha sido realizada en el Centro Andaluz de Biología del Desarrollo (CSIC-UPO-JA) y financiada por el Ministerio de Educación del Gobierno de España desde el año 2014 hasta el año 2018. Esta tesis está inscrita al Departamento de Fisiología, Anatomía y Biología Celular de la Universidad Pablo de Olavide.

Marina Villanueva Paz

Sevilla, 2019

EL DIRECTOR

José Antonio Sánchez Alcázar

Catedrático de la Universidad Pablo de Olavide

D. JOSÉ ANTONIO SÁNCHEZ ALCÁZAR, Doctor en Medicina por la Universidad Complutense de Madrid y Catedrático del área de Biología Celular en el departamento de Fisiología, Anatomía y Biología Celular de la Universidad Pablo de Olavide de Sevilla

INFORMA

Que **DÑA. MARINA VILLANUEVA PAZ,** licenciada en Biotecnología por la Universidad Pablo de Olavide de Sevilla, ha realizado bajo su dirección la tesis doctoral titulada **AUTOPHAGY AND MITOPHAGY FLUX DISRUPTION IN CELLULAR MODELS OF MERRF SYNDROME**, y que a su juicio reúne los méritos suficientes para superar el programa de Doctorado en Biotecnología, Ingeniería y Tecnología Química.

Y para que conste, firmo el presente en Sevilla, a 18 de marzo de 2019

Fdo.: José Antonio Sánchez Alcázar

Esta Tesis Doctoral ha sido realizada dentro del programa de Doctorado en Biotecnología, Ingeniería y Tecnología Química, en el Grupo de Investigación de Fisiopatología Celular en la Enfermedad y el Desarrollo del Centro Andaluz de Biología del Desarrollo, Departamento de Fisiología, Anatomía y Biología Celular de la Universidad Pablo de Olavide y bajo la dirección del Dr. José Antonio Sánchez Alcázar gracias a la financiación del proyecto de investigación en salud PI13/00129 del Instituto de Salud Carlos III. El trabajo del doctorando ha sido financiado por una ayuda predoctoral de Formación de Profesorado Universitario (FPU), referencia FPU13/01335, concedida por el Ministerio de Educación del Gobierno de España.

“La verdadera ciencia enseña,
por encima de todo,
a dudar y a ser ignorante.”
Miguel de Unamuno

A mis padres y mi hermano.

A Juan.

ABSTRACT

MERRF (Myoclonic Epilepsy with Ragged-Red Fibers) syndrome is one of the most common mitochondrial disorders, principally caused by the m.8344A>G mutation in mitochondrial DNA (mtDNA). This mutation affects the translation of mtDNA-encoded proteins; therefore, the assembly of the electron transport chain (ETC) complexes is disrupted, leading to a reduced mitochondrial respiratory function.

In this thesis, we report how the autophagy flux and the selective degradation of defective mitochondria (mitophagy) become essential mechanisms for the balance between survival and cell death in this disease. We evaluated autophagy and mitophagy flux in transmitochondrial cybrids and fibroblasts derived from MERRF patients, reporting that Parkin-mediated mitophagy is increased in MERRF cell cultures harbouring the m.8344A>G mutation. Our results suggest that supplementation with coenzyme Q_{10} (CoQ) prevents Parkin translocation to mitochondria. In addition, CoQ acts as an enhancer of autophagy and mitophagy flux, improving cell pathophysiology. Our findings support the hypothesis that both a regulated autophagy and Parkin-mediated mitophagy act as cell survival mechanisms in a mitochondrial dysfunction background.

However, the use of cybrids and skin fibroblasts as MERRF cellular models has shortcomings, since they are not the cell types mostly affected in MERRF patients and they are not much vulnerable to energy-dependent defects resulting from mitochondrial dysfunction. For that reason, in this thesis we report how patient-specific induced neurons (iNs) are originated by direct reprogramming of dermal fibroblasts derived from different individuals carrying the m.8344A>G mutation. The pathophysiological characterization of MERRF iNs indicates that they can be used as an excellent cellular model to elucidate the mechanisms underlying MERRF syndrome, as well as a screening platform for testing drugs that can correct the phenotype of the disease.

According to our results, iNs generation would provide an opportunity to study mitochondrial diseases in one of the cell types primarily affected.

RESUMEN

MERRF (del inglés, *Myoclonic Epilepsy with Ragged-Red Fibers*) es una de las enfermedades mitocondriales más comunes, principalmente causada por la mutación m.8344A>G en el ADN mitocondrial. Esta mutación afecta a la traducción de proteínas codificadas por el ADN mitocondrial; por lo tanto, el ensamblaje de los complejos de la cadena de transporte de electrones está alterado, provocando una disminución de la función respiratoria mitocondrial.

En esta tesis se estudia cómo el flujo autofágico y la degradación selectiva de mitocondrias disfuncionales (mitofagia) son mecanismos esenciales para el balance entre supervivencia y muerte celular en esta enfermedad. Evaluamos los flujos autofágico y mitofágico en cíbridos transmitocondriales y fibroblastos dérmicos procedentes de pacientes con síndrome MERRF, observando que la mitofagia mediada por Parkina está aumentada en los cultivos celulares MERRF con la mutación m.8344A>G. Nuestros resultados sugieren que el tratamiento con coenzima Q_{10} (CoQ) previene la translocación de Parkina a la mitocondria. Además, la CoQ actúa como un acelerador del flujo autofágico y mitofágico, mejorando la fisiopatología celular. Nuestros hallazgos respaldan la hipótesis de que una autofagia y mitofagia mediada por Parkina reguladas actúan como un mecanismo de supervivencia celular en un contexto de disfunción mitocondrial.

Sin embargo, el uso de cíbridos y fibroblastos dérmicos como modelos celulares del síndrome MERRF presenta desventajas, ya que no son las células más afectadas en los pacientes y no son demasiado vulnerables a defectos dependientes de la falta de energía provocada por la disfunción mitocondrial. Por esta razón, en esta tesis se presenta la generación de neuronas inducidas mediante reprogramación celular directa a partir de fibroblastos dérmicos de pacientes con la mutación m.8344A>G. La caracterización fisiopatológica de las neuronas inducidas MERRF indica que éstas pueden constituir un excelente modelo para dilucidar los mecanismos moleculares de la enfermedad, así como una plataforma de cribado para el estudio de moléculas que puedan corregir su fenotipo.

CONTENTS

ABBREVIATIONS

ABBREVIATIONS

3D: Three-dimensional
AAA: ATPases associated with diverse cellular activities
AAV: Adeno-associated virus
AD: Alzheimer's disease
ADP: Adenosine diphosphate
AHSCT: Allogenic hematopoietic stem cell transplantation
AICAR: 5-aminoimidazole-4-carboxamide 1-β-D-ribofuranoside
AIF1: Allograft inflammatory factor 1
AKT: Protein kinase B
AL: Albumin
ALS: Amyotrophic lateral sclerosis
AMN: Apoptotic microtubule network
AMP: Adenosine monophosphate
AMPK: 5'-adenosine monophosphate-activated protein kinase
AOX: Alternative oxidase
APS: Ammonium persulfate
Arg: Arginine
ASCL1: Achaete-scute complex-like 1
ATG: Autophagy-related
ATP: Adenosine triphosphate
ATP6: ATP synthase F0 subunit 6
BAF: Bafilomycin A1
BCL11B: B-cell lymphoma 11b
BCL2: B-cell lymphoma 2
BDNF: Brain-derived neurotrophic factor
bFGF: Basic fibroblast growth factor
BN-PAGE: Blue Native-PAGE
BNIP3: Bcl2/adenovirus E1B 19 kDa protein-interacting protein 3
Bp: Base pair
BRN2: Brain-2
BRN3A: Brain-specific homeobox/POU domain protein 3A
BSA: Bovine serum albumin
CaMKK: Calmodulin-dependent protein kinase-kinase
cAMP: Cyclic AMP
Cas9: CRISPR-associated protein 9
CCCP: Carbonyl cyanide m-chlorophenylhydrazone
CDKN2A: Cyclin dependent kinase inhibitor 2A
CLPP: ATP-dependent Clp protease proteolytic subunit
CM-H2DCFDA: Chloromethyl H2DCFDA
CMA: Chaperone-mediated autophagy
CMs: Cardiomyocyte-like cells
CMT2A: Charcot–Marie–Tooth neuropathy type 2A
CNTF: Ciliary neurotrophic factor
CO: Cytochrome c oxidase
CoA: Coenzyme A
CoQ: Coenzyme Q10
CoQH2: Ubiquinol

COX: Cytochrome oxidase
CRISPR: Clustered Regularly Interspaced Short Palindromic Repeats
CSF: Cerebral spinal fluid
cTNT: Cardiac troponin T
CYTB: Cytochrome B
Cyt. c: Cytochrome c
DAPI: 4′,6-diamidino-2-phenylindole
db-cAMP: Dibutyryl-cyclic AMP
DCF: 2′,7′-di-chlorofluorescein
DLXs: Distal-less homeobox proteins (1,2 and 5)
DMEM: Dulbecco's modified Eagle's medium
DMSO: Dimethyl sulfoxide
DNA: Deoxyribonucleic acid
DNP: 2,4-dinitrophenyl
DNPH: 2,4-dinitrophenylhydrazine
dNTP: Deoxyribonucleotide triphosphate
DPI: Days post infection
DRP1: Dynamin-like protein 1
EBV: Epstein-Barr virus
ECAR: Extracellular acidification rate
EDTA: Ethylenediaminetetraacetic acid
EE: Ethylmalonic encephalopathy
EGTA: ethylene glycol-bis (β-aminoethyl ether)-*N*, *N*, *N*′, *N*′-tetraacetic acid
EIF4EBP1: Eukaryotic translation initiation factor 4E-binding protein 1
EN1: Homeobox protein engrailed-1
EPCs: Endothelial progenitor cells
ER: Endoplasmic reticulum
ESCs: Embryonic stem cells
ETC: Electron transport chain
ETF: Electron-transferring-flavoprotein
FACS: Fluorescence-Activated Cell Sorting
FAD+: Oxidized Flavin adenine dinucleotide
FADH2: Reduced Flavin adenine dinucleotide
FBS: Fetal bovine serum
FCCP: Carbonyl cyanide-4-(trifluoromethoxy)phenylhydrazone
FD: Familial dysautonomia
FDA: Food and Drug Administration
FEV: Fifth Ewing variant protein
FF: Form factor
FGF8: Fibroblast growth factor 8
FIP200: 200 kDa FAK family kinase-interacting protein
FIS1: Mitochondrial fission 1
FITC: Fluorescein Isotiocyanate
FOXAs: Forkhead box A proteins (1,2 and 3)
FOXG1: Forkhead box G1
FP: Forward primer
FUNDC1: FUN14 Domain containing 1
Gag: Group-specific antigen (retrovirus)
GAPDH: Glyceraldehyde-3-phosphate dehydrogenase
GATAs: GATA binding proteins (2 and 4)

GDNF: Glial cell derived neurotrophic factor
GFP: Green fluorescent protein
Gln: Glutamine
Glu: Glutamic acid
Gly: Glycine
GRACILE: Growth retardation, aminoaciduria, cholestasis, iron overload and early death
GSH: Glutathione
GTP: Guanine triphosphate
GuttaQ: Guttaquinon CoQ10
H_2DCFDA: 2′,7′-dichlorodihydrofluorescein diacetate
HAND2: Heart and neural crest derivatives expressed 2
HBSS: Hank's balanced salt solution
HD: Huntington's disease
HDAC6: Histone deacetylase 6
HEK293T: Human embryonic kidney 293 cell line
HEPES: 4-(2-hydroxyethyl)-1-piperazineethanesulfonic acid
HIF1: Hypoxia-inducing factor-1
hiPSCs: Human iPSCs
His: Histidine
hmtPAP: Mitochondrial poly-A polymerase
HNFs: Hepatocyte nuclear factors (1 and 4)
HRP: Horseradish peroxidase
HSC-70: Heat shock cognate protein of 70 kDa
HSP60: 60 kDa heat shock protein
HUVECs: Human umbilical vein endothelial cells
IDD: Intervertebral disc degeneration
IGFs: Insulin-like growth factors (1 and 1R)
Ile: Isoleucine
IBM: Inner boundary membrane
IMM: Inner mitochondrial membrane
iNs: Induced neurons
iPSCs: Induced pluripotent stem cells
IS: Intermembrane space
ISLS: Insulin gene enhancer proteins (1 and 2)
JC-1: 5,5',6,6'-tetrachloro-1,1'3,3' tetraethylbenzimidazolecarbocyanine iodide
KA: Kainic acid
KEAP1: Kelch-like ECH-associated protein 1
KLFs: Kruppel-like factors (4 and 7)
KSS: Kearns–Sayre syndrome
LC3-I: LC3 cleaved at the C terminus by Atg4
LC3-II: LC3-I lipided by conjugation to PE
LC3: Microtubule-associated proteins 1A/1B light chain 3
LC3B: LC3 isoform (antibody against LC3B was used during this thesis)
LCLs: Lymphoblastoid cell lines
Leu: Leucine
LHON: Leber hereditary optic neuropathy

LHXs: LIM/homeobox proteins (3 and 6)
LIR: LC3-interacting region
LMX1A: LIM homeobox transcription factor 1 alpha
LMX1B: LIM homeobox transcription factor 1 beta
LONP1: Lon peptidase 1
Lys: Lysine
MAFA: MAF bZIP transcription factor A
MAM: Mitochondria-associated ER membrane
MAP-2: Microtubule-associated protein 2
Mdivi-1: Mitochondrial division inhibitor 1
MEF2C: Myocyte enhancer factor 2C
MEFs: Mouse embryonic fibroblasts
MELAS: Mitochondrial Encephalomyopathy, Lactic Acidosis, and Stroke-like episodes
MERRF: Myoclonic Epilepsy with Ragged-Red Fibers
MFN1: Mitofusin-1
MFN2: Mitofusin-2
MILS: Maternally inherited Leigh syndrome
miR: Micro-RNA
miRNA: Micro-RNA
MIRO: Mitochondrial rho GTPase
mLST8: Mammalian lethal with SEC13 protein 8
MMPs: Matrix metalloproteinases
MNGIE: Mitochondrial neurogastrointestinal encephalopathy
Mnm (E, G, A): 5-carboxymethylaminomethyluridine-tRNA synthase GTPase subunit (E, G, A)
MnSOD: Superoxide dismutase
MNX1: Motor neuron and pancreas homeobox 1
MOI: Multiplicity of infection
MPP: Mitochondrial processing peptidase
MPT: Mitochondrial permeability transition
MRC: Mitochondrial respiratory chain
MRI: Magnetic resonance imaging
mRNAs: Messenger RNAs
MRS: Magnetic resonance spectroscopy
mt-aaRSs: Aminoacyl mt-RNA synthetases
mt-rRNAs: Mitochondrial ribosomal RNAs
MT-TK: Mitochondrially encoded tRNA lysine
mt-tRNA: Mitochondrial transfer RNA
mtDNA: Mitochondrial DNA
MTDR: MitoTracker™ Deep Red
MTO1: Mitochondrial tRNA translation optimization 1
mTOR: Mammalian target of rapamycin
mTORC1: mTOR complex 1
mTORC2: mTOR complex 2

MTS: Mitochondrial targeting sequence
mtSSBP: Mitochondrial single strand binding protein
mtTERM: Mitochondrial transcription terminator factor
mtTFA: Mitochondrial transcription factor A
mtTFB: Mitochondrial transcription factor B (1,2).
MTU1: tRNA 5-methylaminomethyl-2-thiouridylate methyltransferase
MUL1: Mitochondrial E3 ubiquitin protein ligase 1
MYC: MYC proto-oncogene
MYLs: Myosin light chains (2 and 7)
MYOD1: Myoblast Determination 1
MYT1L: Myelin transcription factor 1 like
N or N0: Number of cells
N-CAM: Neural cell adhesion molecule
n: Proliferation rate
NAC: N-acetylcysteine
NADH: Reduced nicotinamide adenine dinucleotide
NARP: Neuropathy, ataxia and retinitis pigmentosa
NBR1: Neighbour of BRCA1 gene 1
ND: NADH dehydrogenase
ND5: NADH-ubiquinone oxidoreductase chain 5
nDNA: Nuclear DNA
NDUFS4: NADH-ubiquinone oxidoreductase core subunit S4
NDUFV1: NADH: ubiquinone oxidoreductase core subunit V1
NEUROD: Neurogenic Differentiation factor (1 and 4)
NGN1: Neurogenin 1
NGN2: Neurogenin 2
NGN3: Neurogenin 3
NIX: NIP3-like protein X
NKX2-2: NK2 homeobox 2
Np: Nucleotide positions
NP: Nucleus pulposus
NPCs: Neural progenitor cells
NRF1: Nuclear respiratory factor 1
NRF2: Nuclear factor (erythroid-derived 2)-like 2
Nt: Nucleotide
NT3: Neurotrophin-3
NuoL: NADH: quinone oxidoreductase subunit L
NURR1: Nuclear receptor related 1 protein
O/N: Overnight
OAβ: Oligomeric amyloid β
OCR: Oxygen consumption rate
O_H: Replication origin of heavy strand of mtDNA
O_L: Replication origin of light strand of mtDNA
OMM: Outer mitochondrial membrane
OPA1: Optic atrophy 1
OPTN: Optineurin
OXPHOS: Oxidative phosphorylation

P: P-value (statistics)
P62/SQSTM1: Sequestosome-1
p70S6K: Ribosomal S6 kinase
PAGE: Polyacrylamide gel electrophoresis
PANK2: Pantothenate kinase 2
PARK2: Parkin gene
PARL: Presenilins-associated rhomboid-like
PAS: Phagophore assembly sites
PAX: Paired box (6 and 7)
PBS: Phosphate-buffered saline
PCR: Polymerase chain reaction
PCR-RFLP: PCR-Restriction fragment length polymorphism
PD: Parkinson's disease
Pdr-1: E3 ubiquitin-protein ligase parkin
PDX1: Pancreas and duodenum homeobox 1
PE: Phosphatidylethanolamine
PEI: Polyethyleneimine
PEO: Progressive external ophtalmoplegia
PFA: Paraformaldehyde
PFK2: Phosphofructokinase 2
PFL: Polyornithine-fibronectin-laminin
PGC1A: Peroxisome proliferator-activated receptor gamma coactivator 1-alpha
PGK: Phosphoglycerate kinase
Phe: Phenylalanine
Pi: Inorganic phosphate
PI3K: Phosphatidylinositol kinase type III
PI3P: Phosphatidylinositol 3-phosphate
PINK1: PTEN-induced putative kinase 1
PITX3: Pituitary homeobox 3
PKB: Protein kinase B
Pol: Polymerase (retrovirus)
POLRMT: Mitochondrial RNA polymerase
POLγ: Mitochondrial DNA polymerase
POU5F1: POU class 5 homeobox 1
PPAR: Peroxisome proliferative-activated receptor
PRAS40: Proline-rich Akt substrate of 40 kDa
Pro: Proline
PT: Permeability transition
PTB: Polypyrimidine tract-binding
qPCR: quantitative PCR
RE: Restriction enzyme
REST: RE-1 silencing transcription factor
Rev: Regulator of virion (retrovirus)
RHEB: Ras homolog enriched in brain
RIPA: Radioimmunoprecipitation assay (buffer), 50 mM Tris-HCl, 150 mM sodium chloride, 1.0% Triton X-100, 0.5% sodium deoxycholate, 0.1% SDS, pH 8.0.
RNA: Ribonucleic acid
RNS: Reactive nitrogen species
ROI: Region of interest

ROS: Reactive oxygen species
RP: Reverse primer
rRNAs: Ribosomal RNAs
RT: Room temperature
SC: Supercomplex
SD: Standard deviation
SDH: Succinate dehydrogenase
SDR: Strand displacement replication
SDS: Sodium dodecyl sulphate
Ser: Serine
sgRNA: Single guide RNA
Shh: Sonic hedgehog
shRNA: Short hairpin RNA
SIRT1: NAD-dependent protein deacetylase sirtuin-1
SLM3: tRNA-5-taurinomethyluridine 2-sulfurtransferase
SMA: Spinal muscular atrophy
SMURF1: SMAD specific E3 ubiquitin protein ligase 1
SOX2: SRY-box 2
SV40: Simian virus 40
T-TBS: TBS with 0.05% Tween
TAL: Transcription activator-like
TALENs: Transcription activator-like effector nucleases
TBK1: TANK binding kinase 1
TBS: Tris-buffered saline
TBX5: T-box 5
TEMED: Tetramethylethylenediamine
TG: Transfer buffer (
TGS: Running buffer (25 mM Tris, 190 mM glycine, 0.1% SDS, pH 8.3)
Thr: Threonine
TIM: Translocase of inner membrane
TOM: Translocase of outer membrane
TOMM20: Translocase of outer mitochondrial membrane 20
TrkB: Tropomyosin-related kinase B
TRMU: Mitochondrial tRNA-specific 2-thiouridylase 1
tRNAs: Transfer RNAs
Trp: Tryptophan
TSC: Tuberous Sclerosis Complex (1 and 2)
TYMP: Thymidine phosphorylase
TUJ1: βIII-Tubulin
UBA: Ubiquitin-associated
UBL: Ubiquitin-like
ULK1: Unc-51 Like Kinase 1
UPR^{mt}: Mitochondrial unfolded protein response
UPS: Ubiquitin-proteasome system
URFs: Unidentified reading frames
VDAC1: Voltage-dependent anion-selective channel 1
VHL: Von Hippel-Lindau
VPA: Valproic acid
VPS: Vacuolar protein sorting
VSV-G: Vesicular stomatitis virus G
WPRE: Woodchuck Hepatitis Virus Posttranscriptional Regulatory Element
WT: Wild-type
ZFNs: Zinc-finger endonucleases
ΔΨm: Mitochondrial membrane potential

INTRODUCTION

INTRODUCTION

Mitochondria

Structure, morphology and functions

Mitochondria are vital organelles for every nucleated cell as they generate energy by producing adenosine triphosphate (ATP) by the oxidative phosphorylation (OXPHOS) system. Therefore, these organelles are necessary for the energetic survival of the cell without being dependent on anaerobic glycolysis. They are also important for several aspects of the cell metabolism, since they regulate apoptosis, calcium homeostasis and the response against oxidative stress, mainly caused by the mitochondrial production of reactive oxygen species (ROS)[1]. Mitochondria were first identified during the nineteenth century and it is widely accepted that they have an endosymbiotic origin[2]: mitochondria are suggested to evolve from bacteria that endocytosed in a primal eukaryotic cell which acquired bacteria's OXPHOS system[3].

Structure, organization and functions of mitochondria are strongly interconnected. However, it is difficult to stablish a static mitochondrial morphology due to the plastic and dynamic nature of the organelle. Besides, mitochondria can be observed as discrete entities or interconnected as tubular networks by which they can move, fuse and fission. Therefore, mitochondria have no permanent size, but typically they can be defined as rod-like shaped organelles with dimensions of 3-4 μm (length) and 0.5-1 μm (diameter)[4].

Mitochondria contain two different, highly specialized membranes: the outer mitochondrial membrane (OMM) and the inner mitochondrial membrane (IMM). They create two independent internal compartments: the mitochondrial matrix and the intermembrane space (IS)[5] **(Figure I1).** The biochemical composition, the morphology and the roles of the two membranes are different.

The OMM is a phospholipid bilayer similar to the plasma membrane, which is freely permeable to small molecules and ions smaller than 6 kDa. The OMM contains many copies of a transport channel protein called VDAC1 (Voltage-Dependent Anion Channel 1) which allows the free diffusion of molecules. Therefore, the IS and the

cytosol share a similar biochemical composition and the presence of specific proteins such as cytochrome c[5].

Moreover, OMM associates mitochondria with the cytoskeleton, allowing mitochondrial movement across the cell[6]. Recently, interaction areas between OMM and the endoplasmic reticulum (ER) have been observed (mitochondria-associated ER membrane, [MAM])[7]. These contact areas are required for crucial cellular events including the import of calcium and phosphatidylserine into mitochondria, the autophagosomes formation or the regulation of the mitochondrial morphology and motility[8].

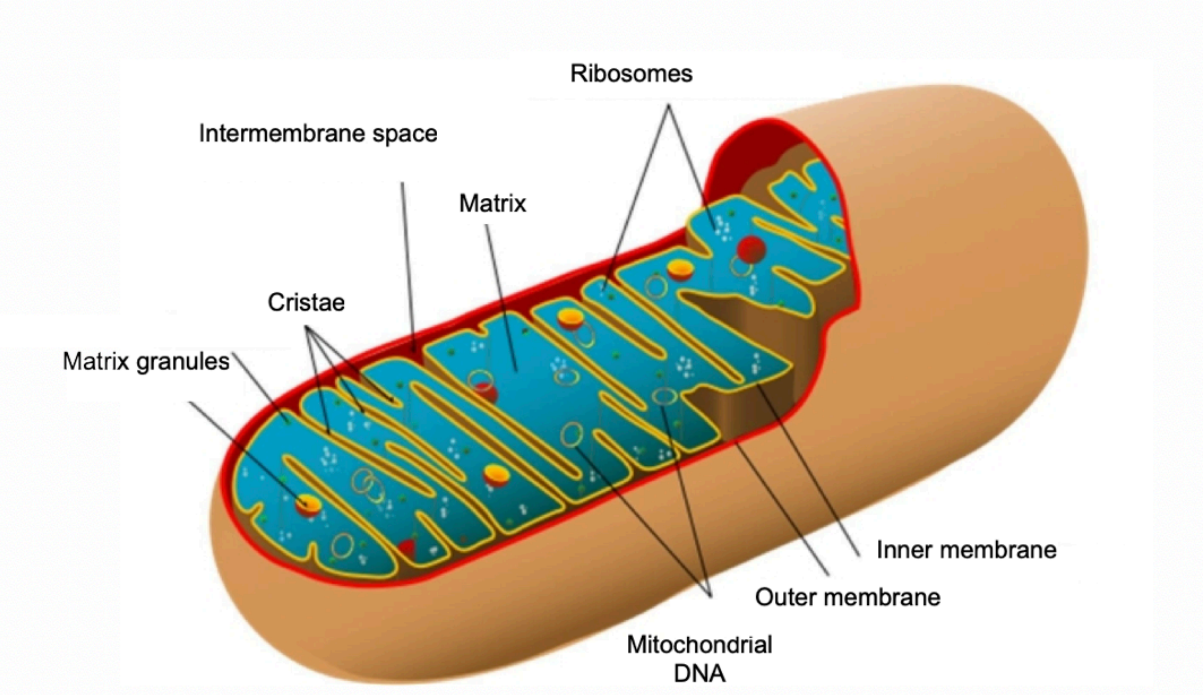

Figure I1. Structure of mitochondrion (diagrammatic).
Mitochondria are bounded by a double membrane: a smooth outer membrane and a folded inner membrane. The folds of the inner membrane are called cristae. The gap between both membranes is called the intermembrane space. The space within the inner membrane is called the matrix, which contains DNA, ribosomes and granules.

In contrast to OMM, the lipid composition of the IMM is special, since it contains a huge percentage of cardiolipin, a phospholipid with four fatty acids that helps IMM to be impermeable to most ions and small molecules. This allows the maintenance of the proton gradient that drives OXPHOS. Besides, it is postulated that cardiolipin may be essential for either the assembly of the complexes of the mitochondrial

respiratory chain (MRC) in the IMM or their maintenance in their functional conformation.

The IMM forms numerous invaginations named cristae which expand IMM surface area and contain mainly proteins (70% of the total components) which have an essential role in OXPHOS (ATP generation) and the import and export of metabolites or small molecules required by the enzymes of the matrix. Due to the presence of these invaginations, IMM can be divided into two distinct regions, the inner boundary membrane (IBM) and cristae[9].

The number and morphology of cristae are likely to reflect the response of the mitochondria to the energy demands of the cell. Recently, technical advances in ultrastructure analysis of mitochondria have led to the current view of cristae as tubules, in which three components can be observed: cristae junctions (sites where a given crista extends inward from the IBM), cristae stalks (digitiform segments which harbor ETC supramolecular complexes) and cristae tips (regions which cap the cristae, seal the membranes and contain the ATP synthase complex)[9].

The matrix contains the mitochondrial DNA (mtDNA), mitochondrial ribosomes, different mitochondrial transfer RNAs (mt-tRNAs) and the enzymes responsible for the central reactions of oxidative metabolism **(Figure I1)**: the catabolism of pyruvate and fatty acids to produce acetyl coenzyme A (CoA) and its oxidation in the citric acid cycle. The oxidation of acetyl CoA to CO_2 produces the bulk of reduced nicotinamide adenine dinucleotide (NADH), which is the main source of electrons for transport along the MRC.

Despite of the specialized mitochondrial compartmentalization, mitochondrial sections are interconnected by transport protein complexes, such as the translocase of outer membrane (TOM) and the translocase of inner membrane (TIM)[10], which allow the import of proteins into the IS or the mitochondrial matrix.

The main function of mitochondria is the ATP production in aerobic organisms, a metabolic process termed OXPHOS that is carried on through the MRC by transferring electrons from reduced species (NADH or reduced Flavin adenine dinucleotide, [$FADH_2$]) to O_2, obtaining water as an end product. This process is

coupled to a proton pumping through the IMM from the mitochondrial matrix to the IS, generating an electrochemical gradient, which provides mitochondrial membrane potential (ΔΨm).

Among the components of MRC that carry on the OXPHOS process, four are multiprotein complexes (complex I-IV) located in the IMM, which are connected through two electron transporters: coenzyme Q_{10} (CoQ) and cytochrome c, and the ATP synthase (complex V)[5] (**Figure I2**).

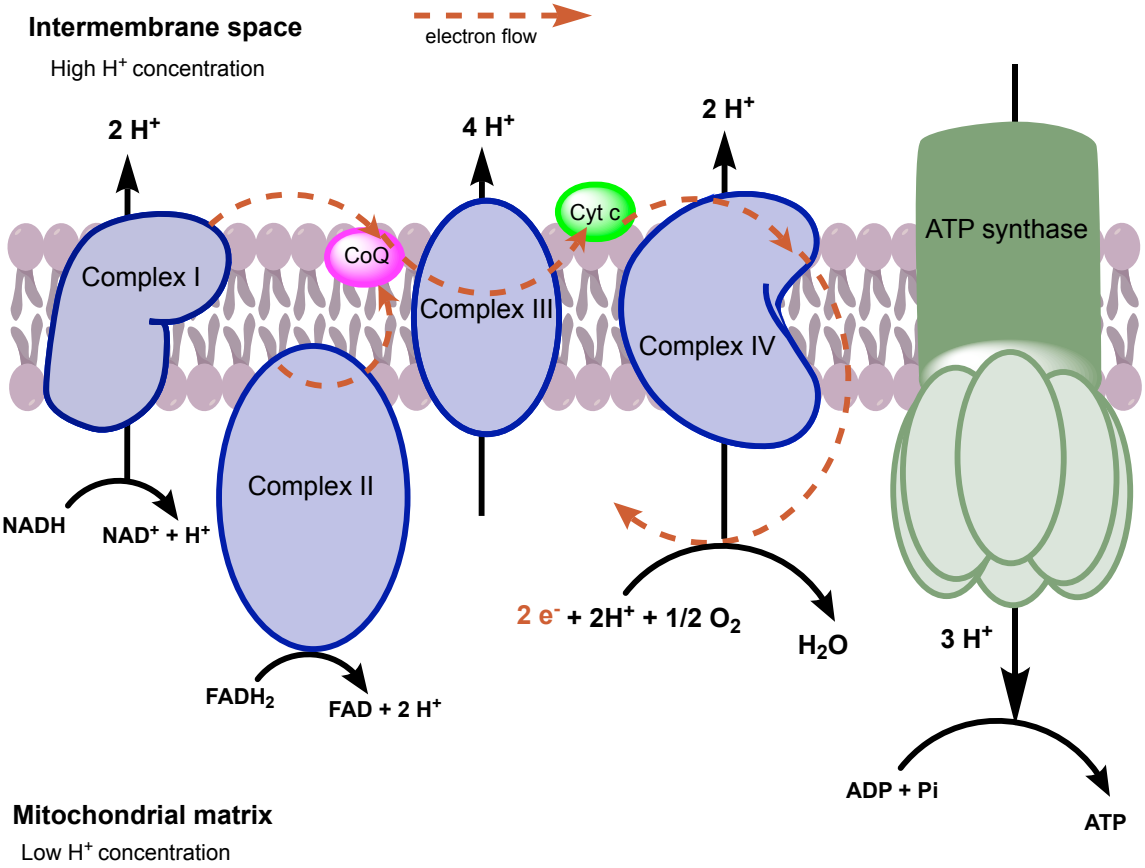

Figure I2. Mitochondrial electron transport chain.
The mitochondrial electron transport chain consists of a series of large proteins bound to the inner mitochondrial membrane. Four large proteins are associated with electron transport, called complexes I through IV. The electron transport chain and OXPHOS are coupled by a proton gradient across the inner mitochondrial membrane, which creates an electrochemical gradient that is used by ATP synthase (complex V) to produce ATP.

The complex I or NADH dehydrogenase is the largest enzyme of the MRC and has a characteristic L shape with an extensive part being embedded in the IMM and a smaller part protruding into the mitochondrial matrix[11]. This multiprotein complex takes 2 electrons from NADH and transfers them to one CoQ molecule, which is

reduced to ubiquinol ($CoQH_2$). This process generates a pumping of 2 protons through the IMM from the matrix to the IS.

The other main entry way to the MRC is the complex II or succinate dehydrogenase, whose fourth subunit is part of the Krebs cycle and oxidizes succinate to fumarate, reducing one oxidized Flavin adenine dinucleotide (FAD^+) molecule to $FADH_2$ at the same time. This reduced molecule feeds the electrons into the electron transport chain (ETC) by transferring them to one CoQ molecule. Complex II does not pump protons across the IMM and therefore does not contribute to the generation of the $\Delta\Psi m$[12].

$FADH_2$ reducing equivalents also can enter MRC through other proteins such as the electron-transferring-flavoprotein (ETF) dehydrogenase, which directly reduces CoQ[13]. $CoQH_2$ is oxidized by the dimer complex III or cytochrome c oxidoreductase and as a result four protons can be pumped to the IS. The electrons from $CoQH_2$ are passed to the electron carrier cytochrome c *via* cytochromes b and c_1 of complex III.

The last component of the ETC is the complex IV or cytochrome c oxidase, which is able to get electrons from cytochrome c and transfer them to an oxygen molecule to convert it to two water molecules. Two protons are pumped to the IS during this process[11].

Complexes I, III and IV produce a proton pumping that provides an electrochemical proton gradient through the IMM, the mitochondrial membrane potential, that indicates the functional state of mitochondria. Complex V or ATP synthase uses the dissipation of protons from the IS to the mitochondrial matrix to generate ATP from adenosine diphosphate (ADP) and inorganic phosphate (Pi)[14].

Currently, there is a consensus about the existence of higher-order organization of the OXPHOS-ETC: MRC complexes are organized into supercomplexes (SCs) of varying stoichiometry. In mitochondria from mammalian tissues, BN-PAGE has revealed SCs including $CI/CIII_2/ CIV_{1-4}$, $CI/CIII_2$, and $CIII_2/CIV_{1-2}$. Respirasomes are considered SCs that contain CI, CIII, and CIV and are capable of $NADH:O_2$ oxidoreduction *in vitro*[15].

Mitochondrial DNA

As a relic of their evolutionary past, mitochondria contain their own genetic material (mtDNA)[16]. In 1981, the complete sequence of human mtDNA was published[17], but the complete characterization of all the Unidentified Reading Frames (URFs) was achieved in 1986[18,19].

Several differences between mtDNA and nuclear genome can be found. For example, there is little non-codifying or regulatory mtDNA in humans, almost every nucleotide (nt) is part of a coding sequence and there are no introns.
Moreover, the mitochondrial genetic system uses a slightly different genetic code, with a relaxed codon usage, which is different from the "universal" genetic code used by both prokaryotic and eukaryotic cells. Human mtDNA only encodes 22 transfer RNA (tRNA) species, and these are the only ones used for translation of mitochondrial messenger RNAs (mRNAs). This is accomplished by an extreme form of wobble in which the uracil (U) in the anticodon of the tRNA can pair with any of the four bases in the third codon position of the mRNA, allowing four codons to be recognized by a single tRNA. In addition, some codons specify different amino acids in mitochondria than in the universal code[17] (**Table I1**).

Codon	Universal code	Human mitochondrial code
UGA	STOP	Tryptophan
AGA	Arginine	STOP
AGG	Arginine	STOP
AUA	Isoleucine	Methionine

Table I1. Differences between the Universal and Mitochondrial genetic codes.

The human mitochondrial genome is a compact, 16,569 base pair (bp), circular, double-stranded molecule found in the mitochondrial matrix and present in multiple copies[20], which are usually distributed in several clusters, called *nucleoids*. *Nucleoids* are thought to be attached to the IMM and are made up of an aggregate of mtDNA genomes (5-7 copies per *nucleoid*)[21] and a group of mitochondrial proteins

such as mitochondrial transcription factor A (mtTFA), mitochondrial single strand binding protein (mtSSBP) and the mitochondrial helicase TWINKLE[22]. The *nucleoid* may also serve as a mitochondrial genetic unit as it has been shown that there is very little mtDNA exchange between individual *nucleoids*[23].

Most mitochondrial genes were transferred to the nucleus along evolution, so most of the proteins in mitochondria are encoded by special genes devoted to this purpose in nuclear DNA (nDNA) and imported into the mitochondria[24], with the exception of 37 genes encoded by mtDNA: 13 protein-coding genes together with two mitochondrial ribosomal RNAs (mt-rRNAs, 16S and 12S) genes and 22 mt-tRNA genes (*MTT*)[17,25], necessary for the mitochondrial proteins synthesis. The 13 proteins encoded by mtDNA are structural subunits of the MRC: constituents (ND1–6, ND4L) of complex I (NADH-coenzyme Q oxidoreductase), complex III (cytochrome b), cytochrome oxidase (COI, COII, COIII of complex IV), and ATP synthase or complex V (ATPase 6, 8). However, the rest of components of the MRC are encoded by nuclear genes; therefore, the mitochondrial and nuclear genomes must work together to ensure the normal functioning of the mitochondria[26] (**Figure I3**).

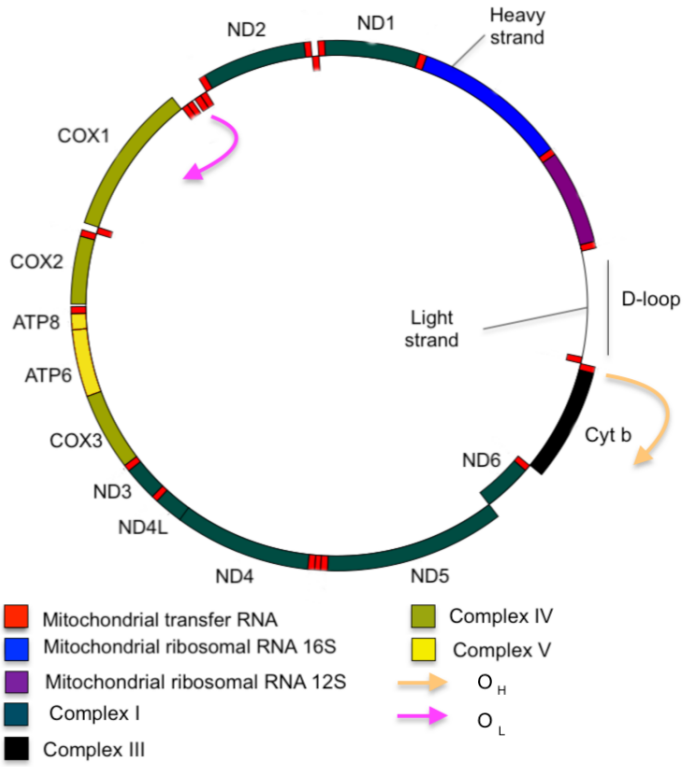

Figure I3. Mitochondrial DNA structure.

The two DNA strands of the human mtDNA differ in their nucleotide composition. Therefore, they are identified as either the heavy (H) strand or the light (L) strand. The H strand has more guanine nucleotides; the L strand has more cytosine nucleotides.

The unique non-coding control region of the human mtDNA is located into the displacement loop (D loop) region, which has the promoters of both H and L strands and the replication origin of H strand.

Replication and transcription are coupled in mitochondria, with unique machinery that carries out these processes.

Each strand has a single promoter site and both strands are transcribed at the same rate, so two different enormous polycistronic RNAs precursors are produced during transcription by the mitochondrial RNA polymerase (POLRMT), which is recruited by mtTFA to the promoter sites. Other proteins, such as the mitochondrial transcription factors B1 and B2 (mtTFB1 and mtTFB2) and the mitochondrial transcription terminator factor (mtTERM) are involved. Then, RNAs precursors are fragmented in individual RNA molecules[27], but not in the same way.

The transcripts made on the H strand are extensively processed by nuclease cleavage to yield the two mt-rRNAs, 14 mt-tRNAs, and 12 proteins (poly-A-containing RNAs, mt-mRNAs). In contrast, the transcript of the L strand is processed to produce only 8 mt-tRNAs and 1 protein (poly-A-containing RNA, mt-mRNA). The mt-mRNAs lack a cap structure at their 5' end and the poly-A tail at their 3' end is posttranscriptionally added by a mitochondrial poly-A polymerase (hmtPAP)[17].

Translation of the mt-mRNAs takes place in the mitochondrial matrix by the mitoribosomes and different proteins responsible for translation, initiation and elongation processes and mitoribosomes recycling[28].

Human mtDNA has two origins of replication, one responsible for each strand: O_H (origin of H-strand synthesis) and O_L (origin of L-strand synthesis). RNA processing of L-strand transcripts is the first critical step in the initiation of mtDNA replication, since necessary RNA primers are generated[29].

Two different mechanisms of human mtDNA replication have been elaborated[30]: a) the Strand Displacement Replication (SDR), in which a leading strand synthesis starts at a specific site and advances approximately two thirds of the way around the molecule before the second-strand DNA synthesis initiates[31]. In this model, initiation

and elongation of the H-strand is the first event, and it proceeds a considerable distance around the circle. Only after the second origin (O_L) is displaced as a single-stranded template, DNA replication of the other strand in the opposite direction will begin. Therefore, O_H is dominant. b) the coupled leading and lagging strand DNA synthesis, in which a fully double-stranded structure is formed[32].

Anyway, there are different proteins involved in mtDNA replication: the mtDNA polymerase (POLγ) has 3'–5' exonuclease and 5'-deoxyribose phosphate lyase activities. TWINKLE is essential to loosen the mtDNA duplex and mtSSBP maintains the mtDNA molecule as a single strand[27].

Heteroplasmy

Each cell contains a variable number of mitochondria, and mitochondria are polyploid: each mitochondrion contains several copies of mtDNA, so there can be several hundred or thousand copies of their genome per cell.

The polyploidy aspect of mitochondrial genetics invokes the concepts of homoplasmy and heteroplasmy.

Usually, all copies of mtDNA of a human cell are identical between them (homoplasmy). However, heteroplasmy is considered when mutations of mtDNA are present in some but not all copies, so there is a mixture of mutant and wild-type (WT) mtDNA within each cell (**Figure I4**).

The ratio of different types of mtDNAs in a heteroplasmic population may be variable, being usually one mitotype prevalent over the rest of alternative configurations, which are present at very low proportions. Generally, the phenotype of the organism is determined by the predominant mtDNA variant[33]. Furthermore, it has been demonstrated that low levels of heteroplasmy are maternally inherited in humans[34].

Therefore, mtDNA populations may frequently contain variable proportions of mutant and WT mtDNA (heteroplasmy load)[35]. At least 20% of the population harbours heteroplasmy loads that have been reported to be implicated in several diseases[36].

Heteroplasmy origin.

The mitochondrial genome has a high mutation rate compared to the nuclear genome due to many factors: the lack of a protective chromatin-type packaging of mtDNA, insufficient mechanisms of mtDNA repair and high ROS production in mitochondria[37]. Therefore, the presence of heteroplasmy in the cell can be caused by different phenomena.

- Spontaneous mutations in mtDNA:

The most common cause of heteroplasmy is the appearance of single nucleotide mutations: single base insertions or single base deletions which provoke point mutations, deletions or duplications in mtDNA[38]. These mutations are usually consequences of the harmful action of ROS. MRC complexes-derived ROS are thought to have the highest impact on oxidative damage of mtDNA. In fact, evidences suggest that mtDNA is more affected by ROS than nDNA[39]. Nucleotide misincorporations by POLγ or spontaneous base hydrolysis are responsible for the accumulation of point mutations in mtDNA[40].

- mtDNA recombination:

Although mtDNA recombination has been described in mammals[41], heteroplasmy of human mtDNA driven by that process has been rarely described[42]. Recombinant mtDNA molecules are able to be inherited; however, to have a real repercussion on the cell, recombination must occur between two different mtDNA molecules, when there is previous heteroplasmy[43].

- Paternal mtDNA leakage:

Mitochondria are transferred by a single progenitor, almost exclusively the mother (maternal inheritance pattern). Paternal mtDNA is almost never passed on to progeny[44]. However, it has been proven that heteroplasmy can be produced by occasional paternal mtDNA leakage resulted from a failure in mechanisms that normally maintain maternal mtDNA inheritance[45,46]. However, this is a rare phenomenon and only a few cases of paternal mtDNA transmission are reported in humans[47].

Heteroplasmy segregation and expansion.

The variation of the heteroplasmy load between the offspring of a mother carrying a mtDNA mutation is stablished before the formation of the primary oocyte.

During the early development of the oocyte, a restriction of the mtDNA copy number occurs (bottleneck phenomenon): mitochondrial genomes are distributed by chance during cytokinesis; therefore, only a subset of all embryo cells and consequently mtDNAs present in the zygote will ultimately contribute to the embryo itself[48].

This process is responsible for heteroplasmy load variation between the offspring, but it does not explain the clinical heterogeneity of mitochondrial diseases[49].

When a heteroplasmic cell divides, the mtDNA molecules randomly pass to the daughter cells in a process called vegetative segregation (**Figure I4**).

By chance, each daughter cell can receive a different proportion of mutant mtDNA. When vegetative segregation occurs in somatic cells, phenotypic variation can emerge in the same organism: different cells of the organism differ in the heteroplasmy load, with different phenotypes between tissues. In the case of pathological mtDNA mutations, disease phenotypes are only observed in the tissue once the proportion of WT mtDNA drops below a threshold level. This phenomenon is called mitochondrial threshold effect[50] (**Figure I4**).

The threshold level required to trigger the mitochondrial dysfunction depends on each mutation, tissue or patient[51]. Tissues and organs with high energetic demand such as neurons, renal and endocrine systems and muscle (including heart) are more vulnerable to low proportions of heteroplasmic mutations, meanwhile tissues with low energetic demand have higher threshold levels[52].

Regarding heteroplasmy load of specific somatic tissues or cell cultures, mitochondrial dynamics has an essential role in heteroplasmy expansion and, for hence, in mitochondrial quality control.

During mitochondrial fission and fusion, mitochondria mix their genome and gene products[53]. Thus, balancing fission and fusion is crucial for both combining mtDNA genomes which allows functional complementation and promoting the elimination of defective mitochondria (with mutant mtDNA) by mitophagy[54].

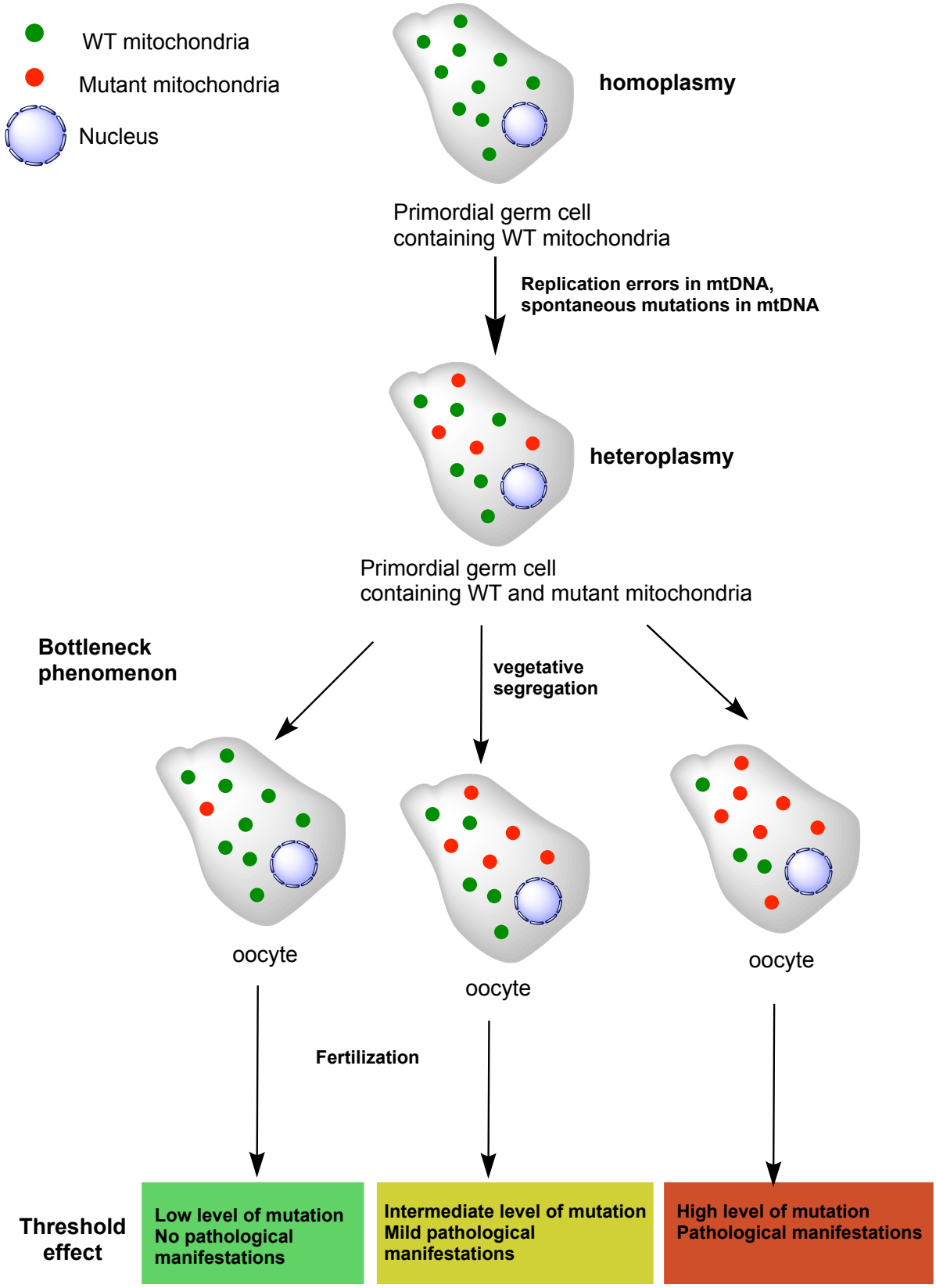

Figure I4. Heteroplasmy origin, segregation and expansion.

Mitochondrial quality control

Currently, how dysfunctional mitochondria are distinguished from functional ones on a molecular level is not fully understood. However, it is known that mitochondria have different quality control mechanisms that keep them functional. These pathways act at the molecular, mitochondrial and cellular level and form an efficient integrated network[55]. At the molecular level, the ROS scavenging process mainly catalyzed by the manganese superoxide dismutase (MnSOD) is the first line of defense in the mitochondrial quality control pathways. Other key components of the mitochondrial ROS scavenging system are small molecules, such as thioredoxin and glutathione, and other enzymes such as glutathione peroxidase or peroxiredoxin[56,57]. The second molecular quality control pathway is the damaged mtDNA repair machinery[58]. Moreover, mitochondrial proteins homeostasis machinery is able to repair oxidized mitochondrial proteins by reductase systems and refold back misfolded proteins by mitochondrial chaperones and the activation of the so-called "mitochondrial Unfolded Protein Response" (UPR^{mt})[59,60]. Currently, since protein damage can impair mitochondrial function, mitochondrial proteases are considered to have a key role in damaged soluble mitochondrial proteins degradation, maintaining mitochondrial functional and structural integrity (**Figure I5**). Lon peptidase 1 (LONP1) and ATP-dependent Clp protease proteolytic subunit (CLPP) are the most important matrix proteases. Both proteins belong to the AAA (ATPases Associated with diverse cellular Activities) proteins family[61,62]. LONP1 is involved in oxidized proteins degradation[63] and also prevents the accumulation of misfolded proteins due to its chaperone activity[64]. CLPP is also able to degrade oxidatively damaged proteins and it has an important role in the UPR^{mt} too[61].

The molecular quality control pathways are not enough to counteract the adverse effects of mitochondrial function, and different strategies at mitochondrial and cellular level are needed: removal of mitochondria by both bulk or selective autophagy (mitophagy), mixing and separating mitochondrial content by fusion and fission processes and producing new mitochondria by *the novo* biogenesis. If mitochondrial damage is not counteracted by molecular, mitochondrial or cellular quality control, apoptosis is finally induced (**Figure I5**).

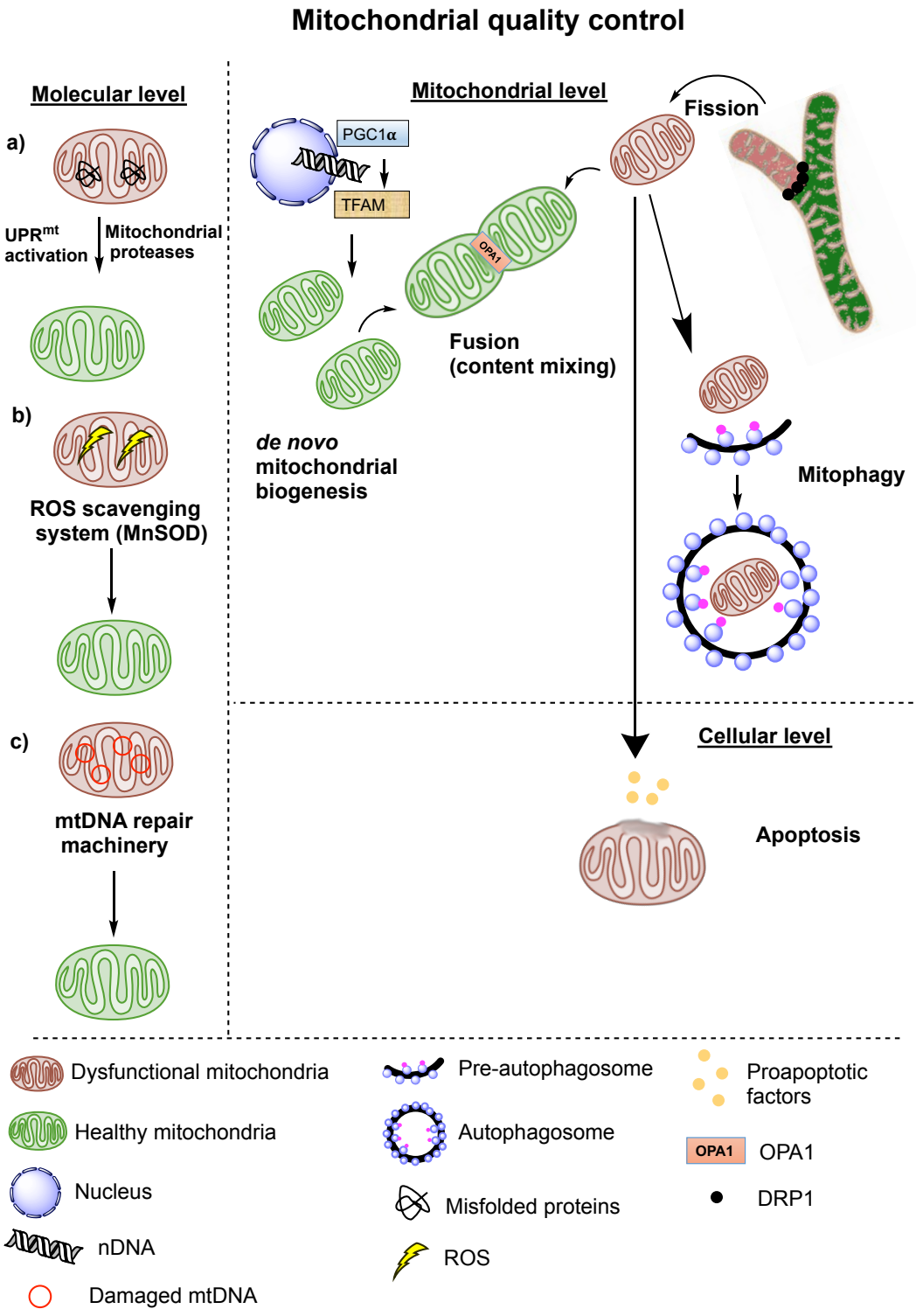

Figure I5. Mitochondrial quality control mechanisms.

Autophagy

Autophagy is an intracellular degradation system by which cytosol and organelles are sequestered within *de novo*-formed double-membrane vesicles (pre-autophagosomes) that deliver the contents to the lysosome/vacuole (autolysosome)

for hydrolytic degradation and recycling of the resulting macromolecules. Autophagy is typically activated by fasting and nutrient deprivation for generating amino acids and metabolic intermediates to maintain ATP production[65]. Furthermore, autophagy allows the removal of defective or useless organelles. In that context, some authors describe bulk autophagy or macroautophagy as a survival mechanism of the cell, because it represents a way to adapt to stressful situations, preventing death by apoptosis[66]. Therefore, an appropriate regulation of autophagy is essential for cellular homeostasis, since only aberrant or defective organelles have to be degraded.

Three main types of autophagy have been described: macroautophagy, microautophagy and Chaperone-Mediated Autophagy (CMA). In macroautophagy (hereinafter, autophagy), cargo is sequestrated from the rest of the cytosol by the autophagosome and is degraded upon fusion of this vesicle with secondary lysosomes, which contain a broad range of enzymes required for hydrolysis of the cargo[67]. By contrast, during microautophagy, the lysosomal membrane invaginates to engulf the cytosolic components without any intermediaries[68]. In CMA, the cytosolic chaperone protein HSC-70 recognizes targeted proteins through the exposure of a pentapeptide motif biochemically related to the pentapeptide KFERQ. The interaction between the chaperone and the substrate in the cytosol forms a complex, which is specifically translocated across the lysosomal membrane[69].

The molecular mechanism underlying autophagy has been extensively researched in the past decade, and the genes participating in this process, denoted ATGs (AuTophaGy-related genes), were found to be conserved from yeast to humans[70,71]. Among these ATGs, two major cytosolic kinase complexes, the Beclin-1/phosphatidylinositol kinase type III (PI3K) complex and mammalian Target Of Rapamycin (mTOR) kinase, together with its accessory proteins regulate induction of autophagy, whereas autophagic-auxiliary proteins and lipids are involved in the formation of autophagosomes[72].

There are different pathways which regulate induction of autophagy, being the 5' Adenosine Monophosphate-activated Protein Kinase (AMPK) and mTOR pathways the most important ones[73].

The autophagy checkpoint is a major mechanism for the maintenance of intracellular homeostasis that can be up-regulated by nutrient deprivation and/or organelle damage. Therefore, autophagy is controlled by several metabolites, including the AMP/ATP ratio and the availability of acetyl CoA, which affect the activity of various acetyltransferases[74]. Since AMPK was primarily characterized as a kinase allosterically activated by adenosine monophosphate (AMP)[75], it was logical to hypothesize that AMPK would have a critical role in autophagy regulation.

Energy levels reduction manifested in the form of an increased AMP/ATP ratio triggers autophagy by activating AMPK[76]. Moreover, oxidative stress activates AMPK by different pathways, some of them in an AMP-independent manner[77-79].
In addition to energy levels, it has been hypothesized that others stimuli trigger autophagy by AMPK activation, such as intracellular calcium (Ca^{2+}) levels[80-82].
Independently of the stimuli, AMPK activation can induce the autophagic process through two different mechanisms: inhibition of mTOR and direct phosphorylation of Unc-51 Like Kinase 1 (ULK1), a mammalian orthologue of Atg1.
mTOR is a main regulator of diverse intracellular pathways that control growth, proliferation and survival. It is an effector in the PI3K/Protein Kinase B (PKB) pathway, and it carries out its action by two different complexes, called mTOR Complex 1 (mTORC1) and mTOR Complex 2 (mTORC2). mTORC1 promotes protein synthesis, lipid biogenesis and cell growth as well as anabolism and inhibits cellular catabolism by preventing autophagy. Instead, mTORC2 regulates cell survival, cell proliferation and metabolism.
mTOR name comes from its sensitivity to rapamycin, which inhibits autophagy by solely affecting mTORC1, which is formed by the serine/threonine kinase mTOR, mLST8, PRAS40 and raptor, a regulatory protein which recruits downstream substrates such as EIF4EBP and p70S6K. mTORC1 inhibits autophagy by blocking the autophagy initiator complex activity, which is formed by ULK1, ATG13, ATG101 and FIP200[83,84]. ULK1 is the essential protein for autophagy initiation in mammalian cells[85-87]. The autophagy initiator complex is assembled independently of mTOR activity or nutrients conditions. However, under fed conditions, mTORC1 phosphorylates ULK1 in Serine (Ser) 638 and Ser758 and inhibits its kinase activity, preventing autophagy initiation[88]. ATG13 is also a substrate of mTOR kinase and its phosphorylation has negative effects on ULK1 activity[84]. Moreover, ULK1

phosphorylation by mTOR disrupts its interaction with AMPK, preventing autophagy. Under starvation conditions, mTORC1-dependent phosphorylation of ULK1 is removed and ULK1 autophosphorylates and phosphorylates ATG13 and FIP200, initiating autophagy.

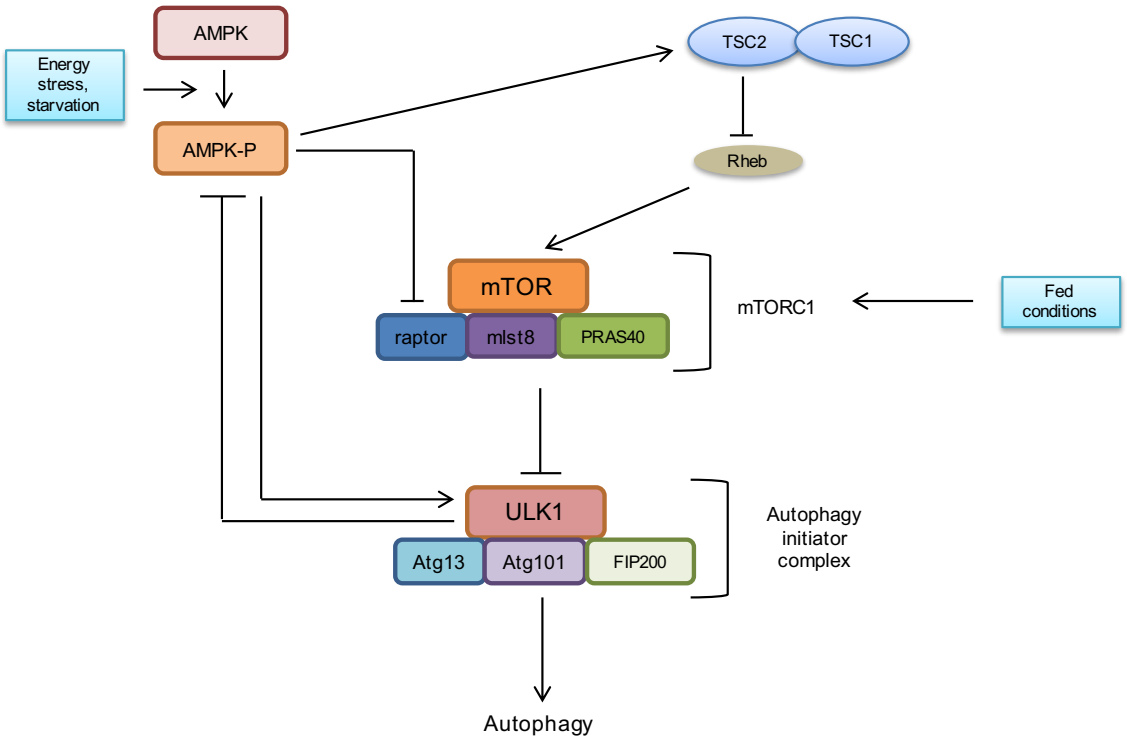

Figure I6. Dual regulation of autophagy by mTOR and AMPK. Adapted from Villanueva-Paz et al. (2016)[89].

Since activation of mTORC1 is the principal mechanism to inhibit autophagy in mammalian cells, one of the mechanisms of AMPK-dependent induction of autophagy is inhibition of mTORC1 activity. AMPK is able to inhibit mTORC1 in a direct way by phosphorylating raptor, the mTORC1 binding partner[90] and through an indirect way by phosphorylating TSC2, an upstream inhibitor of mTORC1 which inactivates RHEB, an activator of mTORC1[91,92].

More recently, it has been observed that AMPK can also activate autophagy by direct phosphorylation of ULK1[93,94].

Interestingly, the patterns of activation of AMPK and mTOR are opposite, regulating by this way the activation of autophagy depending on the nutrient conditions[95,96] (**Figure I6**).

Autophagy can be a nonselective or selective process, because autophagy receptors and proteins of the growing autophagosome can specifically interact with the cytoplasmic component that needs to be eliminated[97-100].

There is a controversy about considering whether autophagy promotes or prevents cell death. If autophagy removes damaged organelles that would otherwise activate caspases and apoptosis, then autophagy could be protective. On the other hand, some authors describe autophagy as other way of programmed cell death different from apoptosis, since autophagy is essentially a catabolic process that could potentially be used by the cell to its self-destruction[101]. Therefore, regulation of autophagy in the cell appears to be essential for the balance between survival and cell death.

Mitophagy

Although autophagy usually refers to the non-selective elimination of any component of the cytoplasm, the term mitophagy was coined by J.J. Lemasters in 2005 to exclusively define the selective degradation of mitochondria by autophagy[98]. Damaged or useless mitochondria are selectively degraded by a regulated and complex process which allows controlling the number of functional mitochondria in the cell, both for satisfying the metabolic demand and performing a mitochondrial quality control. Within the mitochondria, the main ROS produced is superoxide anion (O_2•−), most of which is converted to hydrogen peroxide (H_2O_2) by the action of superoxide dismutase. The production of O_2•− by mitochondria has been assigned to several enzymes of the ETC, including complexes I and III and glycerol-3-phosphate dehydrogenase[102]. If mitochondria are defective or cellular respiration is inhibited, the level of ROS produced by mitochondria increases. Due to the production of these reactive species, mitochondria are highly exposed to oxidative stress, which causes both the opening of permeability transition (PT) pores in the IMM and the permeability of mitochondrial membranes to molecules of less than 1.5 KDa. Induction of the mitochondrial PT (MPT) can lead to mitochondrial swelling and cell death through apoptosis or necrosis depending on the particular biological situation[103]. Moreover, induction of MPT causes mitochondria to become uncoupled and depolarized, and as a consequence, mitochondria show a defective synthesis of ATP. In addition, ROS are implicated in genotoxicity and cause the accumulation of

mutations in the mtDNA. The accumulation of oxidative damage in the mitochondria over time causes the dysfunction of the organelle and can even cause cell apoptosis due to release of proapoptotic proteins. Therefore, mitochondrial quality control must occur in the cell to eliminate ancient or damaged mitochondria that produce high levels of ROS. This process is mainly performed by mitophagy[104]. In fact, ROS-induced mitochondrial damage may be an important upstream activator of mitophagy[105].

Mitophagy is a complex process that shares elements and mechanisms of bulk autophagy. For example, besides activating macroautophagy, AMPK is demonstrated to promote mitophagy[73]. In mammals, loss of AMPK resulted in aberrant accumulation of the autophagy adaptor protein Sequestosome-1 (P62/SQSTM1) and defective mitophagy[93]. P62 binds to specific cargo targeted for autophagy-mediated degradation. Especially, P62 is bound to dysfunctional mitochondria targeted for mitophagy, and is involved in mitochondrial aggregation and clearance[106]. Moreover, although the best-known function of the autophagy initiating factor ULK1 is the autophagy induction[107,108], recent studies suggest that ULK1 has a more selective function in mitophagy[109,110]. It has been described that ULK1 translocates to dysfunctional mitochondria in response to hypoxia or carbonyl cyanide-4-(trifluoromethoxy)phenylhydrazone (FCCP) treatment. Translocated ULK1 phosphorylates FUN14 Domain Containing 1 (FUNDC1) protein (a mitophagy receptor located in the OMM) allowing its interaction with the microtubule-associated protein-light chain 3 (LC3) and inducing mitochondria degradation by autophagy[111].
In relation to this novel role of ULK1, it has been demonstrated that specific phosphorylation of ULK1 at Ser555 by activated AMPK is crucial for ULK1 translocation to the mitochondria[112]. Therefore, AMPK-mediated phosphorylation of ULK1 is essential for mitophagy initiation under stress conditions such as hypoxia.

Understanding of mitophagy mechanisms at the molecular level was pioneered in yeasts[113-116]. Although mitophagy needs autophagy machinery to initiate and keep going; interestingly, there are a few genes that are specifically required for mitophagy, but not for other forms of autophagy. Atg32 is of particular interest because of its role as a mitophagy receptor. It is anchored to the OMM and recruits Atg8, a protein essential for autophagosome formation. Mitochondria-derived ROS,

at low concentrations, may act as signalling molecules and trigger mitophagy through regulation of Atg4, an essential cysteine protease in the autophagic pathway[117]. The formation of autophagosomes depends on Atg4-mediated cleavage of Atg8 and its subsequent conjugation to phosphatidylethanolamine (PE) at autophagosomal membranes.

In mammals, autophagosome formation proceeds in morphologically and biochemically distinct phases referred to as the initiation, execution and maturation phases[118]. The process starts with the formation of a sickle-shaped isolation membrane, called phagophore, in the phagophore assembly sites (PAS)[119]. The ER[120], mitochondria[121] and plasma membrane[122] are membrane sources for phagophores. The formation of the phagophore requires two Vacuolar Protein Sorting (VPS) proteins, VPS34 and VPS15, which act in a macromolecular complex, along with Beclin-1 (mammalian Atg6) and ATG14 to form phosphatidylinositol 3-phosphate (PI3P)[123].

The expansion and closing of the phagophore give rise to the autophagosome by the action of different ubiquitin-like systems: first, ATG12 is conjugated to ATG5 by ATG7. Then, the ATG5–ATG12 complex interacts with ATG16L1 and this resulting complex associates with phagophores but dissociates from completed autophagosomes.

Second, LC3, the mammalian homologue of yeast Atg8, is conjugated with a molecule of PE by ATG7 and ATG3, resulting in a lipidated form of the protein (LC3-II) that anchors the autophagosome membrane. The ATG5–ATG12–ATG16L complex may determine the sites of autophagosome synthesis by regulating the targeting of LC3-II to ATG5–ATG12-associated membranes, forming the double membrane of the autophagosome that engulfs the content to be degraded.

Finally, the autophagosome fusions with the lysosome to form the autolysosome, where the cargo is degraded by hydrolysis. At this point, the LC3-II inside the autolysosomes is degraded and the LC3-II on the cytoplasmic surface is delipidated (LC3-I) and recycled[123].

Documentation of changes in autophagic proteins levels provides an incomplete picture of the process of autophagy within cells. A difficulty in assessing autophagy and mitophagy is that they are highly dynamic processes and static measures are difficult to interpret. Therefore, measures of autophagy flux are required. The term

autophagy flux refers to the whole process of autophagy, including autophagosome formation, maturation, fusion with lysosomes, subsequent breakdown and the release of macromolecules back into the cytosol[124,125].

Considering that LC3-II is present in the initiation, elongation and maturation of the autophagosome, this protein is an essential marker to study autophagy flux and autophagosome dynamics[126]. The accumulation of autophagosomes (LC3-II protein) could indicate either autophagy activation or a blockage of downstream steps in autophagy, such as inefficient fusion or decreased lysosomal degradation. Therefore, to monitor autophagy flux, detection of LC3-II or other autophagosome markers in the presence and absence of lysosomal degradation inhibitors is necessary. Bafilomycin A1 is widely used since it inhibits vacuolar H+ ATPase (V-ATPase), preventing fusion between autophagosome and lysosome[127] (**Figure I7**).

At the same way, mitophagy flux can be evaluated by detecting mitochondrial mass changes in the presence and absence of lysosomal degradation inhibitors such as bafilomycin A1. An increase in mitochondrial mass markers in presence of autophagy flux inhibitors suggests a proper mitophagy flux, meanwhile the absence of accumulation of mitochondrial mass markers suggests a mitophagy flux slowdown or blockage. Moreover, mitophagy flux enhancers or inhibitors can be discovered using this methodology[128,129].

In mammals, three different mechanisms of mitophagy are known[130]. First of all, most mammals' erythrocytes lose their mitochondria by mitophagy during maturation. NIP3-like protein X (NIX), located in the OMM, has a WXXL-like domain in its cytosolic side, which is capable of binding to LC3 protein. The binding of NIX and LC3 promotes the isolation of mitochondria in the phagophore[131,132].

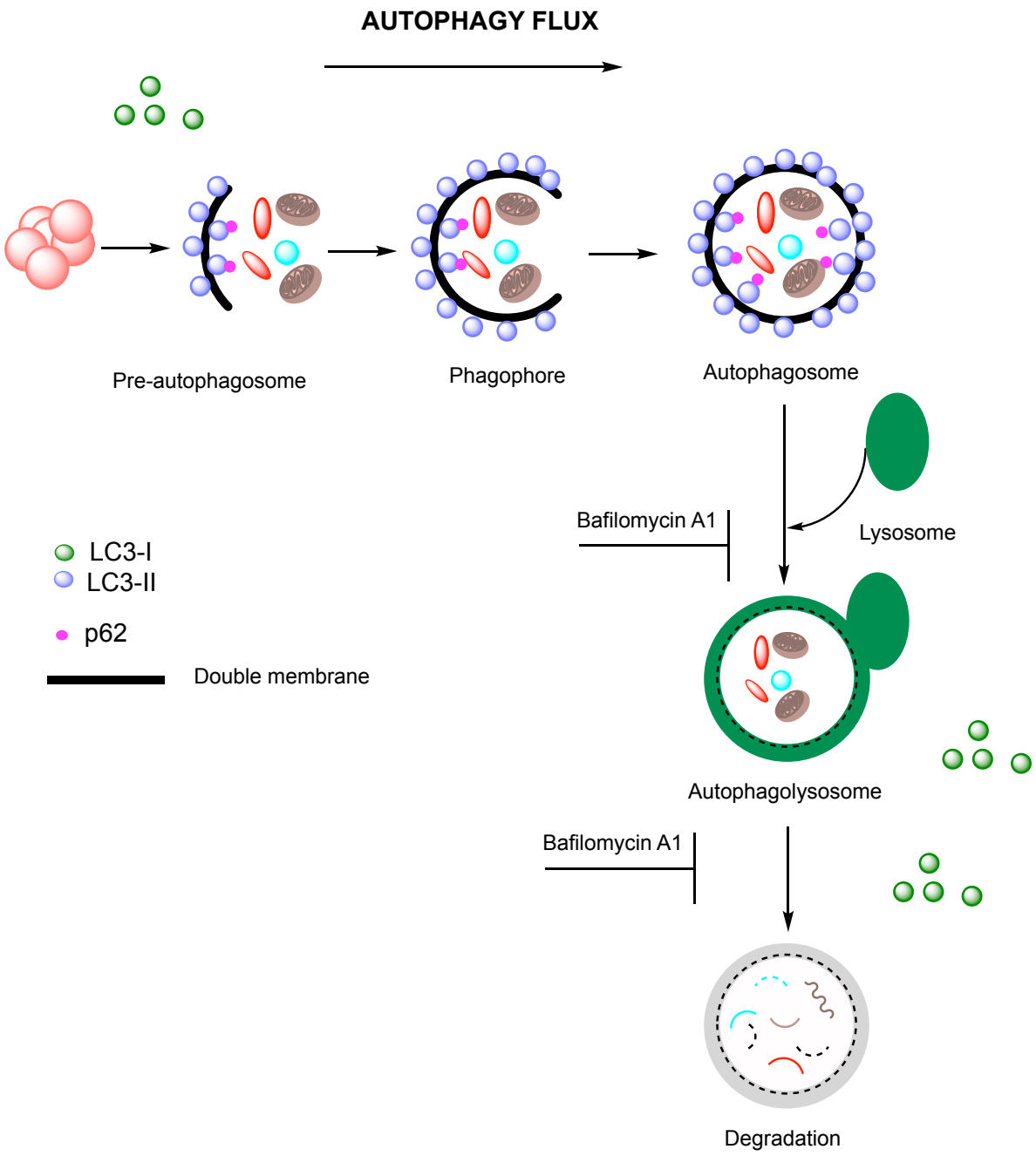

Figure I7. The process of autophagy flux and the effect of bafilomycin A1, the lysosomal inhibitor generally used.
A normal autophagy flux includes the autophagosome formation and maturation step, the autophagolysosome formation step and the degradation step. Under pathological conditions or autophagy inhibitors, autophagy flux may be blocked, leading to the accumulation of dysfunctional autophagosomes and autophagolysosomes.

The second and most important mitophagic mechanism in mammals is considered to be induced by depolarization of the mitochondrial membrane due to damage

accumulation and the action of harmful agents in mitochondria, such as ROS[105]. This process is dependent on the interaction between PTEN-induced putative kinase 1 (PINK1) and the ubiquitin ligase Parkin.

Finally, as a third mechanism of mitophagy, the existence of a Parkin-independent mitophagic mechanism mediated by iron metabolism has been recently suggested[133]. It has been observed in different cell lines that cellular iron chelation induces mitophagy without altering the normal conditions of PINK1 and Parkin. However, more studies are needed to determine the influence of iron on mitophagy.

Parkin-mediated mitophagy

PINK1/Parkin-mediated mitophagy is the best characterized mechanism for the elimination of damaged mitochondria by autophagy in mammalian cells.

In 2008, Parkin recruitment to depolarized mitochondria and the subsequent degradation of mitochondria by mitophagy was described[134]. Parkin is a cytosolic E3 ubiquitin ligase with a ubiquitin-like (UBL) domain in its N-terminal end, which allows the transference of ubiquitin to lysine residues of target proteins, including Parkin itself[135]. Parkin catalyzes a range of different ubiquitination events, from mono-ubiquitination (which has various cellular functions) until polyubiquitination of proteins, which results in a signalling to the proteasome, aggregates formation and therefore, proteins degradation. PINK1 is a serine/threonine kinase whose cellular localization is not yet clear, as it is found both in the cytosol and some mitochondrial compartments, most likely anchored to the OMM by a transmembrane domain.

Under steady-state conditions, PINK1 and Parkin regulate cell morphology by interacting with mitochondrial fusion/fission machinery. In these conditions, PINK1 is imported to mitochondria in a voltage-dependent manner and is rapidly degraded by proteolytic processing in a mitochondrial membrane potential-dependent manner, cleaved by the presenilins-associated rhomboid-like (PARL) protein in the IS and by the mitochondrial processing peptidase (MPP) in the mitochondrial matrix[136-138] (**Figure I8**). Moreover, under these physiological conditions, Parkin maintains an inactive conformation due to the association of its N-terminal UBL and RING1 domains.

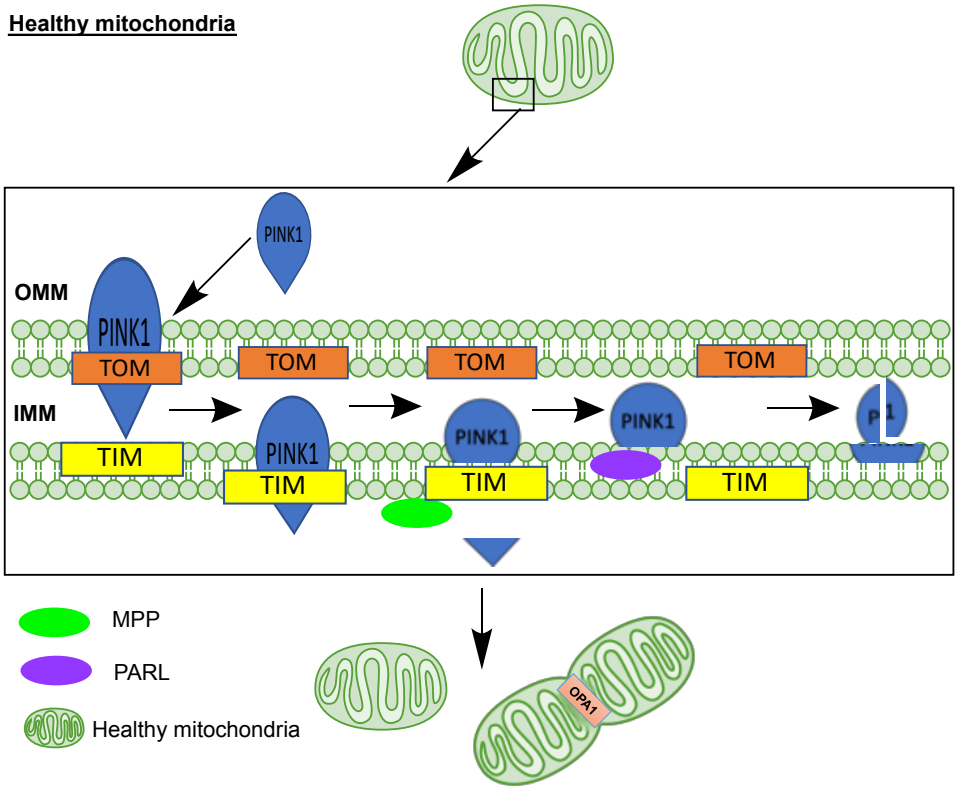

Figure I8. PINK1 degradation in mitochondria under physiological conditions.

Thus, while PINK1 is normally kept at low levels on healthy mitochondria, it rapidly and selectively accumulates on mitochondria that have lost membrane potential[130,139]. Under dissipation of mitochondrial membrane potential due to mitochondrial damage (ROS), loss of cellular respiration, mtDNA mutations, use of uncoupling agents, etc., PINK1 is recruited to the OMM by TOM/TIM complex and it is stabilized in a voltage-dependent manner. Therefore, PINK1 is kept in the OMM of depolarized mitochondria interacting with the TOM complex[139]. In these conditions, PINK1 autophosphorylates[140,141], dimerizes and recruits Parkin to mitochondria through direct phosphorylation at Ser65, increasing Parkin ubiquitin ligase capacity by promoting a conformational change[142,143]. A second PINK1-mediated phosphorylation of a ubiquitin molecule also at Ser65 is essential for full activation of Parkin. The phosphorylated ubiquitin binds to the UBL domain of Parkin to fully activate its E3 ligase activity[144,145]. Once Parkin is phosphorylated, it remains in the OMM and ubiquitinates numerous proteins on the OMM and in the cytosol, including VDAC1, mitochondrial rho (MIRO) GTPase, translocase of outer mitochondrial membrane 20 (TOMM20), Mitofusin-1 (MFN1) and Mitofusin-2 (MFN2)[146]. Following Parkin-mediated ubiquitination of OMM proteins, the selective autophagy adapter

protein P62 and the Neighbor of BRCA1 gene 1 (NBR1) protein are recruited to mitochondria to initiate mitophagy[106,147]. These proteins are able to interact with both ubiquitinated proteins of the OMM (through its ubiquitin-associated [UBA] domain) and autophagic membrane proteins such as LC3 (through its LC3-interacting region [LIR] domain). The interaction between P62 and NBR1 with LC3 allows the sequestration of depolarized mitochondria by the membrane of the autophagosome[106,134] (**Figure I9**).

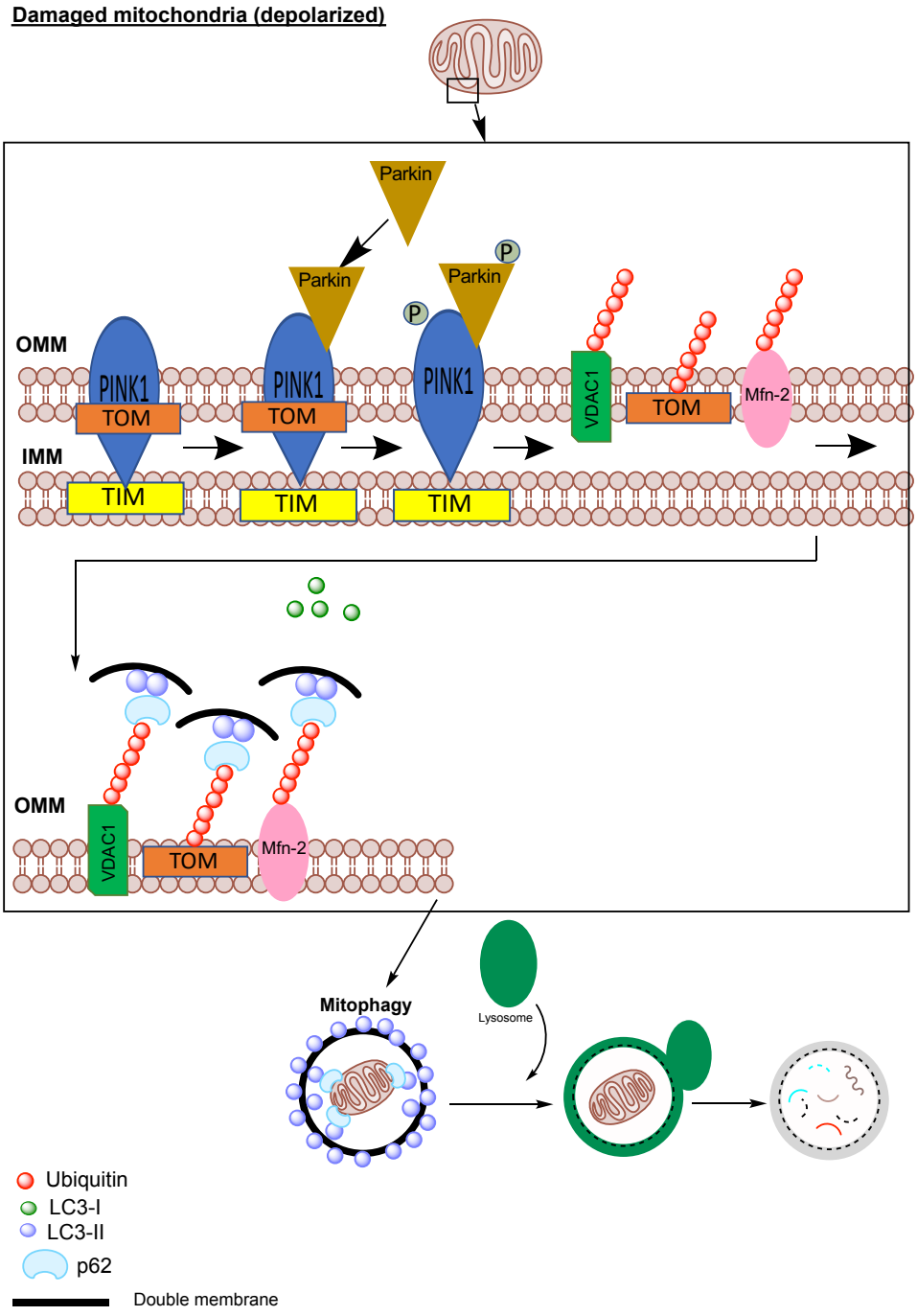

Figure I9. PINK1/Parkin-mediated degradation of damaged mitochondria by autophagy.

The adaptor protein histone deacetylase 6 (HDAC6) has also an important role in mitophagy. This cytosolic protein is able to bind ubiquitinated proteins to the microtubule transport system (by interaction with dynein protein), and concentrates depolarized mitochondria near to the nucleus to be removed by selective autophagy. Finally, in this particular area, this structure called “mito-agresomme” is fused with lysosomes. Then, autophagolysosomes are formed and the subsequent degradation of mitochondria is performed[135].

Ubiquitination and proteasomal degradation of MFN1 and MFN2 result in mitochondrial fission and fragmentation[148]. Mitochondrial fission has been shown to be important for mitophagy induction given that mitochondrial depolarization prevents fusion and leads to mitochondria isolation and subsequent degradation by mitophagy[149]. In contrast, increased mitochondrial fusion has been shown to inhibit the mitophagic process[150].

Mitochondrial dynamics

As dynamic organelles, mitochondria are constantly undergoing fission and fusion to adapt toward changes in the cellular environment.

Fission produces small spherical mitochondria, whereas fusion produces tubular or elongated mitochondria. It is well established that mitochondrial dynamics plays a crucial role in the quality control of mitochondria[151]. When mitochondria are functional, fusion and fission occur in a constant and balanced manner to adapt the morphology of the mitochondrial network to the metabolic needs of the cell[152]. Healthy mitochondria form elongated tubules that continually divide and fuse to form a dynamic interconnected network. The molecular machinery that mediates this organelle fission and fusion is necessary to maintain mitochondrial integrity, perhaps by facilitating DNA or protein quality control[153]. The fusion process is critical for the maintenance of mitochondrial function, as interruption of mitochondrial fusion results in a loss of mitochondrial membrane potential[154]. In fact, mitochondrial fusion allows the spreading of metabolites and mitochondrial gene products throughout the entire mitochondrial compartment. This serves to optimize mitochondrial function and to counteract the accumulation of mitochondrial mutations during aging. Therefore, it is suggested that mitochondrial fusion prevents the induction of mitophagy[150].

Mitochondrial fusion in mammals is mediated by the proteins MFN1, MFN2 and optic atrophy 1 (OPA1). MFN1 and MFN2 are dynamin-related GTPases which are responsible for fusion of OMMs. OPA1 is also a dynamin-related GTPase, which is responsible for fusion of IMMs[155] (**Figure I10**). In fact, mutations in MFN2 can cause neurodegenerative diseases such as Charcot–Marie–Tooth neuropathy type 2A (CMT2A)[156], suggesting that these protein is necessary to preserve the correct function of mitochondrial fusion, to satisfy energy demands of the cell and to keep mtDNA molecules under control by mixing mitochondria and their content.

In contrast, mitochondrial fission plays an important role in the removal of damaged organelles by selective autophagy. As soon as individual parts of the mitochondrial network become dysfunctional, fission events, induced by proteins like mitochondrial fission 1 (FIS1) and dynamin-like protein 1 (DRP1), permit damaged mitochondria to become spatially isolated (**Figure I10**). Thus, dysfunctional mitochondria are distinguished on a morphological basis from the rest and can be presumably degraded by selective autophagy[157]. Since mitochondrial fission may be necessary for the beginning of mitophagy, ubiquitination of MFN2 by Parkin could be important for dysfunctional mitochondria signalling[149]. In fact, it is hypothesized that Parkin facilitates mitophagy by eliminating functional mitofusins and increasing the fission process, thus there is an increase in the number of small and isolated mitochondria which can be easily handled by the phagosome. However, mitochondrial fission would be necessary but not sufficient for mitophagy activation, since mitochondria have to be depolarized and/or dysfunctional to prevent mitochondrial fusion and induce mitophagy[158].

Besides mitochondrial fusion and fission, mitochondrial mobility through the cytoskeleton is very important for mitochondrial quality control. Mitochondria make use of the kinesin-dynein motor to move along the microtubules.
The attachment between the mitochondria and microtubules is performed by the interaction between a mitochondrial membrane protein (MIRO) and the adapter protein Milton[159] (**Figure I10**).
Although it is not clear if mitochondrial motility prevents mitophagy, it has been demonstrated in HeLa cells that knockdown of MIRO accelerates the mitochondrial

removal by mitophagy[160]. Moreover, Parkin ubiquitinates MIRO, preventing mitochondrial movement and facilitating mitochondrial isolation[161].

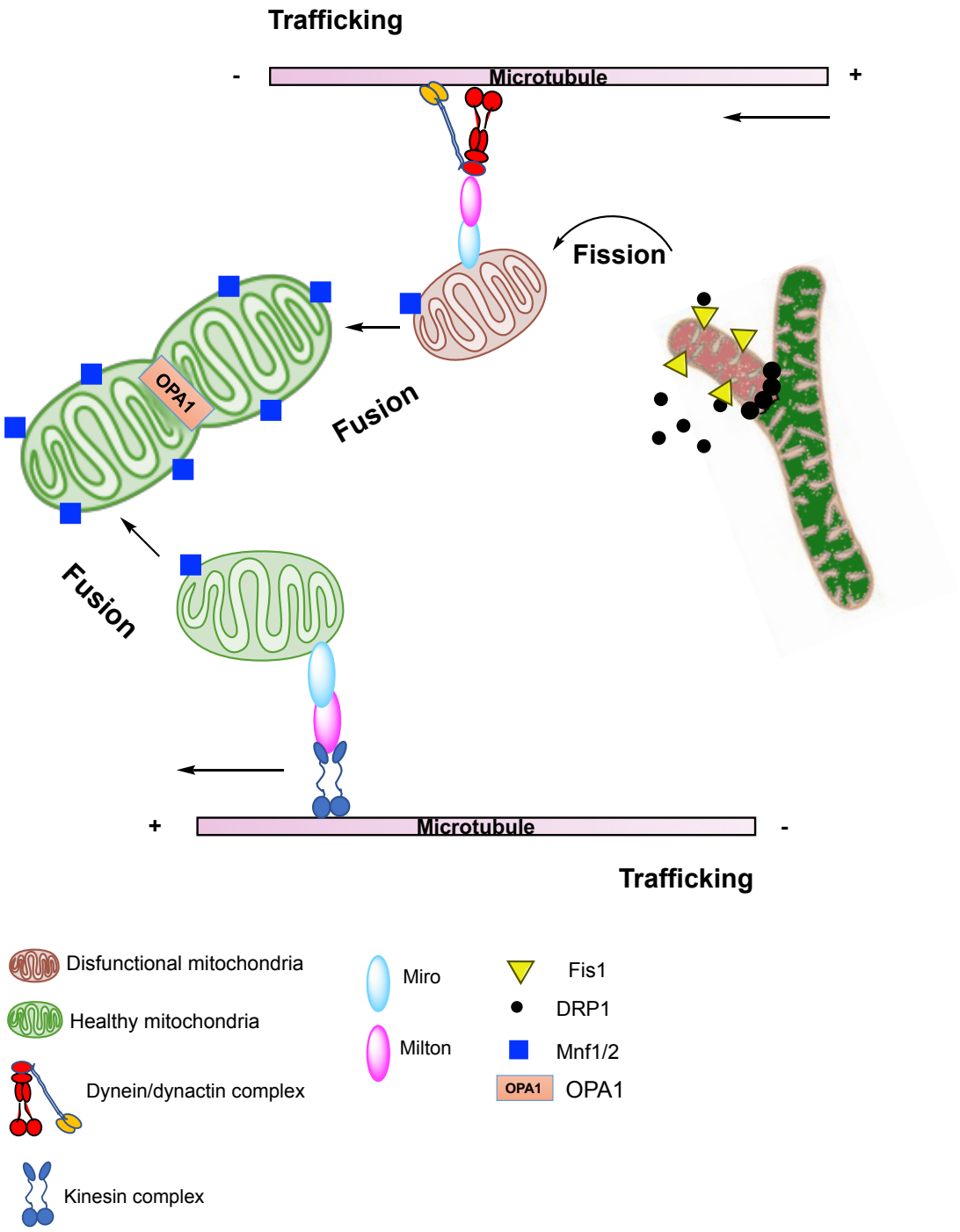

Figure I10. Mitochondrial dynamics.

Mitochondria are highly dynamic organelles that remodel their network in order to maintain their shape, distribution and size. The balance between fission and fusion events modulates mitochondrial morphology depending on the metabolic needs of the cell.

Mitochondrial biogenesis

Extensive mitophagy of dysfunctional mitochondria can suppose a loss of mitochondrial mass resulting in energy disruption of the cell. The lack of energy input would increase mitochondrial damage and eventually it would trigger cell death by apoptosis. Therefore, it is reasonable to hypothesize that mitophagy in the presence of defective mitochondrial function must be accompanied by an increase in mitochondrial biogenesis to preserve cell homeostasis. If mitochondrial elimination is not compensated by mitochondrial biogenesis, mitophagy is no longer protective and becomes detrimental for cell survival. For example, during subacute sepsis in the liver, mitochondrial function is impaired and mitochondria are removed by autophagy. However, clearance of mitochondria is followed by mitochondrial replenishment[162]. Moreover, it has been observed an increase in mitochondrial biogenesis after promoting mitochondrial dysfunction by oxidant injury in renal cells[163].

Mitochondrial biogenesis can be triggered by characteristic signals of mitochondrial dysfunction. When cells contain low levels of ATP, the AMP/ATP ratio increases and AMPK is activated and promotes mitochondrial biogenesis to maintain the overall ATP-generating capacity of cells and avoid cell death. The most important regulator of mitochondrial biogenesis is peroxisome proliferator-activated receptor gamma coactivator 1-alpha (PGC1A)[164]. It has been observed that PGC1A is directly phosphorylated and transactivated by AMPK[165]. PGC1A can also be activated by Sirtuin 1 (SIRT1)-mediated deacetylation, which is also induced by AMPK activation[166]. PGC1A upregulates the activity of transcription factors involved in mitochondrial biogenesis, such as Nuclear respiratory factor 1 (NRF1) and Nuclear factor (erythroid-derived 2)-like 2 (NRF2), which in turn modulate the expression of other factors such as mtTFA, important for the regulation of mtDNA replication and transcription.

Therefore, although mitochondrial biogenesis and mitophagy are opposite processes, they must be highly linked and coordinated to determine the mitochondrial function, structure and homeostasis. In fact, both processes regulate cellular adaptation to mitochondrial dysfunction. Interestingly, AMPK is able to initiate a dual response that promotes mitophagy as well as mitochondrial biogenesis[167]. It is important to highlight that mitochondrial biogenesis in the absence of balanced

mitophagy to remove defective mitochondria may be detrimental, since there would be high ROS generation, accumulation of damaged mitochondria and finally cellular degeneration and death. Therefore, a balanced function of these two processes is essential for cellular adaptation and dysfunction resistance.

Other mitochondrial quality control mechanisms

Recently, other less known mechanisms to perform mitochondrial quality control have been suggested, such as Parkin-independent mitophagic pathways or mitochondrial spheroids formation[155].

It has been observed that mitophagy induction during hypoxia can be mediated by different proteins such us Bcl2/adenovirus E1B 19 kDa protein-interacting protein 3 (BNIP3), NIX and FUNDC1. Both BNIP3 and NIX are hypoxia-inducing factor-1 (HIF1) target genes that contain a LIR domain to interact with LC3, which can promote mitophagy by recruiting autophagosomes to damaged mitochondria and protect against ROS[168]. In fact, depletion of both BNIP3 and NIX inhibits the mitophagic response to hypoxic conditions[169].

Moreover, during hypoxia, FUNDC1 is dephosphorylated, which allows for it to interact with LC3 on autophagosome membranes via its LIR motif[170].

Other mitochondrial E3 ubiquitin ligases play a role in mitophagy induction, such as SMURF1[171] and MUL1[172].

Moreover, it has been observed that peroxidation status of cardiolipin can regulate both apoptosis and mitophagy[173]. After mitochondrial depolarization, cardiolipin translocates to the OMM. If cardiolipin is peroxidized, cell death through apoptosis is initiated, whereas non-peroxidized cardiolipin initiates mitophagy to prevent cell death.

On the other hand, recently a novel mitochondrial quality control mechanism called mitochondrial spheroids has been described[174,175]. Mitochondrial spheroids are mitochondria with a cup-like morphology that can envelop different contents of the cytosol. Formation of mitochondrial spheroids is independent of autophagy pathways but requires the presence of ROS and either MFN1 or MFN2. These structures may allow mitochondrial remodelling in response to different stresses avoiding mitophagy activation.

Mitochondrial diseases

General considerations

Mitochondrial diseases are a group of rare genetic disorders with very heterogeneous origins. The estimated prevalence of these diseases is at least 1 out of 5,000 people, even though it could be much higher[176]. In fact, together they represent the most common cause of inherited metabolic disease. In general, the term "mitochondrial disease" refers to those disorders caused by total or partial dysfunction of the mitochondrial ETC coupled to the OXPHOS system[177]. This alteration leads to an energy deficiency in the cell. Therefore, clinical manifestations of mitochondrial diseases typically involve organs with high energy requirements, such as the neuronal tissue, muscle, heart, kidney and the endocrine system[178]. The age of onset of mitochondrial diseases may range from very early in the neonatal period to very late in adulthood. Some symptoms may be precipitated by environmental factors and the natural course of the illness can be slowly progressive or punctuated with periods of good health[179].

Genes responsible for mitochondrial metabolism (including OXPHOS components) are encoded by both nDNA and mtDNA; therefore, mitochondrial diseases can be caused by mutations in both genomes. This double genetic control of mitochondrial function gives rise to different patterns of inheritance of mitochondrial diseases, and consequently complicates their characterization and diagnosis.

Additionally, it is still difficult to establish the relationship between the molecular pathology of mitochondrial diseases and the variety of phenotypes associated with them, because the phenotype depends on the type of mutation, the patient genetic background and the existence of other mutations, among other features[180].

The nuclear genome encodes over 1,500 proteins that contribute to all aspects of mitochondrial structure and function, including MRC subunits or assembly factors, protein import machinery, intergenomic signalling, mitochondrial motility and dynamics or lipid composition of the IMM. Therefore, there is a great number of nuclear genes associated with mitochondrial diseases[181-183] (**Table I2**).

Function	Genes
MRC subunits	**Complex I**: *NDUFS1-8, NDUFV1-2, NDUFA1-2, NDUFA9-13, NDUFAF2, NDUFAF6, NDUFB11* **Complex II**: *SDHA, SDHB, SDHC, SDHCD, SDHAF1* **Complex III**: *UQCRB*, *BCS1L, UQCRQ*, *UQCRC2*, *CYC1*, *TTC19*, *LYRM7*, *UQCC2, UQCC3* **Complex IV**: *COA5, SURF1, COX10, COX14, COX15, COX20, COX6B1, FASTKD2, SCO1, SCO2, LRPPRC, TACO1, PET100* **Complex V**: *ATPAF2, TMEM70, ATP5E, ATP5A1*
Electron transporters	*PDSS1, PDSS2, COQ2, COQ4, COQ6, COQ8A, COQ8B, COQ9* *ETFDH*
MRC assembly factors	*ACAD9, AIFM1,FOXRED1,NUBPL, HCCS, FAM36A,SCO1-2*
mtDNA replication and maintenance	*APTX, ANT1 ,TWINCLE, POLG1, POLG2, DGUOK, DNA2, MGME1, MPV17, RRM2B, SUCLA2, SUCLG1, TDP1, TK2, TYMP, RNASEH1*, *C10orf2*
mtDNA transcription and translation	*MTO1*, *GTP3BP*, *TRMU*, *PUS1*, *MTFMT*, *TRIT1*, *TRNT1, TRMT5, AARS2*, *DARS2*, *EARS2*, *RARS2*, *YARS2*, *FARS2*, *HARS2*, *LARS2*, *VARS2*, *TARS2*, *IARS2*, *CARS2*, *PARS2*, *NARS2*, *KARS*, *GARS*, *SARS2, MARS2, C12orf65, TUFM*, *TSFM, GFM1, MRPS16*, *MRPS22*, *MRPL3*, *MRP12, MRPL44*, *ELAC2*, *PNPT1*, *HSD17B10*, *MTPAP, PTCD1, SPG7, AFG3L2*
Mitochondrial dynamics	*OPA1, MNF2, MFF, DLP1*
Mitochondrial membrane integrity	*AGK*, *SERAC1, TAZ , CHKB, GDAP1, LP1N1*
Mitochondrial protein transport	*TIMM8A, HSP60*
Mitochondrial metabolism	*HIBCH*, *ECHS1*, *ETHE, SCLC25A3*
Mitochondrial iron metabolism	*ISCU*, *BOLA3*, *NFU1, IBA57, FXN, GLRX5, ABCB7*

Table I2. Main nuclear gene mutations associated with mitochondrial diseases classified by their function.

Mutations in these genes can have autosomal dominant, autosomal recessive or X-linked inheritance patterns. These mutations in the nDNA, which encodes proteins with a role in mtDNA maintenance, manifest with a wide variety of clinical syndromes, such as Mitochondrial NeuroGastroIntestinal Encephalopathy (MNGIE) or Progressive External Ophtalmoplegia (PEO), both caused by mtDNA deletions. Other mitochondrial diseases caused by mutations in nDNA are characterized by mtDNA depletions or MRC defects; for example, Alpers syndrome, Leigh syndrome or Growth Retardation, Aminoaciduria, Cholestasis, Iron overLoad and Early death

(GRACILE). Defects in CoQ synthesis or failures in iron metabolism cause encephalomyopathy and different types of ataxias. Finally, failures in mitochondrial motility and dynamics cause CMT2A or optic atrophy[184].

Sequencing the human mitochondrial genome in 1981 allowed the further identification of numerous pathogenic point mutations in mtDNA, representing a breakthrough in the molecular diagnosis and understanding of multiple mitochondrial diseases[17]. Two types of mutations of mtDNA can be distinguished[179,185,186].
First, point mutations, which can affect 1 of the 13 genes encoding mtDNA proteins, the 2 genes encoding ribosomal RNAs (rRNAs) or the 20 genes encoding tRNAs which globally affect mitochondrial protein synthesis. For example, Mitochondrial myopathy, Encephalopathy, Lactic Acidosis and Stroke-like episodes (MELAS) and Myoclonic Epilepsy with Ragged-Red Fibers (MERRF) syndromes, which are mainly caused by point mutations in genes codifying mt-tRNAs[187,188] or Neuropathy, Ataxia and Retinitis Pigmentosa (NARP) and Leber Hereditary Optic Neuropathy (LHON) syndromes, caused by mutations in genes encoding mtDNA proteins, ATP6 and ND1, respectively[189,190].
Second, some mitochondrial diseases are caused by mtDNA rearrangements: large deletions, insertions or mtDNA duplication. For example, Kearns–Sayre Syndrome (KSS) and Pearson syndrome are mitochondrial diseases caused by a single, large-scale deletion which includes several genes[191,192] **(Table I3).**

In the case of mitochondrial diseases caused by mtDNA mutations, understanding the phenotypes is even more complicated due to the characteristic presence of heteroplasmy (coexistence of WT and mutant mtDNA in the same cell).
Almost 55% of the reported mtDNA mutations involved in mitochondrial diseases have been observed at sites known to be prone to heteroplasmy[193].

In general, it is accepted that the higher the percentage of heteroplasmy is, the more severe the symptomatology of the patient is, but it depends on the patient's background and the disease[53]. Mutational load of the tissues varies, usually being higher in the muscle (the best choice for diagnosis) and buccal mucosa and lower in the blood cells. The mutational load can be also detected in urine sediment and dermal fibroblasts[194]. This uneven distribution of mutant mtDNA leads to a mosaic

respiratory chain deficiency in affected tissues that is an important determinant in disease pathophysiology[195].

Mitochondrial disorder(s)	mtDNA mutation	Affected genes
MELAS	Point mutation	Protein synthesis gene *mt-tRNA(Leu(UUR))* Protein-encoding genes *MT-ND1, MT-ND5*
MERRF	Point mutation	Protein synthesis gene *mt-tRNA(Lys)* Protein-encoding genes *MT-ND1, MT-ND5*
Leigh syndrome	Point mutation	Protein-encoding gene *MT-ND2, MT-ND3, MT-ATP6*
Hypertrophic cardiomyopathy, neuropathy, ATP deficiency	Point mutation	Protein-encoding gene *MT-ATP8*
LHON	Point mutation	Protein-encoding gene *MT-ND1, MTND4, MTND4L, MT-ND6, MT-CYTB*
NARP, MILS (if homoplasmic)	Point mutation	Protein-encoding gene *MT-ATP6*
Mitochondrial myopathy	Point mutation	Protein synthesis genes *mt-tRNA(Ala), mt-tRNA(Asn), mt-tRNA(Leu(CUN)), mt-tRNA(Phe), mt-tRNA(Tyr), mt-tRNA(Ser(AGY)), mt-tRNA(Ser(UCN))* Protein-encoding genes *MT-CYTB* *MT-CO1, MT-CO2, MT-CO3*
PEO, Kean-Sayre syndrome, Pearson syndrome	mtDNA rearrangement (deletion/ depletion)	Protein synthesis genes
Diabetes and deafness	mtDNA rearrangement (deletion)	Protein synthesis genes

Table I3. Main mitochondrial disorders associated with mutations in mtDNA.

Mutational load increases with age in most tissues. However, in lymphocytes mutational load decreases with age, which is due to a selection of positive clones that have more WT mtDNA. This fact explains why there is no correlation between the degree of heteroplasmy detected in blood and the clinical symptoms of the patient[196].

Disease phenotypes are only observed once the proportion of WT mtDNA drops below a threshold level associated with high accumulations of heteroplasmic mutations: this phenomenon is called mitochondrial threshold effect[50]. Generally, a

critical threshold level above 60-80% of heteroplasmy is required to trigger the OXPHOS defects in specific tissues, but it depends on each mutation, organ or patient[51]. Tissues and organs with high energetic demand such as neurons, renal and endocrine systems and muscle (including heart) are more vulnerable to low proportions of heteroplasmic mutations[52]. Differences in the levels of heteroplasmy and the precise thresholds are thought to contribute to the characteristic patterns of organ vulnerability observed in different mitochondrial diseases and the clinical heterogeneity observed in patients harbouring the same mtDNA mutation[197].
Therefore, increasing the proportion of WT mtDNA in affected tissues is seen as a viable therapeutic strategy for the treatment of diseases caused by mtDNA mutations.

Clinical features of mitochondrial diseases are very complex due to the wide range of tissues affected and the variety of phenotypes involved, depending on the mutational load, patient's background and the existence of other mutations. The most common features in mitochondrial diseases involve several clinical areas: neurological symptoms (migraine, epilepsy, dementia, ataxia, dysphagia, etc.), cardiomyopathy (heart muscle weakness), respiratory problems (hypoventilation, apnea, pneumonia), diabetes, ophtalmoplegia and optic atrophy, muscular problems (ptosis, dystonia, myopathy) and, less commonly, renal tubular defects and hepatic failures[198] **(Figure I11).**

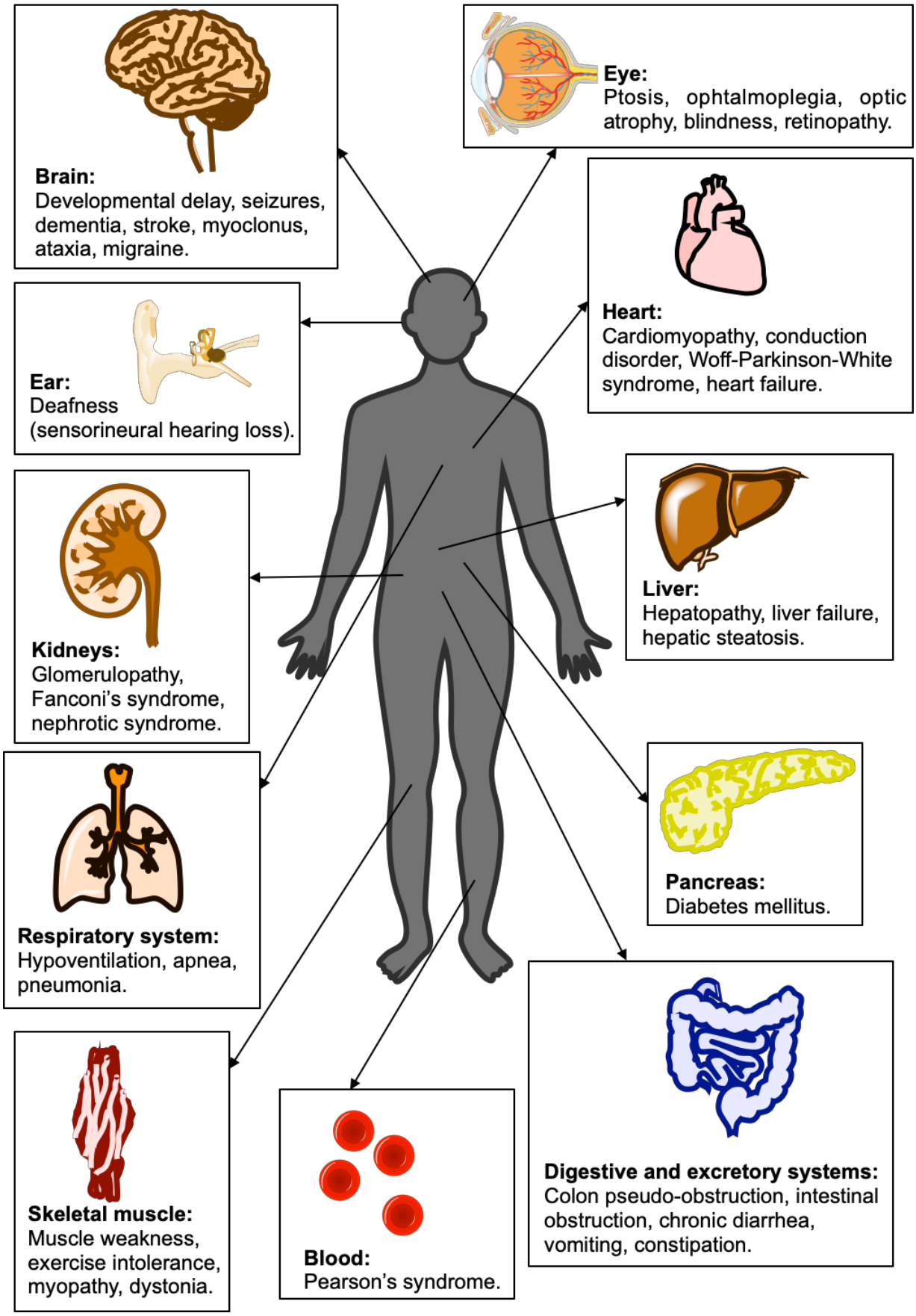

Figure I11. Common clinical features of mitochondrial diseases.

Pathophysiological features of mitochondrial diseases

Due to the heterogeneous origin of mitochondrial diseases, the understanding of their pathogenic mechanisms is still very limited. ATP shortage and ROS excess are the main pathogenic factors that cause most of clinical manifestations of mitochondrial diseases[199,200]. In most of the cases, ATP shortage is due to a dysfunction in the OXPHOS system. Due to the reduction of ATP synthesis capacity, cells with mitochondrial dysfunction show a chronic stage of energy insufficiency which finally induces a disruption of cell homeostasis.

Other specific molecular features of mitochondrial diseases are:

i. Decrease in the activity of the complexes of the OXPHOS system.

ii. Increase in glycolytic pathways, anaerobic metabolism of glucose.

iii. Increase in lactate production.

iv. Lower respiratory capacity per mitochondrion.

v. Lower $\Delta\Psi m$.

vi. Increase in cytosolic calcium levels.

vii. Increase in ROS production.

viii. Premature aging.

ix. Decrease in CoQ levels.

x. Reduction of insulin secretion.

xi. Increase of apoptosis levels.

Besides these characteristics, it has been demonstrated that several cellular models of mitochondrial diseases show high levels of bulk autophagy and/or mitophagy. These processes are gaining importance nowadays due to their regulation could be a promising therapeutic target for mitochondrial dysfunctions. There is not a common agreement about the presence of autophagy/mitophagy activation and/or disruption in mitochondrial diseases, and different authors show diverse hypothesis about the importance and role of both processes.

Autophagy and mitophagy in mitochondrial diseases

In the recent years, increased or imbalanced autophagy has been reported in several cellular and murine models of mitochondrial diseases. Autophagy could be induced as a compensatory mechanism to obtain energy or to eliminate damaged

organelles whose accumulation could exacerbate the mitochondrial dysfunction. Thus, in a mouse model of mitochondrial myopathy due to a mutation in the mitochondrial helicase TWINKLE, an increased recycling of mitochondria through autophagy in muscle fibers has been observed[201]. Furthermore, an increase of autophagy has also been observed in muscle biopsies of patients harbouring the m.8344A>G mutation, the most common mutation that causes MERRF syndrome[202]. Recently, the role of bulk autophagy in fibroblast models of mitochondrial dysfunctions due to deficiencies in OXPHOS system has been described[203]. The authors found an accumulation of autophagosomes and lysosomes in the cells, but a selective process of mitochondria degradation could not be detected. The increase of autophagic markers in these models of mitochondrial diseases can be due to an impairment of the autophagy flux, which causes an accumulation of autophagosomes. This blockade of lysosome flux can be caused by a depletion of ATP levels, a characteristic of mitochondrial dysfunction, because ATP is necessary to maintain lysosome function and seclude the cytosolic components[203,204].

Although there is no longer doubt about the importance of autophagy in mitochondrial diseases, there is not a common consensus about if autophagy has a protective or pathological role during the course of these diseases.

The protective role of autophagy has been confirmed in multiple cellular types and situations by a large number of studies. Among others, it has been observed that autophagy activation has a neuroprotective role during brain damage[205] and improves resistance under hyperoxia situations and oxidative stress in the lung endothelium[206]. In fact, protection of autophagy has been suggested to be a possible future therapy for brain disorders like schizophrenia[207]. However, autophagy has been demonstrated to be harmful in different situations such as establishment and progression of tumors[208] or progression of pathogenesis of different lung diseases[209]. Moreover, a recent study shows a protective effect of inhibition of autophagy on MRC disruption by an mTOR-independent mechanism[210]. Recently, the protective role of autophagy in diseases with mitochondrial dysfunction like osteoarthritis has been suggested. Autophagy protects chondrocytes with mitochondrial dysfunction from oxidative stress; therefore, regulation of autophagy could be a promising therapeutic target for age-related skeletal disorders[211]. In the same way, deficient or disrupted autophagy is characteristic of other diseases that present mitochondrial

dysfunction, mostly neurodegenerative disorders, since deficient elimination of toxic aggregates in neurons and other cell types promotes cellular stress and death. Dysregulation of autophagy is a contributing factor of chronic, disabling diseases like Alzheimer's disease (AD), Parkinson's disease (PD), Huntington's disease (HD), and amyotrophic lateral sclerosis (ALS)[212].

In the same way, mitophagy seems to exert a protective role on cell homeostasis in many situations. For example, mitophagy is considered to be an adaptive metabolism to prevent oxidative damage and hypoxia[168].

Selective degradation of mitochondria by autophagy can be considered as a defense mechanism to face stress situations caused by mitochondria alterations. Thus, it has been demonstrated that mitophagy is activated during sepsis and the activity of Parkin is implicated in cardiac recovery[213]. In neurodegenerative diseases like AD, an alteration in mitochondrial function has been suggested. Some mitochondrial dysfunctions have been found in the preliminary stages of AD, such as an imbalance in the oxidative status, bioenergetics deficit, decrease in cytochrome oxidase (COX) activity, and an increase in oxidative damage that occurs prior to senile plaque formation[214-216]. Currently, the role of mitochondrial fission/fusion and mitophagy in AD is gaining importance. Although there is evidence of mitophagy in AD[217], it is not clear if a correct degradation of sequestered mitochondria is being performed or if all the degraded mitochondria are damaged. In addition, it has been suggested that mitochondrial fission is upregulated in AD, probably in an attempt to segregate damaged mitochondria in order to facilitate degradation by mitophagy. However, if mitophagy is efficient or not has to be clarified[218].

In the case of mitochondrial diseases, an augmented mitophagic response in cellular models of MELAS and MERRF syndromes has been observed. In both disorders, cells show low membrane potential, high level of ROS and CoQ deficiency. In fact, CoQ supplementation restored mitochondrial morphology, membrane potential and levels of ROS, as well as mitophagy levels[204,219-221].

However, in the specific case of mitochondrial diseases, there is not a common agreement about the failure of mitophagy regulation. Since the expression levels of PINK1 and/or Parkin in the cell are critical for mitophagy, some authors propose that cells with mutant mtDNA have decreased levels of PINK1 and/or Parkin, possibly due to unknown transcriptional inhibition mechanisms. In fact, it has been observed

that cybrids cells with mtDNA mutation (A3243G) have less Parkin expression levels than WT cybrids cells, and this fact may impair mitophagy of dysfunctional mitochondria[222]. In light of these data, some authors have hypothesized that mitochondrial dysfunction *per se* is not sufficient to recruit mitophagic factors to damaged mitochondria and to activate mitophagy. Although high levels of ROS and/or low ΔΨm are necessary to promote mitophagy, Parkin expression levels may be critical to allow the degradation of dysfunctional mitochondria. Likewise, the presence of the non-selective autophagy machinery would be necessary for the progression of mitophagy[223].

Therapies for mitochondrial diseases

Treatments for mitochondrial diseases in general are largely inadequate[224]. Nowadays, there is only supportive therapy for mitochondrial diseases and its effectiveness is not total for most of them.

Among the challenges for finding a successful mitochondrial disorder treatment are the lack of large groups of similar patients and the heterogeneity of the symptoms. The partial accessibility of bioactive molecules to mitochondria is also a difficulty that needs to be overcome[225].

Due to the intrinsic difficulties in the design of clinical trials for rare diseases, few randomized double-blinded placebo-controlled trials for mitochondrial diseases have been completed[226,227].

However, in the last decade, due to advances in defining the pathophysiology of these diseases, new therapies are being developed in the laboratory and are entering human clinical trials[228].

We can divide the therapies for mitochondrial diseases in different groups:

1. Clinical therapies

- Pharmacological and dietary supplement therapies

Multiple vitamins and cofactors are used in patients with mitochondrial diseases, although currently, only a few compounds seem to be effective. The effects of these compounds are thought to be: 1) increase MRC flux, 2) counteract the effects of

oxidative stress caused by ROS (antioxidants), 3) act as cofactors, 4) act as mitochondrial substrates (e.g. l-carnitine).

In practice, the majority of patients take a cocktail of at least four dietary supplements.

Most of current therapies are a combination of creatine, CoQ (in its reduced form, ubiquinol) and alpha-lipoic acid[229]. Antioxidants such as riboflavin, thiamine and vitamins C and E or analogues with water-solubility (trolox ornithylamide hydrochloride) are also used to counteract the effects of oxidative stress caused by ROS[230,231].

- CoQ

CoQ is the most common utilized treatment for mitochondrial diseases therapy, since it has demonstrated to be effective in different *in vitro* and *in vivo* models of mitochondrial dysfunctions and no serious side effects have been reported from the treatment with CoQ, even with high dosage.

CoQ molecule was characterized for the first time by Festenstein and Crane in the second half of the XX century[232,233]. Its structure was determined by Folkers and collaborators in 1958[234].

CoQ is described as a lipophilic molecule composed by a benzoquinone ring conjugated in the third position to a carbon isoprenoid side chain. The number of isoprenoid units of the carbon chain determines the type of coenzyme Q. The predominant form of coenzyme Q in humans is coenzyme $Q_{10,}$ which contains 10 isoprenoid units in the tail[235].

Functionally, CoQ is an essential component of the MRC and thus in the generation of ATP. Moreover, ubiquinol (reduced CoQ), works as a ROS scavenger, being able to repeatedly suffer reduction and oxidation[236]. Therefore, it is an excellent membrane antioxidant that can be found in many cell organelles and compartments such as lysosomes, Golgi apparatus or plasma membrane[237]. In addition, CoQ exerts its antioxidant function by re-establishing the antioxidant properties of other molecules such as vitamin E and ascorbate[238].

Moreover, CoQ has other different functions in the cell metabolism such as apoptosis inhibition[239,240], regulation of the MPT[241], stimulation of cell growth[242,243] and regulation of inflammatory response[244,245].

CoQ also regulates the expression of genes involved in metabolism, autophagy and mitophagy[204,219-221], as well as cellular signalling and transport.
Although CoQ is synthesized *de novo* by the cell[246], its dietary supplementation can provide health benefits in a great variety of disorders that undergo mitochondrial dysfunction. However, only CoQ supplements with more water-soluble formulations, such as idebenone, are able to act on mitochondria and other cellular compartments and cross the blood-brain barrier. Therefore, CoQ analogues with increased water-solubility, similar effect and better bioavailability are being investigated[237].

Physiological levels of CoQ are altered in different disorders such as cardiovascular[247] and neurodegenerative diseases[248] and some mitochondrial dysfunctions[236], mainly primary and secondary CoQ deficiencies[224,249]. Moreover, CoQ levels diminish with age, and this decline might contribute in part to some of the manifestations of aging[250,251].
CoQ supplementation has had different effects in patients with mitochondrial dysfunctions. In patients with primary CoQ deficiencies causing encephalomyopathy, muscle symptoms improved after CoQ therapy[252]. Moreover, in patients showing myopathy caused by primary CoQ deficiency, CoQ supplementation improved clinical symptoms with a synergistic effect in conjunction with riboflavin[253].
The CoQ treatment of secondary deficiencies of CoQ (resulted from mutations in genes not involved in CoQ synthesis) has shown benefits in cellular models of mitochondrial diseases such as MELAS or MERRF syndromes[204,219-221,254].
Moreover, oral administration of CoQ to patients with mitochondrial dysfunctions has shown improvements in exercise intolerance, muscle weakness, neurological function, lactate levels, ataxia and stroke-like episodes[255-260].
The CoQ analogue idebenone has demonstrated benefits in a subgroup of patients with LHON and in some cases of MELAS[261].
In spite of all the research carried out, the clinical evidence supporting the beneficial effects of CoQ treatment in mitochondrial diseases is scarce, probably due to the heterogeneity of mitochondrial diseases included in clinical trials.

- Exercise therapies

Endurance training has been proven to be beneficial in some patients with mitochondrial diseases[262-264]. Aerobic exercise training has demonstrated some

improvements in exercise capacity and quality of life in patients with mtDNA mutations, since mitochondrial biogenesis and activities of mitochondrial enzymes are stimulated.

2. Pre-clinical (emerging) therapies

There are some potential treatments under study which target different molecular features of mitochondrial diseases.

These new approaches can be divided in “disease-tailored” strategies, designed to act on characteristics of specific mitochondrial diseases, and “non-tailored” strategies, acting on common pathways relevant to different mitochondrial diseases[265].

2.1. Disease-tailored therapies

- Scavenging of specific toxic compounds

Mitochondrial diseases are often characterized by accumulation of different toxic substances. For example, patients with ethylmalonic encephalopathy (EE) accumulate high levels of hydrogen sulphide (H_2S), which provokes COX activity inhibition. Treatments such as N-acetylcysteine (NAC) are able to buffer H_2S in a mouse model of EE, although this treatment has not been tested in clinical trials yet[266]. Other possible strategy may be removing the toxins by hemodialysis, although it has not been effective yet[267].

- Deoxynucleotide bypass therapies

Some mitochondrial diseases caused by mtDNA depletions or mutations in enzymes involved in mitochondrial deoxynucleotide triphosphate (dNTP) metabolism show dNTP pool unbalance with a consequent mtDNA instability.

Supplementation with deoxyribonucleotides and deoxyribonucleosides has been shown to ameliorate mtDNA instability *in vitro*[268] and *in vivo*[269].

- Cell replacement therapies

*Enzyme replacement therapies

MNGIE syndrome is the first mitochondrial disorder treated by this approach, using erythrocyte-encapsulated thymidine phosphorylase to revert the loss-of-function

mutation of *TYMP*, which encodes thymidine phosphorylase. The first preliminary results of the therapy in a patient are promising[270].

*Allogenic hematopoietic stem cell transplantation (AHSCT)

Thymidine phosphorylase activity has been restored by performing AHSCT in patients with MNGIE syndrome. However, the immunosuppression treatment required after the transplantation can damage the mitochondria[271].

*Organ transplantation

Recently, liver transplantation in a patient with EE has been able to replace the deficient persulfide dioxygenase enzyme and ameliorate the symptoms of the disease[272].

- Gene therapy approaches

*Tissue-specific adeno-associated virus (AAV)-mediated gene therapy

AAV-mediated gene therapy has been performed in different mouse models of mitochondrial diseases. For example, AAV vector targeted to retina was used to express AIF1 in the eye of the Harlequin mouse and restore complex I deficiency[273]. Moreover, AAV vectors have been used to deliver mitochondrial proteins by using a viral capsid protein which can be fused with a mitochondrial targeting sequence (MTS). AAV vectors carrying the *MT-ND4* gene targeted to mitochondria were used to express ND4 in cells with the G11778A mutation (LHON syndrome) and restoration of defective ATP synthesis was observed[274].

In patients with LHON, AAV-mediated gene therapy has demonstrated to be safe and ameliorate visual acuity[275].

*Clustered Regularly Interspaced Short Palindromic Repeats (CRISPR)/Cas9 system based gene therapy

Using the CRISPR/Cas9 system approach in induced pluripotent stem cells (iPSCs), mitochondrial dysfunctions due to *COQ4* gene mutation have been rescued[276].

- Heteroplasmy shiftment

Since the percentage of heteroplasmy is directly proportional to the severity of mitochondrial diseases[53], the modulation of heteroplasmy could be a promising

therapeutic strategy. Nowadays, several heteroplasmy removal/reduction strategies have been proposed[277].

*Pharmacological approach

An important role of mitophagy in mitochondrial diseases caused by mtDNA mutations could be its capability to modulate the percentage of heteroplasmy. Stimulating mitophagy seems to be a possible strategy to decrease the level of heteroplasmy, because only defective mitochondria, with high percentage of heteroplasmy, will be eliminated and healthy mitochondria will proliferate.

This strategy has been examined by using the autophagy activator rapamycin.

Lengthy treatment with rapamycin in a culture of cybrids harbouring the heteroplasmic mitochondrial mutation m.11778G>A, the most common in patients with LHON, has demonstrated to decrease the mutational load from 71% to 13% after 20 weeks of treatment[278].

*Protein overexpression or silencing

Overexpression of Parkin in cybrids with 80% of mutated mtDNA (*COX-I* mutation) led to an increase in mitophagy, which allowed a reduction of the mutational load up to 26.7%. Importantly, the reduction of heteroplasmy load remained over time[279]. Moreover, COX activity was restored in cybrid cells enriched for WT mtDNA, indicating that decrease of heteroplasmy could improve the pathophysiology of the disease. Therefore, upregulation of Parkin expression may be beneficial for mitochondrial diseases.

The importance of Parkin in heteroplasmy regulation has been recently examined in an *in vivo* model of mitochondrial dysfunction. Thus, in a strain of *Caenorhabditis elegans* carrying a heteroplasmic mtDNA truncation, it has been demonstrated that mutations in *pdr-1* (*PARK2* orthologue) caused an increase in the ratio mutant/WT mtDNA (up to 2.2-fold)[280]. These results showed the first evidence of Parkin involvement in heteroplasmy modulation *in vivo*.

Furthermore, targeting mitochondrial dynamics can be another strategy to modulate heteroplasmy. Thus, it has been suggested that mitochondrial fission prevents the increase of heteroplasmy in cellular models of mitochondrial diseases. In fact, it has been observed that the knockdown of DRP1 causes an increase of the percentage of heteroplasmy from 80% to 96% of m.3243A>G in a human cell culture of rhabdomyosarcoma[281].

*Mitochondrial genome editing

All of the genetic approaches are based on the elimination of mutant mtDNA and the reduction of the levels of the mutant copies below the threshold levels[282].

1. Mitochondrial-targeted endonucleases:

If the mutation of the mtDNA is located in a recognition site of a restriction enzyme (RE), the development of mitochondrial-targeted endonucleases by modifying bacterial REs could be a possible therapeutic strategy[283].

In human cells, a recombinant mitochondrial-targeted SmaI was used to reduce the heteroplasmy load of the m.8993T>C mutation (related to Leigh and NARP syndromes) in a cybrid cell line[284].

Although mitochondrial-targeted endonucleases have been reported to change mtDNA heteroplasmy, their clinical application is limited due to the fact that only a few mtDNA mutations create restriction sites. To solve this limitation, there are nucleases which can recognize multiple sequences: transcription activator-like effector nucleases (TALENs) and zinc-finger endonucleases (ZFNs).

2. Mitochondrial TALENs (mitoTALENs):

TALENs are engineered restriction enzymes made by fusing a TAL effector DNA-binding domain to a DNA-cleavage domain.

MitoTALENs are TALENs designed to exclusively target mitochondria and work as endonucleases producing a double-strand break point in the sequence followed by a quick degradation. MitoTALENs have been used to induce heteroplasmy shiftment in different cybrid cells models of mitochondrial diseases such as MERRF, MELAS or Leigh syndromes, ameliorating also the OXPHOS function[285].

MitoTALENs have also been effective in reducing heteroplasmy levels in mammalian oocytes[286]. This approach to induce heteroplasmy shiftment in the germline might be an effective alternative to mitochondrial replacement techniques to prevent the maternal transmission of mitochondrial diseases caused by mtDNA defects.

3. ZFNs:

ZFNs are artificial restriction enzymes generated by fusing a zinc finger DNA-binding domain to a DNA-cleavage domain. ZFNs are DNA-binding proteins adapted to operate in the nucleus, even in the absence of nuclear localization signals[287]. Designed ZFNs which manipulate mtDNA incorporate mitochondrial localization signals and nuclear export sequences[288].

ZFNs technology has been used to target pathogenic mtDNA mutations in cybrid cell lines, such as those harbouring the mutation mt.8993T>G (NARP)[289].

4. CRISPR/Cas9 system:

The CRISPR/Cas9 system has been broadly used for nDNA editing to generate specific mutations or correct pathogenic alleles[290]. Recently, its functional application for mitochondrial genome editing has been demonstrated by attaching MTS to Cas9 protein and using mtDNA specific single guide RNAs (sgRNAs)[291].

- Stabilization of mutant mt-tRNA

Most of mtDNA mutations are located in mt-tRNA genes. Therefore, overexpressing aminoacyl mt-tRNA synthetases (mt-aaRSs) or their fragments can be a novel therapeutic approach for the treatment of these diseases. In fact, there are some studies that confirm that the overexpression of mt-aaRSs stabilizes mt-tRNAs and attenuates the detrimental effect of the mtDNA mutations located in tRNA genes in human cellular models of MELAS[292,293].

2.2 Non-tailored therapies

- Activation of mitochondrial biogenesis

Most of the new strategies for the treatment of mitochondrial diseases mainly promote mitochondrial biogenesis with the intention of increasing mitochondrial function by having a greater mitochondrial mass[227], thus ameliorating the phenotype. For example, it has been observed that an increased mitochondrial content in LHON patients' cells decreases the pathogenic effects of the mtDNA mutation[294].

Increasing mitochondrial biogenesis is driven by the activation of PCG1A. Just as mentioned before, PCG1A activation can be targeted by AMPK, SIRT1 or peroxisome proliferative-activated receptors (PPARs), whose functions result in increased transcription of nDNA-encoded mitochondrial genes and therefore increased mitochondrial biogenesis[295].

Currently, PGC1A stimulators such as benzafibrate (PPAR agonist), epicatechin and RTA 408 (isoprenoid that activates NRF2) are under clinical study to assess their effectivity in patients with different mitochondrial diseases[295].

Other compounds such as resveratrol (SIRT1 activator) and the AMP analogue 5-aminoimidazole-4-carboxamide 1-β-D-ribofuranoside (AICAR) have demonstrated to

possess potential therapeutic utility in mitochondrial diseases, although they have not been tried in patients yet[296,297].

However, controversy exists regarding whether increasing biogenesis of dysfunctional, as well as healthy mitochondria will ultimately be beneficial or harmful.

- Bypassing OXPHOS defects

The use of enzymes derived from yeast or low eukaryotes to bypass MRC defects has been tested in *in vitro* and *in vivo* models[228]. For example, the alternative oxidase (AOX) is present in lower eukaryotes and bypasses complex III and IV by accepting electrons from CoQ. Expression of these enzymes has been used to bypass complex I and complex III-IV deficiencies in human cells[298], but not in patients.

- Mitochondrial genome replacement therapy

The prevention of pathogenic mtDNA transfer is a novel method to avoid maternal transmission of mtDNA mutations. Using mitochondrial donation techniques such as maternal spindle transfer and pronuclear transfer, mutant mtDNA in the oocyte or fertilized embryo is substituted with normal copies of the mitochondrial genome[299]. The procedure involves removing the mtDNA from an oocyte or zygote containing mutated mtDNA and transferring its nuclear content to an enucleated oocyte or zygote that contains WT mtDNA from a healthy donor. In 2017, the first human birth after using mitochondrial genome replacement therapy to reduce transmission of the m.8993T>G mutation causing Leigh syndrome was published[300].

- Hypoxia

Another interesting therapeutic strategy for the treatment of mitochondrial diseases is the activation of the hypoxic response pathway[301]. In a recent study, the von Hippel Lindau (VHL) factor (a key regulator of the hypoxia response pathway) was identified as the most effective genetic suppressor of mitochondrial diseases.

VHL negatively regulates the HIFs, whose transcriptional response shifts cellular bioenergetic reliance on mitochondrial OXPHOS. Studies using zebrafish and mouse models of mitochondrial dysfunctions support this new therapeutic approach[301].

- Regulating autophagy/mitophagy and mitochondrial dynamics

Autophagy and mitophagy modulation has been proposed as a possible therapy for numerous different diseases which present mitochondrial dysfunctions (**Table I4**).

Autophagy/mitophagy as targets for different diseases		
Disease	**Characteristics**	**Potential treatments**
Neurodegenerative diseases (e.g. PD, AD, HD)[212]	Failed elimination of damaged mitochondria. Extensive accumulation of autophagosomes. Defects in mitochondrial dynamics.	Autophagy inducers[302]
Cancer	Autophagy is essential for tumor suppression in pre-malignant stages. Autophagy promotes the pathogenesis of established malignancies.	Autophagy inducers: Temsirolimus, rapamycin[303]. Autophagy inhibitors: chloroquine, hydroxychloroquine.
Mitochondrial diseases	Autophagy/mitophagy imbalance.	Autophagy/mitophagy inducers[296,304]
Chronic inflammation diseases (e.g. Chron disease)[305]	Defects of autophagy have been associated with higher production of proinflammatory cytokines implicated in pathogenesis of inflammation diseases.	Autophagy inducers
Lung diseases[209]	Protective or harmful role of autophagy depending on the type of lung disease	Autophagy inducers Autophagy inhibitors
Diabetes type 2[306]	Autophagy deficiency in β-cells could help to the progression from obesity to diabetes	Autophagy inducers (metformin)
Liver diseases[307]	Autophagy has a protective role (eliminating lipid droplets and protein aggregates), except for hepatitis B and C infections (virus promote their replication by autophagy)	Autophagy inducers Autophagy inhibitors

Table I4. Autophagy and mitophagy as therapeutic targets for different diseases. Adapted from Villanueva-Paz et al. (2016)[89].

Various autophagy inducers such as rapamycin, rapalogs (rapamycin derivatives), metformin[278,308] and trehalose and autophagy inhibitors (chloroquine, hydroxychloroquine) are already approved for the treatment of various diseases.

Moreover, the nicotinamide adenine dinucleotide pathway, with nicotinamide mononucleotide and riboside[309], has been explored as a potential option for future therapies.

Because the accumulation of defective mitochondria seems to be the main cause of the worsening of mitochondrial diseases, autophagy and mitophagy are gaining importance as future therapeutic targets for these disorders. The most studied strategies to pursue this approach are targeting two different autophagy regulation pathways: AMPK and mTOR pathways.

AMPK pathway

AMPK is gaining attention as a potential therapeutic target for mitochondrial diseases in the future, because it has many functions related to maintain the mitochondrial and cellular homeostasis.

As we have mentioned before, AMPK functions as an initiator of autophagy *via* mTOR complex inhibition and ULK1 activation. It also participates in the transcriptional control of lipogenesis and mitochondrial proliferation and regulates other metabolic processes such as glycolysis, lipolysis or fatty acid oxidation.

AMPK can be activated by Food and Drug Administration (FDA)-approved drugs, including AICAR or the anti-diabetic biguanide metformin and several natural products[310].

Although autophagy is a general process in the cell, some authors suggest that activation of autophagy is necessary for mitophagy progression[222]. Therefore, induction of autophagy by activated AMPK and the recruitment of Parkin to defective mitochondria contribute to the induction of mitophagy in mammalian cells. In fact, it has been demonstrated that cells with AMPK deficiency exhibit defective mitophagy[93]. Therefore, increasing the activity of AMPK could ameliorate the symptoms of mitochondrial diseases that course with dysfunctional mitophagy. Thus, it has been recently proved that AICAR partially corrects the mitochondrial dysfunction in a mouse model of COX deficiency[311].

Moreover, besides its importance in autophagy regulation, AMPK activation is also crucial for the metabolic switch from respiration to glycolysis caused by mitochondrial dysfunction[73], and activation of AMPK pathway could contribute to the adaptation of mitochondrial diseased cells to oxidative stress.

mTOR machinery

The use of pro-autophagic agents as a therapy for different diseases is increasing in the recent years. Among these compounds, rapamycin and its derivatives are the most studied as therapeutic agents for the treatment of tumors[303] and neurodegenerative diseases such as HD[302].

Rapamycin exerts its pro-autophagic effect by competitive inhibition of mTOR complex by affecting mTORC1.

Recently, the beneficial effect of rapamycin treatment in mitochondrial diseases and other pathologies that undergo mitochondrial dysfunctions has been demonstrated. For example, it has been observed that treatment with rapamycin after cerebral ischemia promotes a reduced infarct volume, improves neurological outcomes and inhibits mitochondrial dysfunction in experimental animals. The beneficial effects of rapamycin are due to an increase in mitophagy[312]. In addition, promotion of mitophagy by rapamycin has demonstrated to be protective against the effects of rotenone, a complex I inhibitor which causes mitochondrial dysfunction[313]. Using human chondrocytes treated with oligomycin to induce mitochondrial dysfunction, it has been proven that autophagy induction by rapamycin treatment protects chondrocytes from oxidative stress[211]. Therefore, regulation of autophagy could be a promising therapeutic target for aging-related musculoskeletal disorders too, because mitochondrial dysfunction has an important role in these diseases. Rapamycin benefits have been also demonstrated in *in vivo* models of mitochondrial diseases. Rapamycin treatment has been shown to improve survival and attenuate the progression of the disease in a mammalian model of Leigh syndrome, the *NDUFS4* knockout (*NDUFS4−/−*) mouse[314]. Improved motor function was observed, as well as a decrease in brain inflammation and prevention of the brain lesions characteristic of Leigh syndrome.

Manipulating mitochondrial dynamics is potentially an attractive approach to treat mitochondrial diseases, because shifting the equilibrium of fission and fusion may allow damaged mitochondria to be rescued by mitochondrial fusion or else be selectively eliminated by mitophagy.

Genetic approaches have shown that inhibiting mitochondrial fusion shifts the fusion/fission equilibrium towards fission[154] and vice versa[315]. Thus, adding a pharmacological agent that inhibits fission to cells containing fragmented

mitochondria should increase the proportion of tubular mitochondria. In fact, a compound termed mitochondrial division inhibitor 1 (mdivi-1), a DRP1 inhibitor, selectively inhibits mitochondrial division[316]. More recently, mdivi-1 has been demonstrated to rescue mitochondrial morphological and functional defects induced by mutations in PINK1[317].

MERRF syndrome

MERRF syndrome is a rare, maternally inherited, multisystemic mitochondrial disease[318], that is defined as a mitochondrial encephalomyopathy characterized by myoclonic seizures. MERRF syndrome was described for the first time in 1980 by Fukuhara et al. after the study of the symptoms and pathology of two patients with dyssynergia cerebellaris myoclonica and mitochondrial myopathy. Muscle biopsies of these patients revealed ragged-red fibers[319]. MERRF is estimated to affect about 1 in 5,000 people worldwide[320].

Two important medical landmarks are ascribed to MERRF syndrome. MERRF was the first human disease in which a maternal inheritance pattern was clearly demonstrated, suggesting a defect in mtDNA. MERRF was also the first disorder in which a molecular defect was associated with a particular form of epilepsy[321].

Genetics

There are at least 18 mutations responsible for MERRF syndrome[321], majority of them affecting mt-tRNA genes, although mutations in *MTND5* gene or *POLG* gene are also described[318] (**Table I5**). However, 80% of MERRF patients possess an adenine to guanine transition in the 8344 position in the $tRNA^{Lys}$ gene of mtDNA (*MT-TK* gene)[187,322], with a frequency of between 0 and 1.5: 100,000 in populations from Western Europe[323]. The m.8344A>G mutation is localized in the T-arm of the mt-tRNA[324] and causes low aminoacylation of the mutant mt-tRNA, incomplete translation at some lysine codons[325] and hypomodification of its anticodon wobble-position due to the lack of the taurine-containing modified uridine τm^5s^2U[326]. This fact hinders the translation of both AAA and AAG codons (**Figure I12**), resulting in marked defects in the whole mitochondrial proteins synthesis and dysfunction of the MRC[327].

Mutation	Affected gene
mtDNA mutation	
m.8344A>G[187,322]	*MT-TK* (mt-tRNALys)
m.8356T>C[328]	*MT-TK* (mt-tRNALys)
m.8361G>A[329]	*MT-TK* (mt-tRNALys)
m.8363G>A[330]	*MT-TK* (mt-tRNALys)
m.611G>A[331]	*MT-TF* (mt-tRNAPhe)
m.3243A>G[332]	*MT-TL1* (mt-tRNALeu(UUR))
m.3255G>A[333]	*MT-TL1* (mt-tRNALeu(UUR))
m.3291T>C[334]	*MT-TL1* (mt-tRNALeu(UUR))
m.4279A>G[335]	*MT-TI* (mt-tRNAIle)
m.4284G>A[336]	*MT-TI* (mt-tRNAIle)
m.15923A>G[337,338]	*MT-TP* (mt-tRNAPro)
m.15967G>A[339]	*MT-TP* (mt-tRNAPro)
m.5521G>A[340]	*MT-TW* (mt-tRNATrp)
m.7512T>C[341]	*MT-TS1* (mt-tRNASer(UCN))
m.12147G>A[342]	*MT-TH* (mt-tRNAHis)
m.12300G>A[343]	*MT-TL2* (mt-tRNALeu(CUN))
m.13042A>T[344]	*MT-ND5* (Complex I, subunit 5)
Multiple deletions of mtDNA[345]	-
nDNA mutation or deletion	
A467T[346]	*POLγ*

Table I5. Mitochondrial and nuclear DNA mutations associated with MERRF syndrome.

The m.8344A>G mutation is heteroplasmic; therefore, both heteroplasmy load and the variation of the tissue distribution of mutant mtDNA have an impact in the clinical manifestations of the disease. Moreover, the threshold effect of each tissue has also a role in phenotype. For the m.8344A>G mutation, the threshold of mutation load seems to be between 75 and 90%[347,348].

The m.8344A>G mutation is usually present in all tissues with a high proportion (above 90%); therefore, it is often detected in mtDNA from blood leukocytes. If the heteroplasmy load is low, it is necessary to detect the mutation in other tissues, such as cultured skin fibroblasts, urinary sediment, oral mucosa, saliva, hair follicles or (most reliably) skeletal muscle.

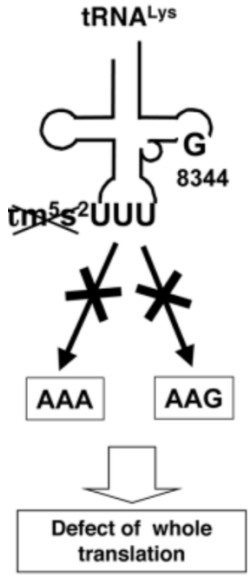

Figure I12. Proposed molecular pathogenesis caused by the wobble modification deficiency of mutant mt-tRNA associated with MERRF syndrome.
The pathogenic point mutation m.8344A>G impairs the wobble modification of the mutant mt-tRNA and the pattern of codon recognition. Adapted from Kirino et al. (2005)[327].

Molecular pathophysiology

Defects in the whole mitochondrial proteins synthesis due to the m.8344A>G mutation provoke lower function of MRC complexes I and IV, decreased mitochondrial respiration rate and reduced $\Delta\Psi m$[349-352]. Complex IV seems to be the most affected in MERRF patients, meanwhile complex II is the least affected[321]. Furthermore, oxidative stress caused by the MRC deficiency has a high impact on the pathogenesis and progression of MERRF syndrome, since high ROS accumulation induces tissue damage[353].

The inhibition of mitochondrial proteins synthesis due to the m.8344A>G mutation was observed for the first time by the accumulation of aberrant polypeptides due to a premature termination of translation.

The main abnormal protein characteristic of MERRF mitochondrial synthesis is a polypeptide translated from MT-COI mRNA, derived from premature termination of translation. Other abnormal polypeptides are different products of premature termination of translation of MT-ND2 mRNA[325].

Therefore, the mechanisms that trigger the main manifestations of MERRF syndrome are thought to be correlated with a combination of neuronal loss and hyperexcitability dysfunction initiated by the failure of the OXPHOS system in specific areas of the brain tissue[321].

Clinical description

Clinically, MERRF is classified as one of the progressive myoclonic epilepsies. There are four canonical features of this disorder: myoclonus, generalized seizures, ataxia and ragged-red fibers within muscle tissue[354].

It is also associated with dementia, muscular weakness and other secondary clinical manifestations such as peripheral neuropathy, renal dysfunction, cardiomyopathy, hearing loss, optic atrophy, short stature and exercise intolerance[355,356]. Less common findings are ophthalmoparesis and multiple lipomas.

MERRF patients also suffer from lactic acidosis and elevated pyruvate levels in serum at rest, and especially after moderate exercise[357], and often complain of vomiting, abdominal pain, fatigue, muscle weakness and difficulty breathing. Depression may be an under-recognized feature of MERRF syndrome[358].

Sometimes, patients showing the clinical manifestations for MERRF also have strokes (MERRF/MELAS overlap)[342,344] or progressive external ophtalmoplegia and retinopathy, symptoms of KSS[333,334].

Age onset of MERRF syndrome is diverse. Early development is usually normal before presentation in adolescence or early adulthood. However, a late onset in adults is not uncommon in patients with MERRF[359].

Diagnostic methods

MERRF is diagnosed based on clinical, biochemical/molecular and genetic testing[360].

Clinical testing:

-Measurement of lactate and pyruvate concentrations in blood and/or cerebral spinal fluid (CSF). In individuals with MERRF, the concentrations of lactate and pyruvate are commonly elevated at rest and excessively increase after moderate activity[357].

-Measurement of CSF protein. Levels of this protein may be elevated in MERRF syndrome, but rarely exceed 100 mg/dL.

-Magnetic resonance imaging (MRI). This technique looks for stroke-like lesions. MERRF patients often show brain atrophy and basal ganglia calcification. MERRF syndrome preferentially involves the inferior olivary nucleus, cerebellar dentate nucleus, red nucleus and pons of the brainstem, as well as the gray matter[361].

-Magnetic resonance spectroscopy (MRS). It is used to look for lactate in the brain.

-Electrocardiogram. It is used to diagnose heart rhythm abnormalities. MERRF patients often show pre-excitation events.

-Electroencephalogram. It usually shows generalized spike and wave discharges with background slowing, but focal epileptiform discharges may also be seen.

-Muscle biopsy. It usually shows ragged-red fibers with the modified Gomori-trichrome staining and hyperactive fibers with the succinate dehydrogenase (SDH) staining, COX negative muscle fibers and lactate accumulation[362] (**Figure I13**).

Biochemical/Molecular testing:

Biochemical analysis of respiratory chain enzymes in muscle extracts of MERRF patients usually shows decreased activity of respiratory chain complexes containing mtDNA-encoded subunits, especially COX deficiency.

Genetic testing:

Two main genetic strategies can be followed:

-Serial single-gene molecular genetic testing, which is based on the order in which pathogenic variants most commonly occur: *MT-TK* (analysis for the m.8344A>G, m.8356T>C, m.8363G>A, and m.8361G>A pathogenic variants), *MT-TF*, *MT-TL1*, *MT-TI*, and *MT-TP.*

-Full mtDNA sequencing, which looks for pathogenic variants that are not exclusive for MERRF syndrome.

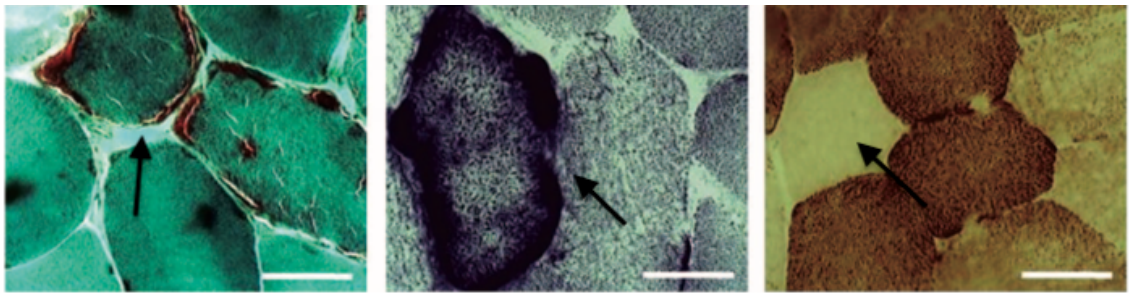

Figure I13. Common examination of muscle tissue biopsies derived from MERRF patients.
Arrows indicate ragged-red fibers stained with modified Gomori-trichrome, SDH and COX stainings, respectively. Adapted from Lorenzoni et al. (2014)[321].

Treatments for MERRF syndrome

Like many mitochondrial diseases, there is no specific cure for MERRF syndrome and treatment is primarily symptomatic.

Seizures can be treated with conventional anticonvulsant therapies (Levetiracetam[363], clonazepam, zonisamide[187]), but valproic acid (VPA) should be administered with care and in association with L-carnitine[320], since VPA may cause secondary carnitine deficiency and a subsequent worsening of the mitochondrial dysfunction. However, no controlled studies have compared the efficacy of different anticonvulsants.

In the absence of proper clinical trials, it is difficult to evaluate the effect of proposed supportive treatments such as CoQ (50-100 mg 3x/day) and its analogue idebenone or L-carnitine (1000 mg 3x/day), although all of them have been beneficial in some patients of heterogeneous mitochondrial diseases by increasing energy production[360].

In addition, physical therapy and aerobic exercise have shown to be helpful for any impaired motor abilities in MERRF and other mitochondrial diseases[364].

MERRF patients with low CSF folate can be also treated with folinic acid, although there is no a clear consensus[323].

Models of MERRF syndrome

The development of new potential treatments for mitochondrial diseases is complicated due to the rarity of patients and the lack of animal models to study this group of disorders in general and MERRF syndrome in particular. This situation has

led to the development of different systems in order to study the tissue specific effects of mtDNA mutations (**Figure I14**).

Microorganisms

- *Escherichia coli*

Prokaryotic bacteria have proven to be a useful model system to investigate MRC proteins structure and function. For example, *E. coli* can be beneficial for comprehensive studies investigating effects of mtDNA mutations known to cause human complex I deficient mitochondrial diseases. *E. coli* complex I is a powerful model system to exploit the gene manipulation (especially site-specific mutagenesis), which is virtually impossible in human complex I for mtDNA-encoded subunits such as ND5. For example, mutational analyses of the corresponding mutations at E144 and D400 of the *E. coli* NuoL (ND5) subunit suggested that these residues are critical for the complex I functions of electron transfer and/or proton pumping[365].

Moreover, the equivalent *E. coli* mutant of the common M64V LHON mutation in ND6 demonstrated a mild effect on *E. coli* complex I activity[366].

Although there is no an equivalent mutation to m.8344A>G in *E. coli*, xm5 and xm5s2U (being x ammonium, glycine or taurine) modifications of the wobble position of mt-tRNA are a result of enzymes that are evolutionary conserved from bacteria to humans[367-369].

Bacterial proteins MnmE-MnmG and MnmA form an enzymatic complex that modifies the 5 position of wobble U position of $tRNA^{Lys}$, $tRNA^{Glu}$, $tRNA^{Gln}$, $tRNA^{Gly}$, $tRNA^{Leu}$ and $tRNA^{Arg}$. Mutations in these proteins are associated with alterations in protein synthesis, growth deficiency, acid pH sensitivity and lethality[368,370-374].

However, although *E. coli* model is very easy to use in the laboratory, there are some limitations to the utilization of the bacterial system due to its prokaryotic nature and the lack of phenotypes caused by some mutations.

- Yeast models

Mitochondrial functions are highly conserved between humans and *Saccharomyces cerevisiae*. Therefore, yeasts are a good model to study mitochondrial diseases, providing insight into both physiological and pathophysiological processes.

Moreover, yeasts have the ability to survive with fermentable carbon sources in the absence of mitochondrial function. Therefore, pathogenic mutations that lead to mitochondrial dysfunction are able to be maintained in yeast, as long as a fermentable carbon source is available[375].

The ability to transform yeast mtDNA and the conservation between yeast and human mt-tRNAs allow pathogenic mt-tRNA mutations to be modelled in yeast[376,377]. In fact, the molecular consequences of pathogenic mutations at conserved sites are the same in yeast as in humans. For example, the A14G mutation in $tRNA^{Leu}$ (UUR) in yeasts is equivalent to the m.3243A>G mutation causing MELAS in humans[378]. This yeast model has been successfully used as a screening platform to find new drug candidates for the treatment of MELAS disease[254].

Although there is no an equivalent mutation to m.8344A>G in yeasts, other yeasts models have been used to study the pathophysiology of MERRF syndrome.

As before commented, human mt-$tRNA^{Lys}$ has a taurine-containing modified uridine (τm^5s^2U) at its anticodon wobble position and the m.8344A>G mutation in humans provokes that the mt-$tRNA^{Lys}$ lacks that τm^5s^2U modification.

The tRNA-modifying enzyme TRMU (tRNA 5-methyl aminomethyl-2-thiouridylate methyltransferase) is responsible for the 2-thiolation of the wobble position of mt-$tRNA^{Lys}$ and other mt-tRNAs in human and yeasts. Yeast *SLM3* gene is homologous to human *TRMU*, and it has been observed that disruption of this gene eliminated the 2-thio modification of mt-tRNAs and impaired mitochondrial proteins synthesis, which led to reduced respiratory activity, similar phenotypic features observed in MERRF human cellular models. Furthermore, when *MTO1*, which is responsible for the C5 substituent of the modified uridine, was disrupted along with *MTU1*, a much more severe reduction in mitochondrial activity was observed[379].

However, the aspect of heteroplasmy cannot be modelled in yeasts, since yeasts become homoplasmic within a few generations[380]. Therefore, using this model it is

not possible to study the threshold effect, which has an essential role in the pathophysiology and appearance of symptoms of MERRF syndrome.

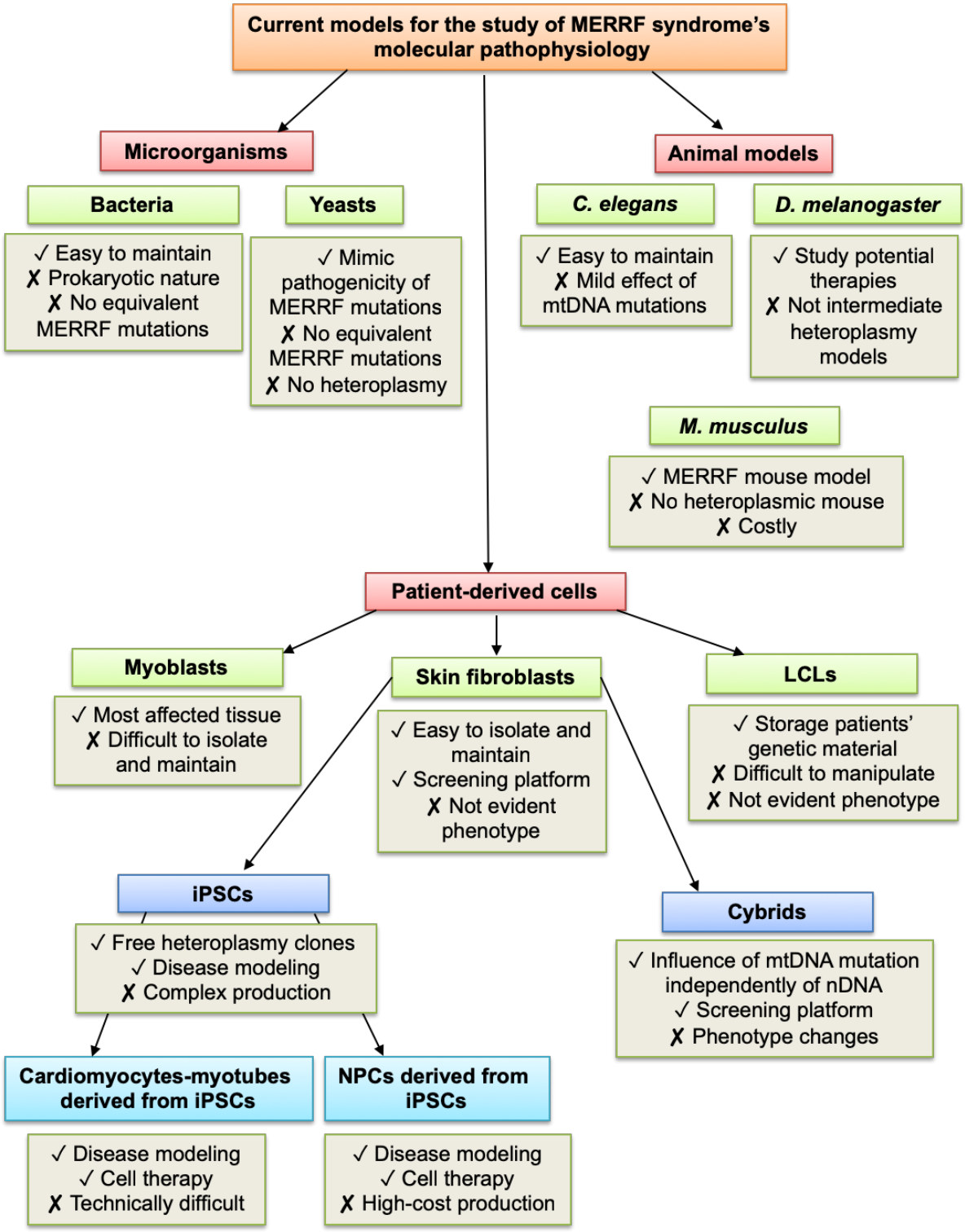

Figure I14. Current models for the study of MERRF syndrome's molecular pathophysiology.

Animals models

- *Caenorhabditis elegans*

Extensive evolutionary conservation exists in mitochondrial composition, function and mtDNA between humans and *C. elegans*[381]. In fact, several well-characterized strains have been described that harbour classical gene mutations in nuclear-encoded subunits of the MRC. These include missense and/or deletion mutants in subunits of complex I, complex II and complex III, as well as in CoQ biosynthesis genes[382-385]. Moreover, *C. elegans* has been widely used to investigate the effect of oxidative stress in lifespan and the mechanisms and efficacy of different mitochondrial therapies[386]. For example, using the *nuo-1* (*NDUFV1* homologue) mutant worm, which has been observed to show low respiration rate, low ATP production and reduced lifespan, the beneficial effects of riboflavin have been checked[387].

However, in *C. elegans,* mutations in mtDNA have a mild effect, even they do not show any phenotype[388]. In fact, mtDNA mutations have not been reported to affect motility, reproduction, development or other important functions in the worm[389]. Therefore, there is no a worm model for MERRF syndrome that mimics the pathophysiological characteristics of the disease.

Although the worm model is very easy to manipulate in the laboratory (they are transparent, hermaphrodites and reach adulthood in less than three days), the expression of some mitochondrial diseases phenotypes and their maintenance over time is intriguingly[386].

- *Drosophila melanogaster*

The fruit fly *D. melanogaster* offers many advantages as a model system since its genetics has been studied for a long time and there are a lot of genetic tools developed[390].

The utility of modelling human diseases in the fly has been repeatedly demonstrated, in particular for neurodegenerative diseases[391-393]. Markedly important are *D. melanogaster* mutants for the orthologues of the genes *PARK2* and *PINK1* that show distinctive mitochondrial morphology and phenotypes[394,395].

Apart from *Drosophila* mutants of MRC components that show neurodegeneration, motor dysfunction, increased ROS production and abnormal mitochondrial

morphology[396,397], some fly mutants of mtDNA have been described, such as a model of Leigh syndrome (conserved homoplasmic mutation in *ATP6*)[398] that revealed altered IMM structure and has been used as a well characterized model of mitochondrial encephalomyopathies pathophysiology.

Moreover, fly has been used to investigate the efficacy of new mitochondrial therapies such as heteroplasmy shiftment[399].

However, currently it is not possible to introduce an engineered precise mitochondrial genome and generate intermediate mutant heteroplasmy in *Drosophila*[400]; therefore, there are no fly MERRF models yet.

- Mouse models

Mammalian *in vivo* model systems are ultimately necessary for answering the many questions regarding mtDNA biology, mitochondrial diseases pathogenesis and tissue specificity that still remain.

With the possibility to make transgenic mice at will, different murine models with mutations in several nuclear genes encoding mitochondrial proteins have been reported[401-403].

This is far from being the case for diseases due to mutations in the mtDNA, which modelling is technically difficult[404].

Different mutagenesis methods to generate mutations in mouse mtDNA have been described, and besides, several groups have shown that mtDNA mutations can be transferred from cultured cells into mice, thereby creating transmitochondrial mice (mito-mice)[405-409].

However, the generation of heteroplasmic mice with pathological mtDNA mutations has proven challenging due to the multicopy nature of the mitochondrial genome. Furthermore, the transfection of plasmids or modified mtDNA into mouse mitochondria has not been successful[410].

Recently, a mito-mice carrying a G7731A mutation in the $tRNA^{Lys}$ gene encoded by mtDNA has been generated. This mutation is equivalent to the human mtDNA mutation G8328A, which provokes mitochondrial encephalomyopathy, COX-deficient fibers, myopathy and exercise intolerance[411,412]. Mito-mice-$tRNA^{Lys7731}$ expressed respiration defects and disease-related phenotypes; therefore, it can be used as a model for diseases caused by mutations in the mt-$tRNA^{Lys}$ gene, such as MERRF, MELAS or PEO.

However, generating and maintaining transgenic mice is costly and time-consuming and thus unfeasible for each individual mutation.

Patient-derived cells

- Skin fibroblasts model

Obtaining skin fibroblasts is a little invasive procedure that can be requested at a later stage. Moreover, they are convenient to maintain in culture as primary cells that show most of pathophysiological features of the mitochondrial disease, at least the nuclear-encoded ones. For example, patient-derived fibroblasts have been used to study the assembly of MRC complexes I[413] and IV[414], the process of mtDNA translation[415] and mitochondrial structure[416].

Moreover, skin fibroblasts have been widely used as a screening tool for searching individualized treatments, for example in the case of patients with complex I defects[417] or MELAS[220,254].

In the case of MERRF syndrome, it has been observed that primary skin fibroblast cultures established from MERRF patients show imbalanced gene expression of antioxidant enzymes, excessive ROS production, OXPHOS system disruption and increased levels of matrix metalloproteinases (MMPs), which are a progressive marker of neurodegenerative diseases[219,349,353,418].

However, patient-derived fibroblasts show some disadvantages as cellular models of mitochondrial diseases. Skin fibroblasts, unlike the cell types mostly affected in MERRF patients, are proliferative and rely on glycolytic metabolism for energy production. Therefore, a more relevant *in vitro* model is desired since skin fibroblasts are not much vulnerable to energy-dependent defects resulting from mitochondrial dysfunction.

Moreover, the phenotype may not be evident in defects involving the expression and maintenance of mtDNA.

- Transmitochondrial cytoplasmic hybrids (cybrids) model

Cybrid cell lines can incorporate patients' mitochondria and perpetuate its mtDNA-encoded components, maintaining the same nuclear background.

Cybrids have been very useful to exclusively study the influence of mtDNA mutations on cell function and phenotype alterations, independently of the patient's nuclear background[419].

Transmitochondrial cybrids models for MERRF syndrome have been widely used for the study of the pathophysiology of the disease and also as a screening platform for the discovery of new potential treatments or toxics[219,420-423].

However, the cybrid model shows important limitations and several criticisms of their application in mitochondrial diseases modelling have arisen.

The most important disadvantage of the cybrid model is that the ρ0 (mtDNA-less) cell line (nuclear background) used for cybrid generation can influence the mitochondrial genotype–phenotype relationship. In different studies using MELAS cybrids, it has been observed that MELAS cybrids made using osteosarcoma cell lines required a mutational burden of 85% for phenotypic consequences were observed and only a 30% decrease in COX activity was shown. However, a A549 lung carcinoma MELAS cybrid model required only a 55% mutational burden to observe a 50% reduction in COX activity[424].

Therefore, the loss of patients' nDNA and mtDNA interactions possibly modifies the behaviour of the diseased cells.

- Lymphoblastoid cell lines model

B lymphoblastoid cell lines (LCLs) constitute a valuable source of mitochondria to investigate mitochondrial function in patients affected by respiratory chain disorders[425]. LCLs are mainly generated by transformation of peripheral B lymphocytes by Epstein-Barr virus (EBV)[426].

Recently, LCLs from one patient with MERRF were derived by EBV transformation of peripheral blood mononuclear cells. This model was used to evaluate the feasibility of delivering WT mitochondria using the cell-penetrating peptide Pep-1 as a treatment for MERRF syndrome. Interestingly, a harmful effect on mitochondrial function was observed[427].

Although this model is still the preferred choice of storage for patients' genetic material due to its low somatic mutation rate and ease of maintenance, LCLs have some limitations, such as induction of micro-RNAs (miRNAs) expression due to infection of EBV[428], the presence of two different cellular stages[426] and different

cellular response in comparison to lymphocytes[429,430]. Moreover, LCLs are difficult to manipulate and the phenotype is often not evident.

- Patient-derived myoblasts model

Cultured myoblasts have been an important *in vitro* model for mitochondrial diseases research since tissues that have a higher energy demand such as the muscle and neurons are the most affected in mitochondrial myopathies.

Myoblasts derived from patients with MELAS or different mitochondrial myopathies have been used to study the role of antioxidant enzymes, ATP levels, heteroplasmy distribution and mitochondrial proteins translation in these diseases[431,432].

Cultured MERRF myoblasts have been used to study the distribution and expression of mutant mtDNAs[351]. Moreover, the heteroplasmy threshold for the biochemical expression of the mutation was determined.

However, using myoblasts as a cellular model for mitochondrial diseases has several disadvantages. First, large quantities of proliferative myoblasts are difficult to isolate from muscle tissue biopsy at later stages; therefore, it is probable that more than one muscle biopsy is necessary to obtain enough cells for the analysis required. In the case of OXPHOS dysfunction, a repeat of an invasive muscle biopsy is problematic. Moreover, primary myoblasts require special conditions for optimal growth and myoblasts enrichment protocols are needed in order to obtain a pure cell culture.

- Human iPSCs (hiPSCs) model

In 2006, a hallmark publication by Yamanaka et al. redefined the field of stem cells biology. For the first time, adult fully differentiated somatic cells were dedifferentiated to the pluripotent state using four transcription factors; *OCT4* (also known as *POU5F1*), *SOX2*, *KLF4* and *MYC*, yielding iPSCs, which have the capacity to differentiate into all types of somatic cells[433]. This technology allows to create patient-specific iPSCs that are suitable for studying mitochondrial diseases caused by mtDNA mutations. The development of this model has led to numerous advances in neurodegenerative disorders, as well as in mitochondrial diseases.

For example, the reduction of heteroplasmy load of a MELAS hiPSCs model stablished from skin fibroblasts by a treatment with a specific mtDNA-targeted platinum TALEN has been reported[434].

Moreover, in the recent years, various MERRF-specific hiPSC models have been developed[435-438]. Different MERRF hiPSCs lines have been generated with different heteroplasmy levels, including one with the same heteroplasmy level than the starting somatic cells and one line with no mutant allele. Moreover, MERRF hiPSCs lines exhibited impaired mitochondrial function, reduced growth, fragmented mitochondrial morphology and elevated levels of ROS. All of these features validate MERRF hiPSCs applicability for disease modelling.

However, the use of hiPSCs for disease modelling has several disadvantages, such as its complexity and high cost of production.
Moreover, induction of pluripotency is accompanied by epigenetic reprogramming and a metabolic shift from OXPHOS toward glycolysis and vice versa during differentiation. Furthermore, the high expression of pluripotency genes increases the number of tumorigenic cells remaining in culture after differentiation[439].
In addition, the nuclear genome of hiPSCs was reported to be genetically instable and additionally they frequently harbour mtDNA aberrations[440].
Furthermore, it has been reported that nuclear reprogramming reduces the copy number of mtDNA and may change the proportions of WT and mutant mtDNA, i.e., the degree of heteroplasmy, which determines the onset and severity of the symptoms of the mitochondrial disease. The degree of mtDNA heteroplasmy has been suggested to vary among different iPSC clones, indicating uneven mitochondrial segregation during reprogramming. Therefore, it is possible to obtain mtDNA mutation-free clones of iPSCs from patients with a pathogenic mtDNA mutation. However, this fact can be an advantage since patient-derived mutation-free clones of iPSCs could be used for cell replacement therapies.

- Myotubes or cardiomyocytes derived from hiPSCs

Obtaining muscle cells from iPSCs has been technically difficult. However, not long ago an efficient method to obtain muscle fibers from iPSCs in order to model different diseases has been described[441].
Recently, MELAS and MERRF patients-derived iPSCs were differentiated into iPSC-derived myotubes which retained a non-proliferative PAX7-/Ki67-satellite-like cell niche**,** although further investigations about pathophysiology manifestation using this model are required[442].

Interestingly, MERRF-hiPSC-derived cardiomyocytes-like cells have been recently generated by induction with a cardiac differentiation medium. After two weeks, cells expressed cardiac-specific markers such as cardiac troponin T (cTNT), α-actinin, myosin light chain 7 (MYL7) and myosin light chain 2 (MYL2). Moreover, MERRF-hiPSCs-derived cardiomyocytes-like cells showed a decreased oxygen consumption, increased levels of ROS and mitochondrial fragmentation[438].

- Neural progenitor cells (NPCs) derived from hiPSCs

Nowadays, the most common route to obtain patient- and disease-specific neurons is through reprogramming of somatic cells into hiPSCs, followed by direct neural differentiation. This approach has led to a number of important insights into neurodevelopmental disorders and mechanisms underlying neural pathologies[443-445].
MERRF syndrome is clinically characterized by generalized epilepsy, cerebellar ataxia, deafness, dementia and hereditary polyneuropathies. Therefore, evaluation of mitochondrial function in MERRF neural cells is necessary to understand the pathophysiological mechanisms of the disease.
Patient-derived iPSCs can be differentiated into iPSCs-derived NPCs or neurons by exposing them to a mixture of growth factors and specific cell culture conditions. This technology offers numerous advantages, since a large number of differentiated cells can be obtained. In addition, during iPSCs conversion, mutation-free cells are generated. Therefore, iPSCs approach can be considered an autologous source of cells suitable for cell therapy, without the risk of immune rejection[446].
Moreover, last year NPCs derived from hiPSCs with a deleterious homoplasmic mutation in the mitochondrial gene *ATP6* have been generated by induction with a neurodifferentiation culture medium[447]. The metabolic switch toward OXPHOS was observed in NPCs, as well as defective ATP production and altered calcium homeostasis, indicating that iPSCs-derived NPCs could provide an effective model for drug screening to target mtDNA disorders that affect the nervous system.
Specifically, a recent research demonstrated that MERRF-hiPSCs-derived NPCs showed impaired mitochondrial function, increased ROS production and fragmented mitochondrial network[438].

However, this approach has several disadvantages since the technique is complex, expensive and time-consuming. Besides, it has been reported that it resets cellular

age, thus it could not be the most appropriate approach in order to study age-related neural disorders such as mitochondrial diseases. Moreover, some studies show that iPSCs conversion can rejuvenate mitochondria and the energetic capacity of derived cells[439], a disadvantage in mitochondrial disorders modelling.

Direct reprogramming

Due to the fact that obtaining a brain biopsy is aggressive and not efficient, the establishment of neuronal cells models using reprogramming techniques is necessary in order to elucidate the cellular pathophysiology of different mitochondrial diseases, such as MERRF syndrome, which is considered a mitochondrial encephalomyopathy.

Traditionally, Conrad Hal Waddington's illustration of the cell fate hierarchy has been considered the classic concept of lineage specification: lineage commitment and differentiation have been thought to be unidirectional and irreversible; only uncommitted stem cells differentiate into different tissue-specific cell types.
Waddington's epigenetic landscape model showed the progressive restriction of cell differentiation potential during normal development. The pluripotent cell, at the top of the hill (representing the maximal differentiation potential) falls down a slope with different grooves, which represent distinct tissue-specific cell fates without differentiation potential[448] (**Figure I15**).

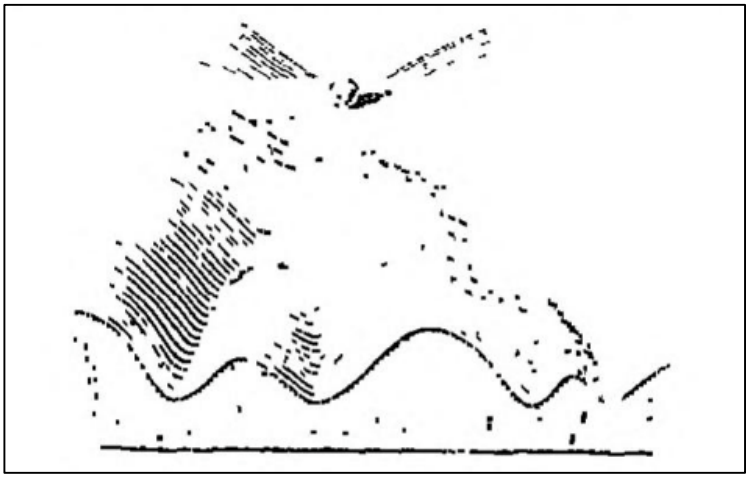

Figure I15. The epigenetic landscape.
Waddington's illustration of the cell fate hierarchy. Adapted from Waddington (1957)[448].

However, although Waddington's model is still very useful in the context of normal development, it does not take account of new progresses in cell reprogramming, such as the advent of iPSCs[449] and advances in direct cell fate conversion. Therefore, currently the Waddington's model has to be modified to include the capacity of a somatic cell to be reprogrammed to pluripotency and the possibility to be directly redifferentiated into another somatic cell type[450] (**Figure I16**).

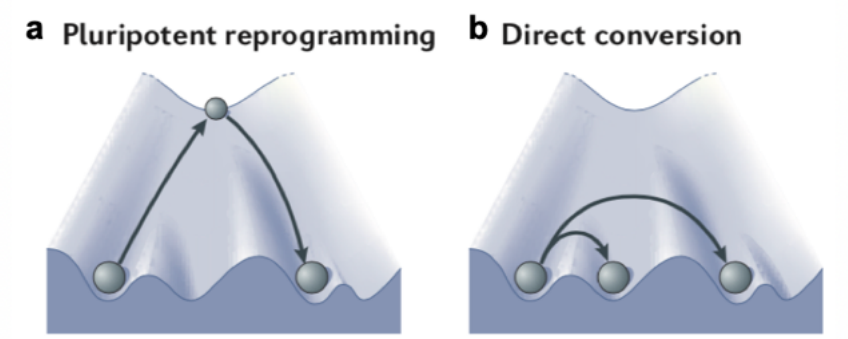

Figure I16. Scheme of Waddington's model.
The model represents a somatic cell which is reprogrammed to pluripotency (a) and a somatic cell which can be directly converted into a cell type of the same or a different germ layer (b). Adapted from Ladewig et al. (2013)[450].

In fact, a few years ago a new epigenetic landscape model was proposed by Ladewig and colleagues to include the advances in cell reprogramming and transdifferentiation across germ layers[450]. In this new model, cell fates are represented in a disc in which the pluripotent state is not higher in hierarchy than other cell states and, therefore, it can be bypassed in the process of cell fate conversion (**Figure I17**).

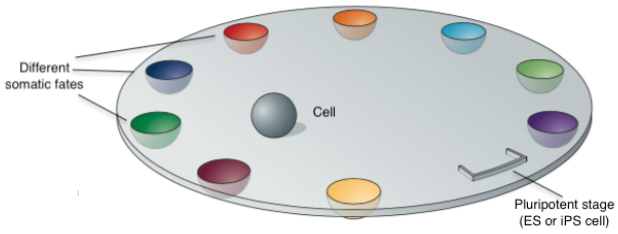

Figure I17. The epigenetic disc model.
It describes an actualization of the Waddington's landscape model that lacks hierarchy between different cell types, being the pluripotent state only one more. Conversion of one cell type into another can be achieved by extrinsic factors that 'tilt' the disc and/or function as guides between distinct fates. Adapted from Ladewig et al. (2013)[450].

Other recent models of cell identity try to represent the current known barriers and facilities to cell reprogramming. One interesting example is the Cook's epigenetic landscape, which represents cellular development as a navigation map in which each island represents a cell stable state and the sea routes the flexibility between different cell fates[451].

The idea that cells from different somatic fates are interconvertible reaches back more than 30 years. Direct reprogramming of a differentiated cell into another cell type was achieved for the first time in 1987 with the conversion of fibroblasts into myoblasts using the expression of a single transcription factor, Myoblast Determination 1 (MYOD1)[452]. It was the first study providing successful cell fate conversion between lineages within the same germ layer (mesoderm). In the following years, several new studies confirmed that direct conversion was possible by only overexpressing transcription factors, at least between lineages within mesoderm such as the smooth muscle[453,454], the blood lineage[455-457] or the cardiac muscle[458]. In fact, using different cocktails of transcription factors (*GATA4*, *MEF2C*, *TBX5* and *HAND2*), *in vivo* conversion of cardiac fibroblasts into functional cardiomyocytes was possible[459,460]. Apart from the use of transcription factors, miRNAs can mediate direct conversion through the direct repression of multiple genes.
For example, it has been observed that combined overexpression of miR-1, miR-133, miR-208 and miR-499 mediated direct conversion from fibroblasts into cardiomyocytes both *in vitro* and *in vivo*[461].

Cell fate conversion between lineages within the endoderm has been very important in different studies about diabetes. For example, only the pancreatic marker Pancreas and duodenum homeobox 1 (PDX1) overexpression was shown to be enough to induce insulin expression in the liver[462,463]. Moreover, recently the overexpression in pancreatic exocrine cells of a combination of the transcription factors NGN-3, PDX1 and MAFA successfully induced b-cell direct conversion *in vivo*[464].

Numerous studies have been focus on cell fate conversion between lineages within the ectoderm due to the importance of cellular development of nervous system. The

first successful researches were carried out using glial cells: both pre- and postnatal astrocytes were converted into functional neurons by the unique or combined expression of three transcription factors: PAX6, Achaete-scute complex-like 1 (ASCL1) and DLX2[465-467].

Due to the successful experiments described above and the advances in generation of iPSCs, a few years ago several groups tried to achieve the direct conversion of somatic cells into cell fates of different germ layers.

For example, different combinations of transcription factors involved in hepatocyte differentiation such as GATA4, HNF1A, HNF4A, FOXA1, FOXA2 or FOXO3 and the inactivation of the tumour suppressor gene *CDKN2A* have been observed to induce direct conversion of mouse fibroblasts into hepatocyte-like cells that expressed hepatocyte-associated markers such as albumin and α-fetoprotein. Moreover, converted cells were able to be engrafted into the adult liver and increase survival in a mouse model of liver failure[468,469].

However, due to the post-mitotic nature of neurons and the lack of models of several diseases that undergo neurodegeneration, direct conversion approach has been mostly exploited in order to obtain neural progenitors or specific neuronal subtypes. The final aim is to study the mechanisms underlying neurodegenerative disorders and use neuron-like cells as screening platforms or for cell replacement therapies.

Direct neuronal reprogramming

Since the first direct reprogramming of a differentiated cell type into another was achieved, it took more than twenty years to reprogram fibroblasts into neuronal cells[470].

The first successful direct conversion of murine fibroblasts into induced neurons (iNs) was achieved in 2010, when Wernig and colleagues identified a combination of three proneural factors (the proneural gene ASCL1 and the transcription factors Brain-2 [BRN2] and Myelin transcription factor 1 like [MYT1L]), which were able to convert murine embryonic and postnatal fibroblasts into functional neurons *in vitro*[471]. The expression of these three transcription factors was required to obtain electrophysiologically functional neurons. Since then, iNs are defined as the product

of directly reprogrammed neurons starting from somatic cells avoiding passing through the pluripotent stage.

About one year later, this approach was transferred to human fibroblasts, using the additional factor Neurogenic Differentiation factor 1 (NEUROD1) to obtain iNs[472]. It was observed that longer conversion times were needed for human cells in comparison to mouse cells.

Since then, the strategy of solely expression of different transcription factors has been successfully used to generate iNs[473-475].

However, from the beginning, the generation of iNs using direct reprogramming has had a main challenge: reaching a high conversion efficiency, which is defined as the percentage of iNs obtained relative to the number of starting cells plated. Although it can be very variable depending on the starting cells and the protocol used, the first approaches using direct reprogramming obtained very poor conversion efficiencies[450,476]. Moreover, it is also necessary to reach a good purity percentage, which is defined as the number of iNs in the final population related to the total cells in the plate. These two parameters are crucial since neurons are post-mitotic cells not able to further expand.

Over the next years, new tools and strategies have been found to improve efficiency and purity of neuronal conversion (**Table I6**).

For example, the expression of different combinations of neuronal specific miRNAs has been shown to direct the conversion of somatic cells into iNs[477,478], although most times the iNs generated were immature and conversion efficiencies were low.

Apart from using miRNAs, it has been demonstrated that derepression of neural genes can be a different approach to neural direct conversion. For example, repression of RNA-binding polypyrimidine tract-binding (PTB) protein enabled the miRNA action on several components of the REST (RE1-silencing transcription factor) complex and the subsequent expression of neuronal-specific genes[479].

REST is considered a relevant guardian for reprogramming, since it is expressed in non-neuronal cells where it represses neuronal genes[480].

A few years ago, it was shown that combinations of small molecules inhibiting both glycogen synthase kinase-3β and SMAD signalling together with the expression of neurogenic factors could improve conversion efficiency[481]. In fact, recently it was

demonstrated that it is possible to undergo direct reprogramming into iNs by only chemically manipulating pathways involved in neural differentiation[482].

Currently, the combination of the different strategies seems to be the best approach to achieve high conversion efficiencies during iNs generation (**Table I6**).

For example, a combination of proneural genes overexpression (*ASCL1*, *MYT1L* and *NEUROD1*) with miRNAs such as miR9/9* or miR124 resulted in the generation of functional neurons with mature physiological properties from human fibroblasts[476].

Combinations of small molecules together with the overexpression of proneural factors have successfully converted adult somatic cells into iNs[483,484]. Some strategies have combined small molecules, transcription factors and miRNAs expression[485] or repression of p53, hypoxic conditions and expression of proneural transcription factors[486].

Strategies for neuronal direct conversion *in vitro*

Pan-neuronal induced population

Starting population	Transcription factors used	Other factors used	Efficiency of conversion	Reference(s)
Mouse and human fibroblasts	ASCL1	Hypoxia	Up to 10%	Chanda, S. *et al.*[487]
Mouse hepatocytes	ASCL1 BRN2 MYT1L	-	12-15%	Marro, S. *et al.*[488]
Mouse embryonic fibroblasts (MEFs) and murine tail fibroblasts	ASCL1 BRN2 MYT1L	-	1.8–7.7%	Vierbuchen, T. *et al.*[471]
Human fibroblasts (post-mortem)	ASCL1 BRN2 MYT1L	-	-	Iovino, M. *et al.*[489]

Human fibroblasts (schizophrenia)	ASCL1 BRN2 MYT1L	SB-431542 Noggin CHIR99021 cAMP VPA GDNF NT3	-	Passeri, E. *et al.*[490]
Human fibroblasts (schizophrenia)	ASCL1 BRN2 MYT1L	bFGF	-	Siegert, S. *et al.*[491]
Human postnatal fibroblasts	ASCL1 MYT1L NEUROD1	miR-9/9* miR-124 VPA db-cAMP	Up to 50%	Yoo, A. S. *et al.*[476]
Human fibroblasts	ASCL1 MYT1L NEUROD1	miR-9/9* miR-124 VPA	-	Bavamian, S. *et al.*[492]
Pericyte-derived cells	ASCL1 SOX2	-	-	Karow, M. *et al.*[493]
Human fibroblasts (PD, HD, ALS, AD)	ASCL1 BRN2 REST knockdown	LM-22A4 GDNF NT3 db-cAMP CHIR99021 SB431542 Noggin LDN-193189 VPA	Up to 50%	Drouin-Ouellet, J. *et al.*[494]
Postnatal human fibroblasts	BRN2 MYT1L	miR-124	-	Ambasudhan, R. *et al.*[495]
Human fibroblasts	P16 and p19 knockdown	db-cAMP bFGF BDNF NT3	-	Sun, C.K. *et al.*[496]
MEFs	PTB protein knockdown	-	Up to 15%	Xue, Y. *et al.*[479]

Human fibroblasts (PD)	PTB protein knockdown	bFGF, BDNF, GDNF, NT3, CNTF	-	Fiesel, F. *et al*.[497] and Puschmann, A. *et al*.[498]
Human fibroblasts (HD)	PTB protein knockdown	bFGF, BDNF, GDNF, NT3, CNTF	-	Liu, Y. *et a*l.[499]
Human fibroblasts (ALS)	PTB protein knockdown	bFGF, BDNF, GDNF, NT3, CNTF	up to 90%*	Lim, S. *et al*.[500] * and Su, Z. *et al*.[501]
Postnatal human fibroblasts	ASCL1 NGN2	SB-431542 Noggin CHIR99021	Up to 200%	Ladewig, J. *et al*.[481]
Human fibroblasts (AD)	ASCL1 NGN2	SB-431542 cAMP Noggin LDN-193189 CHIR99021 BDNF GDNF NT3	10-13%	Hu, W. *et al*.[482]
MEFs, postnatal mouse astrocytes	ASCL1/NGN2 BCL2	Calcitriol Alpha-tocotrienol Forskolin	Up to 40%	Gascon, S. *et al*.[502]
Embryonic and postnatal human fibroblasts	ASCL1 BRN2 MYT1L NEUROD1	-	3-5%	Pang, Z. P. *et al*.[472]
Postnatal mouse astrocytes, human fetal astrocytes	NEUROD4	-	Up to 50%	Masserdotti, G. *et al*.[503]
GABAergic neurons				
Mouse Astrocytes	NGN2 DLX2	-	Up to 35%	Heinrich, C. *et al*.[465]

MEFs	ASCL1 SOX2 FOXG1 DLX5 LHX6	-	Up to 10%	Colasante, G. *et al*.[504]
Dopaminergic neurons				
Fetal and adult human fibroblasts (PD)	ASCL1 NURR1 LMX1A	-	3-10%	Caiazzo, M. *et al.*[475]
Human fibroblasts (*PANK2* mutation)	ASCL1 NURR1 LMX1A	-	5%	Santambrogio, P. *et al*.[505]
Mouse fibroblasts	ASCL1 PITX3 NURR1 LMX1A FOXA2 EN1	Shh FGF8	Up to 9%	Kim, J. *et al*.[506]
Lung fetal fibroblasts and MEFs	ASCL1 BRN2 MYT1L LMX1A FOXA2	-	6-8%*	Pfisterer, U. *et al*.[507]* and Sheng, C. *et al*.[508]
Mouse astrocytes	ASCL1 NURR1 LMX1B	-	Up to 20%	Addis, R.C. *et al*.[509]
Mouse prenatal fibroblasts	ASCL1 NURR1 LMX1A	-	-	Dell'Anno, M.T. *et al*.[510]
Motor neurons				
Mouse/human fibroblasts	ASCL1 BRN2 MYT1L LHX3 NGN2 MNX1 ISL1	-	5-7%	Son, E. Y. *et al*. [511]

Mouse/human embryonic and adult fibroblasts	-	Kenpaullone Forskolin Purmorphamine Rosmarinic acid Y-27632	Up to 90%	Qin, H. *et al*.[512]
Human fibroblasts (SMA)	ASCL1 BRN2 MYT1L NEUROD1 NGN2 ISL1 MNX1 LHX3	bFGF BDNF GDNF IGF1 cAMP	Up to 6%	Zhang, Q. J. *et al*.[513]
Human fibroblasts (ALS)	NEUROG2 SOX11 ISL1 LHX3	Forskolin Dorsomorphin	-	Liu, Y. *et al*.[514]
Glutamatergic neurons				
Postnatal mouse and human astrocytes	NEUROD1	-	Up to 90%	Guo, Z. *et al*.[515]
Human astrocytes	-	LDN-193189 SB431542 TTNPB Thiazovivin CHIR99021 DAPT SAG Purmorphamine	Up to 67%	Zhang, L. *et al*.[516]
Serotonergic neurons				
Human fibroblasts	ASCL1 FOXA2 LMX1B FEV	P53 knockdown Hypoxia dorsomorphin, SB431542, BDNF, GDNF, PD0332991	-	Xu, Z. *et al*. [486]

Human fibroblasts	ASCL1 NGN2 NKX2.2 FEV GATA2 LMX1B	Laminin db-cAMP Noggin LDN-193189 A83-1 CHIR99021 Forskolin SB431542	-	Vadodaria, K. C. *et al*.[517]
Striatal neurons				
Human postnatal and adult fibroblasts	MYT1L DLX1 DLX2 BCL11B	miR-9/9* miR-124	Up to 60%	Victor, M. B. *et al*.[478]
Sensory neurons				
Mouse and human fibroblasts (FD)	ASCL1 MYT1L ISL2 NGN1 KFL7	BNDF CNTF GDNF	Up to 20%	Wainger, B. J. *et al*.[518]
Mouse and human fibroblasts	NGN1/NGN2 BRN3A	-	Up to 6%	Blanchard, J.W. *et al*.[519]

Table I6. Strategies for neuronal direct conversion *in vitro*.

Apart from reaching a high conversion efficiency, other obstacles in neural direct reprogramming are the origin and the state of the starting cells. Human iNs take longer to mature and be able to origin action potentials compared to mouse iNs[475,479,520]. Moreover, embryonic or young donor cells are converted with higher efficiency than aged donor cells, which is a challenge for the modelling of late-onset diseases[474,483]

Recently, it was shown that combinations of small molecules and growth factors, the overexpression of two proneural transcription factors (ASCL1 and BRN2) and the silencing of the neural barrier REST complex[480] can improve conversion efficiency up to more than 50% using aged donor cells as a starting material[494,521].

This single-step and single-vector based approach developed by Drouin-Ouellet et al.[470,494,522] can generate very high yields of iNs from patients with

neurodegenerative disorders, independently of the passage number of the skin fibroblasts. This simple method has facilitated the application of direct neuronal reprogramming for disease modelling studies.

Although most studies have been performed on a pan-neuronal or unspecified neuronal subtype, direct reprogramming to a specific subtype of neurons is currently possible (**Table I6**). In the case of some diseases it is important to study the pathophysiological mechanisms in the subtypes of neurons affected[470], since different neuron subtypes may express distinct disease-related phenotypes[523]. In fact, the correct way to study disease-associated phenotypes would be comparing iNs specific subtypes affected in the disease with iNs subtypes not affected.

To date, the predominant method by which identify the iNs population is based on the expression of neuronal markers such as βIII-Tubulin (TUJ1), Microtubule associated protein 2 (MAP-2) and/or Tau protein, apart from the observation of neuronal morphology (decreased nucleus area, elongation, increased number of branches), since it has been observed that antibiotic selection to purify the iNs population is not efficient, obtaining a high percentage of non-converted cells that express reprogramming constructs[478,520,524-526].

Advantages and disadvantages of direct neuronal reprogramming

Direct reprogramming has several advantages in comparison with the generation of iPSCs-derived cells, such as the relative simplicity and short time requirements; thus, the cost in a clinical setting is reduced[450]. In addition; iNs, unlike iPSCs, maintain the ageing[524] and the epigenetic marks of the donor[525,527], making them excellent candidates for modelling neuronal pathophysiology in age-related disorders. Moreover, unlike hiPSCs that are susceptible to form tumors following transplantation[528], it has been demonstrated that iNs obtained through *in vivo* reprogramming do not cause tumorigenic processes. Therefore, in the future they could be a promising tool for cellular therapy, for example, by performing direct reprogramming *in vivo* of endogenous murine astrocytes or transplanted human cells[529]. For that reason, the generation of iNs or other cell types by direct reprogramming from patient-derived fibroblasts suffering from mitochondrial

diseases holds enormous promise for understanding the pathogenesis of these disorders and for discovering new therapy approaches.
Meanwhile proliferating cells are preferred to perform iPSCs reprogramming[530,531], proliferation is neither a prerequisite nor an advantage for direct neuronal conversion[532], which is important to directly convert senescent patient-derived cells.

Nevertheless, it remains unknown whether patient-derived fibroblasts can be directly reprogrammed into iNs that reflect the main pathological features of mitochondrial diseases.
Moreover, the retroviral or lentiviral vectors commonly used to introduce transcription factors are potentially dangerous to cause undesired genetic mutations.
Specifically, iNs have their own challenges as an *in vitro* model to study diseases pathophysiology. First, *in vitro* expansion and passaging of cells prior to reprogramming prevents successful conversion[503,533].
Moreover, maintaining iNs in culture is difficult and achieving a great number of iNs during long-term cultures is very challenging, restrictive and expensive, since cell death can be observed from 30 days post-infection (DPI). This fact may hinder electrophysiological characterization of iNs, since the earliest time point when spontaneous action potentials could be detected to date in human iNs is 46 DPI[486] and they are usually observed at 80-100 DPI[494]. Moreover, iNs tend to form clusters during the reprogramming process, hampering isolation of individual cells for further analysis.

Applications of direct reprogramming

Transdifferentiation holds great promise for biomedical applications such as regenerative medicine and cell-based disease modelling.
Somatic cells (for example, skin fibroblasts) can be directly converted into other tissue-specific cell types. The converted cells can be used in disease modelling (to analyze a disease-specific phenotype in a disease-associated somatic cell type *in vitro*)[482,492,498-500,505,513], pharmacological screening (to identify drugs interfering with the disease phenotype), drug toxicity testing (to identify side effects of potential drugs in different somatic cell types) and cell replacement therapy[534], since it is possible to direct convert cells *in vivo*, avoiding the need of immunosuppression.

Currently, the cell therapy approach best studied and closest to clinical application is transplantation of fetal progenitor cells of the neuronal subtype affected in the disease[535,536]. However, in the last years, several investigations have been focus on *in vivo* neural reprogramming from astrocytes or oligodendrocyte progenitors/NG2 glia[537].

It is important to realize that *in vivo* reprogramming not only takes place in a damaged and non-controlled environment, but also in a complex mixture of many different cell types.

The first attempt was turning reactive glial cells into neurons after brain injury a few years ago[538]. Since then, great advances have been made regarding the efficiency of conversion and maturity of iNs[539]. Many cell types in several different brain regions have been targeted by various neurogenic fate determinants with the use of diverse viral vectors. For example, direct conversion of astrocytes into iNs in the striatum has been achieved using different reprogramming factors combinations, such as ASCL1/BRN2/MYT1L[529], SOX2[540,541] or NEUROD1[542]. Moreover, direct conversion from astrocytes has been achieved in the cortex[515] and the spinal cord[543,544].

Using NG2-glia as starting cells, direct neural conversion has been achieved using similar reprogramming factors (NEUROD1, SOX2) in the spinal cord[544] and cortex[515,545]. Other combinations of transcription factors (NEUROG2 and/or BCL2) have promoted the neural conversion from NG2-glia in striatum[546] and cortex[502].

The potential clinical application of direct reprogramming *in vivo* is increasingly closer. Encouragingly, *in vivo* direct conversion of dopaminergic neurons from striatal astrocytes has been recently achieved, partially recovering the function and behavior in a PD mouse model[547]. Although this approach is still under development, it represents the main strategy to exploit the power of direct neuronal reprogramming.

AIMS

AIMS

MERRF is a mitochondrial disease mainly caused by the m.8344A>G mutation in mtDNA. The molecular pathogenesis of MERRF syndrome remains poorly understood due to the lack of appropriate cellular models, particularly in those cell types most affected in the disease, such as neurons. This thesis arises from the presence of autophagy and mitophagy flux disruptions in primary fibroblasts derived from patients diagnosed with MERRF syndrome and the necessity of new cellular models to study the pathophysiology of the disease. Considering the importance of finding new molecular targets for mitochondrial diseases, we decided to explore the role of autophagy and mitophagy in MERRF cell lines. Given the lack of effective treatments, new and more appropriate cellular models of MERRF syndrome are necessary to characterize the pathophysiology of the disease and perform both drug screening and drug toxicity testing.

To this end, we propose the following aims:

1. To characterize Parkin-mediated mitophagy in fibroblasts derived from MERRF patients and stablish the effect of CoQ treatment.

2. To evaluate the state of autophagy/mitophagy flux in cellular models of MERRF syndrome and stablish the effect of CoQ treatment and autophagy modulators.

3. To elucidate the role of Parkin-mediated mitophagy in MERRF syndrome.

4. To characterize iNs generated from MERRF patients-derived fibroblasts harbouring the m.8344A>G mutation.

5. To confirm the suitability of MERRF iNs to study the pathophysiology of MERRF syndrome and to use them as a new screening platform.

MATERIALS & METHODS

MATERIALS & METHODS

M-I. Reagents

We purchased the following antibodies and chemicals from:

- *Abcam (Cambridge, UK)*: Anti-Parkin, anti-Hsp60.
- *BD Biosciences (New Jersey, USA)*: Anti-CD56 (anti-NCAM).
- *Bio-Rad Laboratories Inc. (Hercules, CA, USA)*: Acrylamide/bisacrylamide solution 37.5:1, Clarity™ Western ECL Substrate, running buffer (TGS), SDS, Triton X-100, turbo transfer buffer (TG), Tween-20, SsoAdvanced™ Universal Probes Supermix.
- *Cell Signalling Technology (Danvers, MA, USA)*: Anti-LC3B, Anti-PINK1.
- *Eurofins Scientific (Luxembourg)*: Albumin (ALB) and WPRE forward and reverse primers.
- *iNtRON Biotechnology (Korea)*: RedSafe™ Nucleic Acid Staining Solution.
- *Invitrogen/Molecular Probes (Eugene, OR, USA)*: Monoclonal antibodies specific for complex IV (subunit II), MitoSOX^{TM} Red, MitoTracker^{TM} Red CMXRos, MitoTracker^{TM} Deep Red, 5,5', 6,6'-tetrachloro-1,1'3,3'-tetraethylbenzimidazolecarbocyanine iodide (JC-1), 2′,7′-dichlorodihydrofluorescein diacetate (CM-H_2DCFDA), Hoechst 3342, 4′,6-diamidino-2-phenylindole (DAPI), secondary antibodies from Alexa Fluor® IgG (H+L) series (488, 555 and 647 nm), Hank's Balanced Salt Solution (HBBS).
- *Jackson ImmunoResearch Laboratories (West Grove, PA, USA)*: Cy2 anti-mouse, Cy3 anti-chicken.
- *Merck Millipore (Burlington, MA, USA)*: OxyBlot™ Protein Oxidation Detection Kit.
- *MSE Pharmazeutika GmbH (Bad Homburg, Germany)*: Guttaquinon CoQ_{10}.
- *Panreac (Barcelona, Spain)*: Potassium acetate, 2-propanol, ethanol, sucrose, n-hexane, methanol, sodium chloride, Tris-base, ammonium persulfate (APS), glacial acetic acid, KOH, KCl.
- *Qiagen (Hilden, Germany)*: Qiagen DNeasy Blood and tissue kit.

- *Roche (F. Hoffmann-La Roche Ltd, Basel, Switzerland)*: Cocktail of proteases inhibitors.
- *R&D System (Minneapolis, MN, USA)*: SB431542, Noggin, LM-22A4, GDNF, NT3.
- *Santa Cruz Biotechnology (Santa Cruz, CA, USA)*: Anti-AMPK, anti-phospho-AMPK, anti-Actin, anti-GADPH, anti-P62, anti-DRP1, Parkin short hairpin (sh) RNA Lentiviral Particles and control scrambled Lentiviral Particles, puromycin hydrochloride.
- *Seahorse Bioscience Inc. (Billerica, MA, USA)*: Mito-stress test kit including oligomycin, FCCP, rotenone & antimycin A, as well as the XFe24 cell culture plates, sensor cartridges and XF base medium.
- *Sigma-Aldrich (St. Louis, Missouri, USA)*: Agarose, anti-cytochrome c, anti-VDAC1, fetal bovine serum (FBS), normal donkey serum, penicillin/streptomycin solution, coenzyme Q_{10}, rapamycin, phenol-chloroform-IAA solution, trypan blue solution, EDTA, sodium deoxycholate, TEMED, pounceau reagent, glycerol, paraformaldehyde, CCCP (carbonyl cyanide m-chlorophenylhydrazone), uridine, Bafilomycin A1, DMEM 4.5 g/L glucose, polyethyleneimine, gelatin, polyornithine, fibronectin, laminin, db-cAMP, CHIR99021, LDN-1931189, VPA, phosphate-buffered saline (PBS), DMSO.
- *Takara Bio Inc. (Nojihigashi, Kusatsu, Japan)*: Ndiff 227 medium.
- *ThermoFisher Scientific (Waltham, MA, USA)*: FastDigest^{TM} PdiI enzyme, DMEM + Glutamax medium, DMEM no glucose medium, Trypsin 10x, anti-Tau clone HT7, ALB probe and WPRE probe.
- *Vector Laboratories (Burlin-game, CA, USA)*: Vectashield mounting medium.

M-II. Fibroblasts cultures

Cultured fibroblasts were derived from a skin biopsy of two patients harbouring a heteroplasmic m.8344A>G mutation. Clinically, the patients had MERRF syndrome. The heteroplasmy of the m.8344A>G mutation was 66% in MERRF 1 fibroblasts and 38% in MERRF 2 fibroblasts. We verified that the heteroplasmy load in MERRF fibroblasts did not significantly change during this study. Control fibroblasts at similar passage number were derived from two healthy volunteers. When indicated in the

figure legends, data were shown as a mean of two control fibroblast cultures. Differential behavior and characteristics of several control and MERRF patient-derived dermal fibroblasts was determined in previous studies of our group[219]. Samples from patients and controls were obtained according to the Helsinki Declarations of 1964, as revised in 2001. Fibroblasts from MERRF patients and controls were cultured at 37°C and 5% CO_2 in Dulbecco's modified Eagle's medium (DMEM) + Glutamax with 100 mg/mL penicillin/streptomycin and 10% FBS.

M-III. Construction and culture of transmitochondrial cybrid cell lines

Transmitochondrial cybrids were a gift from Elena García Arumi from Vall d'Hebron Hospital, Barcelona.

Methodology to generate transmitochondrial cybrids is described below.

Transmitochondrial MERRF cybrids were generated by fusing enucleated fibroblasts from MERRF patients or controls with 143B osteosarcoma cells which lack mtDNA (ρ° cells), using the method described by King and Attardi[548]. These cells thus possess mtDNA from patients or controls in a control nuclear background. Osteosarcoma parental and ρ° cells, control osteosarcoma cybrid cells (100% WT at nucleotide position 8344) and cybrid cells harbouring the m.8344A>G mutation (90% heteroplasmy at nucleotide position 8344) were cultured at 37ºC and 5% CO_2 in DMEM containing 4.5 g/L glucose and 100 mg/mL sodium pyruvate, supplemented with 5% FBS, uridine (50 µg/mL) and penicillin/streptomycin (100 mg/mL). We verified that the heteroplasmy load in MERRF cybrids did not significantly change during the study.

M-IV. Generation of iNs from fibroblasts by direct reprogramming

Neurons were generated from MERRF and control fibroblasts by direct neuronal reprogramming as previously described by Drouin-Ouellet et al.[494,522]. Controls and MERRF patients-derived fibroblasts were plated onto 0.1% gelatin-coated 24-well plates or µ-Slide 4/8 Well Ibidi plates (2.8e4 cells/cm^2) with DMEM + Glutamax with 100 mg/mL penicillin/streptomycin and 10% FBS (hereinafter, fibroblasts medium).

The day after, dermal fibroblasts were transduced with one-single lentiviral vector containing neural lineage-specific transcription factors (ASCL1 and BRN2) and two shRNA against the REST complex, generated as previously described with a non-regulated ubiquitous phosphoglycerate kinase (PGK) promoter[549]. The plasmid was a gift from Dr. Malin Parmar (Developmental and Regenerative Neurobiology, Lund University, Sweden). Transduction was performed at a multiplicity of infection (MOI) of 30. The day after, the cells were switched into fresh fibroblasts medium and after a further 48 h, the medium was replaced with neural differentiation medium (NDiff227; Takara-Clontech) supplemented with neural growth factors and small molecules at the following concentrations[494]: LM-22A4 (Tropomyosin-related kinase B [TrkB] agonist, 2 μM), GDNF (neurotrophic factor, promotes the survival of motoneurons, 2 ng/mL), NT3 (neurotrophic factor, promotes the survival of neurons, 10 ng/mL), dibutyryl cyclic AMP (db-cAMP, promotes neuronal differentiation/survival, 0.5 mM), CHIR99021 (a potent inhibitor of GSK-3, 2 μM), SB-431542 (a neural fate inducing factor, 10 μM), noggin (BMP signalling inhibitor, 50 ng/ml), LDN-193189 (a neural fate inducing factor, 0.5 M) and VPA (a histone deacetylase inhibitor, 1 mM).

Half of the neuronal differentiation medium was replaced every 2-3 days. Eighteen DPI, the medium was replaced with neuronal medium supplemented with only the growth factors until the end of the conversion. The medium was changed every 2-3 days for a further 10 days. We followed up the conversion process by taking pictures every 2-3 days using a Leica DMi1 brightfield microscope (Leica Microsystems GmbH, Wetzlar, Germany).

Neuronal cells were identified by the expression of Tau or Neural cell adhesion molecule (NCAM). DAPI+ and Tau+/NCAM+ cells were considered iNs. Conversion efficiency was calculated as the number of Tau+ cells over the total number of fibroblasts seeded for conversion. Neuronal purity was calculated as the number of Tau+ cells over the total cells in the plate after reprogramming.

Conversion efficiency and neuronal purity were calculated by using images of each whole well obtained with a CellDiscoverer7 microscope (Zeiss, Oberkochen, Germany) fitted with an Axiocam 506 camera. Whole well images (10x magnification) were acquired in a lineal fashion starting from the left of the well. DAPI+/Tau+ cells per well were quantified using the ImageJ software (NIH).

M-V. Lentivirus production and titration

Lentivirus production

Third-generation lentiviral vectors were generated as previously described[549]. HEK293T cells (derived from the HEK 293 cell line, that expresses a mutant version of the SV40 large T antigen) were used for the transfections. On day one, cells were seeded in T175 flasks with DMEM + Glutamax with 100 mg/mL penicillin/streptomycin and 10% FBS. One batch of cells was considered two T175 flask of HEK293T. When a 75-90% confluency was achieved (25 million cells per flask, approximately), cells were transfected with the packaging plasmids and the transfer vector of interest (all of them were a gift from Malin Parmar's Lab, Lund University, Sweden).

Three packaging plasmids were used:

pMDLg/pRRE: 3rd generation lentiviral packaging plasmid. Contains Gag and Pol.

pRSV-Rev: 3rd generation lentiviral packaging plasmid. Contains Rev.

pMD2.G: VSV-G envelope expressing plasmid.

In a vial, the three packaging plasmids were mixed in the following proportions:

- 7.5 µg pMDLg/pRRE per batch
- 3.9 µg pRSV-Rev per batch
- 5.5 µg pMD2.G per batch

Next, 25 µg of the transfer vector containing the proneural genes *ASCL1*, *BRN2* and the two shRNA sequences against the REST complex was added to the mixture per batch. Finally, 3.5 mL PBS 1X and 126 µL polyethyleneimine (PEI) were added to complete the transfection mix per batch. The mixture was incubated at room temperature (RT) for 15 min. Transfection mix was added to the flasks and mixed with the culture medium by tilting the flask. The cells were incubated for 45 hours.

After that period of time, supernatant of each batch was collected in a 50-mL tube and centrifuged at 800g for 10 min at 4ºC to eliminate cellular debris. Then, the supernatant was filtered through a 0.45 µm pore size filter and transferred to a Beckman ultracentrifugation tube. The supernatant was centrifuged at 65000g for 2 hours at 4°C to collect the lentiviral vectors. After, the supernatant was discarded and the lentiviruses were resuspended in 100 µL PBS 1X. The lentiviruses were leaved overnight (o/n) at 4°C, covered with parafilm. The day after, lentiviruses were aliquoted for titration.

Lentivirus titration

For lentivirus titration, we performed quantitative polymerase chain reaction (qPCR) as previously described by Georgievska et al.[550]. Briefly, 50,000 HEK293T cells per well were seeded in 6-well plates. Every titration needed 3 control wells (only cells, without virus infection), 3 reference wells (cells infected with a GFP-expressing virus, previously titrated by Fluorescence-Activated Cell Sorting [FACS]) and 3 wells for the titration of the new viruses. One aliquot of the produced virus was used for titration. A 1:10 dilution of the virus on PBS 1X was used to infect one well with 3 µL, one well with 10 µL and one well with 30 µL. The same procedure was done with the reference virus. The infected cells were incubated for 72 h.

After the period of infection, the medium was aspirated and the cells were trypsinized in order to extract their DNA, using the Qiagen DNeasy Blood and tissue kit (Qiagen, Hilden, Germany).

After DNA quantification, virus titration was performed using qPCR with Taqman probes, since the transfer vector possessed a known sequence, the Woodchuck Hepatitis Virus Posttranscriptional Regulatory Element (WPRE). The expression of WPRE was normalized to Albumin (AL) gene (cellular gene). The sequences of the primers and the probes were the following:

AL Forward Primer (FP): 5'-TGAAACATACGTTCCCAAAGAGTTT-3'
AL Reverse Primer (RP): 5'-CTCTCCTTCTCAGAAAGTGTGCATAT-3'
AL probe:5'Fam-TGCTGAAACATTCACCTTCCATGCAGA-Tamra-3'

WPRE FP: 5'-GGCACTGACAATTCCGTGGT-3'
WPRE RP: 5'-AGGGACGTAGCAGAAGGACG-3'
WPRE probe: 5'Fam-ACGTCCTTTCCATGGCTGCTCGC -Tamra-3'

The program of qPCR was the following:
1X 95ºC
1X 50ºC
45X 60ºC
1X 4ºC

Virus titration ranged from 5E+08 to 2E+09.

M-VI. Treatments

During the conduction of this thesis, both fibroblasts and transmitochondrial cybrids were used to test the effect of different drugs (100 µM CoQ and 100 nM rapamycin) on pathophysiology. iNs were exposed to 1 µM of a water-soluble stock solution of MSE 2001, Guttaquinon CoQ_{10} (MSE Pharmazeutika GmbH, Bad Homburg, Germany) due to the harmful effects of ethanol. Non-confluent fibroblast cultures, iNs and cybrid cells were exposed to these drugs at 37°C and 5% CO_2 during 72 hours. The pharmacological blockage of autophagy and mitophagy flux was achieved with 100 nM bafilomycin A1 during 6 or 12 hours before collecting the cells. The pharmacological induction of mitophagy was achieved with 50 µM CCCP supplementation for 2 hours before the flow-cytometry assay. In cybrids, to make more evident the mitochondrial defects and discard compensatory effects by other pathways, during treatments they were cultured in an oxidative medium (DMEM no glucose supplemented with 0.25 g glucose/L, 0.75 g galactose/L, 5 mM sodium pyruvate, 50 µg/mL uridine, 2 mM glutamine, 100 mg/mL penicillin/streptomycin and 5% FBS).

M-VII. Measurement of heteroplasmy load

Heteroplasmy load was determined by mismatched PCR-Restriction fragment length polymorphism (RFLP) analysis as previously described[187]. Genomic DNA extraction from fibroblasts, cybrids and iNs was performed using the Qiagen DNeasy Blood and tissue kit (Qiagen, Hilden, Germany). DNA was quantified using a Nanodrop™ instrument (Savant SPD111V, Thermo Scientific). To detect the A8344G MERRF mutation, DNA amplification was performed by using reverse primer 5'-GGGGCATTTCACTGTAAAGAGGTGCCGG-3' (nucleotide positions [np] 8372–8345) (mismatched positions underlined) and forward primer 5'-GTATTTACCCTATAGCACCCCCTCTAC-3' (np 8255–8281).

PCR conditions for all reactions were 95ºC for 5 min; 33 cycles at 95ºC for 15 s, at 55ºC for 30 s, and at 72ºC for 1 min; finally, at 72ºC for 7 min and a final hold at 4°C. The primers introduced a cleavage site for the enzyme PdiI when there was a G in the position 8344 (mutant mtDNA). After PCR, the amplicon of 92 bp was digested with PdiI (ThermoFisher Scientific, USA) for 10 min at 37°C and 15 min at 65ºC

(inactivation), generating a 79 bp fragment if there was a G in the position 8344. WT and mutant mtDNA fragments were separated in 15% polyacrylamide gel. Gel stained with RedSafe™ Nucleic Acid Staining Solution (iNtRON Biotechnology, Inc., Korea) was placed on a Molecular Imager ChemiDoc XRS+ System (Bio-Rad Laboratories Inc., USA) and PCR and digested products were visualized. The bands were analyzed using ImageLab™ software (Bio-Rad Laboratories Inc., USA).

In the case of measuring iNs heteroplasmy, this assay was performed using an enriched fraction (more than 90% of iNs) of the cell culture. Twenty-seven DPI, cells were detached from cultureware using accutase (Gibco) and then, they were seeded in culture plates coated with a combination of polyornithine (P, 15 µg/mL), fibronectin (F, 0.5 ng/µL) and laminin (L, 5 µg/mL) (hereinafter, PFL) with neural late medium and placed in a 37°C incubator with 5% CO_2. The seeding of the iNs in a PFL-coated plate has been observed to increase the purity of the iNs culture up to 95% without the need of a purification step[494]. Neuronal purity of reseeded iNs population was confirmed by immunostaining with anti-Tau antibody.

M-VIII. Measurement of mitochondrial generation of superoxide

During oxidative phosphorylation, superoxide anion is produced in the mitochondria as an incidental product[551,552]. In fact, mitochondria are considered the major intracellular source of ROS.

It is known that disruption of the OXPHOS system is the main cause of pathogenicity in mitochondrial diseases since it causes accumulation of ROS[553], being superoxide anion the most predominant in mitochondria.

Therefore, flow cytometric analysis of the mitochondrial generation of ROS was performed by using MitoSOX™ Red mitochondrial superoxide indicator (Invitrogen/Molecular Probes, Eugene, OR, USA), which is a fluorogenic dye for selective detection of superoxide in the mitochondria of live cells. MitoSOX™ Red dye permeates live cells and targets the mitochondria, where is exclusively oxidized by superoxide and exhibits red fluorescence.

Fibroblasts and cybrid cells were cultured in 12-well plates and, at 80% confluence, incubated with 5 µM MitoSOX™ Red prepared in HBSS for 15 minutes at 37°C and

5% CO_2. After incubation, cells were harvested by trypsinization, washed with HBSS 1X and analyzed by flow cytometry (FACScalibur™, BD Biosciences, San Jose, CA, USA). Results were expressed as mean ± SD.

M-IX. Measurement of intracellular generation of ROS

Cell permeant indicators for ROS, such as derivatives of reduced fluorescein, are widely used to estimate the accumulation of general intracellular ROS in live cells. Reduced forms of 2′,7′-di-chlorofluorescein (DCF) are nonfluorescent until the acetate groups are removed by intracellular esterases and oxidation occurs within the cell[554-556]. Therefore, oxidation of these probes can be detected by monitoring the increase in fluorescence using excitation sources and filters appropriate for fluorescein (FITC)[557,558].

During the conduction of this thesis, ROS accumulation in control and MERRF iNs was measured using a derivative of reduced DCF with a thiol-reactive chloromethyl group (CM-H_2DCFDA), that allow for covalent binding to intracellular components, permitting even longer retention within the cell.

iNs generated from fibroblasts were incubated with mouse anti-human CD56 (1:100) (anti-NCAM; BD Biosciences) for 1 h at 37ºC, with goat anti-mouse Alexa Fluor® 555 (1:300) for 1 h at 37ºC, with CM-H_2DCFDA 20 μM for 20 min at 37ºC and with 2 μg/mL of Hoechst 33342 for 5 min at RT. The cells were washed and analyzed by DeltaVision system (Applied Precision; Issaquah, WA, USA) with an Olympus IX-71 microscope. The fluorescence of CM-H_2DCFDA from NCAM+ cells was measured to compare the relative ROS levels.

M-X. Mitochondrial membrane potential determination

To estimate ΔΨm, control and MERRF fibroblasts and cybrids were exposed to 0.5 μM JC-1 (Molecular Probes; Invitrogen, Carlsbad, CA, USA). Approximately 1×10^6 cells were trypsinized, incubated with JC-1 for 20 min at 37 °C, washed twice with PBS, resuspended in 500 μL of PBS and analyzed by flow cytometry. As a control for ΔΨm depolarization, a sample was treated for 4 h with 10 μM of the uncoupling agent CCCP before labelling with JC-1.

JC-1 was excited with the 488-nm argon laser. The fluorescence signals of JC-1 monomers and aggregates were detected through the FL1 (525 ± 5 nm band pass filter) and FL2 channels (575 ± 5 nm band pass filter), respectively.

To confirm the results of the JC-1 assays, cells were loaded with 100 nM MitoTracker™ Red CMXRos for 45 min at 37ºC and immunostaining was performed. Samples were analyzed using DeltaVision system (Applied Precision; Issaquah, WA, USA) with an Olympus IX-71 microscope.

In the case of control and MERRF iNs, cells were incubated in neuronal medium with 100 nM MitoTracker™ Red CMXRos for 45 min at 37ºC. When indicated, cells were previously treated with DMSO (vehicle control) or 10 μM CCCP (negative control) for 4 h. After washing with PBS 1X, iNs were fixed in 4% paraformaldehyde (PFA) for 10 min at RT and permeabilized with 0.1% Triton X-100 for 10 min. Cells were blocked in 5% donkey serum for 60 min at RT and were incubated with mouse anti-Tau (1:500) and, when convenient, with sheep anti-cytochrome-c (1:100) or rabbit anti-Hsp60 (1:200) o/n at 4ºC. The day after, cells were incubated with Cy2 anti-mouse antibody (1:200) and, when convenient, with Alexa Fluor® 647 anti-sheep antibody (1:200) or Alexa Fluor® 647 anti-rabbit antibody (1:200) for 2 hours at RT. After washing twice with PBS 1X, nuclei were stained with DAPI (1 μg/mL) for 15 min at RT. The cells were washed and analyzed using DeltaVision system (Applied Precision; Issaquah, WA, USA) with an Olympus IX-71 microscope and a Nikon eclipse Ti microscope equipped with Plan Apo VC 60x/1.4 objective and a A1R scanner (Nikon, Garden City, NY), using a pinhole of 1.2 airy unit. The fluorescence of MitoTracker™ Red CMXRos from Tau+ cells was measured to compare the relative ΔΨm.

M-XI. Immunoblotting assay

Western blotting was performed by using standard methods. Samples were lysed using RIPA buffer [50 mM Tris-HCl, 150 mM sodium chloride, 1% Triton X-100, 0.5% sodium deoxycholate, 0.1% SDS, pH 8.0] and for cytoplasmic proteins after subfractionation by using a subfractionation buffer [250 mM sucrose, 10 mM Tris, 1 mM EDTA, pH 7.4]. Proteins were quantified by using a Lowry based assay[559] (DC Protein Assay Kit, Bio-Rad, USA) and separated in 12% acrylamide/bisacrylamide SDS-PAGE gels (TGX Stain-Free™ FastCast™ Acrylamide Kit, Bio-Rad, USA), at

120 V in running buffer TGS (25 mM Tris, 190 mM glycine, 0.1% SDS, pH 8.3). After running, gels photoactivation using ChemiDoc™ XRS+ Imaging System was performed to check the running quality. This step allowed the immediate visualization of proteins at any point during electrophoresis and blotting.

Transference of proteins to 0.45 µm nitrocellulose membranes (Hybond-ECL, Amerscham Biosciences) was performed with a Trans-Blot Turbo system (Bio-Rad, USA) at 25 V for 10 minutes using Trans-Blot Turbo transfer buffer (TG). After transference, visualization of proteins was performed using the Stain-free imaging technology.

Blocking step was performed with 5% BSA in 0.05% T-TBS (blocking buffer) at RT for 1 hour. Membranes were incubated with primary antibody at the appropriate dilution (1:500-1:1000) in blocking buffer with gentle agitation o/n at 4°C. Three washes with 0.05% T-TBS were performed to remove the unbound antibody. Then, species-appropriate HRP-conjugated secondary antibodies (1:2500) in blocking buffer were used to detect the protein of interest with gentle agitation for 2 hours at RT. Finally, three washes more were performed with 0.05% T-TBS and proteins of interest were identified using the Clarity Western ECL Substrate (Bio-Rad, USA). ChemiDoc™ XRS+ Imaging System was used to visualize signals in membranes.

M-XII. Cell fractionation and isolation of mitochondrial proteins

Cells were harvested and homogenized using a fractionation buffer containing 250 mM sucrose, 10 mM Tris, 1 mM EDTA and proteases inhibitors cocktail, pH 7.4. Cell suspension was passed through a 25-gauge needle 10 times using a 1 mL syringe. Next, nuclei and intact cells were removed by centrifugation at 1500g for 20 min. The supernatant containing intact mitochondria was transferred into a new tube and centrifuged at 12000g for 10 min. Supernatant (“cytosolic fraction”) was transferred into another new tube, and the mitochondria-enriched pellet (“mitochondrial fraction”) was dissolved in RIPA buffer containing a mixture of proteases and phosphatases inhibitors (Roche). Cytosolic fractions were concentrated using Centricon YM-10 devices (Millipore) according to the manufacturer’s instructions. Proteins of the mitochondrial and cytoplasmic fractions were separated by SDS-PAGE.

M-XIII. Immunofluorescence microscopy

Fibroblasts and cybrids were seeded on 24x24 mm glass coverslips (ThermoScientific™ Gold Seal™, Waltham, MA, USA). iNs were grown on ibiTreat µ-Slide 4/8 Well chamber slides (Ibidi Inc., Martinsried, Germany). Cells were rinsed once with PBS, fixed in 4% PFA for 10 min at RT, washed twice with PBS and permeabilized with Triton X-100 0.1% for 10 min. For immunostaining, cells were incubated with 5% donkey serum (blocking solution) for 1 hour at RT. After, cells were incubated with primary antibodies diluted 1:100-1:500 in blocking solution o/n 4ºC. After two washes with PBS, secondary antibodies were diluted 1:200 in blocking solution and added on the cells. The samples were incubated for 2 h at 37°C. Cells were then washed with PBS, incubated for 20 min with DAPI (1 µg/mL) and washed twice with PBS. Finally, the coverslips were mounted onto microscope slides using Vectashield Mounting Medium (Vector Laboratories, Burlin-game, CA, USA) and the cells were analyzed using a DeltaVision system (Applied Precision; Issaquah, WA, USA) with an Olympus IX-71 fluorescence microscope and/or a Nikon eclipse Ti microscope equipped with Plan Apo VC 60x/1.4 objective and a A1R scanner (Nikon, Garden City, NY), using a pinhole of 1.2 airy unit.

Deconvolution studies and 3D projections were performed using a DeltaVision system (Applied Precision; Issaquah, WA, USA).

M-XIV. Proliferation assay

Fibroblasts were seeded in 12-well plates. Several pictures of different 10X-fields were taken by using a Leica DMi1 brightfield microscope (Leica Microsystems GmbH, Wetzlar, Germany). Cells were counted by using ImageJ software (NIH) before and after CoQ treatment in order to analyze cell growth. To measure proliferation rate, a known initial number of cells (N0) was seeded and after treatment, cells were harvested and quantified (N) by using a TC10^{TM} Automated Cell Counter (Bio-Rad). Cell viability was assessed by trypan blue exclusion.

Proliferation rate (n) was calculated by using the formula $n = Log_2 (N/N0)$, starting from $N=N0x2^n$. Results were expressed as mean ± SD.

M-XV. Cell area measurement

Increase in cell size has been considered one of the evidences of aging fibroblasts in culture[560]. Control and MERRF fibroblasts were treated with 100 μM CoQ for 72 h and cell areas were quantified by ImageJ (NIH) software. More than 150 cells (50 cells per experiment, randomly selected) were measured in three independent experiments. Results were expressed as mean ± SD.

M-XVI. Determination of LC3B puncta as an autophagy marker

Fibroblasts or iNs generated from fibroblasts were fixed in 4% PFA for 10 min at RT and permeabilized with 0.1% Triton X-100 for 10 min. Cells were blocked in 5% donkey serum for 60 min at RT and were incubated with the primary antibodies rabbit anti-LC3B (1:100) and mouse anti-Tau (1:500) in the case of iNs o/n at 4°C. Respective secondary antibodies, Cy2 anti-mouse antibody (Jackson ImmunoResearch Laboratories, West Grove, PA, USA) and Alexa Fluor® 555 anti-rabbit antibody (ThermoFisher Scientific, Waltham, MA, USA) were diluted 1:300 and cells were incubated for 2 h at 37°C. Finally, cells were incubated for 20 min with DAPI (1 μg/mL) and washed with PBS 1X (3 times 5 min). LC3B puncta were analyzed to compare the relative autophagy activation using a DeltaVision system (Applied Precision; Issaquah, WA, USA) with an Olympus IX-71 microscope and a Nikon eclipse Ti microscope equipped with Plan Apo VC 60x/1.4 objective and a A1R scanner (Nikon, Garden City, NY), using a pinhole of 1.2 airy unit. LC3B puncta per cell were quantified using Spot Counter macro, designed to count fluorescent spots in images stacks. In the case of iNs, only LC3B puncta from Tau+ cells were analyzed to compare the relative autophagy activation. Moreover, in order to evaluate autophagy flux, Control 1 and MERRF 1 iNs were treated with DMSO (vehicle control) or 100 nM Bafilomycin A1 for 6 h before immunostaining.

M-XVII. Mitophagy analysis

Fibroblasts, cybrids and iNs generated from fibroblasts were fixed in 4% PFA for 10 min at RT and permeabilized with 0.1% Triton X-100 for 10 min. Then, mitophagy analysis was performed by standard immunofluorescence techniques by using LC3B

(autophagosome marker), Tau (neuronal marker for iNs) and MitoTracker™ Deep Red (mitochondrial selective probe, well retained in both polarized and depolarized mitochondria[561,562]) or cytochrome c (mitochondrial marker). Colocalized signal of LC3B/Mitotracker™ Deep Red or LC3B/cytochrome c was assessed by using DeltaVision system (Applied Precision; Issaquah, WA, USA) with an Olympus IX-71 microscope and calculating the Pearson's coefficient of correlation. In the case of iNs, only colocalized signal of LC3B/MitoTracker™ Deep Red from Tau+ cells was measured. Positive puncta (positive LC3B/MitoTracker™ Deep Red or LC3/cytochrome c) were considered when Pearson's coefficients of correlation were higher than 0.75. To quantify LC3B/MitoTracker™ Deep Red or LC3B/cytochrome c puncta, the Red and Green Puncta Colocalization ImageJ macro developed by Ruben K. Dagda et al.[563] was used. Mitophagic cells were scored when more of 5 puncta were observed per cell. Results were expressed as mean ± SD of three separate experiments.

To study the presence or absence of Parkin-mediated mitophagy activation, a standard immunofluorescence was performed by using Parkin and MitoTracker™ Red CMXRos, cytochrome c or COXIV (mitochondrial markers).
Colocalized signal of Parkin/MitoTracker™ Red CMXRos, Parkin/cytochrome c or Parkin/COXIV was assessed by using DeltaVision system (Applied Precision; Issaquah, WA, USA) with an Olympus IX-71 microscope and calculating the Pearson's coefficient of correlation. Positive puncta (positive Parkin/MitoTracker™ Red, Parkin/cytochrome c or Parkin/COXIV) were considered when Pearson's coefficients of correlation were higher than 0.75. To quantify colocalized puncta per cell, the Red and Green Puncta Colocalization ImageJ macro developed by Ruben K. Dagda et al.[563] was used.

M-XVIII. Mitophagy flux analysis

Mitophagy flux of control and MERRF fibroblasts was assessed using the method of Mauro-Lizcano et al.[128]. Cells were seeded in 12-well plates. When 70% confluency was reached, cells were treated with 50 μM CCCP for 2 hours (as a positive control) or with 100 μM CoQ for 72 h. The pharmacological inhibition of autophagy flux was achieved with 100 nM bafilomycin A1 supplementation for 12 h before trypsinizing

the cells. After these treatments, cells were trypsinized for 5 min at 37ºC and resuspended in complete medium containing 10 nM MitoTracker™ Deep Red (Invitrogen) and then incubated for 30 min at 37ºC.

The fluorescence signal of MitoTracker™ Deep Red (10,000 cells) was detected using flow cytometer BD FACSAria through the APC-A (660/20) channel.

Mitophagy flux was defined as the ratio of fluorescence in the presence of bafilomycin A1 (lysosomal inhibitor) to that in the absence of bafilomycin A1, normalized to the corresponding value in control cells.

M-XIX. Assessment of protein carbonylation by western blotting

Proteins are one of the major targets of oxygen free radicals and other reactive species. Oxidative modification of proteins modifies the side chains of methionine, histidine and tyrosine, and forms cysteine disulfide bonds[564,565]. Metal catalyzed oxidation of proteins introduces carbonyl groups (aldehydes and ketones) at lysine, arginine, proline or threonine residues in a site-specific manner[566,567].

The oxidative modification of proteins can modulate their enzymatic activity[568], DNA binding activities of transcription factors[569] and the susceptibility to proteolytic degradation[570,571]. This fact suggests the importance of oxidative modification of individual proteins in the pathophysiology of diseases that undergo free radical mediated processes, such as mitochondrial diseases.

Therefore, the detection of oxidatively modified proteins by immunoblotting was performed by using OxyBlot™ Protein Oxidation Detection Kit (Millipore, USA), which provides a sensitive methodology for detection and quantification of proteins modified by oxygen free radicals and other reactive species by detecting carbonyl groups (hallmark of the oxidation status of proteins).

Protein carbonyl groups were measured following the protocol provided by the manufacturer. Proteins (5 µg) were incubated with 2,4-dinitrophenylhydrazine (DNPH) to form the 2,4-dinitrophenyl (DNP) hydrazine derivatives by derivatization of carbonyl groups. The DNP-derivatized protein samples were separated by SDS-PAGE and blotted to nitrocellulose membranes. DNP-containing proteins were then immunostained using rabbit anti-DNP antiserum (1:150) and goat anti-rabbit IgG

conjugated to HRP (1:300). Carbonylated proteins were identified using the Clarity Western ECL Substrate (Bio-Rad, USA). ChemiDoc™ XRS+ Imaging System was used to visualize signals in membranes.

M-XX. Analysis of mitochondrial network and morphology

Fibroblasts, cybrids and iNs generated from fibroblasts were incubated with 100 nM MitoTracker™ Red CMXRos for 45 min at 37ºC. After washing with PBS 1X, cells were fixed in 4% PFA for 10 min at RT and permeabilized with 0.1% Triton X-100 for 10 min. In the case of iNs, cells were blocked in 5% donkey serum for 60 min at RT and were incubated with mouse anti-Tau (1:500) o/n at 4ºC. The day after, iNs were incubated with Cy2 anti-mouse antibody (1:200) for 2 hours and with DAPI (1 µg/mL) for 15 min at RT. The cells were washed and analyzed using DeltaVision system (Applied Precision; Issaquah, WA, USA) with an Olympus IX-71 microscope. The fluorescence of MitoTracker™ Red CMXRos was measured to compare the relative mitochondrial morphology using ImageJ (NIH) software. In the case of iNs, only the fluorescence of MitoTracker™ Red CMXRos from Tau+ cells was measured.

Mitochondrial morphology was evaluated using the image processing package Fiji (ImageJ) by the method described by Merrill et al.[572]. Briefly, raw images were preprocessed to remove the background and noise and then they were binarised, thresholded and skeletonized to better detect mitochondria using another ImageJ macro previously described by Merrill et al. When the images were cleaned up, we used the morphometry macro to measure four different parameters of mitochondrial shape (aspect ratio, form factor, area-weighted form factor and length).

Aspect ratio: It is defined as the ratio of the major and short axis of an ellipse fit to an object (mitochondria). It has a minimum value of 1 that indicates a perfect circle, and aspect ratio increases as mitochondria elongates and become more elliptical.

Form factor (ff): It describes mitochondria's shape complexity (0-1). A form factor value of 0 corresponds to a circular, unbranched mitochondrion, and higher ff values indicate longer, more branched mitochondria.

Area-weighted form factor: Variant of form factor that takes into account the mitochondrial network. This parameter averages across the region of interest (ROI) with a bias towards larger mitochondria or mitochondrial networks. It is calculated as the product of the mitochondrial network area and the form factor.

Length: It indicates the average length (number of microns) of the mitochondrial network.

M-XXI. Electron microscopy

Electron microscopy was performed using a protocol previously described[221]. Fibroblasts were fixed for 15 min in the culture plates with 2% glutaraldehyde in culture medium and then for 30 minutes in Buffer A (2% glutaraldehyde, 0.1 M Na Cacodylate/HCl, pH 7.4). Cells were then washed three times with Buffer B (0.2 M Na Cacodylate/HCl, pH 7.4) for 10 minutes and then post-fixed with Buffer C (1% OsO4, 0.15 M NaCacodylate/HCl, pH 7.4) for 30 minutes. After dehydration in increasing concentrations of ethanol, 5 min for each step: 30, 50, 70 and 95%, impregnation steps and inclusion were performed in Epon and finally polymerized at 60°C for 48 hours. 60–80 nm sections were obtained using an ultramicrotome RMC-MTX (Tucson, Arizona, USA), and contrasted with uranyl acetate and lead citrate. Observations were performed on a Philips CM-10 transmission electron microscope. For quantification of autophagic vesicles per μm^2 of cytoplasm, the number of autophagosomes and autophagolysosomes were scored in 50 cells. Data were presented as mean ± SD.

M-XXII. Characterization of iNs: areas, perimeters and neurites features

Imaging of DAPI+/Tau+ control and MERRF cells was performed using the DeltaVision system (Applied Precision; Issaquah, WA, USA) with an Olympus IX-71 inverted microscope hosting a 60x objective (1.42, oil). Control and MERRF iNs (DAPI+/Tau+ cells) neurites structures, total areas, body areas and perimeters were observed and/or quantified by ImageJ (NIH) software. Characterization and measurement of number and length of neurites of Tau+ cells was assessed using Simple Neurite Tracer (SNT), a free software plugin distributed by Fiji-ImageJ that was developed by Longair et al.[573]. More than 150 cells (50 cells per experiment, randomly selected) were analyzed in three independent experiments.

M-XXIII. Parkin silencing

Inhibition of Parkin expression in MERRF cybrids was performed using Parkin shRNA (h) Lentiviral Particles (Santa Cruz, CA, USA), which is a pool of viral particles containing 3 target-specific constructs that encode 19-25 nt (plus hairpin) shRNA designed to knock down *PARK2* gene expression. As a negative control for the different experiments using Parkin shRNA Lentiviral Particles, we used control shRNA Lentiviral Particles, that contain a shRNA construct encoding a scrambled sequence that does not lead to the specific degradation of any known cellular mRNA. MERRF cybrids were infected with Parkin shRNA (shParkin) Lentiviral Particles or control scrambled lentiviral particles (shControl) according to the manufacturer's instructions. Cells were seeded in a 12-well plate for 24 h before the viral infection. Cells were grown to ~50% confluence and then were transduced. Stable clones expressing the shRNA were selected by incubating cells with a mixture of complete medium with puromycin hydrochloride 2 μg/μL (Santa Cruz, CA, USA). Next, the medium was replaced with fresh puromycin-containing medium every 3 to 4 days until resistant colonies were identified. Colonies were expanded and assayed for Parkin protein expression and the subsequent experiments.

M-XXIV. Apoptotic cells quantification

Quantification of apoptotic cells was assessed by fluorescence microscopy analysis, analyzing nuclear fragmentation (*blebbing*) by using DAPI staining, caspase 3 activation and apoptotic microtubule network (AMN) formation. At least ten pictures of different 60x-fields were randomly taken for quantification in all cases. Samples were visualized using a DeltaVision system (Applied Precision; Issaquah, WA, USA) with an Olympus IX-71 microscope.

M-XXV. Microscopy

Widefield microscopy was performed using:

- Leica DMi1 brightfield microscope (Leica Microsystems GmbH, Wetzlar, Germany), fitted with a camera Leica DFC350 FX, with image capture and analysis performed using a Leica Application Suite software.

Fluorescence microscopy was performed using:

- DeltaVision system (Applied Precision; Issaquah, WA, USA) with an Olympus IX-71 microscope.
- CellDiscoverer7 microscope (Zeiss, Oberkochen, Germany) fitted with an Axiocam 506 camera, with image capture and analysis performed using a ZEN software.

Confocal microscopy was performed using:

- Nikon eclipse Ti microscope equipped with Plan Apo VC 60x/1.4 objective and a A1R scanner (Nikon, Garden City, NY), with image capture and analysis performed using a NIS-Elements C software.

M-XXVI. Assessment of mitochondrial respiratory function using Seahorse extracellular flux analyzer.

Mitochondrial respiratory function and profile of controls and MERRF fibroblasts, cybrids and iNs were measured by using Mito-stress test assay by XFe24 extracellular flux analyzer (Seahorse Bioscience, Billerica, MA, USA). The optimal seeding density was determined to be 15,000 cells/well in the case of fibroblasts; 30,000 cells/well in the case of cybrids and 35,000 cells/well in the case of iNs. The optimal concentrations of the injection compounds were determined to be 1 µM oligomycin, 2 µM FCCP and 1 µM and 2.5 µM rotenone & antimycin A, respectively.

Fibroblasts and cybrids were seeded in XFe24 cell culture plates in 100 µL growth medium and placed in 37°C incubator with 5% CO_2. After cells adhered within 1 h, 150 µL growth medium were added and cells were returned to 37°C incubator with 5% CO_2.

In the case of iNs, twenty-seven DPI, cells were detached from cultureware using accutase (Gibco) and they were seeded in XF24 cell culture plates coated with PFL in 100 µL of neural late medium and placed in 37°C incubator with 5% CO_2. After cells adhered within 1 h, 150 µL of culture medium were added and the cells were returned to 37°C incubator with 5% CO_2.

After 24 h incubation, growth medium or neural late medium from each well was removed, leaving 50 µL of media. Cells were washed twice with 500 µL of pre-warmed assay medium (XF base medium supplemented with 10 mM glucose, 1 mM

glutamine and 1 mM sodium pyruvate; pH 7.4). Then, 450 µL of assay medium (500 µL final) were added.

Cells were incubated in 37°C incubator without CO_2 for 1 h to allow pre-equilibration with the assay medium. Pre-warmed oligomycin, FCCP and rotenone & antimycin A were loaded into the injector ports A, B and C of sensor cartridge, respectively. The final concentrations of injections were as follows: 1 µM oligomycin, 2 µM FCCP and 1 µM rotenone & 2.5 µM antimycin A.

The cartridge was calibrated by the XFe24 analyzer and the assay was carried out using cell Mito-stress test assay protocol as described by Nicholls et al.[574]. In the case of fibroblasts and cybrids, protein quantification of each well was performed when the experiment was finished.

In the case of iNs, cell number and neuronal purity of each well was calculated by performing a double staining with DAPI/Tau when the experiment was finished.

Oxygen consumption rate (OCR) and extracellular acidification rate (ECAR) were measured followed by the sequential addition of oligomycin, FCCP and rotenone & antimycin A. This approach allows to determine different parameters of mitochondrial function such as basal respiration, maximal respiration, spare respiratory capacity and ATP production.

Basal respiration: Measurement of the cells' relative utilization of mitochondrial respiration under resting conditions. It is calculated as the value of the last rate measurement before oligomycin injection minus the non-mitochondrial respiration rate.

Maximal respiration: Measurement of the cells' relative utilization of mitochondrial respiration and glycolysis when stressed. It is calculated as the value of the maximum rate measurement after FCCP injection minus the non-mitochondrial respiration rate.

Spare respiratory capacity: Measurement of the cells' ability to respond to an energetic demand. It is an indicator of cell fitness or flexibility. It is calculated as the value of the maximal respiration minus the basal respiration.

ATP-linked respiration: Measurement of the cells' oxygen consumption coupled to ATP production. It is calculated as the value of the last rate measurement before oligomycin injection minus the minimum rate measurement after oligomycin injection.

M-XXVII. Data analysis of Seahorse assays

The XF Mito-stress test report generator automatically calculates the XF Mito-stress test parameters from Wave data that have been exported to Excel. Respiration and acidification rates are presented as the mean ± SD of 3 independent experiments in all experiments performed with 4 replicate wells in the Seahorse XFe24 analyzer. Significance level was determined by performing ANOVA on the complete data set with Tukey's post-hoc testing. The results were considered significant at $P<0.05$.

M-XXVIII. Electrophysiological recordings

Somatic whole-cell patch-clamp recordings were made from iNs after 27 and 60-80 DPI. Individual coverslips were placed in the recording chamber perfused at a flow-rate of 3 mL/min with salt solution consisting of 124 mM NaCl, 2.69 mM KCl, 1.25 mM KH_2PO_4, 2 mM $MgSO_4$, 1.8 mM $CaCl_2$, 26 mM $NaHCO_3$, and 10 mM glucose (pH 7.2, 300 mOsm) (bubbled with 95% O_2, 5% CO_2), at RT (22–25°C). Patch electrodes were made from borosilicate glass and had a resistance of 4–7 MΩ when filled with 120 mM CsCl, 8 mM NaCl, 1 mM $MgCl_2$, 0.2 mM $CaCl_2$, 10 mM HEPES, 2 mM EGTA and 20 mM QX-314 (pH 7.2, 290 mOsm). Current-clamp recordings were performed with a Multiclamp 700B amplifier (Molecular Devices, Foster City, CA, USA). Data were filtered at 4 kHz, digitized at 10 kHz, and stored on a computer using pClamp software (Molecular Devices). Axon pCLAMP software was used to generate command signals and to collect data.

M-XXIX. Statistical analysis

All results are expressed as mean ± SD of the mean, unless stated otherwise. The samples were assumed to come from a Normal distribution. Multiple groups were compared using a one-way ANOVA. Bonferroni post-hoc testing was employed after ANOVA for testing for significant differences between groups. In case of only two groups, they were compared using a Student's t-test with a Welch's correction. Statistical analyses were conducted using the GraphPad Prism 7.0 (GraphPad Software, San Diego, CA). P-values of less than 0.05 were considered significant. Pearson's coefficient of correlation was calculated in order to evaluate colocalization. Correlation was considered when r values were more than 0.7.

RESULTS

RESULTS

R-I. Characterization of mitochondrial dysfunction in skin fibroblasts derived from a MERRF patient and evaluation of the effect of CoQ treatment.

The fibroblast cellular model has been very efficient to study the molecular mechanisms of mitochondrial diseases and to evaluate the effect of potential treatments that ameliorate pathophysiological alterations of mitochondrial dysfunctions[203,204,219-221,254,415-417]. Although CoQ has been widely used as a therapy for MERRF syndrome, there are no evidences of its efficacy and the molecular mechanisms by which CoQ supplementation ameliorates the clinical symptoms of MERRF patients[259,575,576].

Therefore, in this Results subsection, skin fibroblasts derived from one MERRF patient (hereinafter, MERRF) were used for unravelling the pathophysiological manifestations of the disease and the effects of CoQ treatment. The MERRF fibroblasts harboured the heteroplasmic m.8344A>G mutation. The mutational load of MERRF fibroblasts was quantified by mismatched PCR-RFLP resulting in 54% (**Figure R1**). Skin fibroblasts derived from one healthy volunteer (hereinafter, control) were used as a control of heteroplasmy load. Heteroplasmy loads were continuously followed-up during the conduction of this work to rule out any potential changes in the percentage of mutant mtDNA.

To assess the functional consequences of mitochondrial dysfunction in MERRF fibroblasts and the effect of CoQ supplementation on the pathophysiological manifestations of the disease, several parameters such as proliferation rate, cell area, mitochondrial shape, $\Delta\Psi m$ or ROS levels were analyzed.

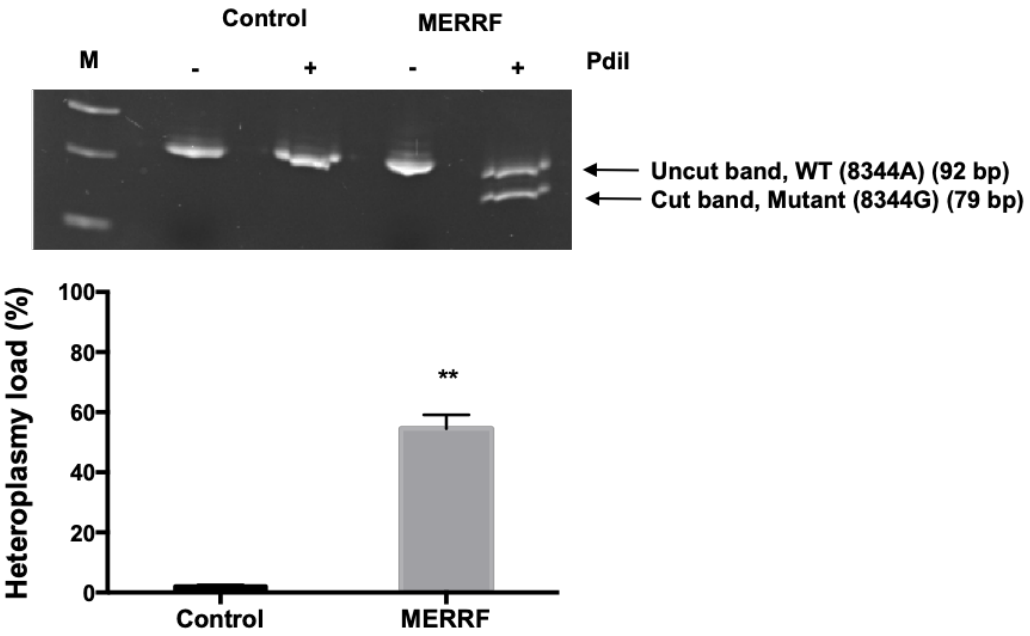

Figure R1. Heteroplasmy load in control and MERRF fibroblasts.
Heteroplasmy loads were determined by mismatched PCR-RFLP assay. Results are expressed as mean ± SD. Significance of MERRF respect to control fibroblasts is represented as **P<0.01.

First, the proliferation assay showed a decreased growth rate by 76.6% in MERRF fibroblasts compared to controls, suggesting a lack of optimum conditions for cell proliferation. Supplementation with CoQ was able to increase MERRF fibroblasts growth rate by 127.3% compared to untreated MERRF fibroblasts (**Figure R2**).

Low proliferation rate has been related with cell size. Aged cells show increased area and less division capacity. Due to this fact, we determined cell size of control and MERRF fibroblasts before and after supplementation with CoQ. Examination of cell morphology by brightfield microscopy revealed that MERRF fibroblasts showed characteristic morphological changes that accompany replicative senescence in cultured cells. The cell size was quantified by determining cell area. This parameter was 2.65-fold higher in MERRF fibroblasts than in controls. Supplementation of CoQ reduced MERRF cells area to control levels (**Figure R3**).

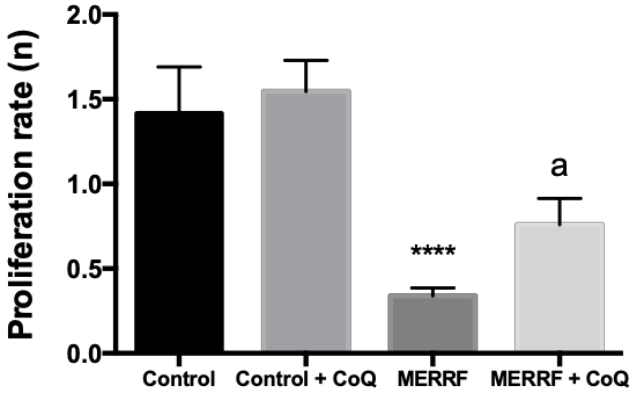

Figure R2. Proliferation rate in untreated and CoQ-treated control and MERRF fibroblasts.

Growth rate of cells without treatment (NT) and treated with CoQ (100 µM) was determined by quantifying the number of cells after 72 hours of incubation, as described in Materials & Methods section. Results are expressed as mean ± SD. Significance of MERRF respect to control fibroblasts is represented as ****P<0.0001. Significance between the presence and the absence of CoQ is represented as ^{a}P<0.05.

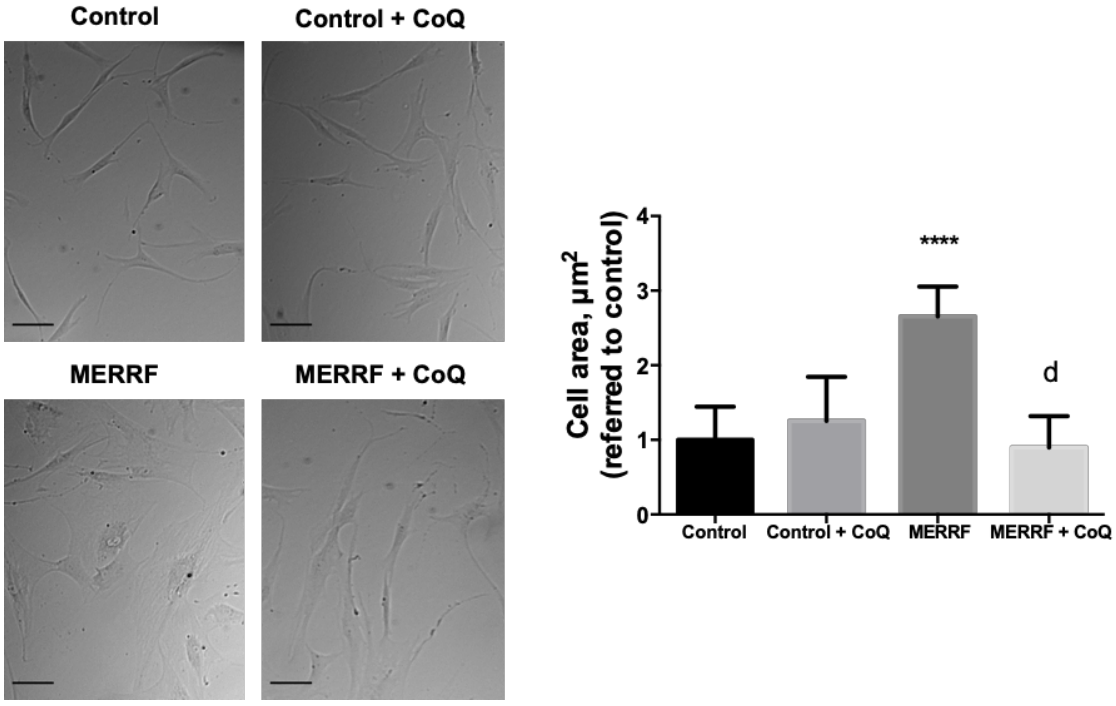

Figure R3. Cell area in untreated and CoQ-treated control and MERRF fibroblasts. Cell area was determined as described in Materials & Methods section. Results are expressed as mean ± SD. Significance of MERRF respect to control fibroblasts is represented as ****P<0.0001. Significance between the presence and the absence of CoQ is represented as ^{d}P<0.0001. [Scale bar = 50 µm].

Low growth rate could easily be associated with defects in the energy production by mitochondria. The complex V or ATP synthase uses the gradient of protons generated from the IS due to the MRC function to generate ATP[14]. Therefore, the assessment of ΔΨm is a good indicator of mitochondrial health, because when some or all MRC complexes are disrupted, ΔΨm is dissipated.

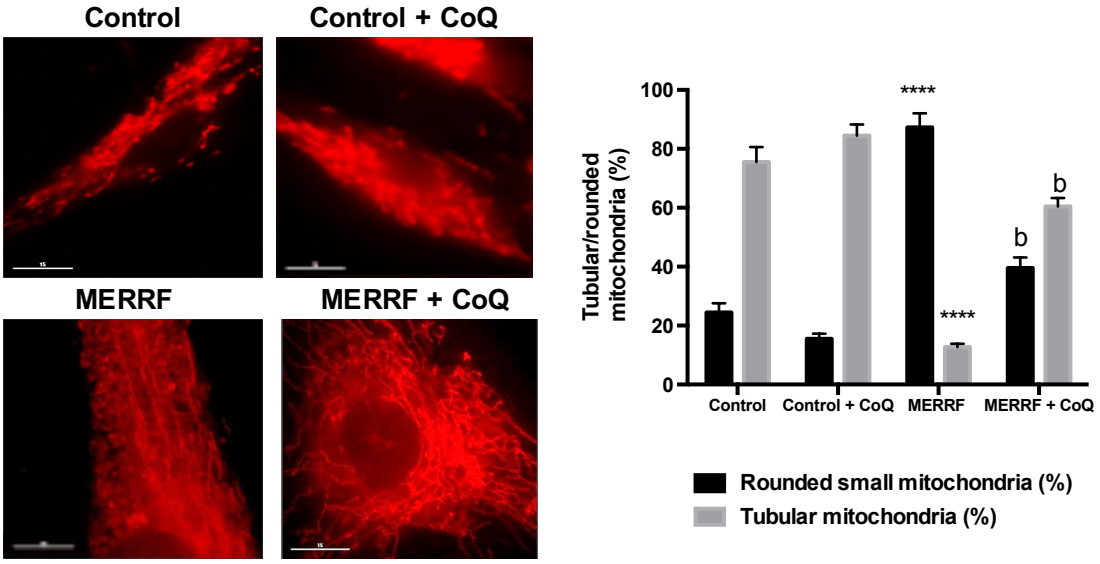

Figure R4. Mitochondrial network morphology assessment in untreated and CoQ-treated control and MERRF fibroblasts.
Tubular and rounded mitochondria were quantified from MitoTracker™ Red CMXRos stained samples as described in the Materials & Methods section. Results are expressed as mean ± SD. Significance of MERRF respect to control fibroblasts is represented as ****P<0.0001. Significance between the presence and the absence of CoQ is represented as ^{b}P<0.01. [Scale bar = 15 μm and 5 μm for MERRF].

For that reason, the ΔΨm of control and MERRF fibroblasts was examined using MitoTracker™ Red CMXRos, a mitochondrion selective dye which is concentrated by active mitochondria in a membrane potential–dependent manner. Staining and imaging analysis revealed discrete staining of mitochondria in control cells, with the mitochondria organized in a tubular network, whilst in MERRF fibroblasts a diffuse staining was observed, indicating reduced mitochondrial uptake of MitoTracker™ Red CMXRos. In addition, the mitochondrial network was fragmented in MERRF fibroblasts, with small rounded mitochondria apparent throughout the cytoplasm. Supplementation with CoQ (100 μM) restored normal mitochondrial morphology and uptake of MitoTracker™ Red CMXRos in MERRF fibroblasts, indicating the

restoration of ΔΨm (**Figure R4**). Additionally, treatment with CoQ partially restored mitochondrial network (**Figure R4 and R5**).

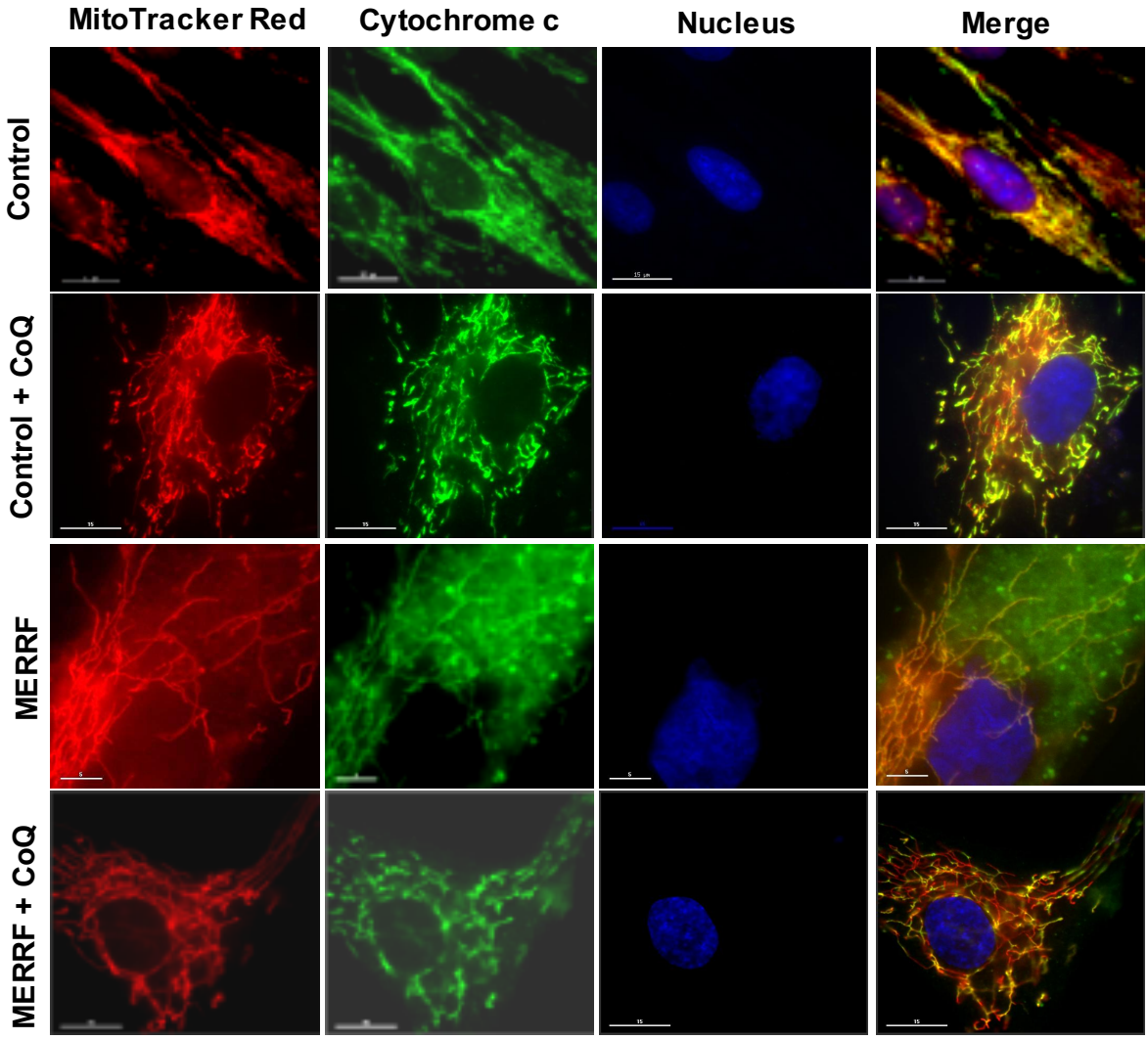

Figure R5. Cytochrome c and MitoTracker™ Red CMXRos staining of mitochondria in untreated and CoQ-treated control and MERRF fibroblasts.
Colocalisation of MitoTracker™ Red CMXRos and cytochrome c signal in mitochondria revealed the specificity of MitoTracker™ to mitochondria. Two relevant populations of mitochondria were found in MERRF fibroblasts; a tubular mitochondrial network with high polarization degree and some smaller, rounded and fragmented mitochondria with low polarization degree. Supplementation with CoQ restored normal mitochondrial network morphology and uptake of MitoTracker™ Red CMXRos in MERRF fibroblasts. [Scale bar = 15 μm and 5 μm for MERRF].

The MitoTracker™ Red CMXRos staining co-localized with cytochrome c, a mitochondrial marker, confirming the specificity of MitoTracker™ staining and verifying that mitochondrial depolarization in MERRF fibroblasts was not a result of cytochrome c release, as occurs in apoptosis[577] (**Figure R5**).

To confirm mitochondrial depolarization in MERRF fibroblasts, cells were stained with JC-1, a fluorescent radiometric probe. The ratio red/green fluorescence was reduced in MERRF fibroblasts and it was significantly improved under CoQ treatment (**Figure R6**).

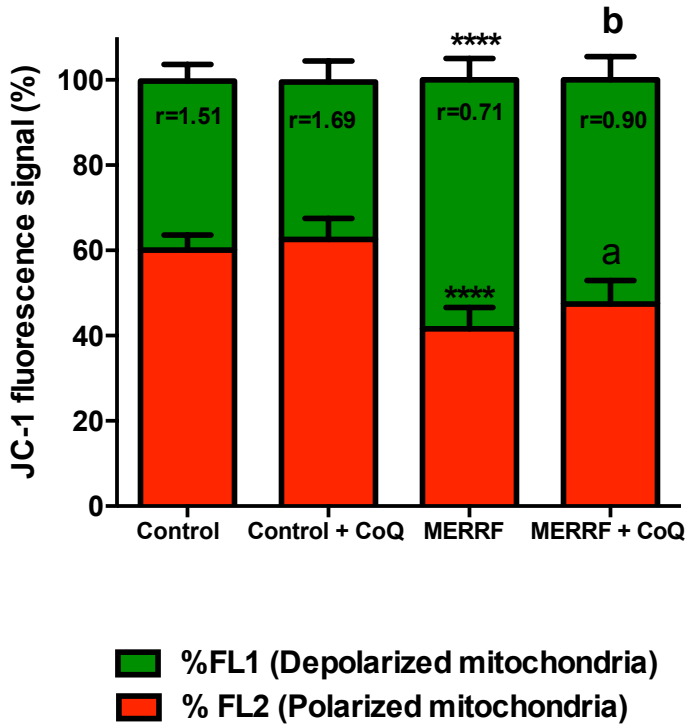

Figure R6. Analysis of mitochondrial membrane potential in untreated and CoQ-treated control and MERRF fibroblasts by using JC-1 as a ratiometric probe. Green and red fluorescence signals were measured by flow cytometry in control and MERRF fibroblasts by using JC-1 as a probe. Whereas green signal (FL1 channel) is associated to JC-1 monomers and dissipated mitochondrial potential, red signal (FL2 channel) represents the aggregated form of JC-1, which indicates the intact mitochondrial membrane potential. The stacked bar graph shows the percentage of main JC-1 fluorescence. Ratio between FL2/FL1 signals was estimated. Significance of MERRF respect to control fibroblasts is represented as ****P<0.0001. Significance between the presence and the absence of CoQ is represented as ^{a}P<0.05 and ^{b}P<0.01.

One of the main causes of mitochondrial depolarization is thought to be the accumulation of high levels of ROS. Therefore, we examined mitochondrial superoxide levels in control and MERRF fibroblasts by flow cytometry by using MitoSOX™ Red, a mitochondrial superoxide fluorescent probe. ROS levels were increased by 2-fold in MERRF fibroblasts and they were significantly decreased by 50% after CoQ treatment (**Figure R7**). These results suggested increased ROS production in MERRF fibroblasts.

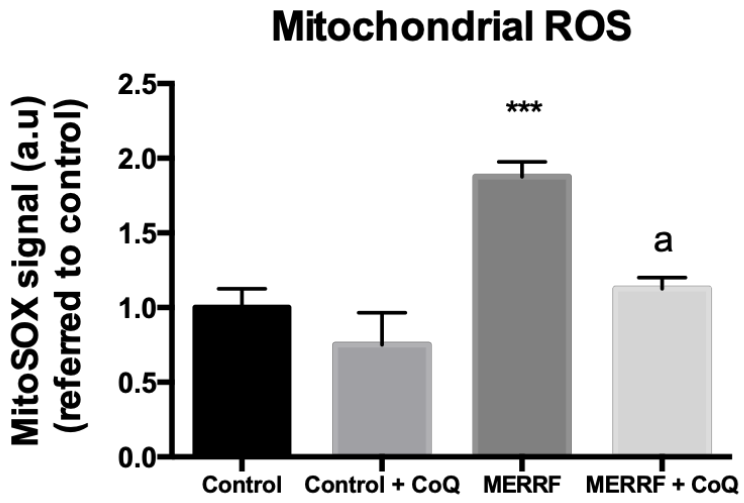

Figure R7. ROS levels in untreated and CoQ-treated control and MERRF fibroblasts.

ROS levels were quantified by using MitoSOX™ as a sensor. Flow cytometry signal is represented as mean fluorescence intensity ± SD (a.u; arbitrary units) of three independent experiments. Significance of MERRF respect to control fibroblasts is represented as $^{***}P<0.001$. Significance between the presence and the absence of CoQ is represented as $^{a}P<0.05$.

Given that mitochondrial ROS levels were elevated in MERRF fibroblasts, we wanted to determine the general cellular oxidative status in control and MERRF fibroblasts and its relationship with CoQ treatment by quantifying the content of carbonylated proteins in cellular extracts by using OxyBlot™ Protein Oxidation Detection Kit (Millipore, USA). The results confirmed that MERRF fibroblasts showed increased carbonylated proteins levels compared to control cells and that CoQ treatment was able to reduce carbonylated proteins in MERRF fibroblasts (**Figure R8**).

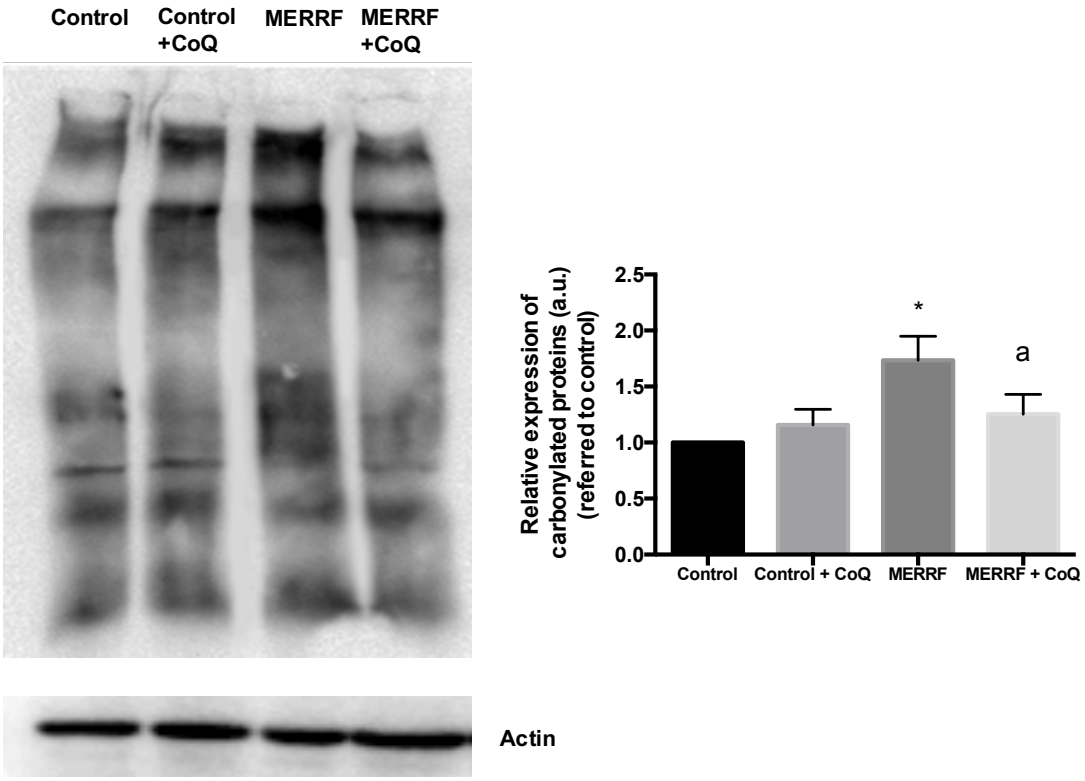

Figure R8. Levels of carbonylated proteins in untreated and CoQ-treated control and MERRF fibroblasts.
Cellular extracts were assayed by the OxyBlot™ Protein Oxidation Detection Kit. One representative of three independent experiments is shown. Carbonylated proteins levels quantification was performed as described in Materials & Methods section. Significance of MERRF respect to control fibroblasts is represented as *P<0.05 Significance between the presence and the absence of CoQ is represented as [a]P<0.05.

Two of the main features in MERRF syndrome are the reduction in mitochondrial proteins synthesis and complex IV deficiency[351,352].

Therefore, we next analyzed mitochondrial proteins expression levels in control and MERRF fibroblasts by immunoblotting. As shown in **Figure R9**, MERRF cells showed decreased mitochondrial proteins expression levels, and CoQ treatment was able to increase the amount of mitochondrial proteins to control levels.

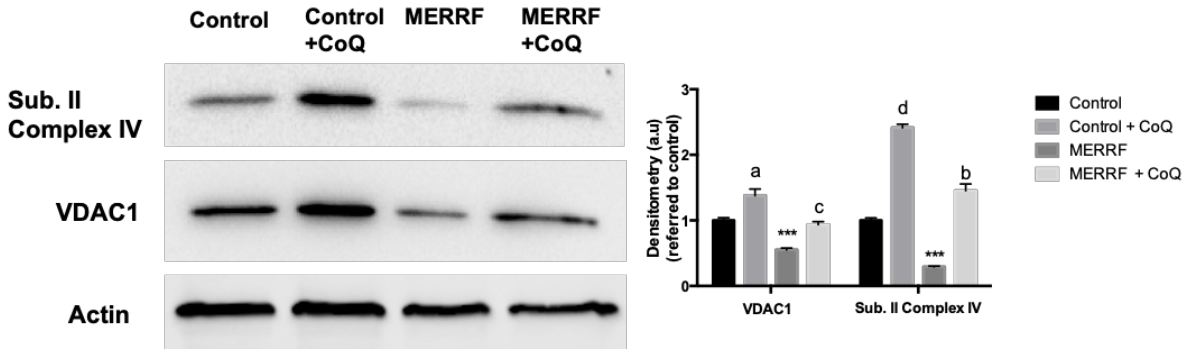

Figure R9. Levels of mitochondrial proteins in untreated and CoQ-treated control and MERRF fibroblasts.
Significance of MERRF respect to control fibroblasts is represented as ***P<0.001. Significance between the presence and the absence of CoQ is represented as ^{a}P<0.05, ^{b}P<0.01, ^{c}P<0.001 and ^{d}P<0.0001.

To test whether reduced mitochondrial proteins expression levels and the different pathological characteristics shown above had an effect on mitochondrial function, we next measured mitochondrial respiratory function and profile of control and MERRF fibroblasts. For that purpose, we performed the Mito-stress test assay by the XFe24 extracellular flux analyzer (Seahorse Bioscience, Billerica, MA, USA), a platform which assesses mitochondrial respiration in living cells by directly measuring the OCR in the extracellular medium. Moreover, we determined if CoQ supplementation restored cellular bioenergetics in MERRF fibroblasts.
The overall respiratory responses of untreated and treated control and MERRF fibroblasts are shown in **Figure R10.** Aerobic respiration (OCR) was reduced in MERRF fibroblasts compared to control cells; meanwhile treatment with CoQ increased OCR both in control and MERRF treated cells.

After carrying out the Mito-stress test, different cellular bioenergetic parameters were calculated using the Seahorse XF Report Generator, a data analysis tool provided by Seahorse Bioscience.

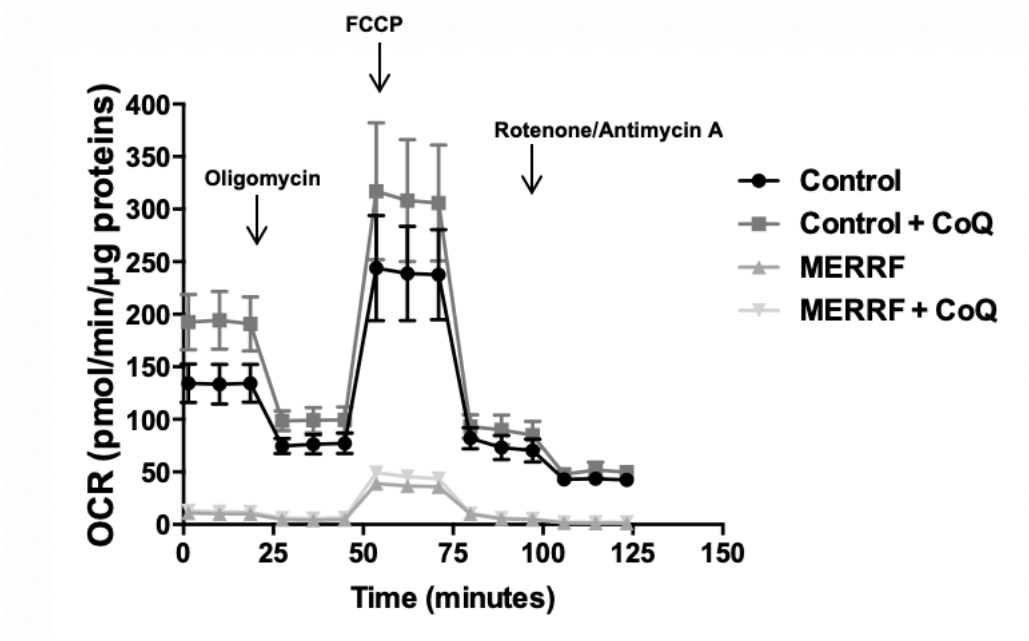

Figure R10. Representative respiratory flux profiles of untreated and CoQ-treated control and MERRF fibroblasts.
One representative of three independent experiments is shown. Addition of ATP synthase inhibitor oligomycin, electron transport chain uncoupler FCCP and complex I and III inhibitors rotenone and antimycin A are indicated. Untreated and CoQ-treated control and MERRF fibroblasts were seeded to 15,000 cells/well and incubated for 24 h. OCR was measured in XF base medium under basal conditions followed by the sequential addition of oligomycin (1 µM), FCCP (2 µM), as well as rotenone (1 µM) & antimycin A (2.5 µM), as indicated. Each data point represents an OCR measurement. Data are expressed as mean ± SD.

The description of the procedure to calculate the most important mitochondrial respiratory parameters is shown in **Figure R11.** For a more detailed explanation of the meaning of the different parameters of mitochondrial respiration (basal respiration, maximal respiration, spare respiratory capacity and ATP production) see Materials & Methods section.

MERRF fibroblasts showed reduced basal respiration, maximal respiration and spare respiratory capacity compared to the control cells. Moreover, OCR coupled to ATP production was also reduced in MERRF fibroblasts (**Figure R12**). This reduced respiratory ability is in agreement with the presence of mitochondrial dysfunction, since different mutations in the mtDNA have been reported to cause impairment of ATP synthesis[200,578,579].

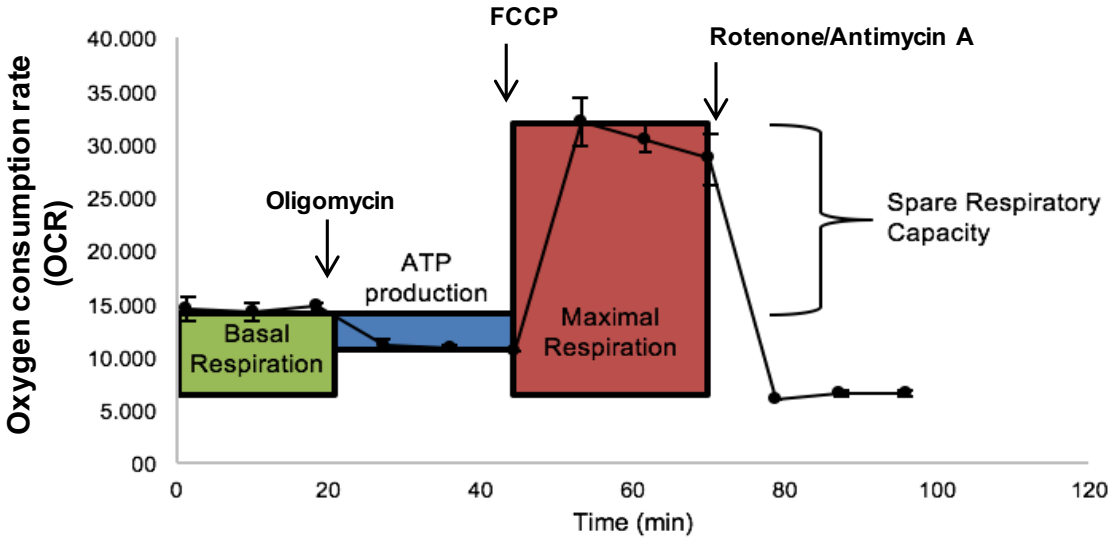

Figure R11. Schematic of oxygen consumption trace from extracellular flux analysis, indicating various parameters of mitochondrial function.
These include: basal respiration (basal OCR measurement minus rotenone/antimycin A response); maximal respiration (FCCP response minus rotenone/antimycin A response); spare respiratory capacity (maximum OCR divided by basal mitochondrial OCR) and ATP-linked OCR (basal measurement minus oligomycin response).

These findings confirmed that the m.8344A>G mutation led to a decreased mitochondrial respiration in a fibroblast model of MERRF syndrome.
CoQ treatment significantly increased maximal respiration, spare respiratory capacity and ATP production of MERRF fibroblasts (**Figure R12**).

Recent data suggest the involvement of ROS and mitochondrial dysfunction in autophagy activation[203,580-582]. To determine whether autophagy was increased in MERRF fibroblasts, we first investigated the conversion of LC3B-I to LC3B-II, as the amount of the latter is closely correlated with the number of autophagosomes. The amount of LC3B-II was significantly increased in MERRF fibroblasts (**Figure R13**), indicating enhanced autophagosome formation in MERRF cells. Supplementation of the culture medium with 100 µM CoQ resulted in a significant decrease in the relative amount of LC3B-II in MERRF cultures.

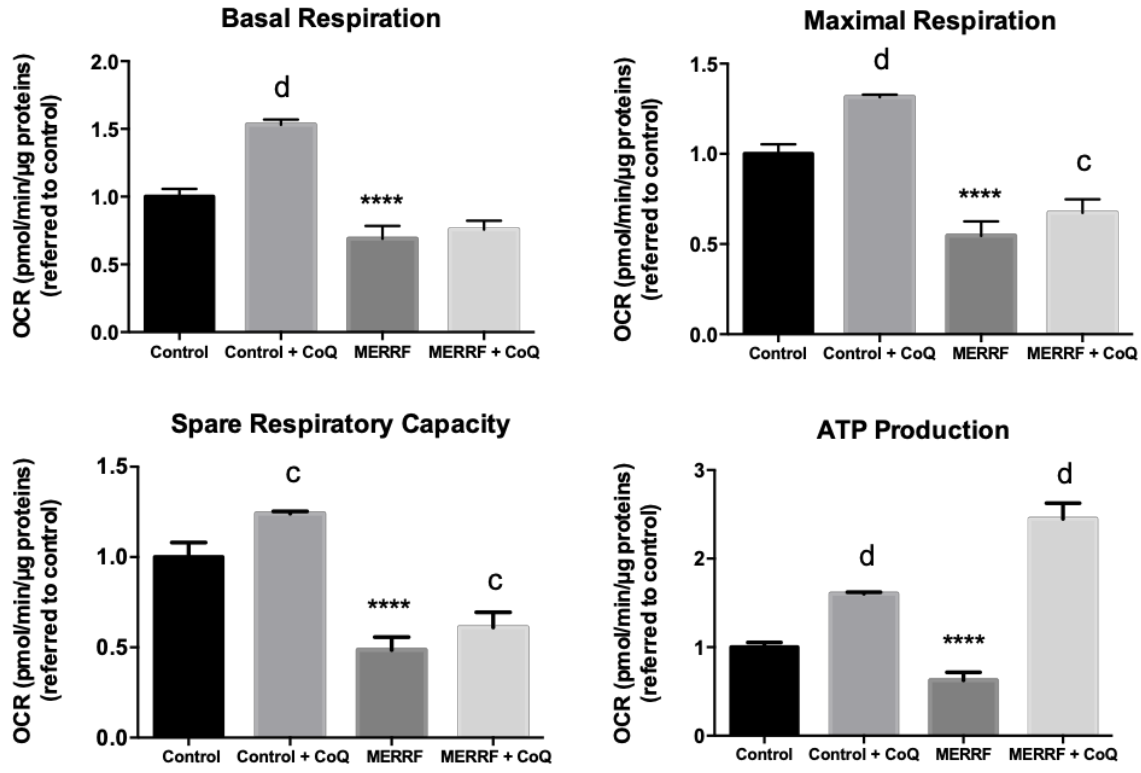

Figure R12. Parameters of mitochondrial respiratory function of untreated and CoQ-treated control and MERRF fibroblasts.
Basal mitochondrial respiration, maximal respiration, spare respiratory capacity and ATP-linked respiration were calculated as described above. Results are expressed as mean ± SD, n = 3 independent experiments. Significance of MERRF respect to control fibroblasts is represented as ****P<0.0001. Significance between the presence and the absence of CoQ is represented as ^{c}P<0.001 and ^{d}P<0.0001. All OCR readings were normalized to µg of proteins as described in Materials & Methods section.

Expression levels of P62, an autophagy substrate that is used as a reporter of autophagy activity and autophagy flux, were also increased in MERRF fibroblasts, indicating autophagy impairment. Treatment with 100 µM CoQ resulted in a significant decrease in the relative amount of P62 in MERRF cultures (**Figure R13**).

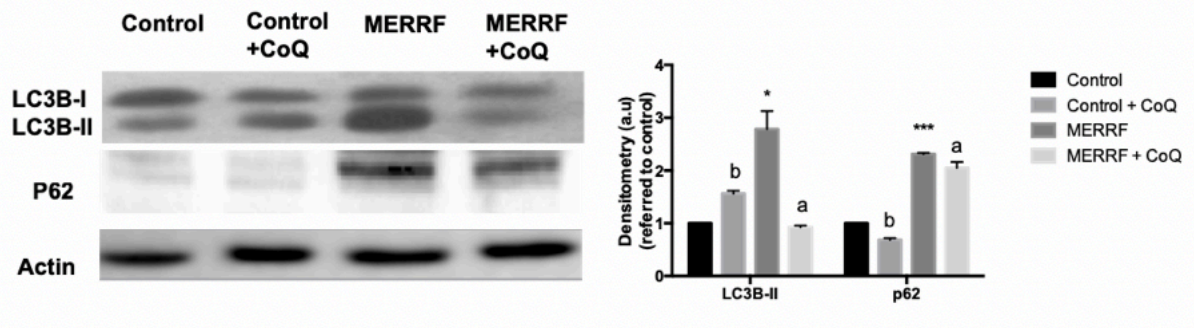

Figure R13. Expression levels of autophagic proteins in untreated and CoQ-treated control and MERRF fibroblasts.
Protein expression levels of LC3B and P62 were determined in control and MERRF fibroblasts cultures before and after CoQ treatment by Western blotting. Densitometry analysis of Western blotting was performed by using ImageLab software. Actin was used as a loading control. Data represent the mean ± SD of three separate experiments. Significance of MERRF respect to control fibroblasts is represented as *P<0.05 and ***P<0.001. Significance between the presence and the absence of CoQ is represented as ^{a}P<0.05 and ^{b}P<0.01.

Given that AMPK is one of the main autophagy activators in the cell[76,164] and MERRF fibroblasts showed high levels of autophagic proteins compared to controls, we checked whether AMPK was involved in autophagy activation in MERRF fibroblasts and the observed beneficial effects of CoQ treatment. AMPK has been shown to be activated in MERRF cellular models in response to cellular stress[583,584], and we have observed in **Figure R7** and **R12** that MERRF fibroblasts showed high levels of ROS and mitochondrial respiration dysfunction. Consequently, we next examined AMPK activation in MERRF fibroblasts by exploring the phosphorylation state of AMPK, since activation of AMPK requires phosphorylation of threonine 172[585]. Phospho-AMPK/total-AMPK ratio was increased by 250% in MERRF fibroblasts (**Figure R14**).

Moreover, we observed the effect of CoQ treatment in AMPK phosphorylation. Interestingly, CoQ treatment stimulated AMPK phosphorylation in MERRF fibroblasts (**Figure R14**), in accordance with recent studies which suggest that CoQ induces AMPK activation[220,586,587].

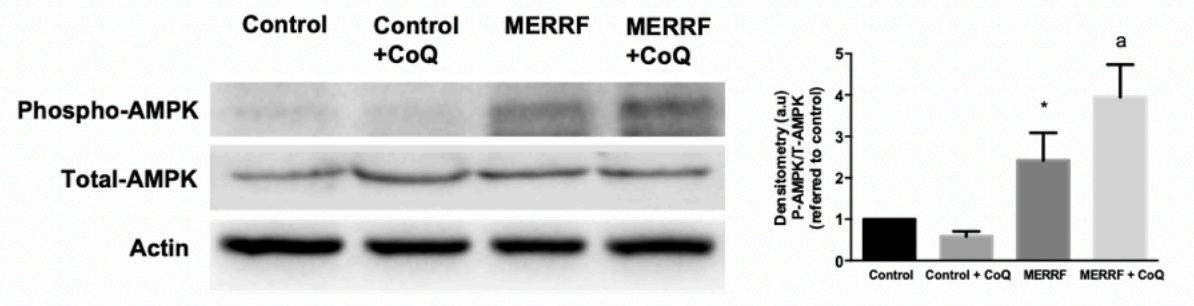

Figure R14. AMPK activation in MERRF fibroblasts and pharmacological stimulation of AMPK pathway through CoQ treatment.
Western blottings of phosphorylated and total AMPK were performed according to standard methods. Densitometry of Western blotting was performed by using the ImageLab software. Actin was used as loading control. Results are expressed as mean ± SD. Significance of MERRF respect to control fibroblasts is represented as $^{*}P<0.05$. Significance between the presence and the absence of CoQ is represented as $^{a}P<0.05$.

Since MERRF fibroblasts showed high levels of phospho-AMPK compared to control cells and some studies suggest that AMPK activation is involved in mitophagy initiation[73,93], we wondered whether mitochondria were selectively being degraded by mitophagy in MERRF cell cultures.

To determine whether bulk autophagy or mitophagy was activated, mitophagic events were detected by colocalisation of LC3B with cytochrome c. Colocalized cytochrome c/LC3B puncta were increased in MERRF fibroblasts. Treatment with CoQ significantly reduced the number of detectable mitophagic events (**Figure R15**).

Colocalisation of cytochrome c/LC3B signal was found in MERRF fibroblasts indicating a general activation of the selective degradation of mitochondria. CoQ treatment reduced the number of cytochrome c/LC3B colocalized puncta per cell to control levels.

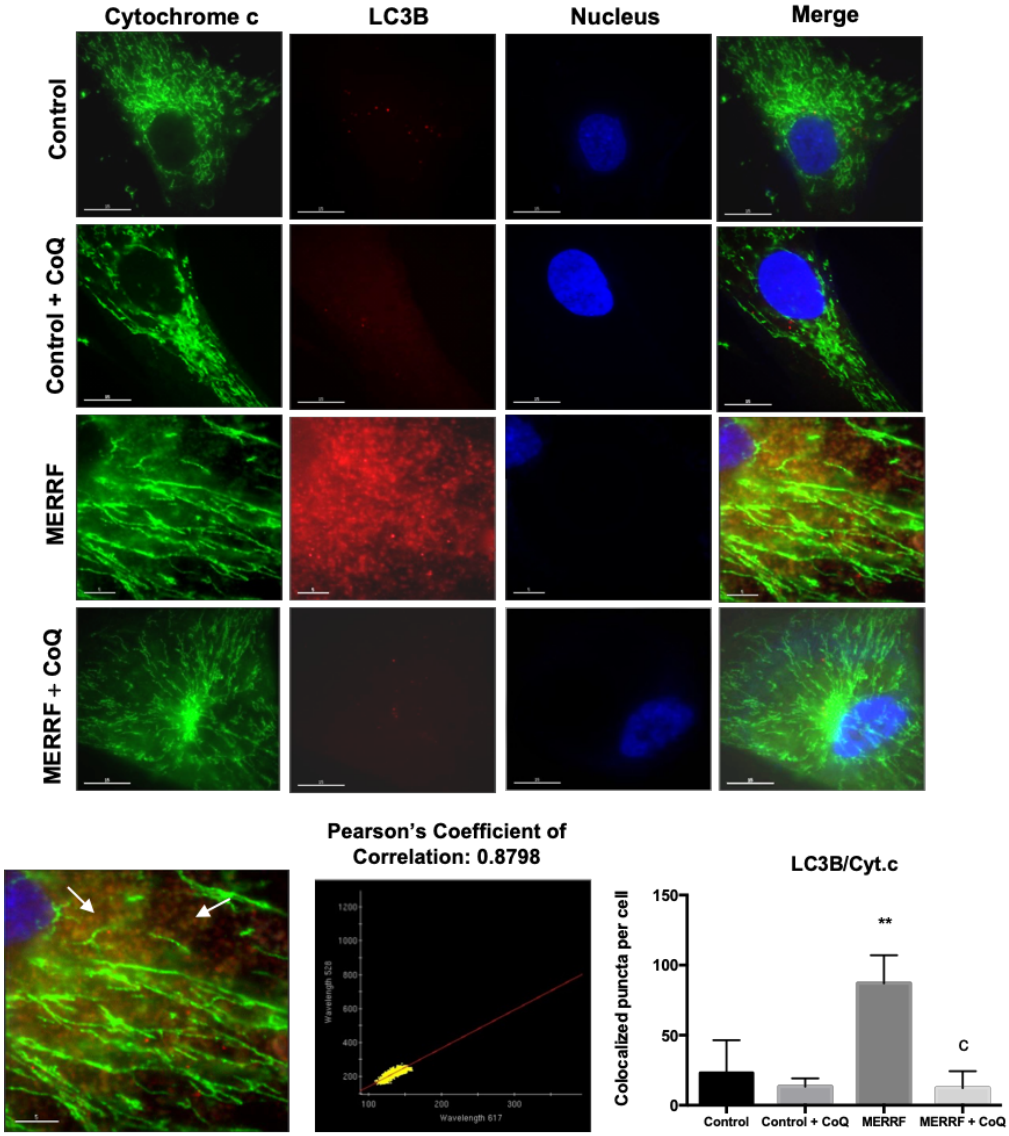

Figure R15. Mitophagy analysis in untreated and CoQ-treated control and MERRF fibroblasts.

Immunostaining of cytochrome c (mitochondrial marker) and LC3B (autophagosome marker) was performed to visualize autophagosomes (puncta) in untreated and treated control and MERRF fibroblasts. Immunostaining of MERRF fibroblasts showed two populations of mitochondria: a smaller, rounded and fragmented one (white arrows) with high cytochrome c/LC3B colocalisation degree (Pearson's coefficient of correlation ~ 0.88) and another tubular with low cytochrome c/LC3B colocalisation degree. To quantify mitophagy, cytochrome c/LC3B colocalized puncta per cell were measured with the Red and Green puncta Colocalization ImageJ macro[563]. Data are shown in the plot as the mean ± SD of three independent experiments (at least 50 cells for each condition and experiment were examined). Significance of MERRF respect to control fibroblasts is represented as $^{**}P<0.01$. Significance between the presence and the absence of CoQ is represented as $^{c}P<0.001$. [Scale bar = 15 μm].

Mitophagy activation in MERRF fibroblasts and CoQ treatment effect on mitophagy were also confirmed by electron microscopy. Control cells showed mitochondria with typical ultrastructure. In contrast, MERRF fibroblasts showed laminar bodies and autophagosomes containing mitochondria-like organelles (white arrows) (**Figure R16**). CoQ treatment reduced the number of autophagosomes in MERRF fibroblasts to control levels.

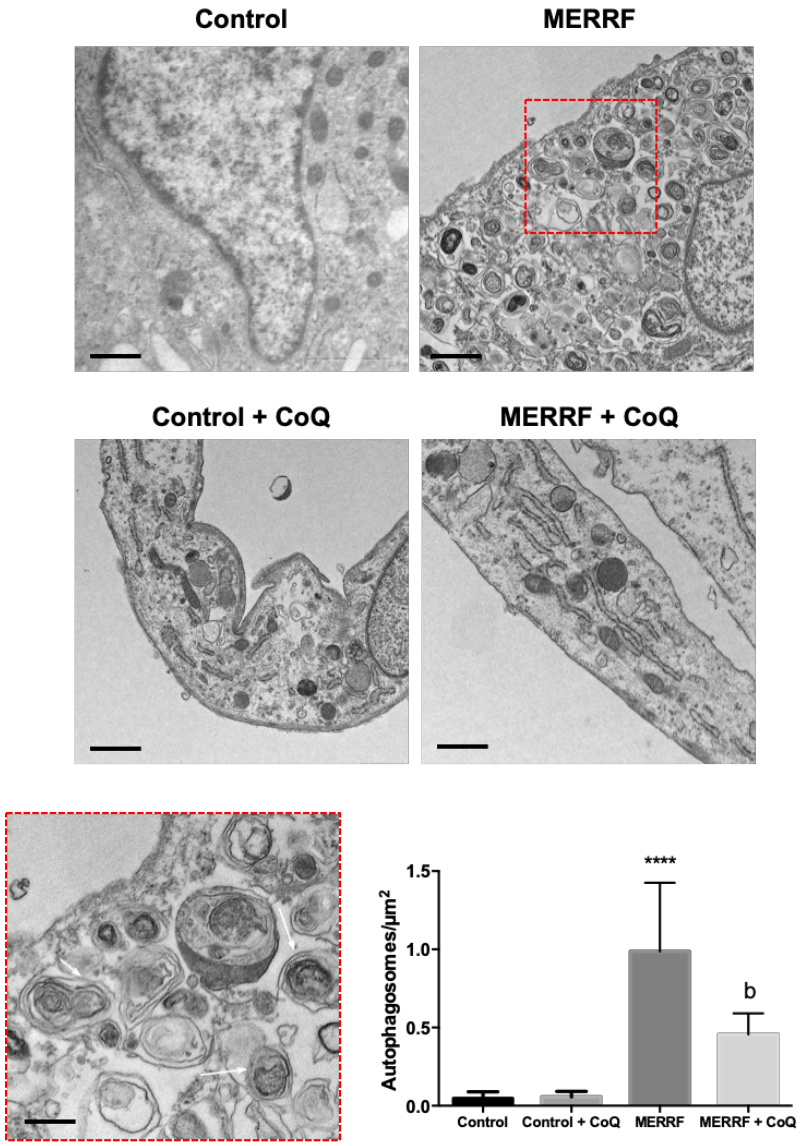

Figure R16. Electron microscopy of untreated and CoQ-treated control and MERRF fibroblasts.

Mitophagy activation in MERRF fibroblasts was detected by using electron microscopy as described in Materials & Methods section. To quantify mitophagy activation, number of autophagosomes per µm^2 were plotted. Significance of MERRF respect to control fibroblasts is represented as ****P<0.0001. Significance between the presence and the absence of CoQ is represented as ^{b}P<0.01. [Scale bar = 1 µm and 0.5 µm in magnified picture].

In conclusion, MERRF fibroblasts showed severe pathophysiological alterations characterized by low $\Delta\Psi m$, high ROS levels, mitochondrial respiration dysfunction and autophagy and mitophagy activation, as well as AMPK activation. CoQ treatment ameliorated most of pathophysiological aspects and induced AMPK activation in MERRF fibroblasts.

R-II. Characterization of Parkin-mediated mitophagy in fibroblasts derived from a MERRF patient and effect of CoQ treatment.

Mitophagy is regulated in most mammalian cell types by the E3 ubiquitin ligase Parkin and PINK1[130]. Moreover, mounting evidence indicate that Parkin also modulates mitochondrial dynamics and autophagy[588].

Depolarization of mitochondrial membrane potential is necessary to induce Parkin-mediated mitophagy[139]. Since depolarized mitochondria have been observed in MERRF fibroblasts in the previous Results subsection, we wonder whether PINK1/Parkin-mediated mitophagy was involved in the pathophysiology of MERRF fibroblasts.

Therefore, in this Results subsection, we deeply investigated the mechanisms of mitophagy observed on the skin fibroblasts derived from a MERRF patient studied in the previous Results subsection.

Protein-specific degradation in cells occurs through the ubiquitin-proteasome system (UPS), by which proteins to be degraded are covalently binded to several ubiquitin molecules trough a specific lysine residue. Then, the polyubiquitinated protein is transported to the proteasome for degradation[589]. Recently, a link between mitochondrial health and the UPS has been observed. Reduced UPS activity and therefore an increase in the amount of ubiquitinated proteins are related to a decline of the mitochondrial function[590,591]. Although Parkin-mediated mitophagy is a more general process leading to global degradation of mitochondria, it is also related to ubiquitination of proteins since Parkin ubiquitinates mitochondrial proteins through its E3 ubiquitin ligase activity[592,593].

For all these reasons, first we checked the amount of ubiquitinated proteins in MERRF and control fibroblasts, untreated and treated with CoQ. The total levels of ubiquitinated proteins were significantly increased in MERRF fibroblasts, and CoQ treatment restored the levels (**Figure R17**).

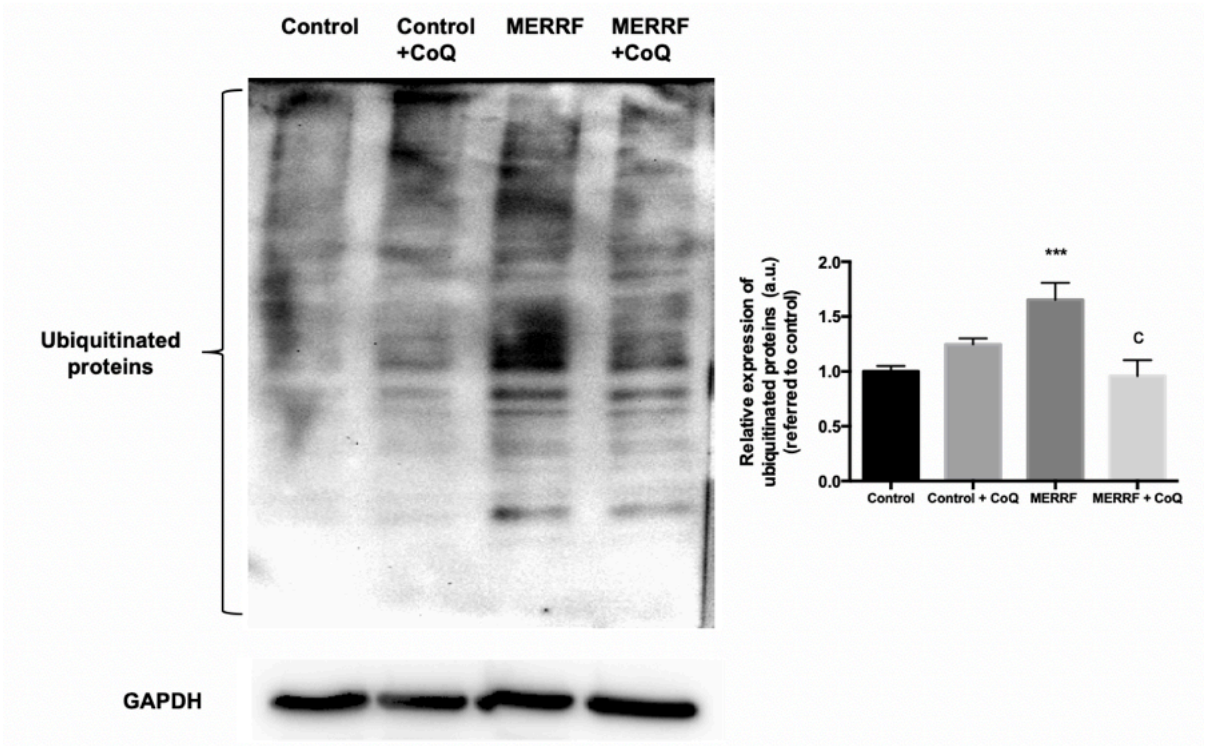

Figure R17. Endogenous levels of ubiquitinated proteins of untreated and CoQ-treated control and MERRF fibroblasts.
Western blotting of ubiquitinated proteins was performed by using standard methods. Protein extracts were separated on a 12.5% SDS polyacrylamide gel and immunostained with antibodies against ubiquitin and GAPDH for loading control. Densitometry of Western blotting was performed by using the ImageLab software. Results are expressed as mean ± SD. Significance of MERRF respect to control fibroblasts is represented as ***P<0.001. Significance between the presence and the absence of CoQ is represented as ^{c}P<0.001.

Therefore, we wanted to further confirm the increase of the amount of ubiquitinated proteins in MERRF fibroblasts and checked if the majority of ubiquitinated proteins were located into the mitochondria targeted for degradation (depolarized mitochondria). Therefore, immunofluorescence of ubiquitin and MitoTracker^{TM} Red CMXRos (a mitochondrial probe which fluorescence is dependent on mitochondrial membrane potential) was performed. Control fibroblasts showed diffuse ubiquitin staining and a healthy mitochondrial network, meanwhile increased expression of ubiquitin and colocalization between ubiquitin and fragmented, depolarized mitochondria were found in MERRF fibroblasts. These effects were prevented by CoQ treatment (**Figure R18**).

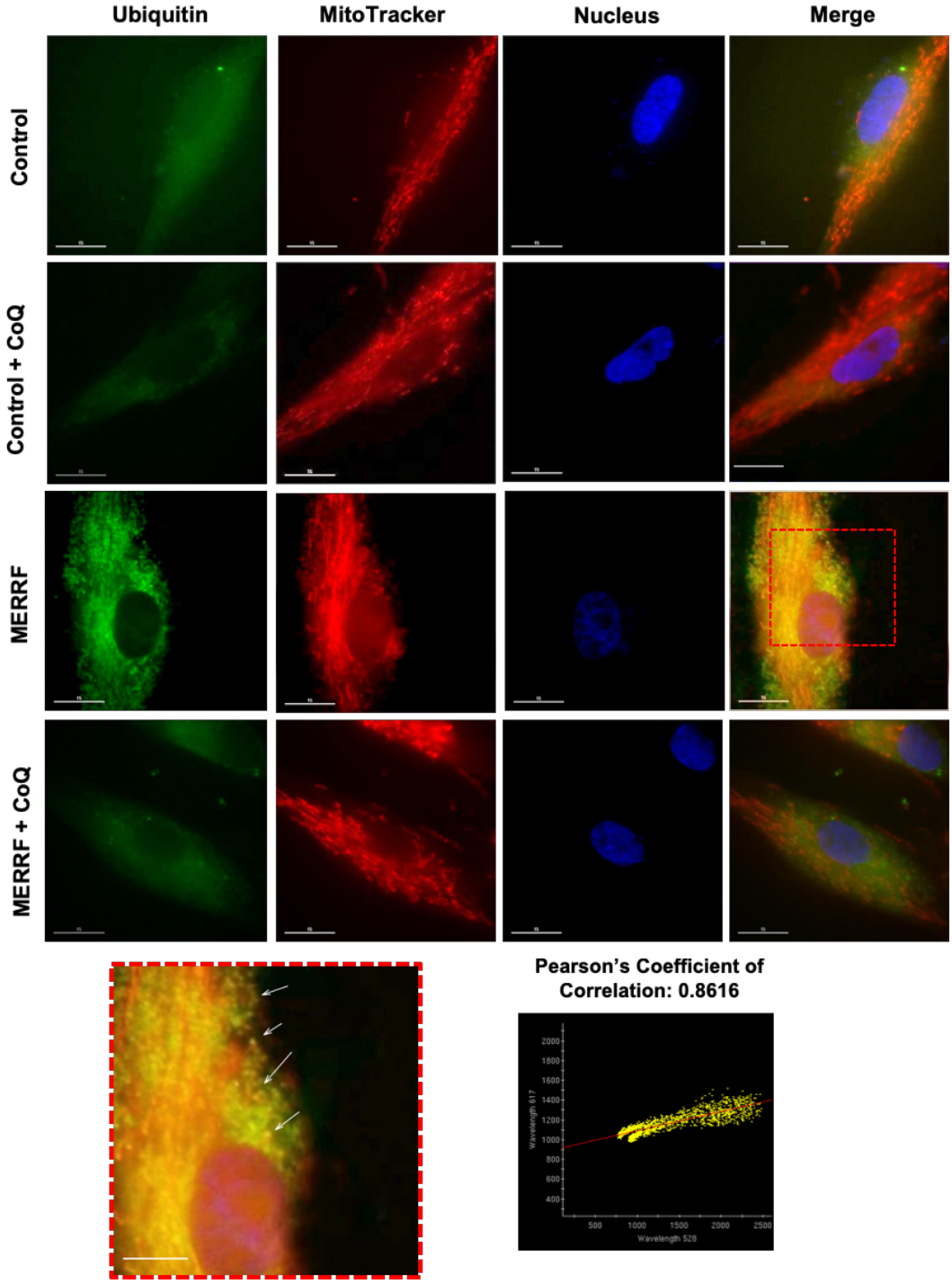

Figure R18. Ubiquitin colocalization with depolarized mitochondria in MERRF fibroblasts.

Immunofluorescence microscopy of MitoTracker™ Red and ubiquitin was performed as described in Materials & Methods section. Magnification of a small area of MERRF fibroblasts showing ubiquitin colocalization with depolarized mitochondria (white arrows) is shown. Colocalisation analysis of ubiquitin and depolarized mitochondria resulted in a high colocalisation (Pearson's coefficient of correlation ~ 0.86). [Scale bar = 15 µm and = 5 µm in magnified picture].

Moreover, since the induction of mitophagy following Parkin recruitment is thought to involve the Parkin-mediated ubiquitination of VDAC1[106], we wanted to observe whether VDAC1 was ubiquitinated in MERRF fibroblasts. Therefore, immunofluorescence of ubiquitin and VDAC1 was performed. Control fibroblasts showed a decreased ubiquitin staining, diffused by the cytoplasm, without specific colocalization with VDAC1. However, increased expression of ubiquitin and colocalization between ubiquitin and VDAC1 were found in MERRF fibroblasts. Moreover, colocalized proteins seemed to stablish aggresome-like structures, typically formed when the protein-degradation system of the cell is overwhelmed (**Figure R19**).

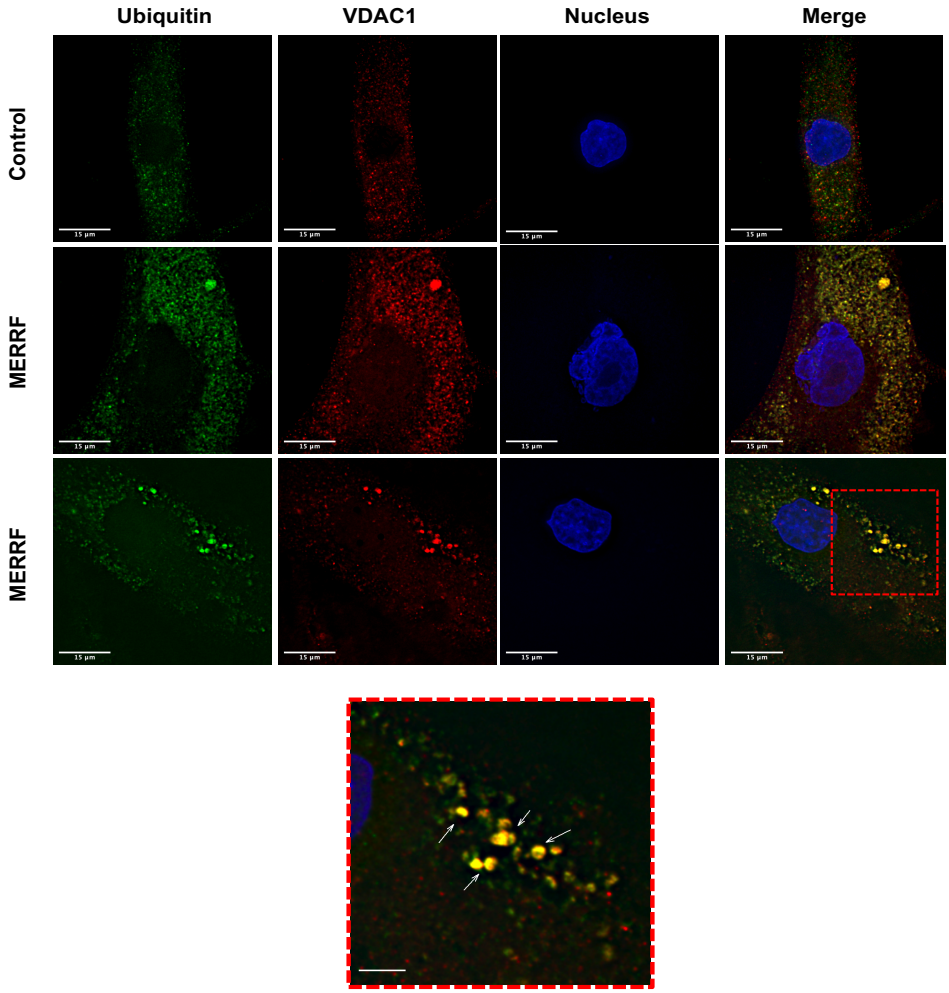

Figure R19. Ubiquitin colocalization with VDAC1 in MERRF fibroblasts. **Immunofluorescence microscopy of VDAC1 and ubiquitin was performed as described in Materials & Methods section. Magnification of a small area of MERRF fibroblasts showing ubiquitin colocalization with VDAC1 in aggresome-like structures (white arrows) is shown. [Scale bar = 15 μm and 5 μm in magnified picture].**

We further observed that the endogenous levels of Parkin, PINK1 and DRP1, a protein involved in mitochondrial fission and required for Parkin-mediated mitophagy, were increased in MERRF fibroblasts and CoQ treatment restored the levels (**Figure R20**).

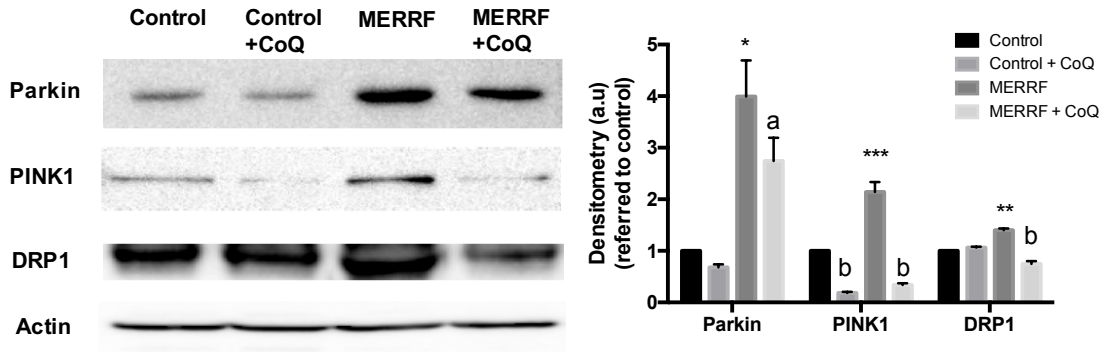

Figure R20. Endogenous levels of proteins involved in Parkin-mediated mitophagy of untreated and CoQ-treated control and MERRF fibroblasts.
Western blotting of Parkin, PINK1 and DRP1 was performed by using standard methods. Protein extracts were separated on a 12.5% SDS polyacrylamide gel and immunostained with antibodies against Parkin, PINK1 and DRP1. Densitometry of Western blotting was performed by using the ImageLab software. Results are expressed as mean ± SD. Significance of MERRF respect to control fibroblasts is represented as $^{*}P<0.05$, $^{**}P<0.01$ and $^{***}P<0.001$. Significance between the presence and the absence of CoQ is represented as $^{a}P<0.05$ and $^{b}P<0.01$.

To further examine the effect of mitochondrial dysfunction in MERRF fibroblasts on Parkin cytosolic/mitochondrial partition, we prepared subcellular fractions from control and MERRF fibroblasts, untreated and treated with CoQ, since a prerequisite for Parkin's actions on mitochondria may be its translocation from the cytosol to mitochondria. These experiments demonstrated that endogenous Parkin was enriched in the mitochondrial fraction of MERRF fibroblasts, and CoQ treatment decreased the traslocation of Parkin to the mitochondrial fraction (**Figure R21**).

To further investigate Parkin mitochondrial translocation in MERRF fibroblasts, immunofluorescence of Parkin and COXIV subunit II, a mitochondrial marker, was performed. To quantify Parkin-mediated mitophagy, Parkin/COXIV colocalized puncta per cell were measured with the Red and Green puncta Colocalization ImageJ macro[563]. Increased expression and mitochondrial traslocation of Parkin

were found in MERRF fibroblasts. These effects were prevented by CoQ treatment (**Figure R22**).

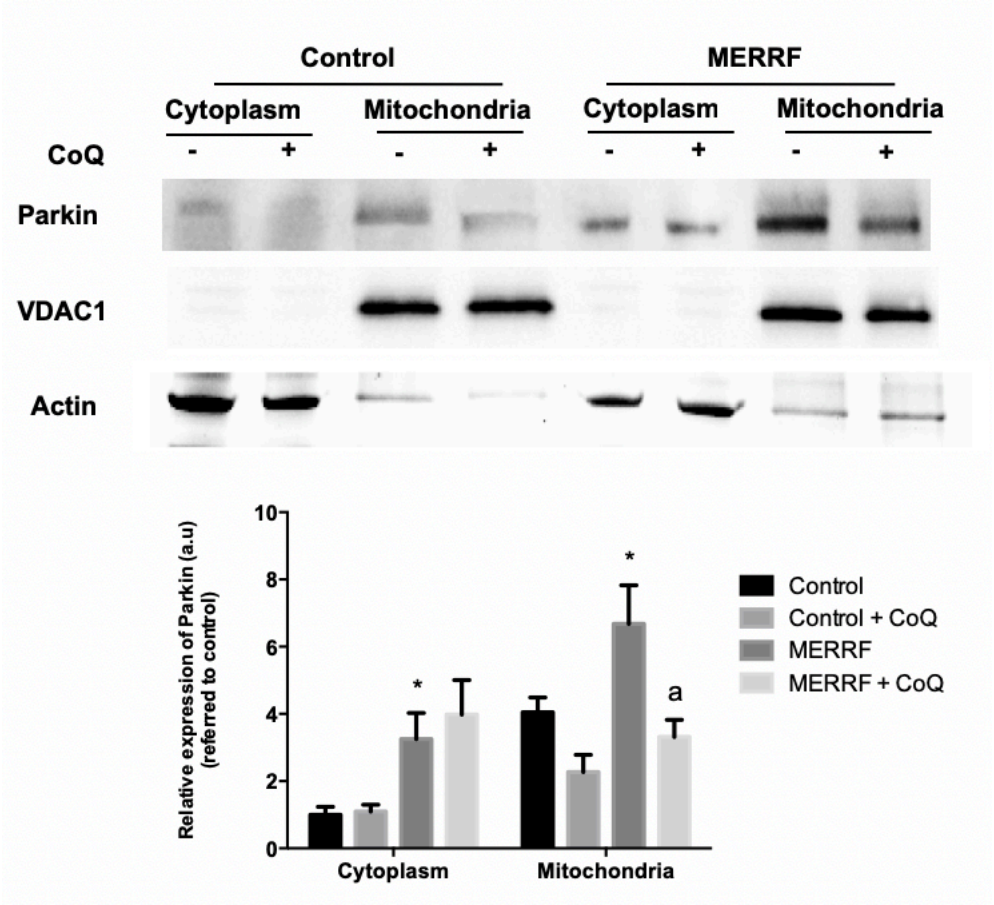

Figure R21. Parkin protein levels in the cytosolic and mitochondrial fractions of untreated and CoQ-treated control and MERRF fibroblasts.
Subfractionation of control and MERRF cells was performed as described in Materials & Methods section, and cellular lysates were processed to isolate cytosolic and mitochondrial fractions. Translocation of Parkin to the mitochondria was determined by standard Western blotting of this protein. Cytosolic and mitochondrial proteins fractions were separated on a 12.5% SDS polyacrylamide gel and immunostained with antibodies against Parkin. The purity of cytosolic and mitochondrial fractions was determined with anti-Actin and anti-VDAC1 antibodies, respectively. The graph shows the increased mitochondrial Parkin levels in MERRF fibroblasts when compared with controls. CoQ treatment prevented Parkin traslocation to mitochondria. Densitometry of Western blotting was performed by using the ImageLab software. Results are expressed as mean ± SD. Significance of MERRF respect to control fibroblasts is represented as $^{*}P<0.05$. Significance between the presence and the absence of CoQ is represented as $^{a}P<0.05$.

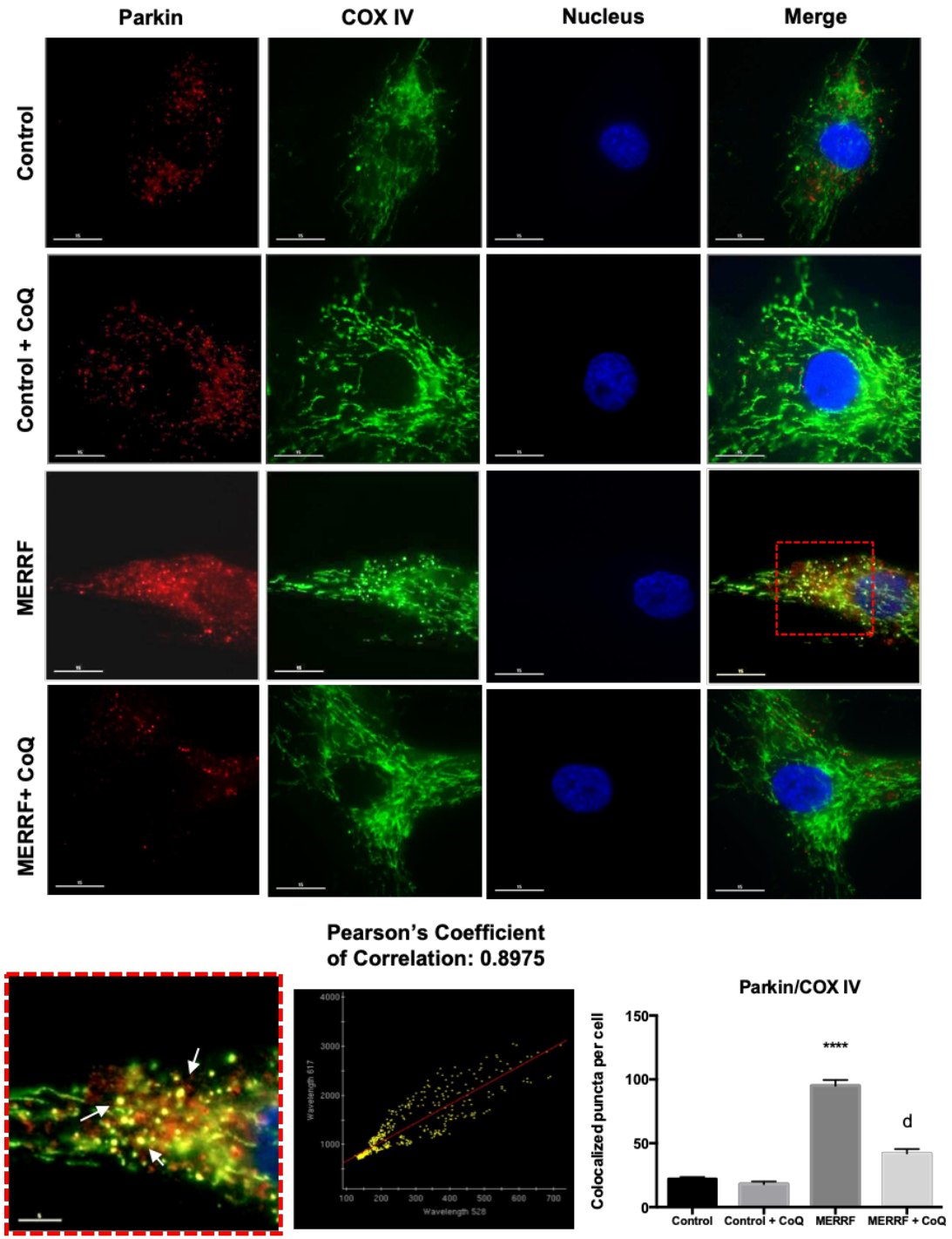

Figure R22. Parkin-mediated mitophagy analysis in untreated and CoQ-treated control and MERRF fibroblasts.

Immunostaining of COXIV and Parkin was performed to visualize Parkin-translocated mitochondria in untreated and CoQ-treated control and MERRF fibroblasts. Data are shown in the plot as the mean ± SD of three independent experiments (at least 50 cells for each condition and experiment were examined). Significance of MERRF respect to control fibroblasts is represented as ****P<0.0001. Significance between the presence and the absence of CoQ is represented as ^{d}P<0.0001. [Scale bar = 15 μm and 5 μm in magnified picture].

Immunostaining of MERRF fibroblasts showed two populations of mitochondria: a smaller, rounded and fragmented one (white arrows) with high Parkin/COXIV colocalisation degree (Pearson's coefficient of correlation ~ 0.90) and another tubular with low Parkin/COXIV colocalisation degree.

Immunofluorescence of Parkin and cytochrome c, other mitochondrial marker, was performed obtaining the same results (**Figure R23**). Immunostaining of MERRF fibroblasts showed two populations of mitochondria: a smaller, rounded and fragmented one (white arrows) with high Parkin/cytochrome c colocalisation degree (Pearson's coefficient of correlation ~ 0.91) and another tubular with low Parkin/cytochrome c colocalisation degree. To quantify Parkin-mediated mitophagy, Parkin/cytochrome c colocalized puncta per cell were measured as previously described in Materials & Methods section.

Moreover, since Parkin translocation occurs to depolarized mitochondria, we also performed an immunofluorescence assay of Parkin and MitoTracker™ Red (**Figure R24**)**.** We observed that in MERRF fibroblasts the mitochondrial network became altered and MERRF cells exhibited colocalization of Parkin with depolarized, fragmented, rounded mitochondria, primarily in the vicinity of the nucleus. CoQ treatment partially restored mitochondrial network and prevented Parkin translocation to mitochondria.

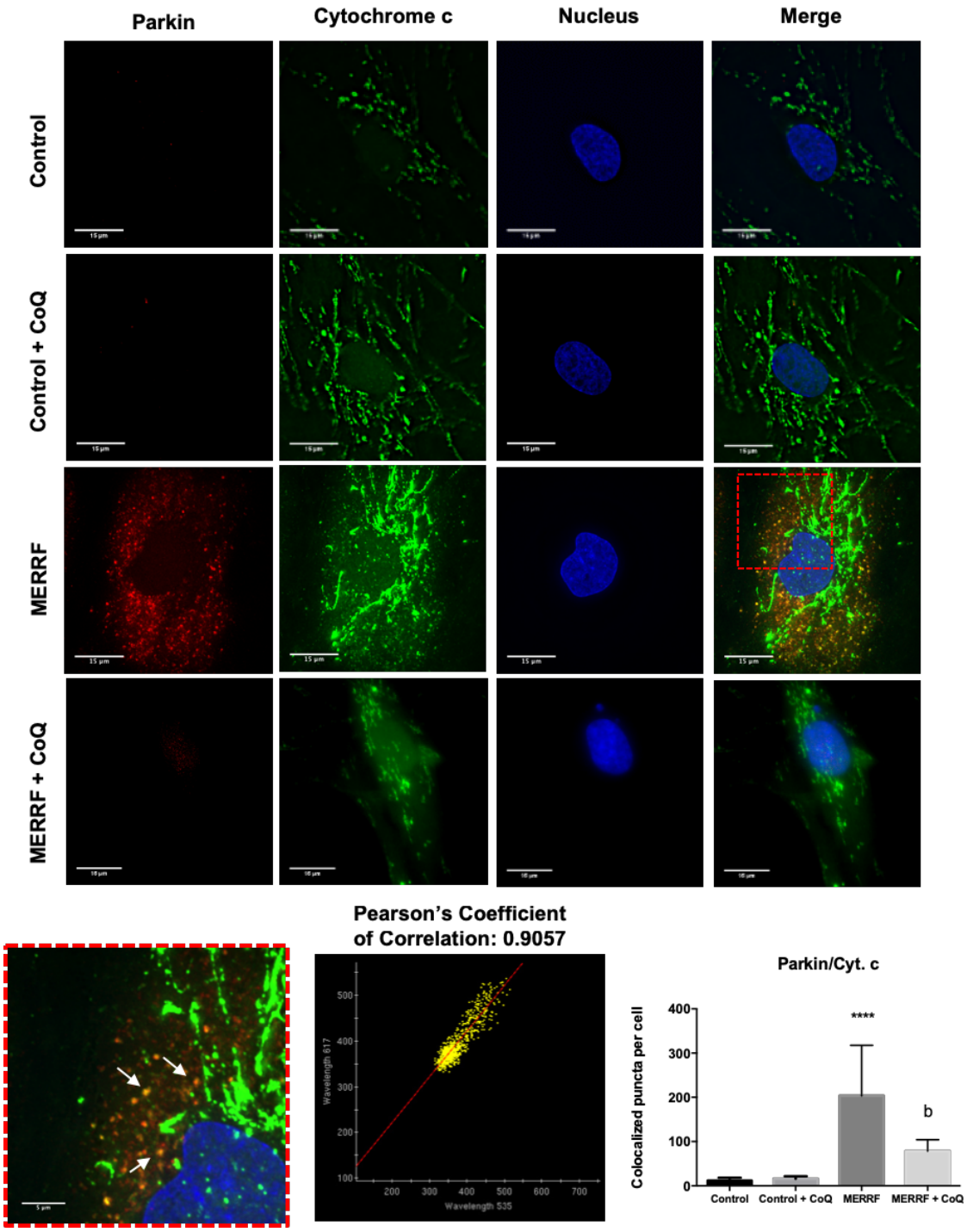

Figure R23. Parkin-mediated mitophagy analysis in untreated and CoQ-treated control and MERRF fibroblasts.

Immunostaining of cytochrome c and Parkin was performed to visualize Parkin-translocated mitochondria in untreated and treated control and MERRF fibroblasts. Data are shown in the plot as the mean ± SD of three independent experiments (at least 50 cells for each condition and experiment were examined). Significance of MERRF respect to control fibroblasts is represented as ****P<0.0001. Significance between the presence and the absence of CoQ is represented as ^{b}P<0.01. [Scale bar = 15 μm and 5 μm in magnified picture].

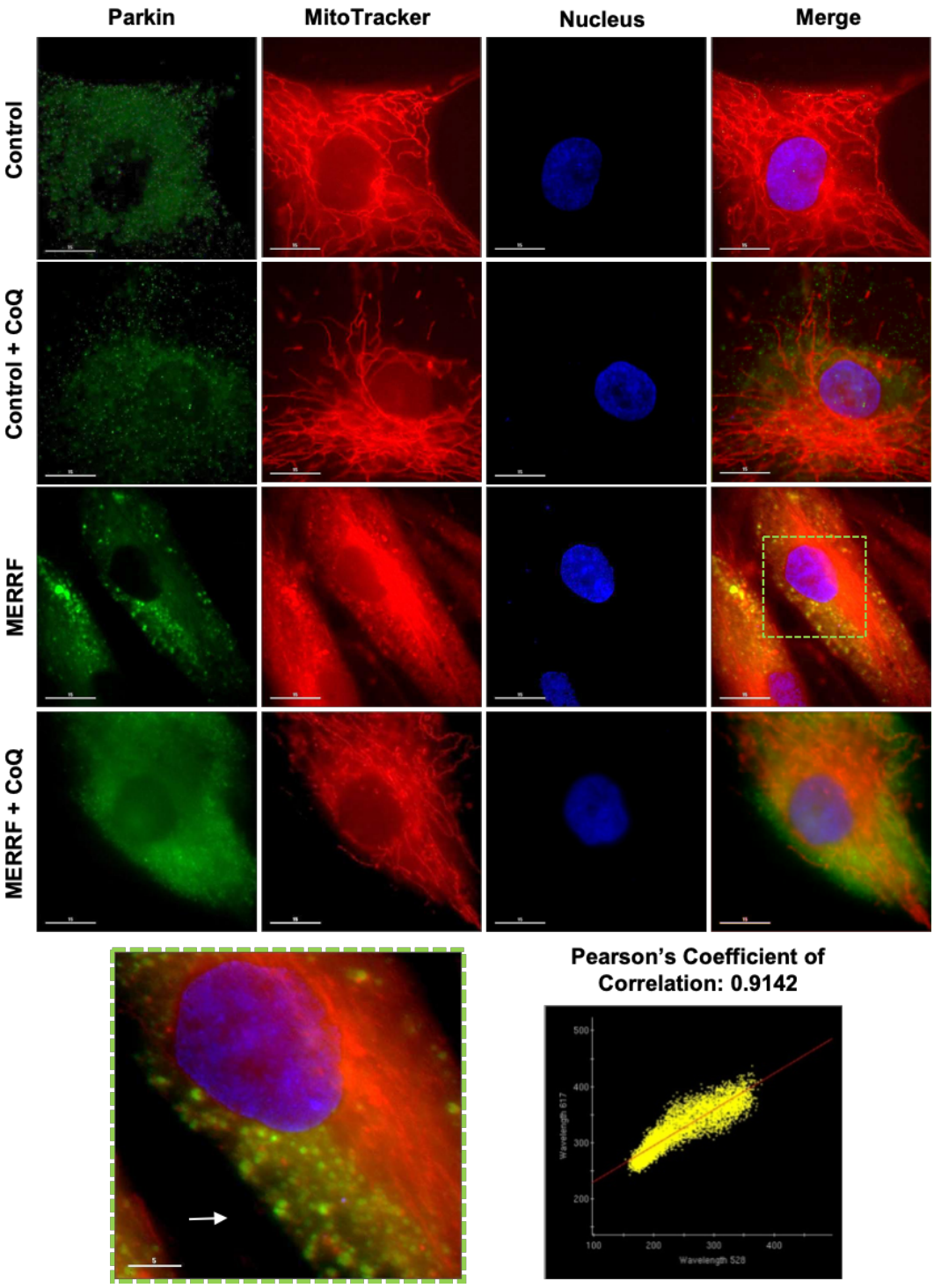

Figure R24. Parkin translocation to depolarized mitochondria in MERRF fibroblasts.

Immunofluorescence microscopy of MitoTracker™ Red and Parkin was performed as described in Materials & Methods section. Magnification of a small area of MERRF fibroblasts showing translocated Parkin into small, rounded depolarized mitochondria (white arrow) is shown. Colocalisation analysis of Parkin and depolarized mitochondria resulted in a high colocalisation (Pearson's coefficient of correlation ~ 0.91). [Scale bar = 15 μm and 5 μm in magnified picture].

In conclusion, MERRF fibroblasts showed Parkin-mediated mitophagy activation, characterized by accumulation of ubiquitinated proteins (presumably most of them mitochondrial proteins) and Parkin translocation to depolarized mitochondria. CoQ treatment prevented high levels of ubiquitinated proteins and diminished Parkin translocation to mitochondria in MERRF fibroblasts, also ameliorating the mitochondrial network.

R-III. Autophagy and mitophagy flux disruption in fibroblasts derived from a MERRF patient and evaluation of the effect of CoQ treatment.

So far, our studies indicated that MERRF fibroblasts showed autophagy and mitophagy activation and the autophagosomes accumulation was prevented by CoQ treatment. The fact that the mitophagic events were detectable without the presence of autophagy inhibitors such as bafilomycin A1 suggested the possibility that the autophagy/mitophagy flux could be disrupted in MERRF fibroblasts. Therefore, in the present Results subsection we deepened into the state of the autophagy/mitophagy flux in this cellular model of MERRF syndrome and the possible effect of CoQ not in the prevention of autophagy but in the enhancement of the autophagy/mitophagy flux.
Moreover, slow or disrupted autophagy flux is a main characteristic of the pathophysiology of different diseases[594-597].

In light of the possible autophagy flux alteration in MERRF fibroblasts, we first studied the effects of bafilomycin A1 and CoQ treatments on the levels of the LC3B-II protein.

As previously shown, the analysis of LC3B-II protein expression in MERRF fibroblasts resulted in high levels of this autophagic protein, which could suggest a higher autophagy activation compared to the controls or a blockage of the autophagy flux due to an inefficient autophagosome-lysosome fusion or autolysosome degradation. To distinguish between these two possibilities, we treated the cells with bafilomycin A1, a specific inhibitor of vacuolar H+-ATPases and a blocker of autophagosome-lysosome fusion[127]. Control and MERRF fibroblasts were incubated for 12 hours with 100 nM bafilomycin A1.
As expected, bafilomycin A1 treatment in control fibroblasts led to a significant increase in the amount of LC3B-II protein, suggesting that autophagy flux was correct in control cells. However, bafilomycin A1 treatment in MERRF fibroblasts had no effect on LC3B-II levels indicating that autophagy flux was disrupted (**Figure R25**).

As shown in the first Results subsection, CoQ treatment reduced the levels of LC3B-II protein in MERRF fibroblasts. However, this reduction could be due to a prevention of autophagy activation or a reduction of autophagolysosome accumulation (autophagy flux enhancing). Therefore, in order to check the specific effect of CoQ on autophagy, CoQ pre-treated control and MERRF fibroblasts were exposed to bafilomycin A1 and LC3B-II expression levels were examined by Western blotting (**Figure R25**).

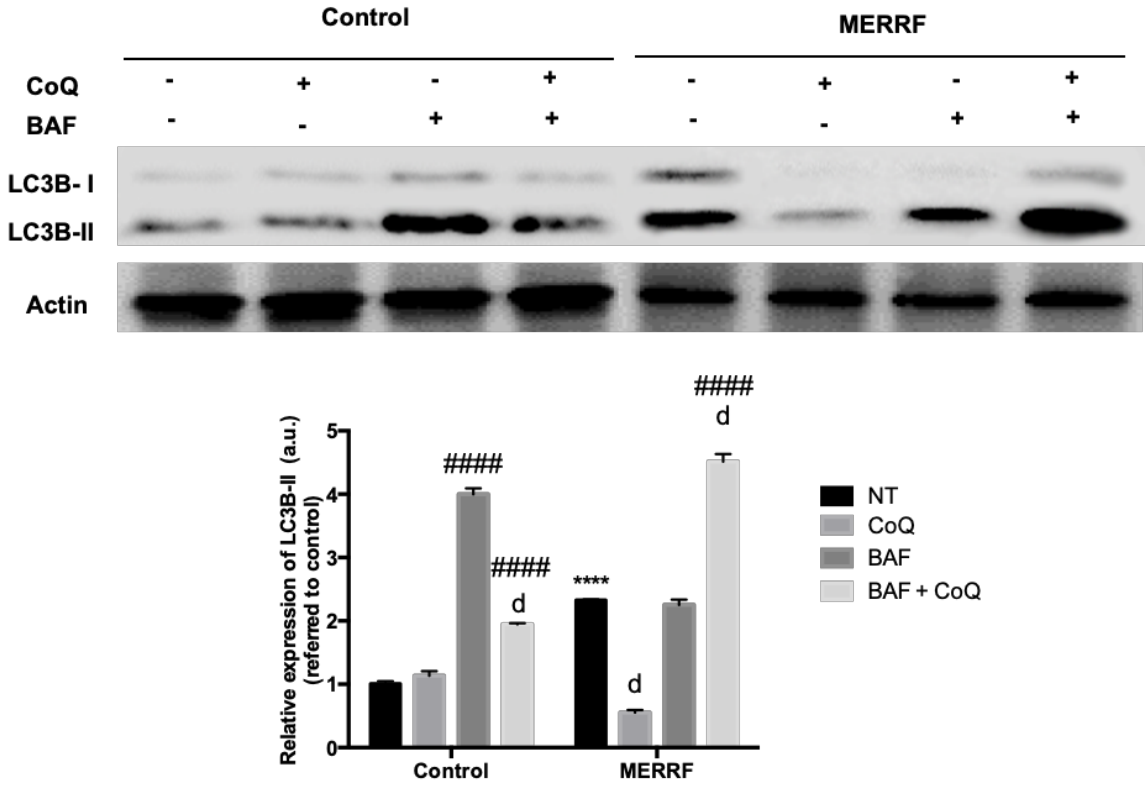

Figure R25. Autophagy flux analysis in control and MERRF fibroblasts and effect of CoQ treatment on autophagy flux.

Autophagy flux was checked by determining LC3B-II protein expression levels in the presence and absence of bafilomycin A1 (BAF). Control and MERRF fibroblasts were incubated with 100 nM BAF for 12 h, and, when indicated, cells were pre-treated with 100 μM CoQ for 72 hours. Total cellular extracts were analyzed by immunoblotting with an antibody against LC3B. Actin was used as a loading control. Densitometry of LC3B-II was performed by using ImageLab software. Data are represented as mean ± SD of three separate experiments. Significance of MERRF respect to control fibroblasts is represented as ****P<0.0001. Significance between presence and absence of CoQ treatment is represented as ^{d}P<0.0001. Significance between presence and absence of bafilomycin A1 treatment is represented as $^{\#\#\#\#}$P<0.0001.

Bafilomycin A1 incubation induced a significant increase on LC3B-II protein expression levels of CoQ-treated MERRF fibroblasts, suggesting that CoQ treatment enhanced autophagy flux by promoting autophagolysosome clearance in pathological cells. This is in accordance with AMPK activation due to CoQ treatment observed in the first Results subsection, since AMPK is considered to enhance autophagy flux[598-600].

Altogether, our results suggested that bulk autophagy flux was disrupted in MERRF fibroblasts. However, we observed in the previous Results subsection that selective degradation of mitochondria by autophagy was also activated in MERRF fibroblasts. Therefore, checking the state of mitophagy flux in this model of MERRF disease was necessary.

Along the last years, there has been a lack of quantitative methods for the study of mitophagy and mitophagy flux, since the colocalization analysis of LC3B and mitochondrial proteins does not provide data about the correct or altered flux of mitophagy. There is thus a great need for novel techniques for the accurate and rapid assessment of mitophagy. Recently, a flow-cytometric assay was developed by Mauro-Lizcano et al.[128] to study mitophagy, mitophagy flux and the effect of different compounds on them.

This method uses the mitochondrial probe MitoTracker™ Deep Red (MTDR), which is not dependent on mitochondrial membrane potential, in combination with lysosomal inhibitors such as bafilomycin A1 (BAF).

By performing this method, mitochondrial population levels of control and MERRF fibroblasts in absence or presence of BAF and/or CoQ were determined. We used CCCP as a control of mitophagy inducer, since it reduces mitochondrial membrane potential promoting Parkin-mediated mitophagy[106,134]. **Figure R26** displays the histogram in which the normalized levels of mitochondrial population in each condition are shown. First, we observed that mitochondrial population was decreased in MERRF fibroblasts compared to controls, which is in relation with the previous results shown in **Figure R9** in the first Results subsection. Moreover, BAF treatment induced an accumulation of MTDR signal in control cells (indicating mitochondrial degradation by mitophagy), but not in MERRF fibroblasts, suggesting that mitophagy flux was disrupted or slower in MERRF cells than in control cells.

Interestingly, CoQ treatment in BAF-treated MERRF fibroblasts significantly increased the mitochondrial population, suggesting that CoQ was acting has an enhancer of mitophagy. CCCP promoted mitochondrial degradation by mitophagy in both control and MERRF fibroblasts (**Figure R26**).

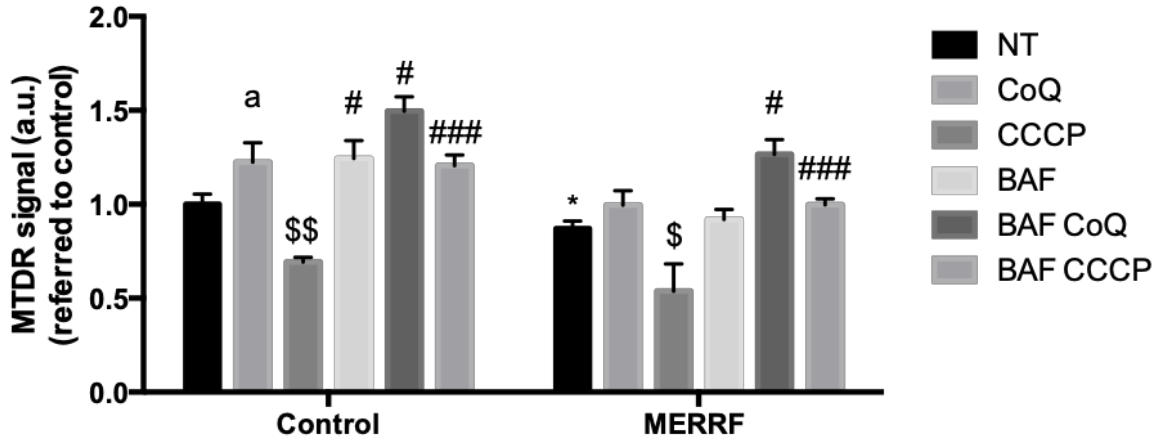

Figure R26. Mitophagy induced by CoQ and CCCP treatments in MERRF fibroblasts is blocked by bafilomycin A1 (BAF) treatment.
Control and MERRF fibroblasts were treated with CCCP or CoQ and also pre-treated with the lysosomal inhibitor bafilomycin A1 6 h before analysis to block autolysosomal degradation. MitoTracker™ Deep Red (MTDR) probe was used to determine mitochondrial population by flow cytometry. * Indicates comparisons between control and MERRF fibroblasts. a Indicates comparisons between the presence or absence of CoQ. $ Indicates comparisons between the presence or absence of CCCP. # Indicates differences between the presence and absence of BAF. *, a, $ or #P<0.05, $$ or ##P<0.01, ###P<0.001.

With all the data shown in **Figure R26**, mitophagy flux index of control and MERRF fibroblasts in each condition could be calculated.
How the index for the measurement of mitophagy flux was calculated is described in **Figure R27**.

$$Mitophagy\ flux = \frac{MTDR\ fluorescence\ in\ presence\ of\ lysosomal\ inhibitor}{MTDR\ fluorescence\ without\ lysosomal\ inhibitor}$$

Figure R27. Mitophagy flux calculation.
Mitophagy flux is defined as the ratio of MTDR fluorescence in the presence of lysosomal inhibitor to that in the absence of inhibitor, normalized to the corresponding value in control cells.

The calculation of mitophagy flux of control and MERRF fibroblasts, untreated and treated with 100 μM CoQ for 72 hours or 50 μM CCCP for 6 hours is represented in **Figure R28**. Mitophagy flux of untreated MERRF fibroblasts was reduced compared to control cells, indicating a disrupted or slower degradation of mitochondria. Interestingly, treatment with CoQ increased the mitophagy flux index in MERRF fibroblasts to control levels, suggesting that CoQ increased the degradation of mitochondria by selective autophagy. CCCP treatment increased mitophagy flux in both control and MERRF cells.

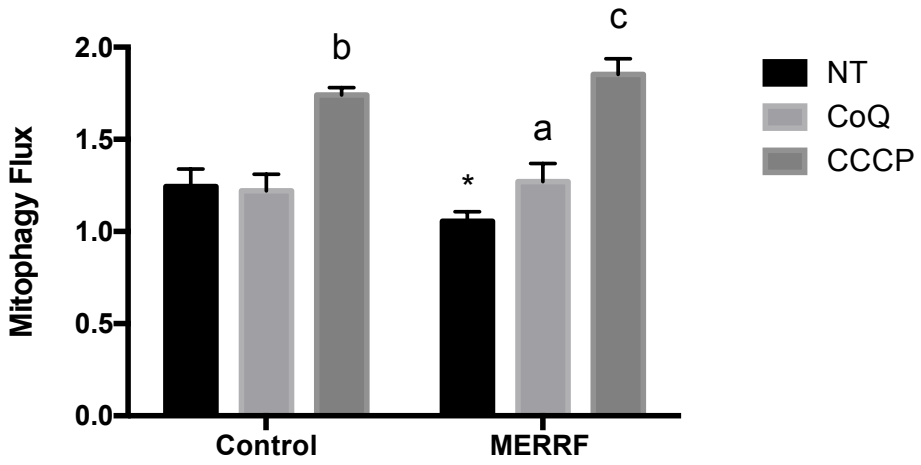

Figure R28. Mitophagy flux determinations of untreated and CoQ-treated control and MERRF fibroblasts.
Mitophagy flux for non-treated (NT), CCCP-treated and CoQ-treated control and MERRF fibroblasts was calculated as described in Materials & Methods section. Significance of MERRF respect to control fibroblasts is represented as $^{*}P<0.05$. Significance between presence and absence of CoQ treatment is represented as $^{a}P<0.05$. Significance between presence and absence of CCCP treatment is represented as $^{b}P<0.01$, $^{c}P<0.001$.

In conclusion, MERRF fibroblasts showed autophagy/mitophagy flux disruption, characterized by a slower degradation of mitochondria by autophagy compared to control cells that could explain the accumulation of autophagosomes and increased Parkin traslocation to mitochondria. CoQ treatment enhanced autophagy and mitophagy flux in MERRF fibroblasts, promoting the degradation of mitochondria by autophagy at a rate similar to control cells.

R-IV. Characterization of mitochondrial dysfunction and autophagy flux disruption in MERRF cybrids harbouring a 90% heteroplasmy load and effect of CoQ treatment.

Our findings indicated the presence of mitochondrial dysfunction, autophagy and Parkin-mediated mitophagy activation and autophagy/mitophagy flux disruption in MERRF fibroblasts with a 57% heteroplasmy load. It is assumed that pathophysiology of MERRF syndrome and other mitochondrial diseases caused by mutations in mtDNA could be related to heteroplasmy load. In order to definitively confirm pathophysiological characteristics associated to the MERRF mutation m.8344A>G, we decided to extend our observations to a transmitochondrial cybrid MERRF cell line harbouring an extremely high heteroplasmy load (90 %). Cybrid cells are very useful tools to exclusively study the influence of mtDNA mutations on cell function and phenotype alterations, independently of the patient's nuclear background[419]. Therefore, there is a loss of patients' nDNA and mtDNA interactions that could modify the behavior of the diseased cells. Cybrids have been widely used for the study of the pathophysiology of MERRF disease and also as a screening platform for the discovery of new potential treatments or toxics[219,420-423].

Accordingly, we investigated different pathophysiological parameters in transmitochondrial cybrid cells harbouring the MERRF mutation m.8344A>G. Moreover, we wanted to observe whether CoQ treatment was also effective on MERRF cybrids with a high heteroplasmy load, independently of the patient's nuclear background.

MERRF cybrids were generated as described in Materials & Methods section.
First, we performed a heteroplasmy analysis to check the mutational load of MERRF cybrids. We confirmed that MERRF cybrids harboured an extremely high heteroplasmy load close to 90 % (86%) (**Figure R29**).

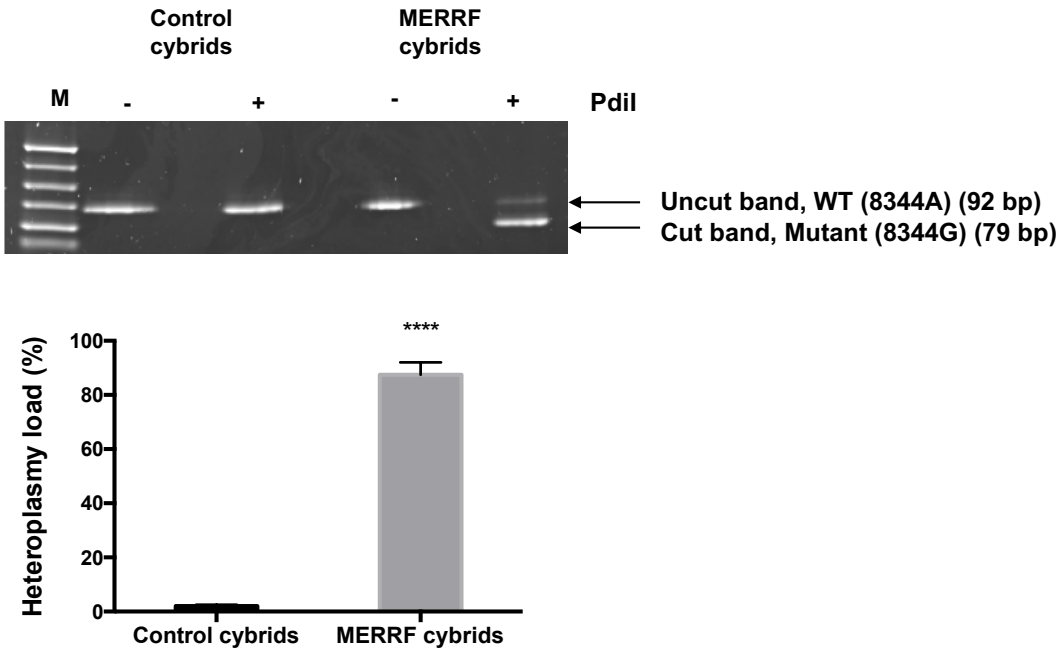

Figure R29. Heteroplasmy load in control and MERRF cybrids.
Heteroplasmy loads were determined by mismatched PCR-RFLP assay. Results are expressed as mean ± SD. Significance of MERRF respect to control cybrids is represented as ****P<0.0001.

Cybrids are supposed to show a glycolytic metabolism due to their tumor nDNA background and their proliferative nature. Therefore, cellular pathophysiology due to mitochondrial dysfunction could be difficult to study. To induce oxidative metabolism, cybrids were cultured in a glucose-restricted medium (hereinafter, oxidative medium) as described in the Materials & Methods section. Then, first we examined the $\Delta\Psi m$ and the ROS levels in control and MERRF cybrids clones. Additionally, we checked the effectiveness of CoQ treatment on these parameters.

First, we determined the $\Delta\Psi m$ of control and MERRF cybrids and the effect of CoQ using the mitochondrial probe JC-1. The ratio red/green fluorescence was significantly reduced by 96% in MERRF cybrids and it was slightly improved under CoQ treatment (**Figure R30**).

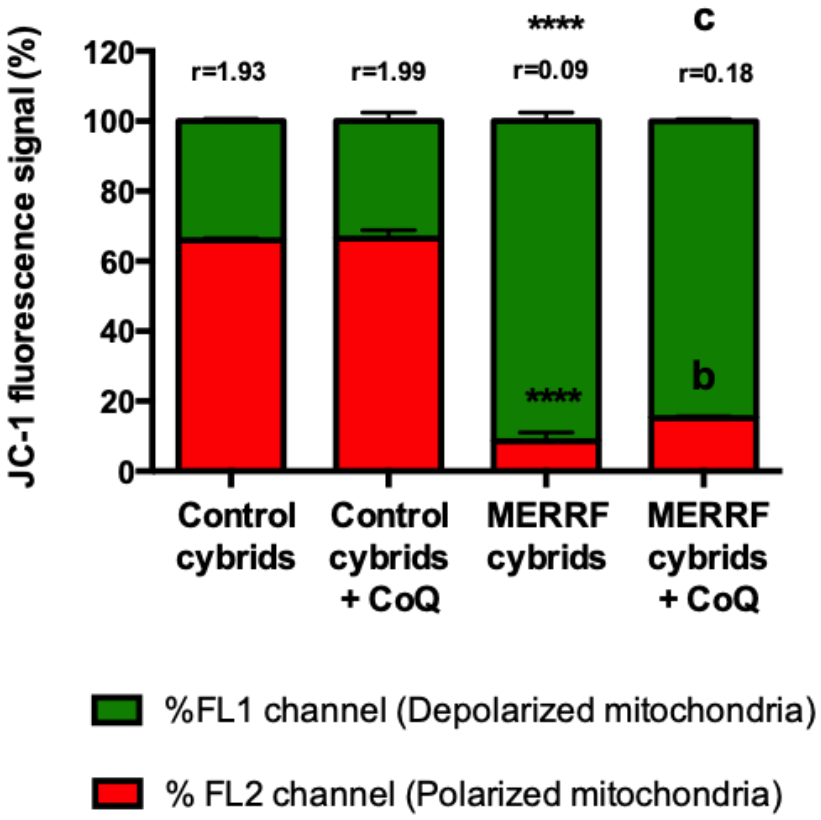

Figure R30. Analysis of mitochondrial membrane potential in untreated and CoQ-treated control and MERRF cybrids by using JC-1 as a ratiometric probe.
Green and red fluorescence signals were measured by flow cytometry in control and MERRF cybrids untreated and treated with CoQ by using JC-1 as a probe. Whereas green signal (FL1 channel) is associated to JC-1 monomers and dissipated mitochondrial membrane potential, red signal (FL2 channel) represents the aggregated form of JC-1, which indicates the intact mitochondrial membrane potential. The stacked bar graph shows the percentage of each JC-1 fluorescence. Ratio between FL2/FL1 signals was estimated. Significance of MERRF respect to control cybrids is represented as $^{****}P<0.0001$. Significance between the presence and the absence of CoQ is represented as $^{b}P<0.01$ and $^{c}P<0.001$.

Moreover, ROS levels were increased in MERRF cybrids and they were significantly decreased by 16% after CoQ treatment (**Figure R31**). These results suggested increased ROS production in MERRF cybrids.

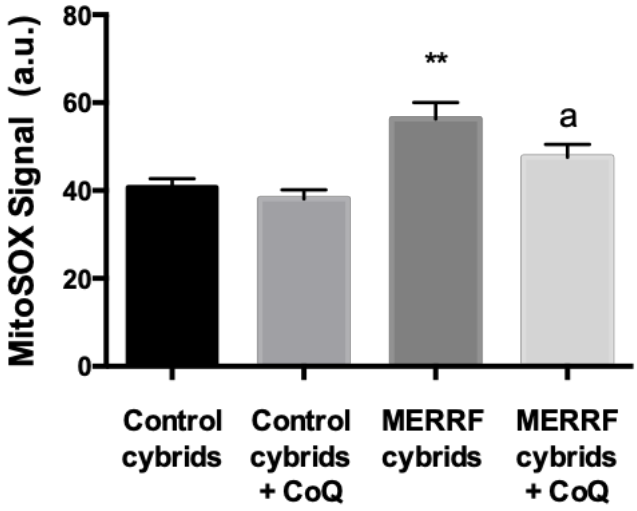

Figure R31. ROS levels in untreated and CoQ-treated control and MERRF cybrids. ROS levels were quantified by using MitoSOX™ as a sensor. Flow cytometry signal was represented as mean fluorescence intensity ± SD (a.u; arbitrary units) of three independent experiments. Significance of MERRF respect to control cybrids is represented as $^{**}P<0.01$. Significance between the presence and the absence of CoQ is represented as $^{a}P<0.05$.

Since mitochondrial ROS levels were elevated in MERRF cybrids, we wanted to determine the general cellular oxidative status in control and MERRF cybrids and its relationship with CoQ treatment by quantifying the content of carbonylated proteins in cellular extracts, using the OxyBlot™ Protein Oxidation Detection Kit (Millipore, USA). The results confirmed that MERRF cybrids showed increased carbonylated protein levels compared to control cells and that CoQ treatment was able to reduce carbonylated proteins levels in both control and MERRF cybrids (**Figure R32**).

As we have explained before, two of the main features in MERRF syndrome are the reduction in mitochondrial proteins synthesis and the complex IV deficiency[351,352]. Therefore, we next analyzed mitochondrial proteins expression levels in control and MERRF cybrids by immunoblotting. As shown in **Figure R33**, MERRF showed decreased mitochondrial proteins expression levels, but CoQ treatment only was able to increase the amount of VDAC1 (OMM protein), not affecting the expression of the subunit II of complex IV (IMM protein).

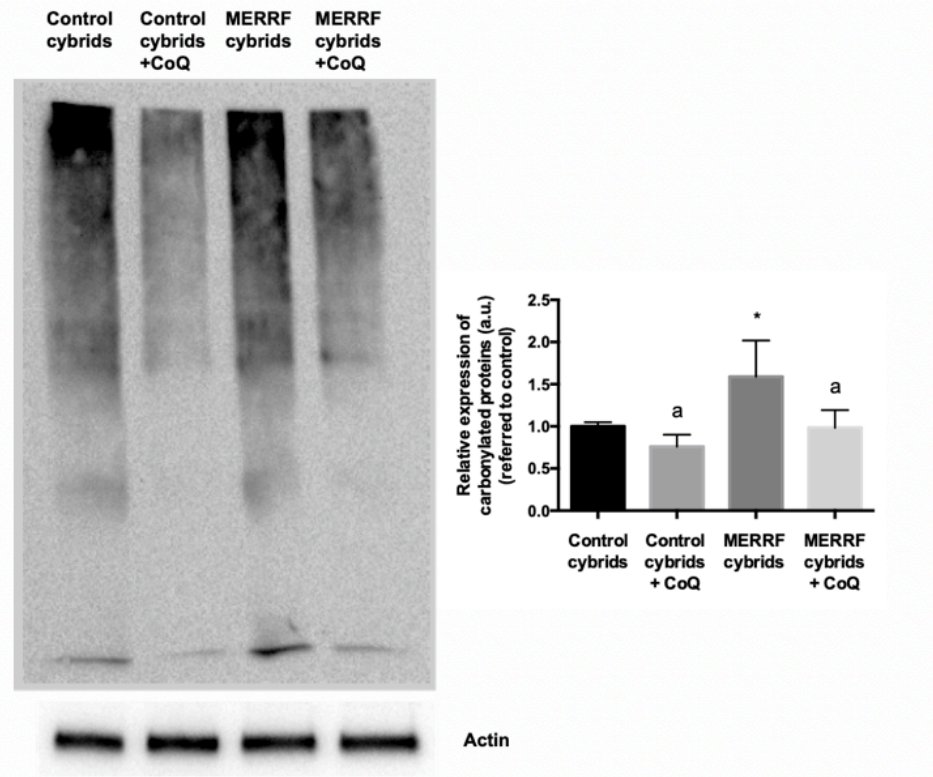

Figure R32. Levels of carbonylated proteins in untreated and CoQ-treated control and MERRF cybrids.

Cellular extracts were assayed by the OxyBlot™ Protein Oxidation Detection Kit. One representative of three independent experiments is shown. Carbonylated proteins levels quantification was performed as described in Materials & Methods section. Significance of MERRF respect to control cybrids is represented as $^{*}P<0.05$. Significance between the presence and the absence of CoQ is represented as $^{a}P<0.05$.

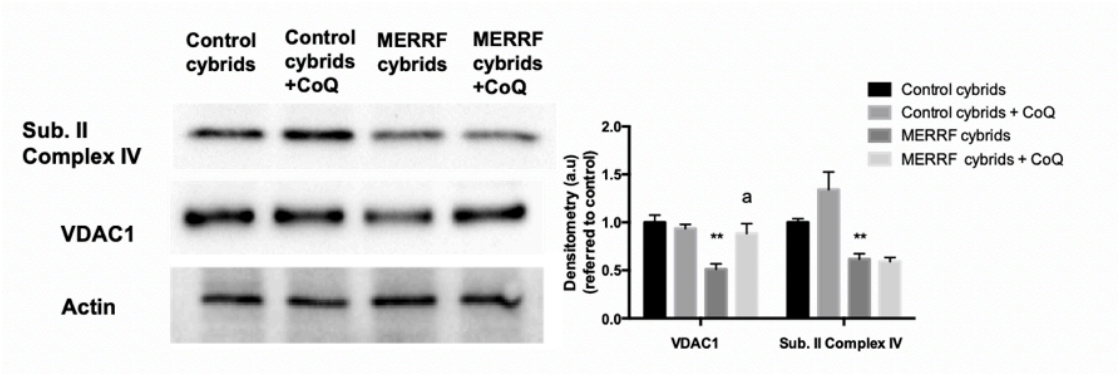

Figure R33. Levels of mitochondrial proteins in untreated and CoQ-treated control and MERRF cybrids.

Significance of MERRF respect to control cybrids is represented as $^{**}P<0.01$. Significance between the presence and the absence of CoQ is represented as $^{a}P<0.05$.

To test whether the different pathological characteristics shown above had an effect on mitochondrial function, we next measured mitochondrial respiratory function and profile of control and MERRF cybrids. For that purpose, we performed the Mito-stress test assay by the XFe24 extracellular flux analyzer (Seahorse Bioscience, Billerica, MA, USA). Moreover, we wanted to determine if CoQ supplementation restored cellular bioenergetics in MERRF cybrids.

The overall respiratory responses of untreated and CoQ-treated control and MERRF cybrids are shown in **Figure R34.** Aerobic respiration (OCR) was reduced in MERRF cybrids compared to controls. Treatment with CoQ did not change OCR neither in control nor in MERRF treated cells.

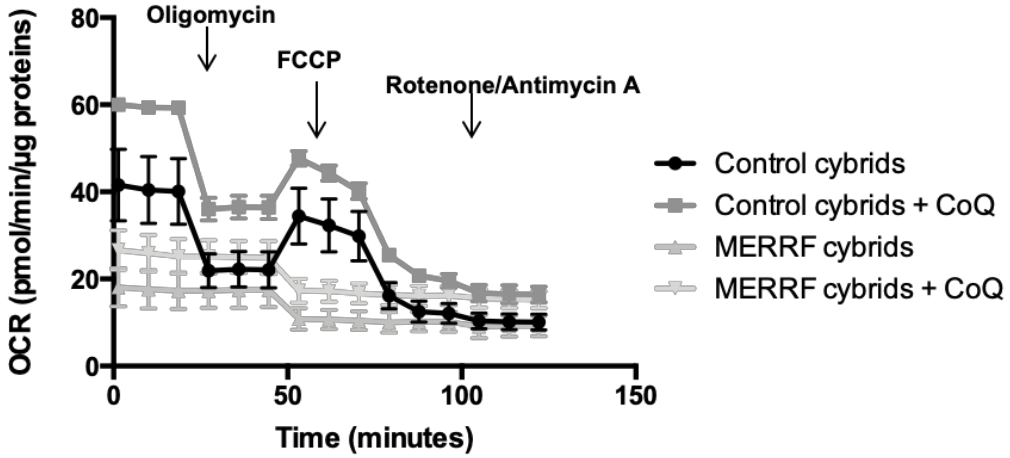

Figure R34. Representative respiratory flux profiles of untreated and CoQ-treated control and MERRF cybrids.

One representative of three independent experiments is shown. Addition of ATP synthase inhibitor oligomycin, electron transport chain uncoupler FCCP and complex I and III inhibitors rotenone and antimycin A are indicated. Untreated and treated control and MERRF cybrids were seeded to 30,000 cells/well and incubated for 24 h. OCR was measured in XF base medium under basal conditions followed by the sequential addition of oligomycin (1 µM), FCCP (2 µM), as well as rotenone (1 µM) & antimycin A (2.5 µM), as indicated. Each data point represents an OCR measurement. Data are expressed as mean ± SD.

After carrying out Mito-stress test, different cellular bioenergetic parameters were calculated using the Seahorse XF Report Generator, a data analysis tool provided by Seahorse Bioscience.

MERRF cybrids showed highly reduced basal respiration, maximal respiration and spare respiratory capacity compared to the control cells. Moreover, OCR coupled to ATP production was also reduced in MERRF cybrids (**Figure R35**).

These findings confirmed that the m.8344A>G mutation led to decreased mitochondrial respiration in a cybrid model of MERRF syndrome, indicating that the mitochondrial dysfunction associated to this mutation is not dependent on the nuclear background.

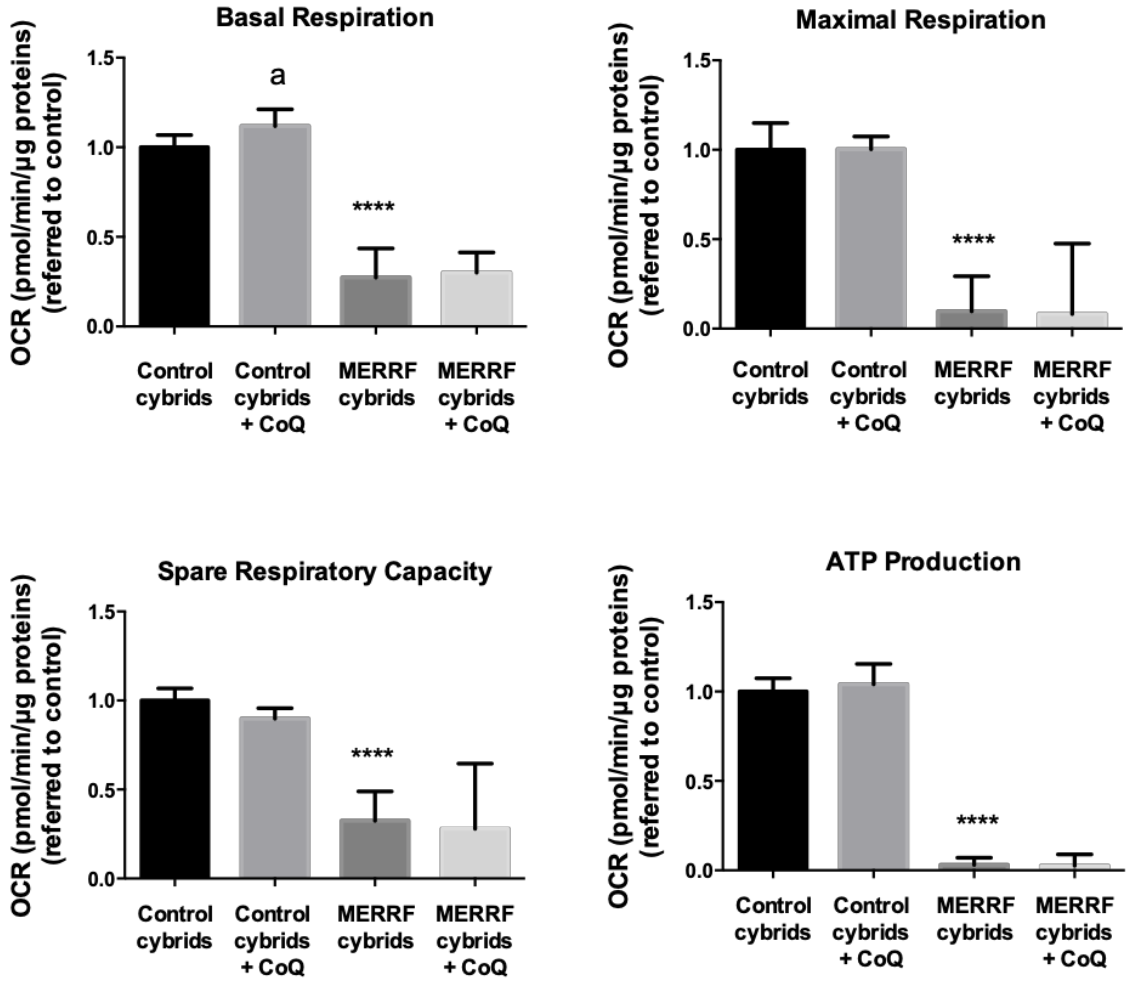

Figure R35. Parameters of mitochondrial respiratory function of untreated and CoQ-treated control and MERRF cybrids.

Basal mitochondrial respiration, maximal respiration, spare respiratory capacity and ATP-linked respiration were calculated as described above. Results are expressed as mean ± SD, n = 3 independent experiments. Significance of MERRF respect to control cybrids is represented as ****P<0.0001. Significance between the presence and the absence of CoQ is represented as ^{a}P<0.05. All OCR readings were normalized to µg of proteins as described in Materials & Methods section.

However, CoQ treatment did not change the levels of any parameters of the mitochondrial function in MERRF cybrids, suggesting that the beneficial effects of this molecule can be altered depending on the heteroplasmy load of the cells (**Figure R35**).

To determine whether autophagy activation in MERRF syndrome was caused by the effect of m.8344A>G mutation, independently of the patient's background, we investigated the conversion of LC3B-I to LC3B-II in MERRF cybrids. The amount of LC3B-II was significantly increased in MERRF cybrids (**Figure R36**), indicating enhanced autophagosome formation in MERRF cells. Supplementation of the culture medium with 100 μM CoQ resulted in a significant decrease in the relative amount of LC3B-II in MERRF cybrids cultures.

P62 expression levels were also increased in MERRF cybrids, indicating autophagy impairment. Treatment with 100 μM CoQ resulted in a significant decrease in the relative amount of P62 in MERRF cybrids cultures (**Figure R36**).

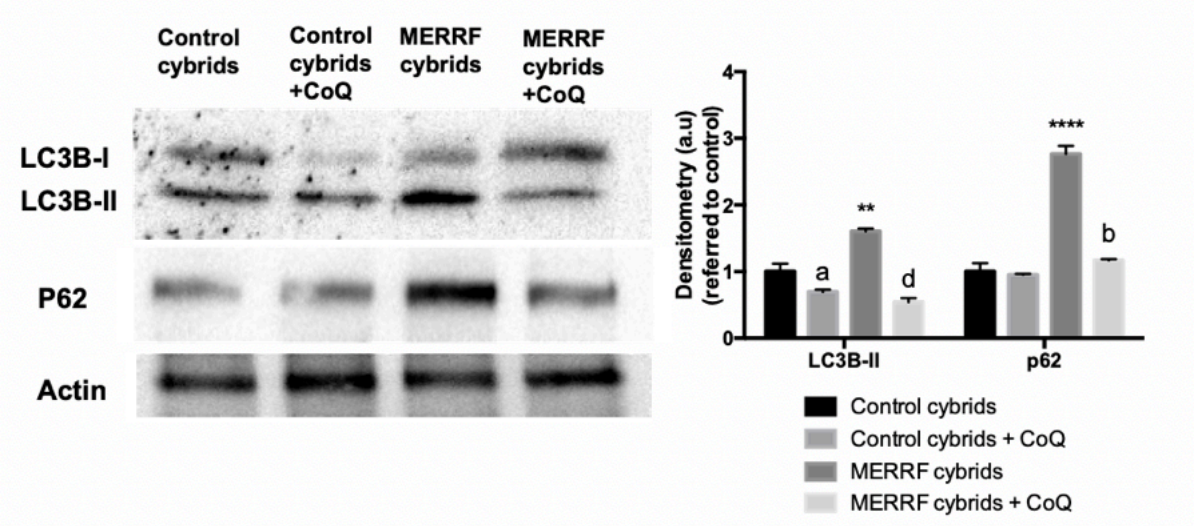

Figure R36. Expression levels of autophagic proteins in untreated and CoQ-treated control and MERRF cybrids.

Protein expression levels of LC3B and P62 were determined in control and MERRF cybrids cultures before and after CoQ treatment by Western blotting. Densitometry analysis of Western blotting was performed by using ImageLab software. Actin was used as a loading control. Data represent the mean ± SD of three separate experiments. Significance of MERRF respect to control cybrids is represented as **P<0.01 and ****P<0.0001. Significance between the presence and the absence of CoQ is represented as ^{a}P<0.05, ^{b}P<0.01 and ^{d}P<0.0001.

The increased LC3B-II protein expression in MERRF cybrids could suggest a higher autophagy activation compared to the controls or a blockage of the autophagy flux. To distinguish between that two possibilities, we treated control and MERRF cybrids with 100 nM bafilomycin A1 for 12 hours.

As expected, bafilomycin A1 treatment in control cybrids led to a significant increase in the amount of LC3B-II, suggesting that autophagy flux was correct in control cells. However, bafilomycin A1 treatment in MERRF cybrids had no effect on LC3B-II levels, indicating that autophagy flux was disrupted (**Figure R37**).
As shown in **Figure R36**, CoQ treatment reduced the levels of LC3B-II in MERRF cybrids. However, this reduction could be due to a prevention of autophagy activation or a reduction of autophagolysosome accumulation (autophagy flux enhancing). Therefore, in order to check the specific effect of CoQ on autophagy, CoQ pre-treated control and MERRF cybrids were exposed to bafilomycin A1 and LC3B-II protein levels were examined by Western blotting (**Figure R37**).
Bafilomycin A1 incubation induced a significant increase on LC3B-II expression levels of CoQ-treated MERRF cybrids, suggesting that CoQ treatment enhanced autophagy flux by promoting autophagolysosome clearance in pathological cells. In control cells, with a correct autophagy flux, CoQ treatment had no effect in BAF-treated cells.

Altogether, our findings indicated that MERRF cybrids with high heteroplasmy load reproduced severe pathophysiological alterations that we had previously observed in patient-derived skin fibroblasts, such as reduced $\Delta\Psi m$, high levels of mitochondrial ROS, increased levels of carbonylated proteins, decreased mitochondrial mass and decreased mitochondrial respiration. However, not all of these alterations could be ameliorated by CoQ treatment, suggesting that the beneficial effects of this molecule can be altered depending on the heteroplasmy load of the cells.

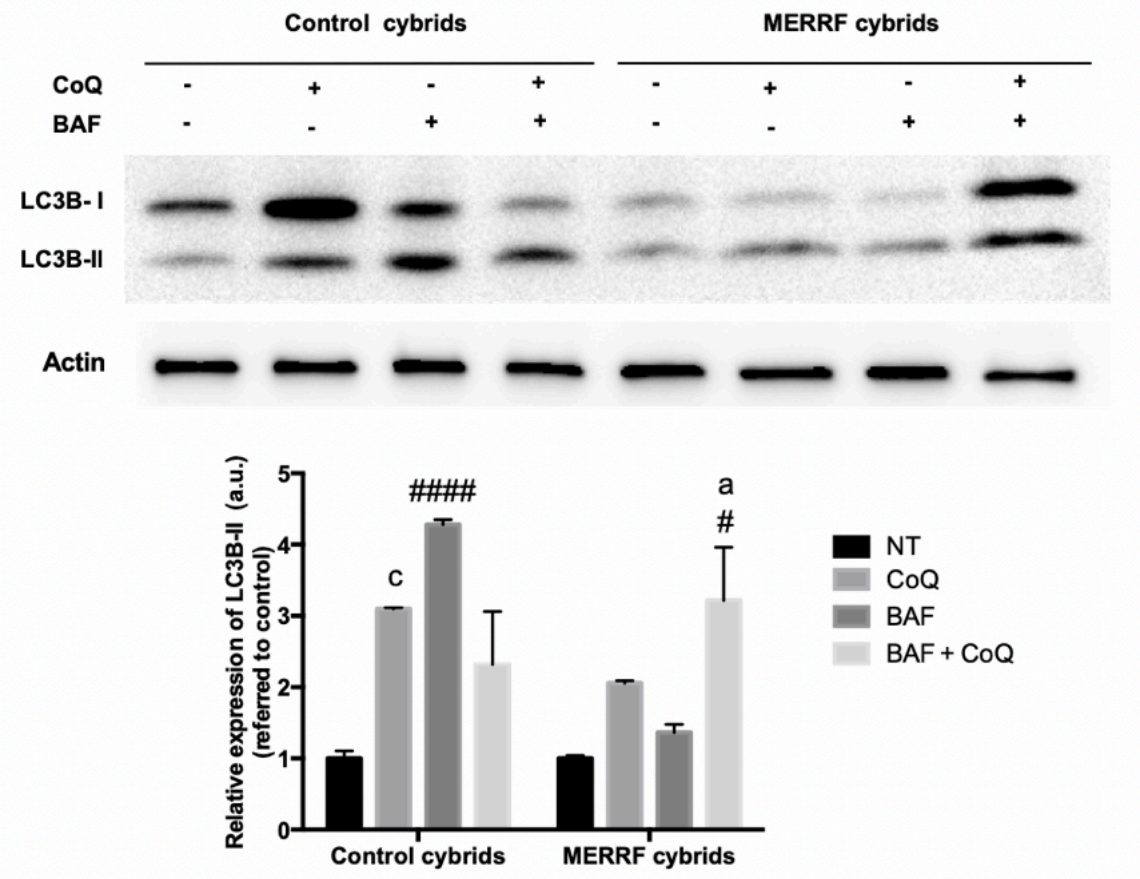

Figure R37. Autophagy flux analysis in control and MERRF cybrids and effect of CoQ treatment on autophagy flux.

Autophagy flux was checked by determination of LC3B-II protein expression levels in the presence and absence of bafilomycin A1 (BAF). Control and MERRF cybrids were incubated with 100 nM BAF for 12 h, and, when indicated, cells were pre-treated with 100 μM CoQ for 72 hours. Total cellular extracts were analyzed by immunoblotting with an antibody against LC3B. Actin was used as a loading control. Densitometry of LC3B-II was performed by using ImageLab software. Data are represented as mean ± SD of three separate experiments. Significance between presence and absence of CoQ treatment is represented as $^{a}P<0.05$ and $^{c}P<0.001$. Significance between presence and absence of bafilomycin A1 treatment is represented as $^{\#}P<0.05$ and $^{\#\#\#\#}P<0.0001$.

Moreover, the use of MERRF cybrid cells model has reinforced the role of autophagy flux in this disease, since we have observed a disruption of the correct functioning of the process as a direct result of the mitochondrial m.8344A>G mutation and not as a consequence of nuclear defects in patient-derived cells.

Furthermore, the role of CoQ as an enhancer of autophagy flux has been confirmed in this cellular model.

R-V. Rapamycin as an alternative to CoQ treatment in MERRF fibroblasts and cybrids.

As far as we have shown in the previous Results subsections, CoQ ameliorates several aspects of the pathophysiology of MERRF fibroblasts and cybrids by enhancing the autophagy/mitophagy flux, which is disrupted in the diseased cells.
However, we wanted to further investigate and confirm the beneficial effects of autophagy/mitophagy induction in MERRF syndrome, since CoQ is a pleiotropic agent that could have an impact in different cellular pathways[601].
Moreover, the use of pro-autophagy agents as a plausible therapy for different diseases has increased in the last years.
The most studied autophagy inducers are rapamycin and its analogues, which are considered potential therapeutic agents for tumors[602,603] or neurodegenerative diseases such as HD[302].
Moreover, the beneficial effect of rapamycin treatment in a mouse model of Leigh syndrome has been recently published[314], and its potential use in the therapy of mitochondrial diseases is being currently discussed.
For all these reasons, we were interested in investigating the potential use of rapamycin in the treatment of MERRF syndrome and its effect on the mitochondrial dysfunction shown by the different MERRF cellular models.

First, we used skin fibroblasts derived from one MERRF patient (the same model used in subsections **R-I-III**) with 54% of heteroplasmy load and control fibroblasts derived from two healthy volunteers. We measured the mitochondrial respiratory function and profile of control and MERRF fibroblasts, untreated and treated with 100 nM rapamycin for 30 days. Moreover, we wanted to observe whether rapamycin effect on mitochondrial function was sustained over time after removing the treatment. Therefore, after rapamycin treatment, we maintained pre-treated MERRF fibroblasts for other 30 days (hereinafter, MERRF post-rapamycin).
To measure mitochondrial respiratory function of all cell populations described above, we performed the Mito-stress test assay by the XFe24 extracellular flux analyzer (Seahorse Bioscience, Billerica, MA, USA).

The overall respiratory responses of untreated and treated controls and MERRF fibroblasts are shown in **Figure R38.** As observed in **R-I** subsection**,** aerobic respiration (OCR) was reduced in MERRF fibroblasts compared to controls. Treatment with rapamycin increased OCR both in control and MERRF treated cells. Moreover, the increase of OCR in MERRF fibroblasts due to rapamycin treatment was sustained over time after rapamycin removal.

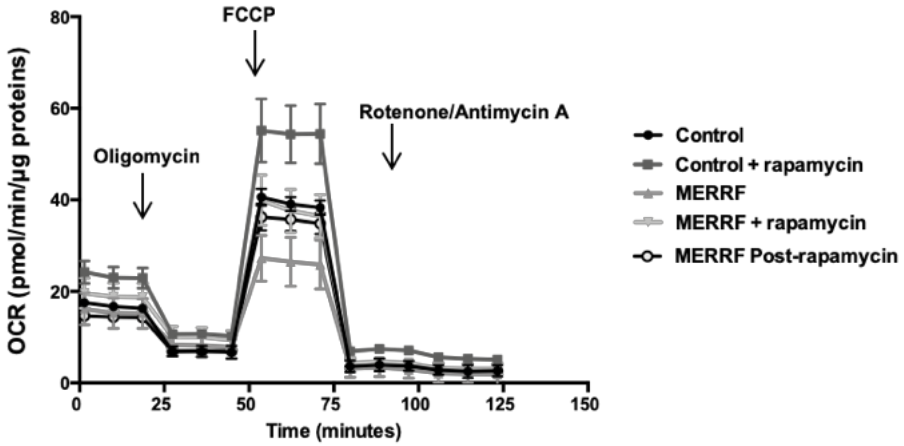

Figure R38. Representative respiratory flux profiles of untreated and rapamycin-treated control and MERRF fibroblasts.
One representative of three independent experiments is shown. Addition of ATP synthase inhibitor oligomycin, electron transport chain uncoupler FCCP and complex I and III inhibitors rotenone and antimycin A are indicated. Untreated and treated control and MERRF fibroblasts were seeded to 15,000 cells/well and incubated for 24 h. OCR was measured in XF base medium under basal conditions followed by the sequential addition of oligomycin (1 µM), FCCP (2 µM), as well as rotenone (1 µM) & antimycin A (2.5 µM), as indicated. Each data point represents an OCR measurement. Data are expressed as mean ± SD.

After carrying out Mito-stress test, different cellular bioenergetic parameters were calculated using the Seahorse XF Report Generator, a data analysis tool provided by Seahorse Bioscience.

As we have observed in subsection **R-I**, MERRF fibroblasts showed reduced basal respiration, maximal respiration and spare respiratory capacity compared to the control cells. Moreover, OCR coupled to ATP production was also reduced in MERRF fibroblasts (**Figure R39**).

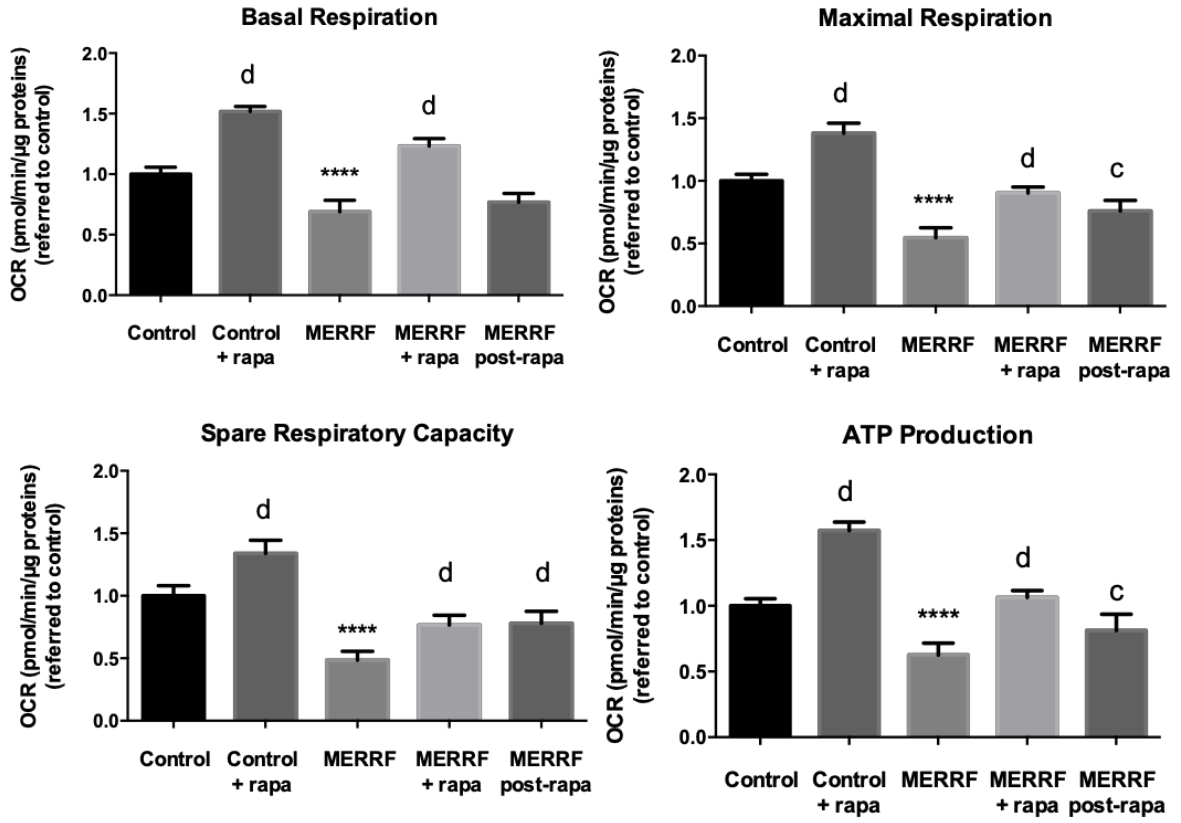

Figure R39. Parameters of mitochondrial respiratory function of untreated and rapamycin-treated control and MERRF fibroblasts.
Basal mitochondrial respiration, maximal respiration, spare respiratory capacity and ATP-linked respiration were calculated as described above. Results are expressed as mean ± SD, n = 3 independent experiments. Significance of MERRF respect to control fibroblasts is represented as ****P<0.0001. Significance between the presence and the absence of rapamycin (rapa) is represented as ^{c}P<0.001 and ^{d}P<0.0001. All OCR readings were normalized to µg of proteins as described in Materials & Methods section.

Rapamycin treatment significantly increased basal respiration, maximal respiration, spare respiratory capacity and ATP production of both control and MERRF fibroblasts (**Figure R39**). Moreover, 30 days after removal of rapamycin treatment, the maximal respiration, spare respiratory capacity and ATP production of MERRF fibroblasts were still increased, almost reaching the levels of the control cells.

Since CoQ was unable to improve any mitochondrial respiratory parameters in MERRF cybrids harbouring an extremely high heteroplasmy load (**Figure R35**), we

wanted to check whether rapamycin, as a direct autophagy promoter, was able to rescue mitochondrial function in this MERRF cellular model.

We measured the mitochondrial respiratory function and profile of control and MERRF cybrids, untreated and treated with 100 nM rapamycin for 72 hours (**Figure R40 and R41**). The overall respiratory responses of untreated and rapamycin-treated controls and MERRF cybrids are shown in **Figure R40.**

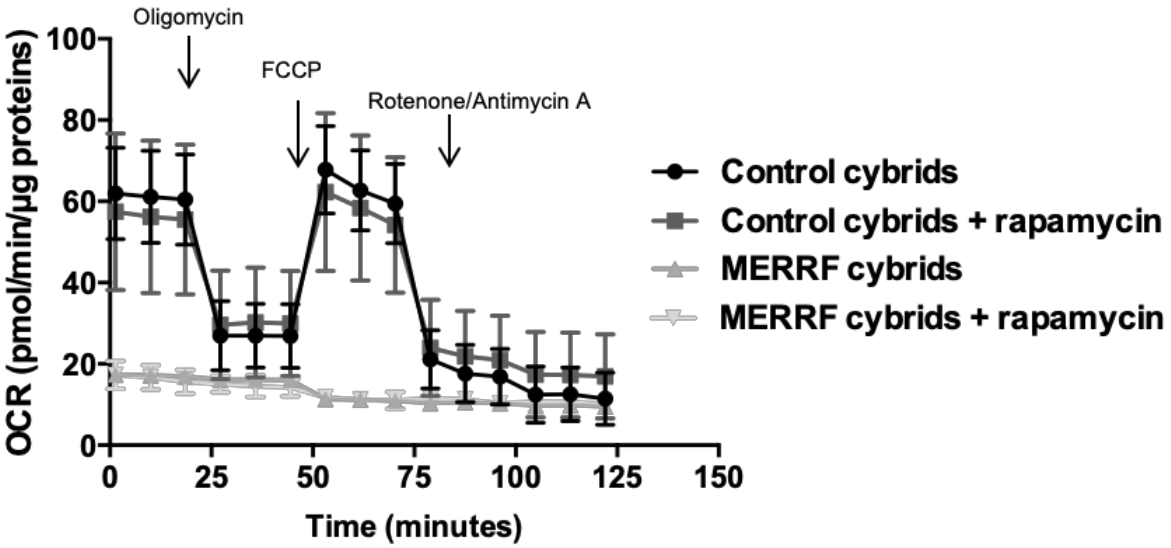

Figure R40. Representative respiratory flux profiles of untreated and rapamycin-treated control and MERRF cybrids.

One representative of three independent experiments is shown. Addition of ATP synthase inhibitor oligomycin, electron transport chain uncoupler FCCP and complex I and III inhibitors rotenone and antimycin A are indicated. Untreated and treated control and MERRF cybrids were seeded to 30,000 cells/well and incubated for 24 h. OCR was measured in XF base medium under basal conditions followed by the sequential addition of oligomycin (1 µM), FCCP (2 µM), as well as rotenone (1 µM) & antimycin A (2.5 µM), as indicated. Each data point represents an OCR measurement. Data are expressed as mean ± SD.

After carrying out Mito-stress test, different cellular bioenergetic parameters were calculated using the Seahorse XF Report Generator, a data analysis tool provided by Seahorse Bioscience.

As we have previously observed in **Figure R35**, MERRF cybrids showed reduced basal respiration, maximal respiration and spare respiratory capacity compared to the control cells. Moreover, OCR coupled to ATP production was also reduced in MERRF fibroblasts (**Figure R41**).

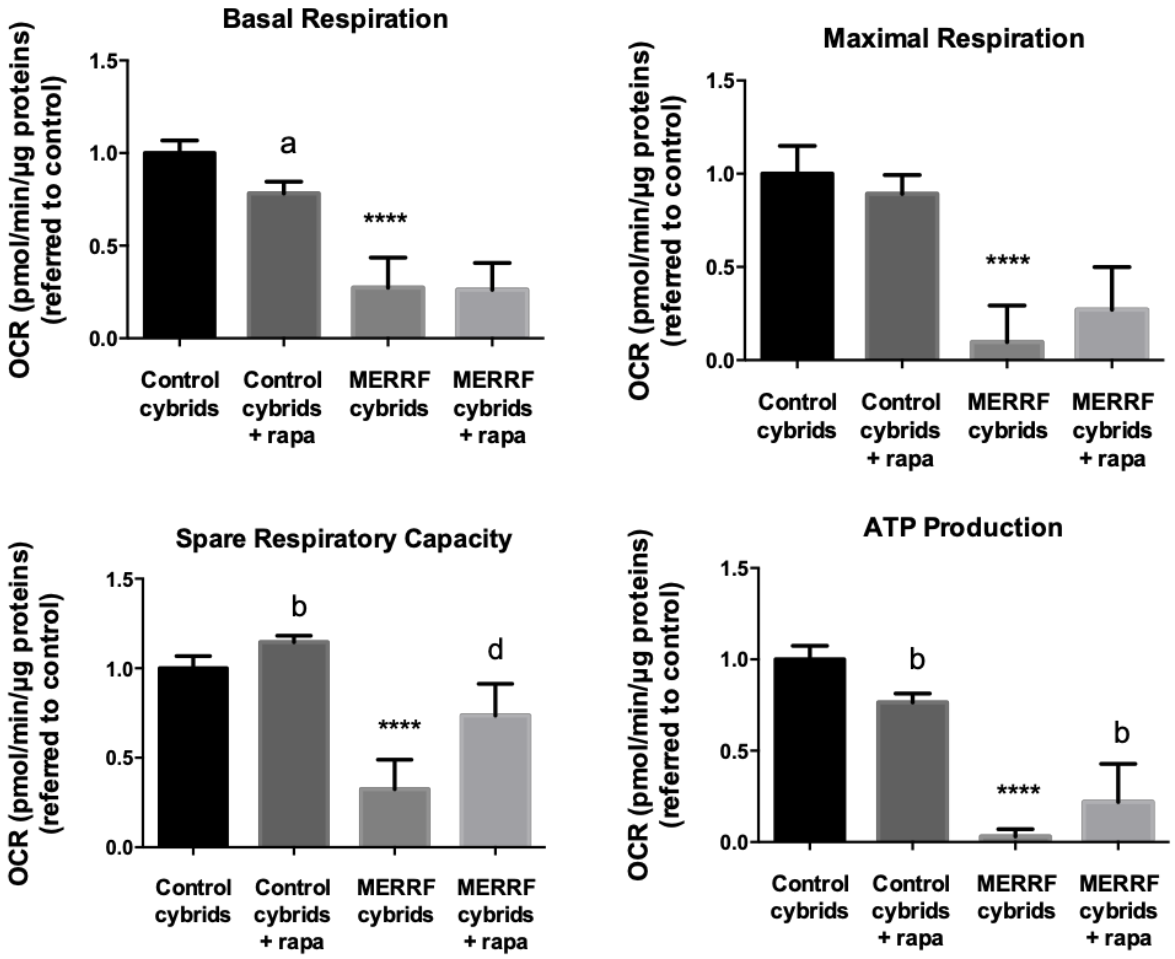

Figure R41. Parameters of mitochondrial respiratory function of untreated and rapamycin-treated control and MERRF cybrids.

Basal mitochondrial respiration, maximal respiration, spare respiratory capacity and ATP-linked respiration were calculated as described above. Results are expressed as mean ± SD, n = 3 independent experiments. Significance of MERRF respect to control cybrids is represented as ****P<0.0001. Significance between the presence and the absence of rapamycin (rapa) is represented as ^{a}P<0.05, ^{b}P<0.01 and ^{d}P<0.0001. All OCR readings were normalized to µg of proteins as described in Materials & Methods section.

Interestingly, rapamycin treatment significantly increased the levels of some parameters of mitochondrial function in MERRF cybrids, such as the spare respiratory capacity and ATP production. However, rapamycin treatment decreased basal mitochondrial respiration and OCR coupled to ATP production in control cybrids (**Figure R41**).

Altogether, these results suggest that rapamycin treatment is able to improve some parameters of mitochondrial respiration in different models of MERRF syndrome. Therefore, autophagy induction in mutant cells exerts a protective role, ameliorating cellular pathophysiology. The differential behavior after rapamycin treatment between MERRF fibroblasts and cybrids could be due to their different mutational load. Indeed, MERRF cybrids showed a much more severe pathological phenotype.

The unexpected effect of rapamycin treatment in basal respiration and ATP production in control cybrids can be due to the concentration of the treatment and/or the response of the tumor cells to the treatment. Although it has been generally accepted that rapamycin impairs mTORC1 function by inhibiting the interaction of raptor with mTOR[604], it has been observed that high concentrations or chronic treatments with rapamycin also interfere with assembly of mTORC2 and inhibits its function[605], decreasing cellular proliferation and cell growth. In fact, rapamycin treatment has been investigated as a potential therapy for many cancers[606-608]. Therefore, a fine regulation of concentration and length of rapamycin treatment is crucial.

Given that, an in-depth characterization of rapamycin effects in MERRF cellular models is necessary to provide new insights for unravelling the role of autophagy/mitophagy promotion in mitochondrial diseases.

R-VI. Role of Parkin-mediated mitophagy in MERRF syndrome.

Currently, there is a controversy whether mitophagy is protective or detrimental for mitochondrial diseases. Although a dysfunction of mitophagy is associated with a lot of pathological conditions, such as PD[161], AD[609,610], HD[611,612] and different chronic kidney diseases[613-615]; in other illnesses, such as lung disease[616,617] or cardiovascular diseases[618], mitophagy factors could be damaging.

In the case of mitochondrial diseases, the role of mitophagy is not clear. In some cases, activation of mitophagy in mitochondrial diseases seems to be protective, because it has been demonstrated that disruption of mitophagy by autophagy sequestration using chemicals such as 3-methyl adenine or wortmannin or by genetic knockdown of *ATG* genes in MELAS or primary CoQ-deficient fibroblasts results in cell death by apoptosis[204,221]. Nevertheless, high activation of mitophagy in these cellular models can suppose a loss of mitochondrial mass, resulting in the energetic collapse of the cell. Therefore, if mitophagy activation is not compensated by increased mitochondrial biogenesis, degradation of dysfunctional mitochondria cannot be protective and becomes detrimental for cell survival[167].

In order to elucidate the role of Parkin-mediated mitophagy in MERRF syndrome, we decided to use MERRF cybrids with silenced Parkin expression (transfected with lentiviral vectors carrying shRNA-Parkin sequences). Lentiviral vectors carrying non-silencing shRNA sequences were used as control. We first checked the knockdown of the expression of Parkin protein by Western Blotting (**Figure R42**).

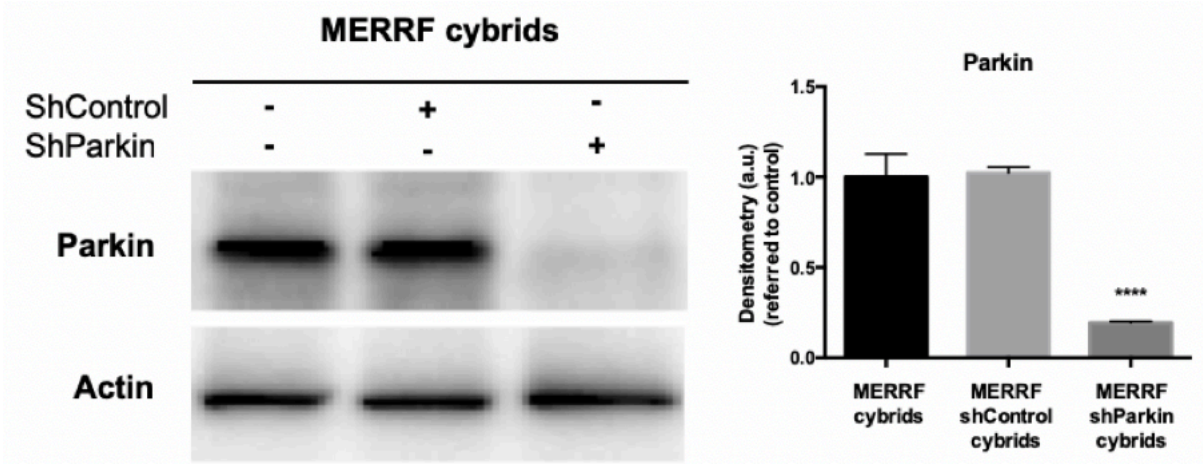

Figure R42. Silencing of endogenous Parkin expression in MERRF cybrids cells. The shRNA-Parkin sequences induced Parkin knockdown in transfected MERRF cybrids. Total cellular extracts of MERRF, MERRF shControl and MERRF shParkin cybrids were analyzed by immunoblotting with an antibody against Parkin. Actin was used as a loading control. Densitometry of Parkin was performed by using ImageLab software. Data are represented as mean ± SD of three separate experiments. Significance of MERRF shParkin cybrids respect to MERRF cybrids is represented as ****P<0.0001.

The expression of Parkin protein was reduced by 80% in MERRF shParkin cybrids.

To further check the drop of Parkin protein expression, we performed a double immunofluorescence with Parkin antibody and MitoTracker^{TM} Red CMXRos (**Figure R43**). This double staining allowed us to also assess whether Parkin was indeed translocated to fragmented, depolarized mitochondria in MERRF cybrids.

The fluorescence of Parkin signal was reduced by 90% in MERRF shParkin cybrids, confirming the reduced expression of the protein in these cells.

Moreover, Parkin translocation to fragmented mitochondria was clearly observed in MERRF cybrids.

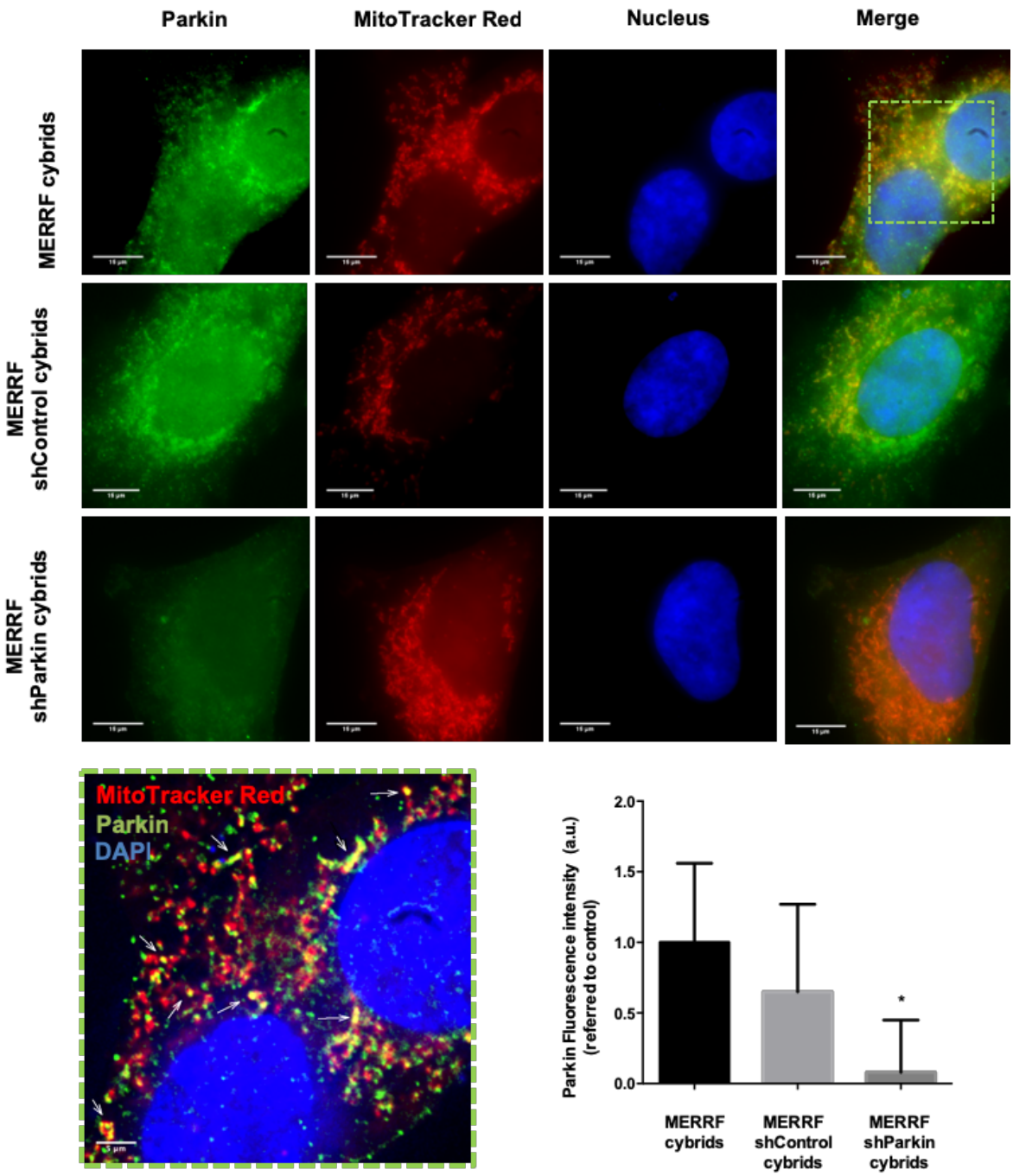

Figure R43. Immunofluorescence microscopy of MitoTracker™ Red CMXRos and Parkin in MERRF cybrids.

Transfection of shRNA Parkin sequences markedly decreased Parkin signal in MERRF cybrids compared with that in scramble shRNA-transfected cells. Magnification of a small area of MERRF cybrids showing translocated Parkin into small, rounded depolarized mitochondria (white arrows) is shown. Data represent the mean ± SD of three separate experiments. Significance of MERRF shParkin cybrids respect to MERRF cybrids is represented as $^{*}P<0.05$. [Scale bar = 15 μm and 5 μm in magnified picture].

Mitochondrial ROS accumulation is thought to be one of the main signals which induce mitophagy in mammalian cells. Damaged or dysfunctional mitochondria produce ROS at levels that exceed the capacity of the antioxidant system and can result in cell death, since ROS accumulation contributes to opening of the MPTP[619].

Therefore, mitophagy is considered a mitochondrial quality control mechanism that can be triggered in response to the high levels of ROS accumulated in dysfunctional mitochondria, which could provoke the oxidative modification of mitochondrial proteins, lipids and mtDNA.

To observe the impact of Parkin-mediated mitophagy in ROS levels regulation in MERRF syndrome, we examined mitochondrial superoxide levels in MERRF cybrids with endogenous Parkin expression and MERRF shParkin cybrids by flow cytometry. For that purpose, we used MitoSOX™ as a mitochondrial superoxide fluorescent probe.

Interestingly, MERRF shParkin cybrids showed an increased by 54% in mitochondrial ROS levels compared to MERRF cybrids (**Figure R44**).

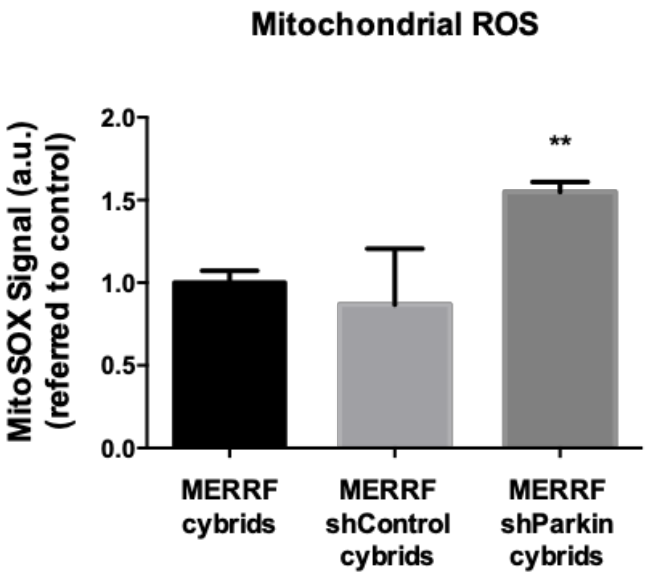

Figure R44. Silencing of endogenous Parkin expression in MERRF cybrids increases mitochondrial ROS levels.

ROS levels were quantified by using MitoSOX™ as a sensor. Flow cytometry signal is represented as mean fluorescence intensity ± SD (a.u; arbitrary units) of three independent experiments. Significance of MERRF shParkin cybrids respect to MERRF cybrids fibroblasts is represented as $^{**}P<0.01$.

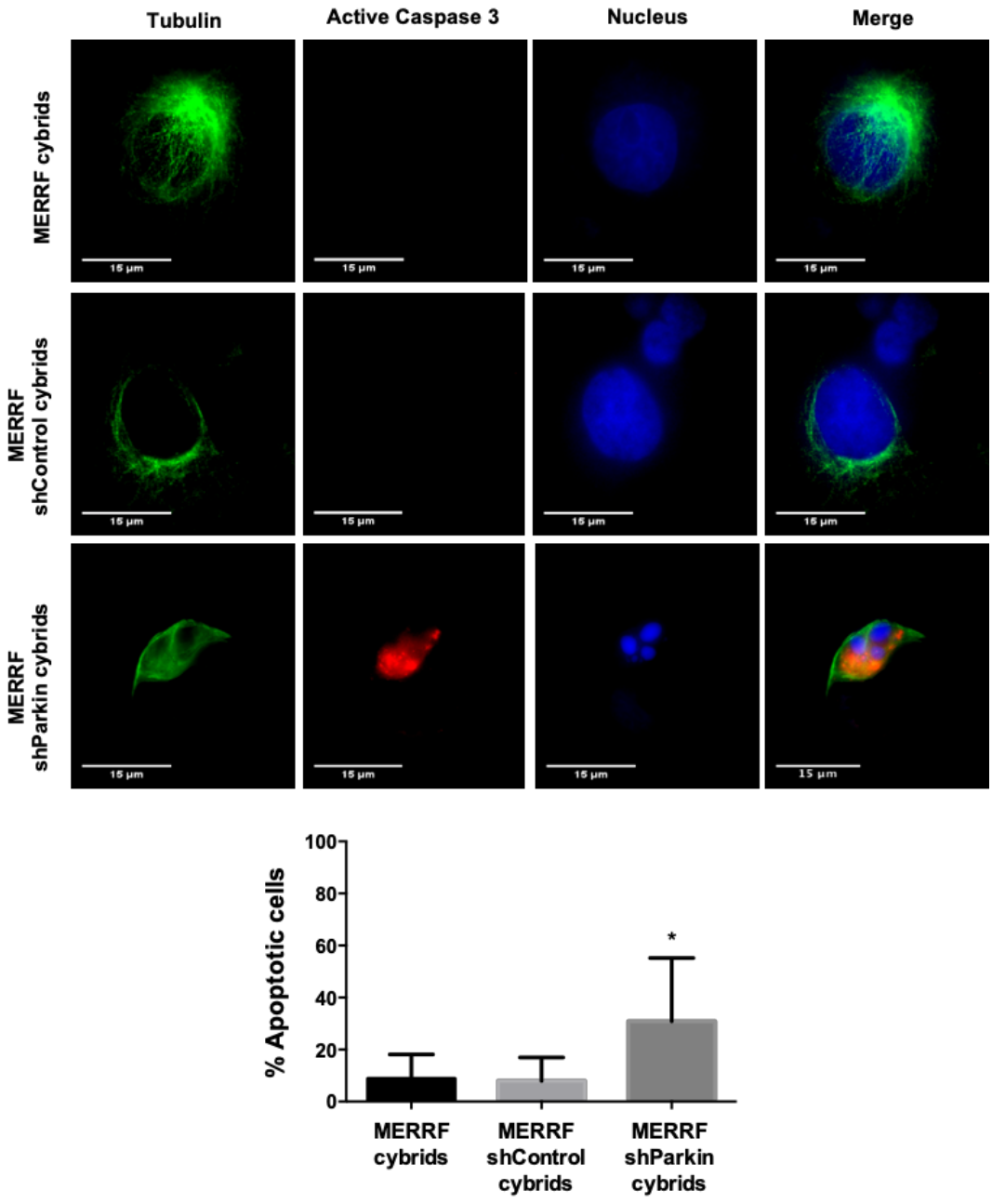

Figure R45. Increased apoptosis levels in MERRF shParkin cybrids.
MERRF cybrids with endogenous or silenced expression of Parkin were cultured in oxidative medium. Immunostaining of tubulin (cytoskeleton protein) and active caspase 3 (apoptotic marker) was performed to visualize apoptosis activation in MERRF cybrids. DAPI staining was used to visualize blebbing or nuclear fragmentation. After, apoptosis levels were analyzed and quantified as described in Materials & Methods section. Data represent the mean ± SD of three separate experiments. Significance of MERRF shParkin cybrids respect to MERRF cybrids is represented as $^{*}P<0.05$. [Scale bar = 15 µm].

Moreover, we were interested in the evaluation of viability of MERRF shParkin cells since there are several studies that link autophagy/mitophagy induction and prevention of cell death[204,221].

Therefore, we verified the role of Parkin-mediated mitophagy in survival of MERRF cells by examining the levels of apoptosis in MERRF cybrids with endogenous levels of Parkin and with knockdown Parkin expression, after 24 hours in oxidative medium. We quantified the number of apoptotic cells by visualization of nucleus fragmentation, caspase 3 activation and the presence of the AMN[620,621].

We observed that MERRF cybrids with knockdown expression of Parkin showed an increase of apoptosis level by 22% compared to MERRF cybrids with endogenous Parkin expression (**Figure R45**).

In conclusion, these results suggest that Parkin-mediated mitophagy could have a protective role in MERRF syndrome. Mitophagy prevented the accumulation of mitochondrial ROS and avoided the induction of apoptotic cell death in MERRF cybrids.

These preliminary results in cellular models of MERRF syndrome are encouraging, because an improvement of mitochondrial pathophysiology after the treatment with autophagy/mitophagy modulators has been observed in different mitochondrial diseases. Therefore, we can speculate that the promotion of elimination of dysfunctional mitochondria by autophagy can be a potential therapeutic approach for mitochondrial dysfunctions.

R-VII. MERRF iNs as a new cellular model to study the pathophysiology of MERRF syndrome.

It is widely known that in diseases that undergo neurodegeneration, such as PD, HD, AD or some neurodegenerative mitochondriopathies such as MELAS or MERRF syndromes, disease molecular pathophysiology is not always exclusive to neurons and as a result, several pathogenic characteristics can be observed in other cell types such as fibroblasts or cybrids[219,254,505,622-625].
In accordance to that, so far, our studies using patient-derived skin fibroblasts and cybrids cells models have shed light on the role of autophagy and mitophagy in the molecular pathophysiology of MERRF syndrome and the importance of the heteroplasmy load in the molecular and clinical phenotype of the disease.

However, these cellular models have shortcomings. Both cybrids and skin fibroblasts, unlike the cell types mostly affected in MERRF patients, are proliferative and rely on glycolytic metabolism for energy production. Therefore, they are not much vulnerable to energy-dependent defects resulting from mitochondrial dysfunction. Moreover, the phenotype may not be evident in defects involving the expression and maintenance of mtDNA. Therefore, they are not the perfect cellular model to study the pathophysiology of mitochondrial diseases.

In fact, the molecular pathogenesis of MERRF syndrome remains poorly understood due to the lack of appropriate cellular models, particularly in those cell types mostly affected in the disease such as neurons.
For that reason, we wanted to stablish a new cellular model for the study of the pathogenesis of the disease, generating patient-specific iNs from dermal fibroblasts (carrying the particular mutation causing the disease) by direct reprogramming. We thought that MERRF iNs generation would provide an opportunity to study mitochondrial diseases in one of the cell types primarily affected.

Therefore, we started from primary fibroblasts derived from skin biopsy samples from two healthy volunteers (hereinafter, Control 1 and Control 2) and two MERRF patients (hereinafter, MERRF 1 and MERRF 2), carrying the most common MERRF

mutation m.8344A>G. For direct reprogramming of fibroblasts into neurons, we employed a recently described method to express proneural genes *ASCL1* and *BRN2* and knock down REST complex by infecting control and MERRF fibroblasts with lentiviral vectors[494] (see Materials & Methods section).

The neural conversion lasted 27 days. During that time, fibroblasts suffered different morphological changes shown in **Figure R46**. Five DPI, fibroblasts' morphology started to change, showing a decreased cell body area. Branches were detectable from 15 DPI both in control and MERRF iNs.

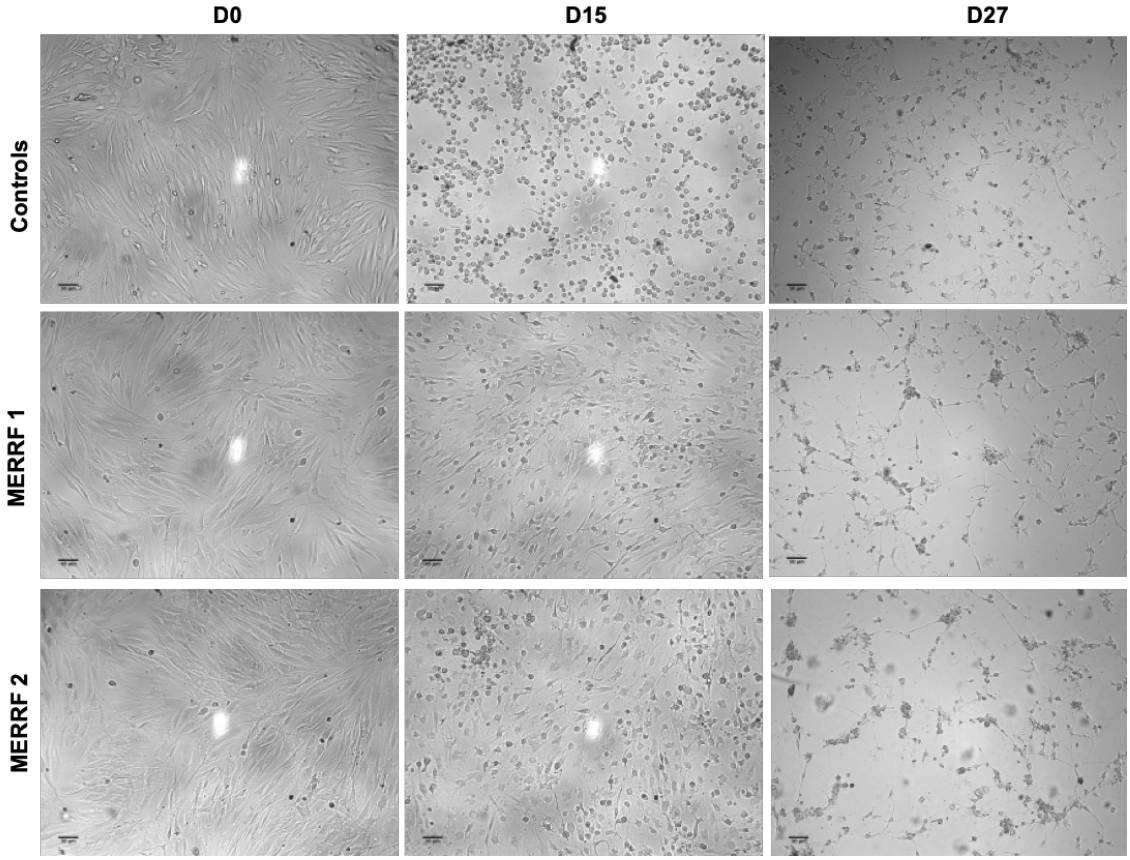

Figure R46. Representative images of the morphological changes of controls and MERRF cells during the days 0, 15 and 27 of neuronal conversion.
Cell morphology was observed using a Leica DMi1 brightfield microscope (Leica Microsystems GmbH, Wetzlar, Germany). [Scale bar=50 µm].

The neural conversion was stopped at 27 DPI, when we observed that most of the cells in the plate exhibited a typical neuron-like morphology, with small body areas, two or more branches and even connections between iNs (**Figure R47**).

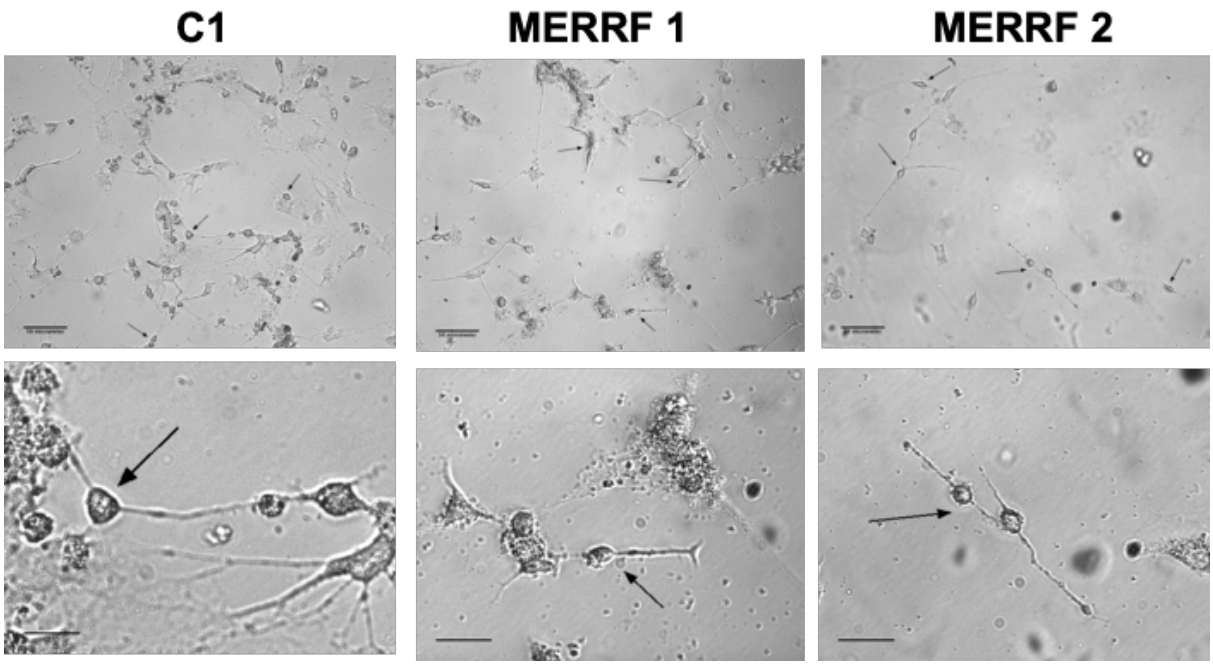

Figure R47. Generation of iNs from controls and MERRF fibroblasts.
Direct reprogramming was stopped twenty-seven DPI and iNs morphology was observed (black arrows) using a brightfield microscope (Leica DMi1, Leica Microsystems GmbH, Wetzlar, Germany). [Scale bar = 50 µm and 15 µm in magnified pictures].

We next analyzed the mature neuronal properties of the resulting iNs. We found that both control and MERRF iNs showed positive immunoreactivity against Tau (a microtubule-associated protein predominantly found in neuronal axons of vertebrate brain that stabilizes neuronal microtubules and is involved in the establishment of neuronal polarity) and MAP-2, which is expressed only in neuronal cells (**Figure 48**). In contrast, undifferentiated cells did not show Tau or MAP-2 staining and only showed the nuclear staining.

We used Tau+ cells to evaluate neuronal conversion efficiency, which was almost 50% in control cells (48.2 ± 2.3 %) and up to 70% in MERRF 1 (70.3 ± 24.5 %) and MERRF 2 cells (74.4 ± 21.4 %). Neuronal purity (percentage of Tau+ cells in the cell culture 27 DPI) was approximately 50% (45.2 ± 8.08 %) in control cells and up to 67% (66.8 ± 7.9 %) in MERRF 1 cells and 78% (78.2 ± 10.2 %) in MERRF 2 cells (**Figure R49**).

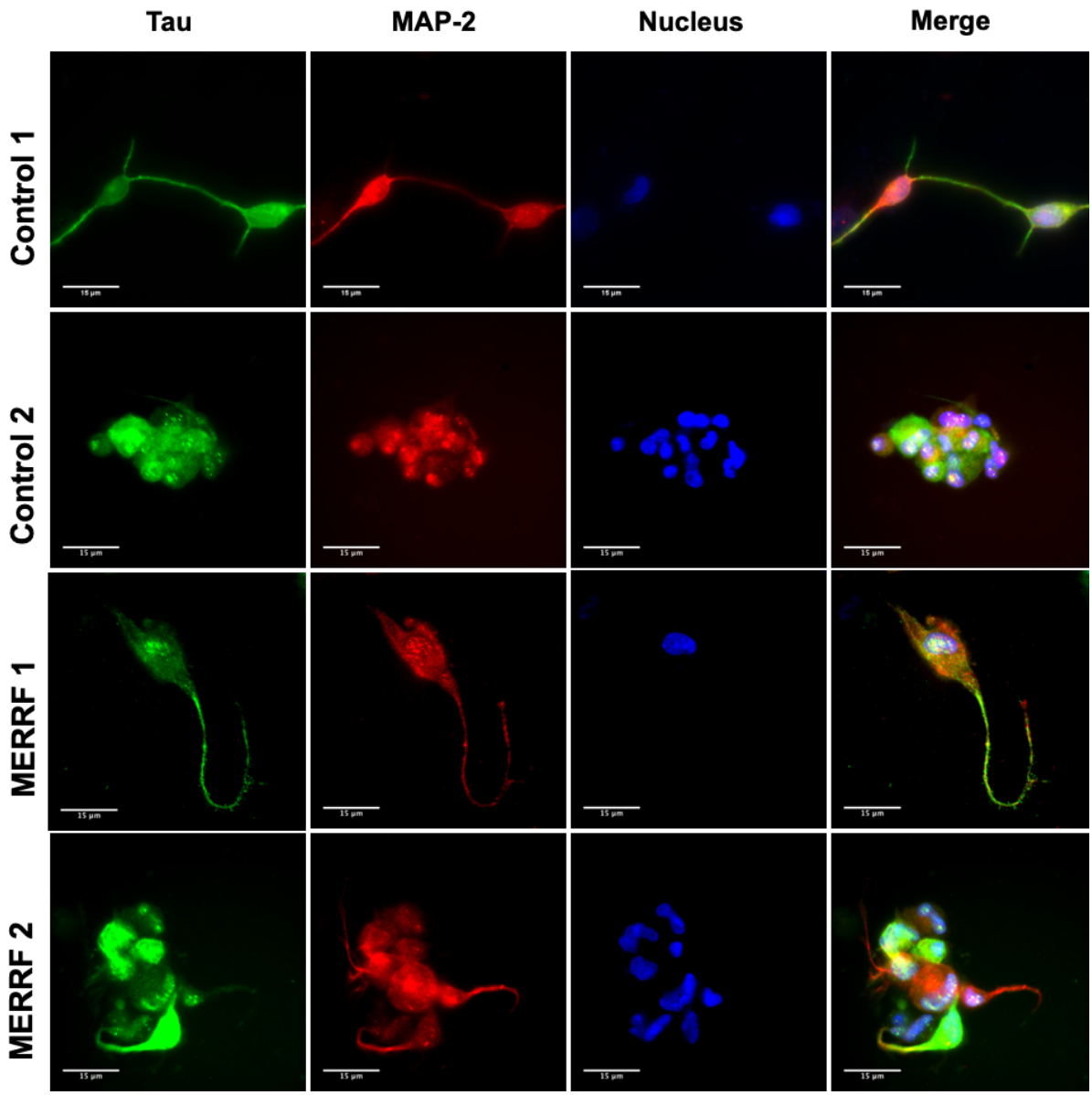

Figure R48. Detection of neuronal markers Tau and MAP-2 in controls and MERRF iNs.

The iNs were immunostained for Tau and MAP-2, different neuronal markers, as described in Materials & Methods section. DAPI was used to stain cell nuclei (in blue). [Scale bar = 15 µm].

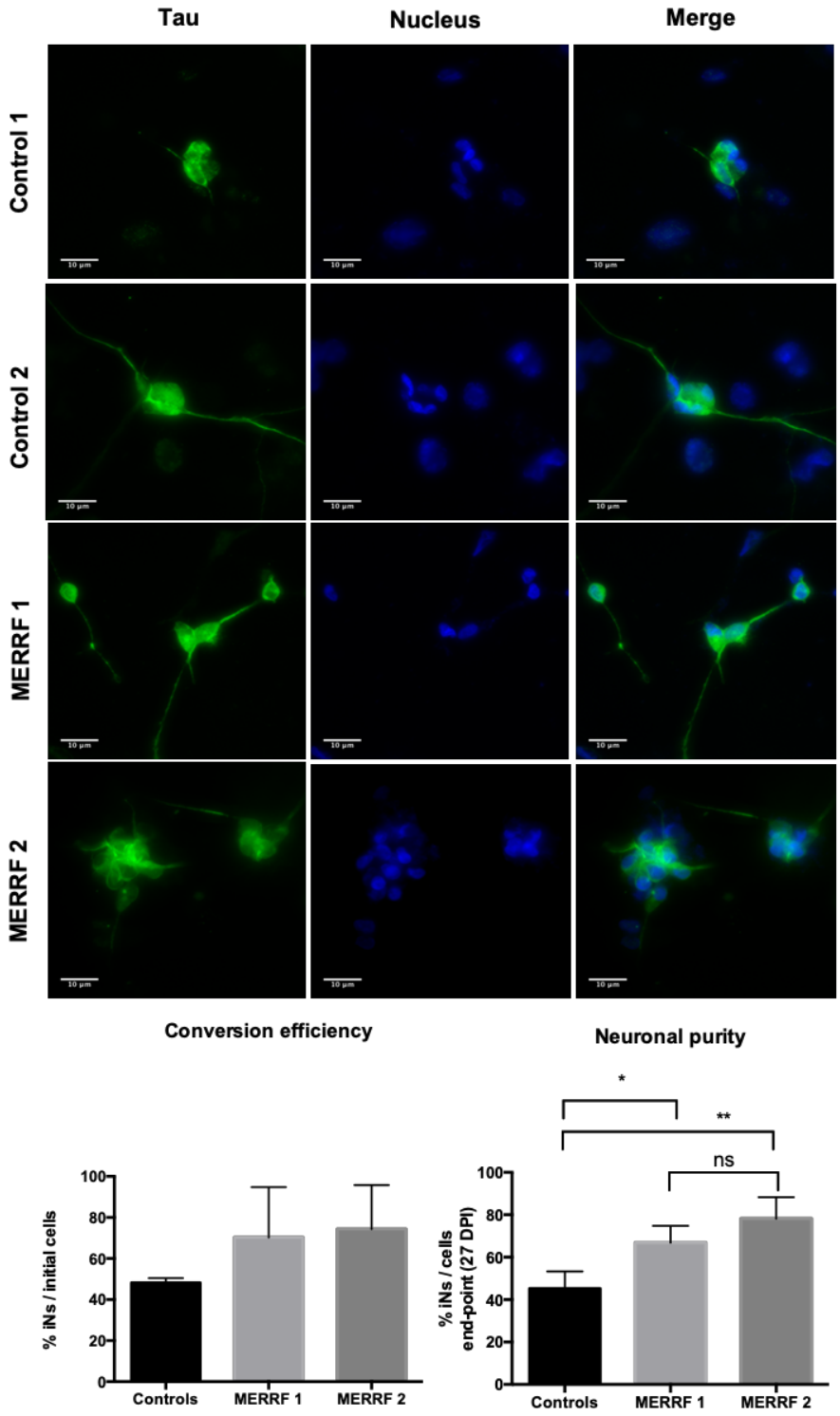

Figure R49. Conversion efficiency and neuronal purity of controls and MERRF iNs.

The iNs were immunostained for Tau, a neuronal marker, in order to calculate conversion efficiency and neuronal purity as described in Materials & Methods section. DAPI was used to stain cell nuclei (in blue). Results are expressed as mean ± SD. Significance of MERRF respect to control iNs is represented as *P<0.05, **P<0.01, ns = no significant. [Scale bar = 10 µm].

To further check iNs maturation, we performed image analysis of controls and MERRF Tau+ cells and this revealed the presence of elongated axons and elaborate neurites with bouton-like structures and/or spine-like protrusions (27 DPI; **Figure R50**), suggesting iNs maturation.

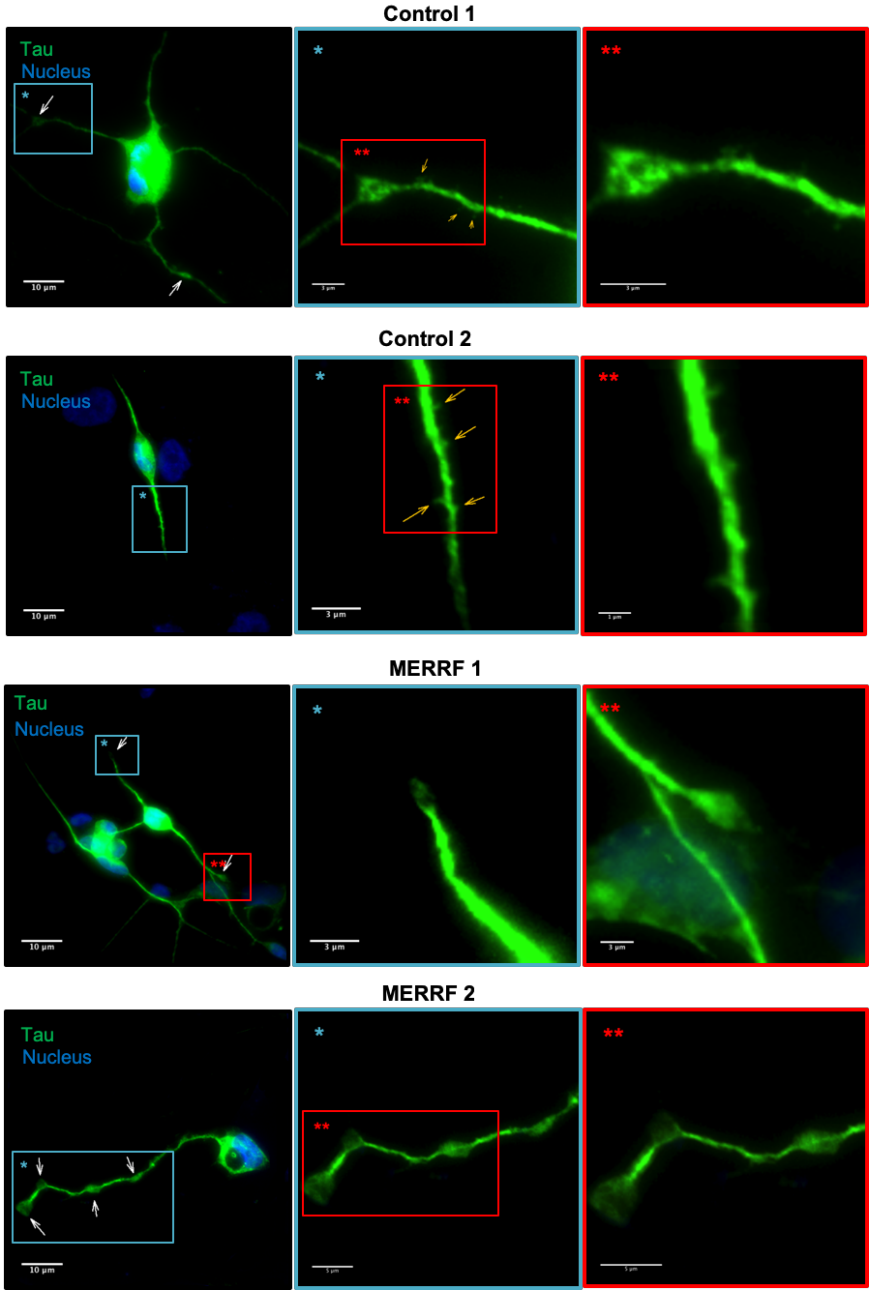

Figure R50. Elaborate neurites with elongated axons and bouton-like and/or spine-like structures in control and MERRF iNs.

Analysis of fluorescence images of Tau/DAPI immunostaining of control and MERRF iNs at 27 DPI revealed very elaborate neurites with elongated axons and bouton-like (white arrows) and/or spine-like (orange arrows) structures. The blue and red boxes (*, **) display higher magnifications of the images. [Scale bars represent 10 µm and 5, 3 or 1 µm in magnified pictures].

Moreover, *in vitro* patch-clamp electrophysiological recordings of the iNs after terminal differentiation and maturation in culture (60-80 DPI) showed that they had acquired the functional properties of neurons (**Figure R51**).

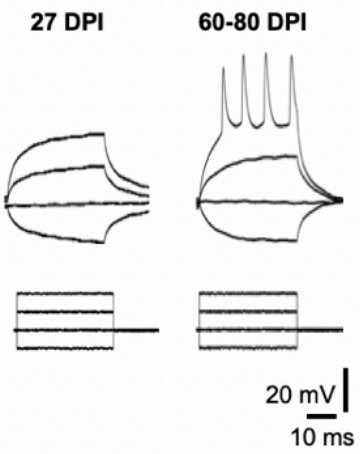

	27 DPI	60-80 DPI
RMP (mV)	-9.4 ± 1.3	-24.8 ± 3.2
Rin (MΩ)	1805.6 ± 467.6	1650.1 ± 430.3
τ (ms)	41.6 ± 9.9	42.8 ± 8
Proportion of spiking cells	0/12	3/17
Threshold (mV)		-32 ± 1.1
AMPLITUDE (mV)		38.2 ± 6
Width (ms)		5.4 ± 0,7

Figure R51. iNs electrophysiological properties.

The electrophysiological properties of cultured cells (iNs) at two different differentiation times (27 DPI, n = 12; 60-80 DPI, n = 17) were investigated using whole-cell recordings. The proportion of iNs firing action potentials increased over differentiation time (27 DPI, 0%; 60-80 DPI, 18%). The resting membrane potential (RMP) of iNs from both populations was weakly polarized (27 DPI, -9.4 ± 1.3 mV; 60-80 DPI, -24.8 ± 3.4 mV). The proportion of iNs firing action potentials increased over differentiation time (27 DPI, 0%; 60-80 DPI, 18%). Rin, Inward resistance, time constant.

Next, we analyzed different functionally relevant morphological characteristics of controls and MERRF iNs generated to evaluate neuronal morphological maturation, as described in Materials & Methods section. Summarized results are shown in **Table R1**. This analysis revealed that iNs from MERRF 1 fibroblasts did show smaller body area than controls iNs. Both MERRF 1 and MERRF 2 iNs did show significantly smaller total area and perimeter compared to controls iNs. Neither MERRF 1 nor MERRF 2 iNs did show significant differences compared to control iNs in relation to the number of neurites per cell, number of branch points and roots. However, both MERRF 1 and MERRF 2 iNs showed significantly shorter neurites compared to controls iNs. These results suggest that MERRF-derived neurons show a decrease in neurite outgrowth and maintenance.

	Controls		MERRF 1			MERRF 2		
	Mean	**SD**	**Mean**	**SD**	**P**	**Mean**	**SD**	**P**
Body area (µm²)	81,80	24,84	**59,97**	4,96	**<0,0001**	80,69	10,23	0,97
Total area (µm²)	116,53	19,14	**87,52**	27,27	**0,0036**	**93,54**	33,60	**0,0253**
Perimeter (µm)	133,48	14,03	**107,88**	12,52	**<0,0001**	**95,00**	8,84	**<0,0001**
Num branch points	0,22	0,05	0,24	0,23	0,9646	0,26	0,36	0,8661
Num roots	2,21	0,14	2,03	0,33	0,0327	2,31	0,14	0,3327
Total neurites/cell	2,34	2,34	2,26	0,49	0,6805	2,59	0,42	0,0138
Media neurite length (µm)	23,02	0,74	**16,08**	3,27	**<0,0001**	**15,40**	2,15	**<0,0001**
Maximal neurite length (µm)	56,79	15,62	**33,11**	3,77	**<0,0001**	**43,56**	12,48	**<0,0001**
Total neurite length (µm)	53,99	5,97	**33,07**	2,66	**<0,0001**	**32,65**	1,68	**<0,0001**
Primary neurites	2,22	0,16	2,05	0,35	0,0711	2,35	0,16	0,2059
Secondary neurites	0,26	0,00	0,26	0,25	0,9999	0,26	0,36	0,9999
Mean primary neurite length (µm)	23,49	1,41	**16,86**	2,57	**<0,0001**	**15,62**	2,08	**<0,0001**
Mean secondary neurite length (µm)	11,47	2,45	**6,48**	5,61	**0,0002**	**4,32**	4,03	**<0,0001**

Table R1. Functionally relevant morphological features of controls and MERRF iNs generated from skin fibroblasts.
SD, Standard deviation on mean; P, p-value of Student's t-test. Measurements pertain to at least 150 cells (50 cells per experiment, randomly selected, in three independent experiments). Bold numbers indicate significant results.

By this way, we have made a further step in mitochondrial diseases' pathophysiology modelling, producing for the first time MERRF patients-derived induced neurons by direct reprogramming from dermal fibroblasts.
Both control and MERRF iNs showed high levels of conversion efficiency and neural purity, as well as presented a high degree of maturation, with the presence of branches, bouton-like structures and spine-like protrusions.

Once MERRF patients-derived iNs were generated, we wondered whether they would be a good model to study the pathophysiology of the disease, conserving the

pathological alterations that we have been previously observed in other models such as skin fibroblasts or cybrids.

The first characteristic we wanted to examine was whether levels of m.8344A>G heteroplasmy of MERRF cells were affected by direct reprogramming, since there are no antecedents in the literature about direct reprogramming of heteroplasmic cells.

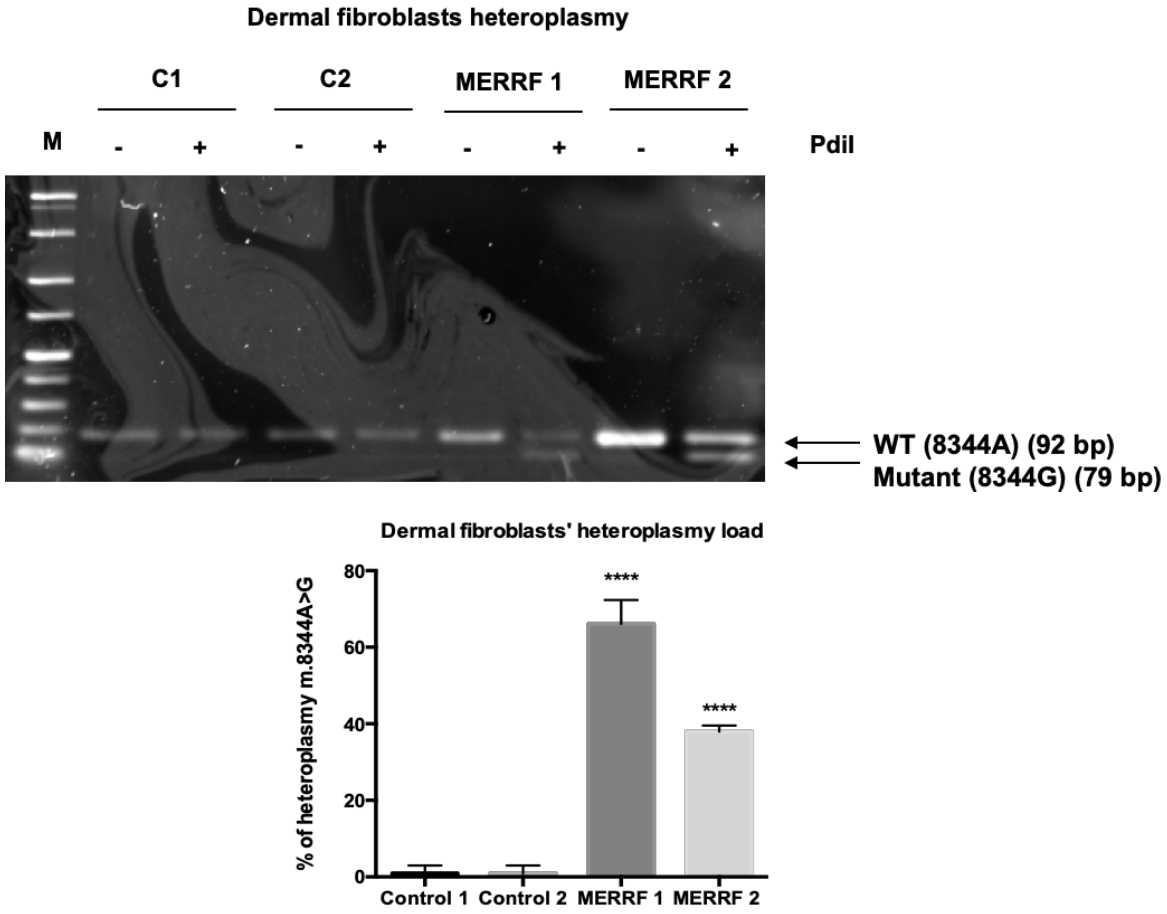

Figure R52. Heteroplasmy load of controls and MERRF patient-derived dermal fibroblasts.
Heteroplasmy load measurement was determined by mismatched PCR-RFLP. Results are expressed as mean ± SD. Significance of MERRF respect to control fibroblasts is represented as ****P<0.0001.

In order to check heteroplasmy maintenance, first the mutational load (m.8344A>G mutation) of MERRF 1 and MERRF 2 skin fibroblasts was quantified by mismatched PCR-RFLP, as described in Materials & Methods section. The heteroplasmy load quantification resulted in 65% for MERRF 1 and 38% for MERRF 2 (**Figure R52**).

Heteroplasmy loads were continuously followed-up during the conduction of this work to rule out any potential changes in the percentage of mutated mtDNA. Then, we compared m.8344A>G heteroplasmy levels between both patient-derived primary fibroblasts and the iNs successfully generated. Twenty-seven DPI and before DNA extraction, controls and MERRF iNs were seeded onto PFL-coated plates in order to enrich the population of neurons, reaching at least a 90% of neuronal purity (see Materials & Methods section).

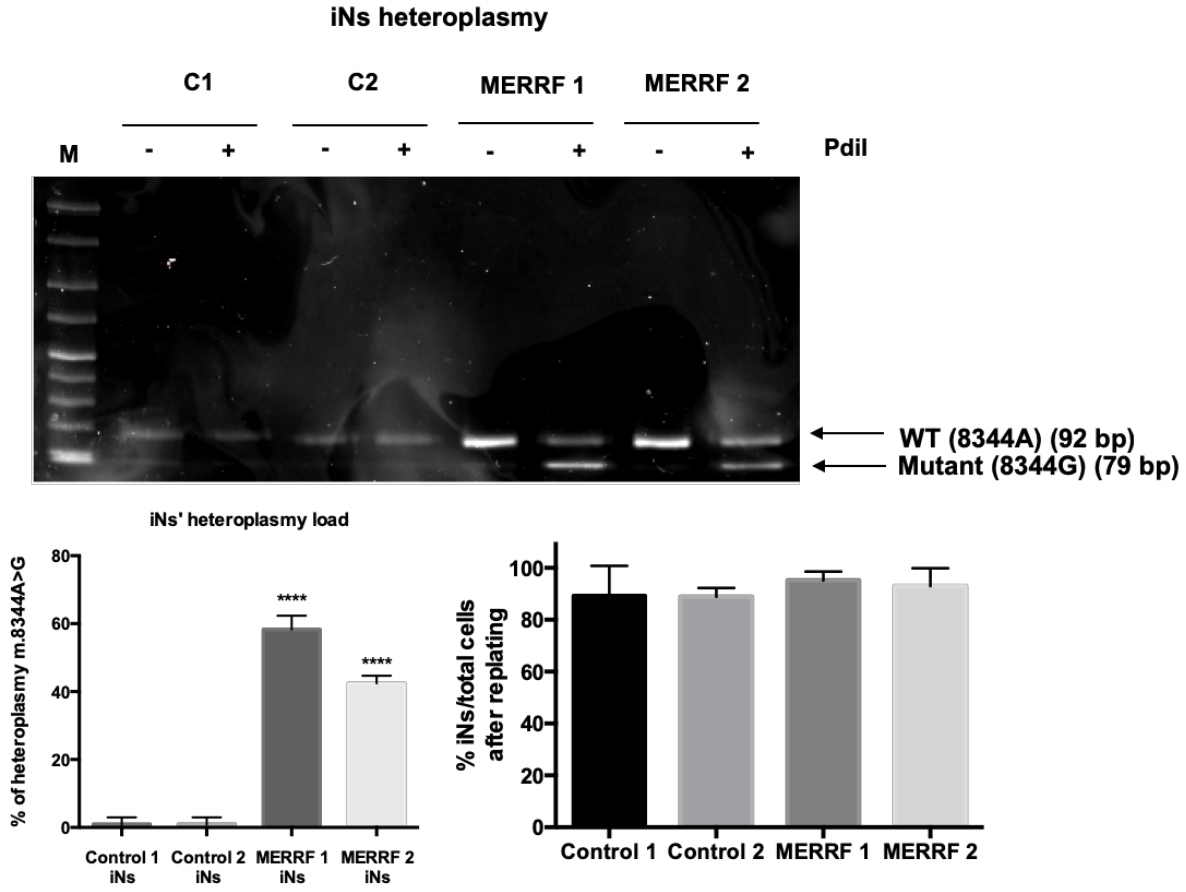

Figure R53. Heteroplasmy load of controls and MERRF patient-derived iNs. Heteroplasmy load measurement was determined by mismatched PCR-RFLP. Results are expressed as mean ± SD. Significance of MERRF respect to control iNs is represented as ****P<0.0001. The neuronal purity was calculated after seeding iNs onto PFL-coated µ-slides 4-well Ibidi plates for DNA extraction.

By mismatched PCR-RFLP analysis, we checked the levels of m.8344A>G heteroplasmy for these iNs, resulting in 58% for MERRF 1 iNs and 43% for MERRF 2 iNs (**Figure R53**).

Heteroplasmy levels of both control and MERRF iNs closely reflected those of the corresponding primary fibroblasts (**Figure R54**). Therefore, we concluded that m.8344A>G proportions did not significantly change during direct cellular reprogramming.

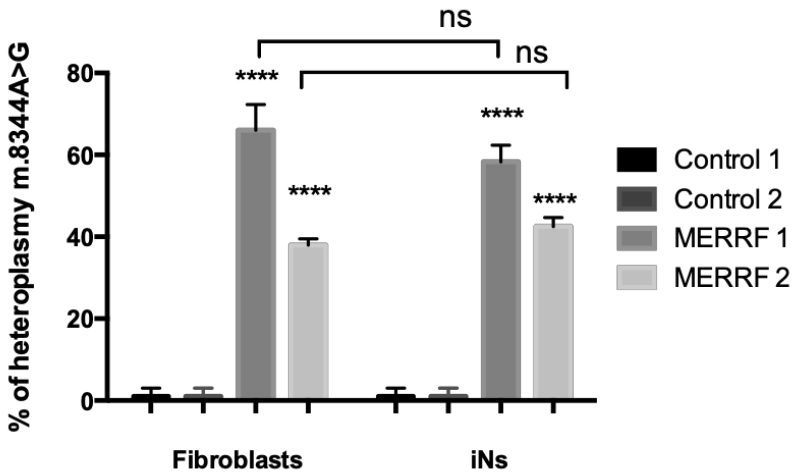

Figure R54. Heteroplasmy load in MERRF 1 and MERRF 2 fibroblasts and iNs derived from them.

Heteroplasmy loads were determined by mismatched PCR-RFLP assay. Results are expressed as the mean ± SD. Significance of MERRF respect to controls fibroblasts or iNs is represented as ****P<0.0001. There were no statistically significant differences (ns) between fibroblasts and iNs heteroplasmy loads.

Since MERRF iNs maintained the heteroplasmy load of m.8344A>G mutation, we wonder whether pathogenic characteristics attributed to the mtDNA mutation were also maintained in MERRF iNs.

First, considering ΔΨm as a good indicator of mitochondrial health, we performed a double immunostaining with MitoTracker™ Red CMXRos and Tau (see Materials & Methods section), and we measured ΔΨm of controls and MERRF iNs by quantifying the MitoTracker™ Red CMXRos fluorescence signal in Tau+ cells. First, to confirm the dependence of MitoTracker™ Red CMXRos fluorescence to mitochondrial membrane potential, we included a negative control with CCCP. After 4 hours of incubation with 10 μM CCCP, ΔΨm was approximately a 60% lower compared to DMSO (vehicle) in control 1 iNs and a 30% lower in MERRF 1 iNs (**Figure R55**).

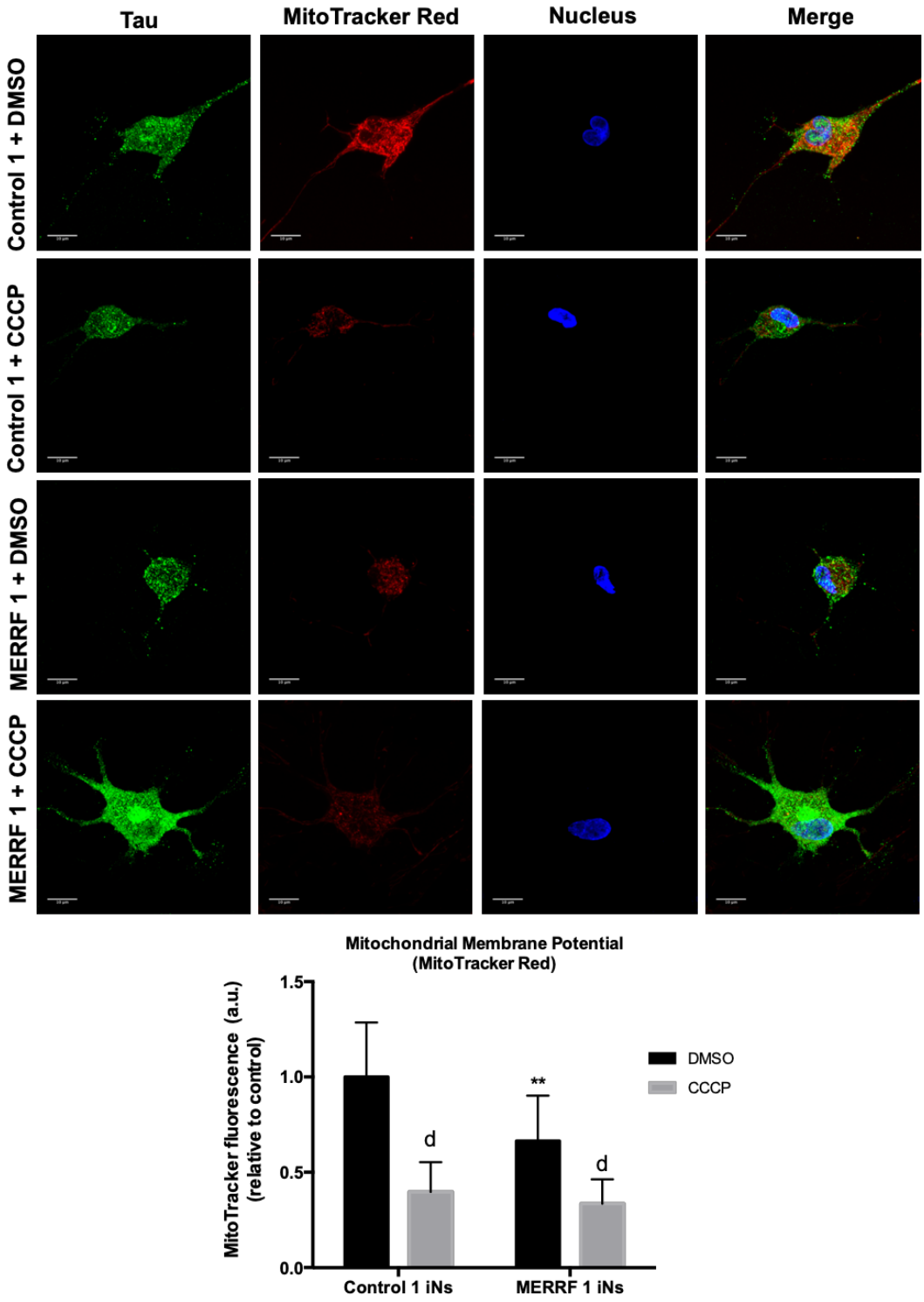

Figure R55. Mitochondrial membrane potential collapse after mitochondrial uncoupling in control 1 and MERRF 1 iNs.

Control 1 and MERRF 1 iNs were treated with 10 µM CCCP or DMSO (vehicle) for 4 hours and then loaded with MitoTracker™ Red CMXRos. MitoTracker™ fluorescence signal from Tau+ cells was quantified, and the data are shown in the plot as mean ± SD of at least 20 iNs. **P<0.01 (difference between control and MERRF cells), ^{d}P<0.0001 (difference between DMSO and CCCP treatments).

The quantification of MitoTracker™ Red CMXRos fluorescence intensity showed that both MERRF iNs had significantly decreased ΔΨm (approximately by 35%) compared to controls iNs (**Figure R56**).

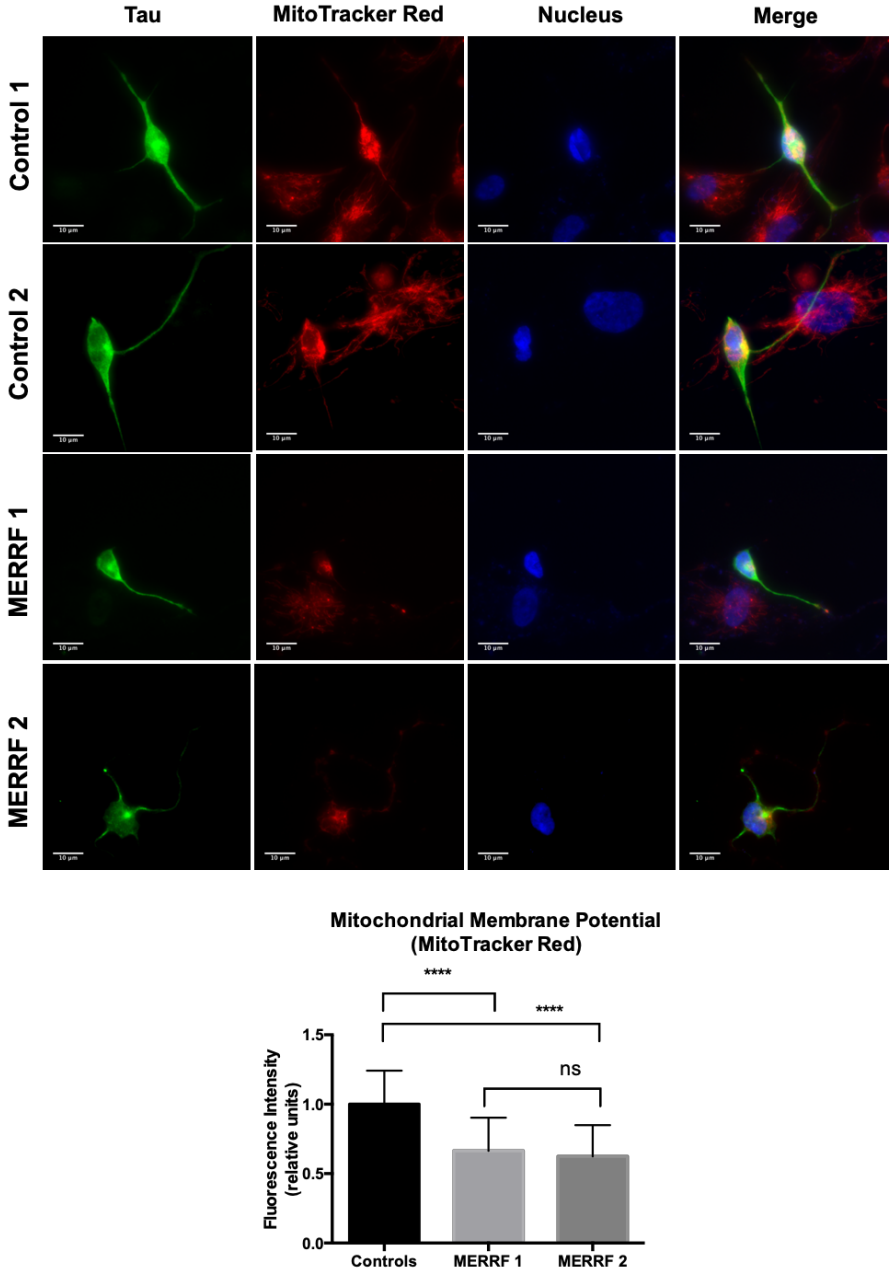

Figure R56. Tau and MitoTracker™ Red CMXRos staining in controls and MERRF iNs.

The merged images are shown in the righter panels, with nuclei stained with DAPI. [Scale bar = 10 μm]. The MitoTracker™ fluorescence signal from Tau+ cells was quantified as described in Materials & Methods section. The data are shown in the plots as the mean ± SD of three independent experiments, ****P<0.0001, ns = not statistically significant.

Moreover, the MitoTracker™ Red CMXRos staining co-localized with cytochrome c, a mitochondrial marker, confirming the specificity of MitoTracker™ Red CMXRos staining to mitochondria and verifying that mitochondrial depolarization in MERRF iNs was not a result of cytochrome c release, as occurs in apoptosis (**Figure R57**).

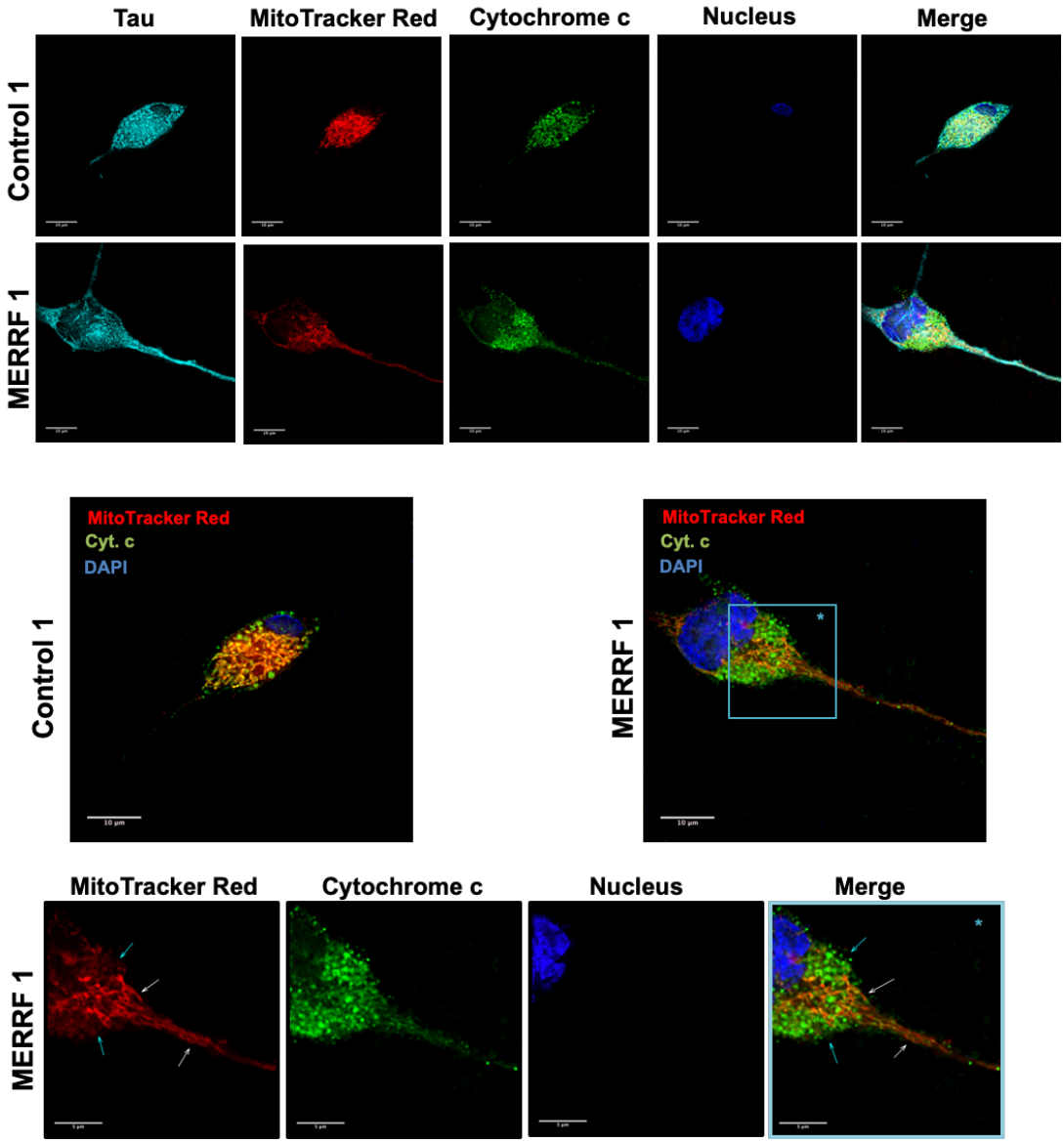

Figure R57. Visualization of mitochondria and ΔΨm by MitoTracker™ Red CMXRos and cytochrome c staining in control 1 and MERRF 1 iNs by fluorescence microscopy.

Nuclei were counterstained by DAPI. Colocalisation of MitoTracker™ Red CMXRos and cytochrome c signal in mitochondria revealed specificity of MitoTracker™ to dyed mitochondria. The magnification of a small area in MERRF iNs revealed two relevant populations of mitochondria: white arrows point out a tubular mitochondrial network with high polarization degree and cyan arrows some smaller, rounded and fragmented mitochondria with low polarization degree. [Scale bar = 10 µm and 5 µm in magnified pictures].

As a further check of the mitochondrial specificity of MitoTracker™ Red CMXRos probe, a double immunofluorescence assay with MitoTracker™ Red CMXRos and the mitochondrial matrix protein Hsp60 was performed (**Figure R58**).

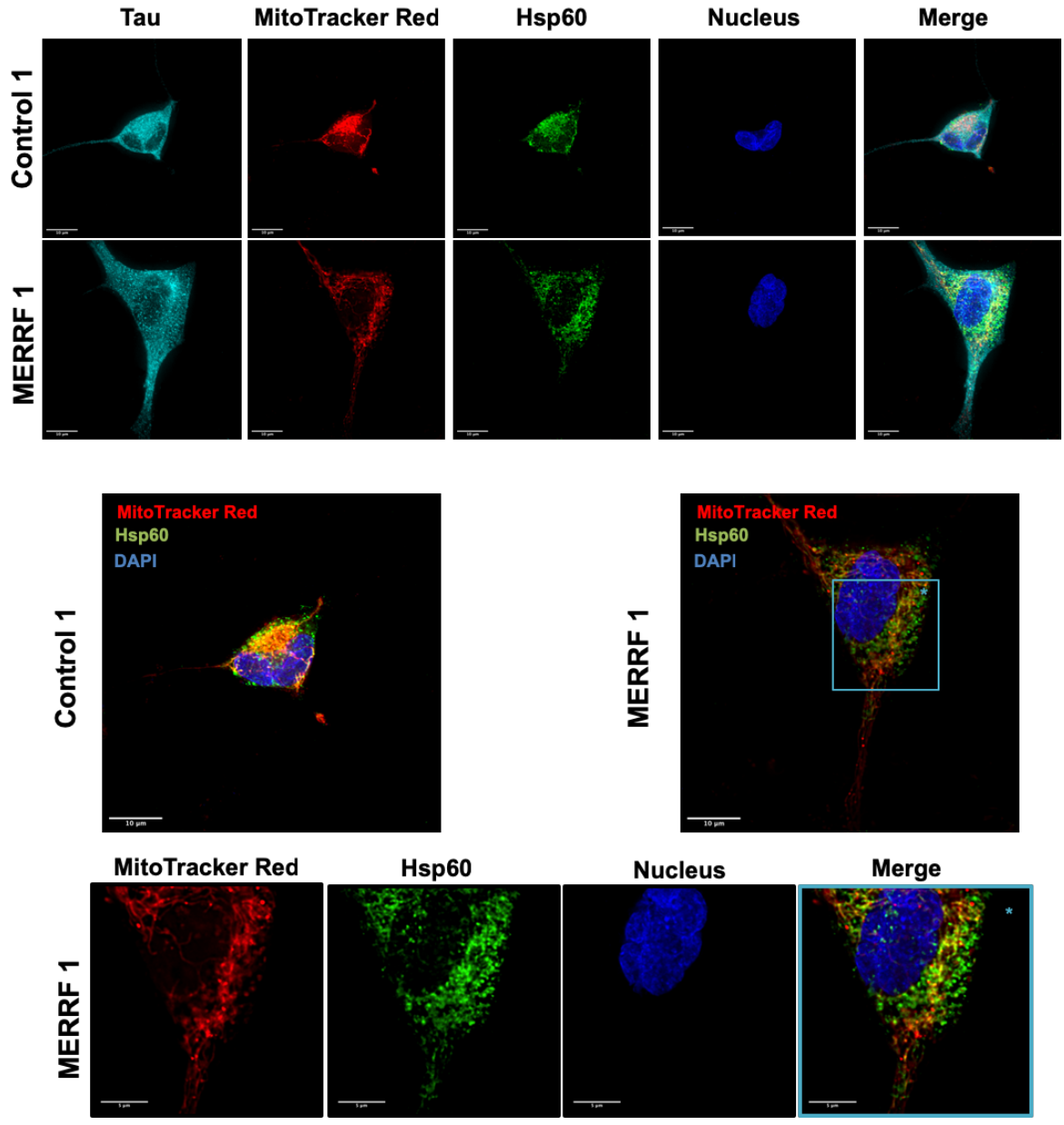

Figure R58. Hsp60 and MitoTracker™ Red CMXRos staining of mitochondria in control 1 and MERRF 1 iNs.

Visualization of mitochondria and ΔΨm by MitoTracker™ Red CMXRos and Hsp60 staining in control and MERRF iNs by fluorescence microscopy (see Materials & Methods). Nuclei were counterstained by DAPI. [Scale bar = 10 µm]. Colocalisation of MitoTracker™ Red CMXRos and Hsp60 signal in mitochondria revealed specificity of MitoTracker™ to dyed mitochondria. Magnification of a small area in MERRF 1 iNs is shown. [Scale Bar = 5 µm].

Visualization of mitochondria in MERRF iNs revealed a distinct mitochondrial population in comparison with control iNs. To check whether there were significant differences in mitochondrial populations between controls and MERRF iNs, we investigated the mitochondrial network morphology after incubating cells with MitoTracker™ Red CMXRos using fluorescence microscopy. By observing controls and MERRF iNs, we could distinguish between different mitochondrial networks. Interestingly, MERRF iNs frequently showed a poorer tubular mitochondrial network compared to control iNs, with the presence of some smaller, rounded and fragmented mitochondria with low polarisation degree. Representative images of these types of mitochondrial morphology are shown in **Figure R57** and **Figure R58**.

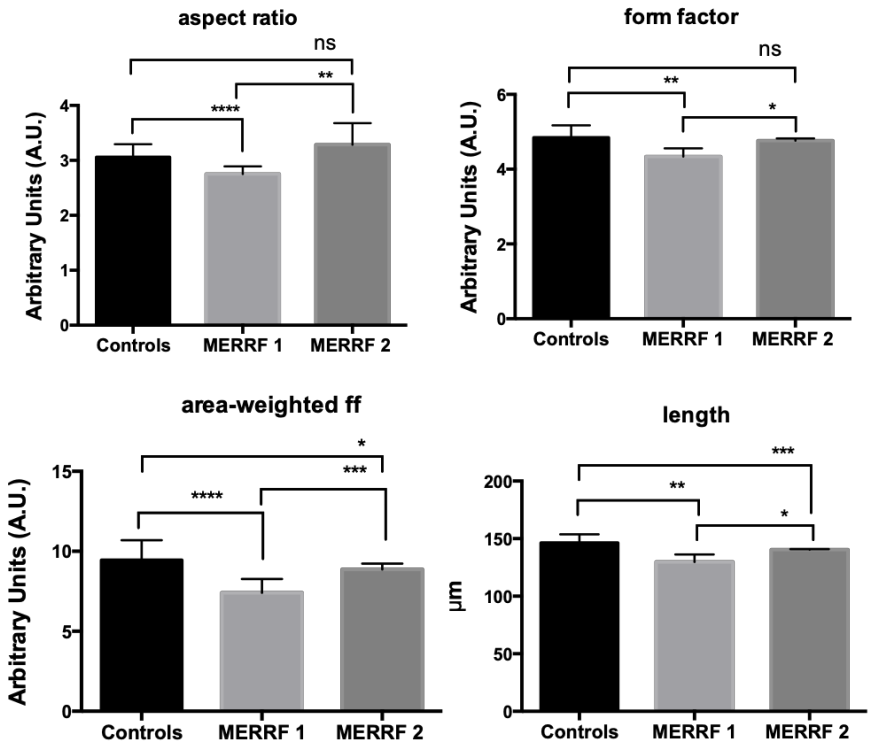

Figure R59. Mitochondrial shape parameters in controls and MERRF iNs.
Controls and MERRF iNs were incubated with MitoTracker™ Red CMXRos fluorescent probe. The evaluation of the mitochondrial shape was performed on images obtained by fluorescence microscopy. Morphometry macro was used to calculate different parameters of mitochondrial morphology. The histograms show the different average metrics of four mitochondrial morphology descriptors between controls and MERRF iNs: aspect ratio, form factor, area-weighted form factor and mitochondrial length. The data are shown in the plots as the mean ± SD of three independent experiments (at least 50 neurons per condition), *P<0.05, **P<0.01, ***P<0.001, ****P<0.0001 and ns = not statistically significant.

The characteristics of the mitochondrial network were evaluated using the method described by Merrill et al.[572] (see Materials & Methods section).
Both the degree of mitochondrial elongation (aspect ratio) and mitochondrial branching (form factor) were lower in MERRF 1 iNs than in controls iNs, indicating that MERRF 1 mitochondria were smaller and less elongated than controls ones (**Figure R59**).

Both MERRF 1 and MERRF 2 iNs showed more mitochondrial fragmentation in comparison with controls iNs, since both showed a decreased area-weighted form factor, a measure of shape complexity that accounts for the object area, since it is described as the product of the area of the mitochondrial network and the form factor (**Figure R59**). Moreover, both MERRF 1 and MERRF 2 iNs had significantly shorter mitochondrial network than controls iNs (**Figure R59**).

One of the main causes of mitochondrial depolarization is thought to be the accumulation of high levels of ROS, which are also accumulated in different models of neurodegenerative diseases[626-628]. Therefore, we analyzed the ROS levels in controls and MERRF iNs 27 DPI by immunofluorescence. The live cells were loaded with the fluorescent general oxidative stress indicator CM-H_2DCFDA (**Figure R60**). The identity of iNs was checked by the expression of the neuron-specific marker NCAM. Only the NCAM+ cells were used to measure the fluorescence of CM-H_2DCFDA. The quantification of iNs fluorescence intensity showed that both MERRF iNs contained higher ROS levels than controls iNs, with a 5-fold increase in MERRF 1 iNs and 3.5-fold increase in MERRF 2 iNs (**Figure R60**).

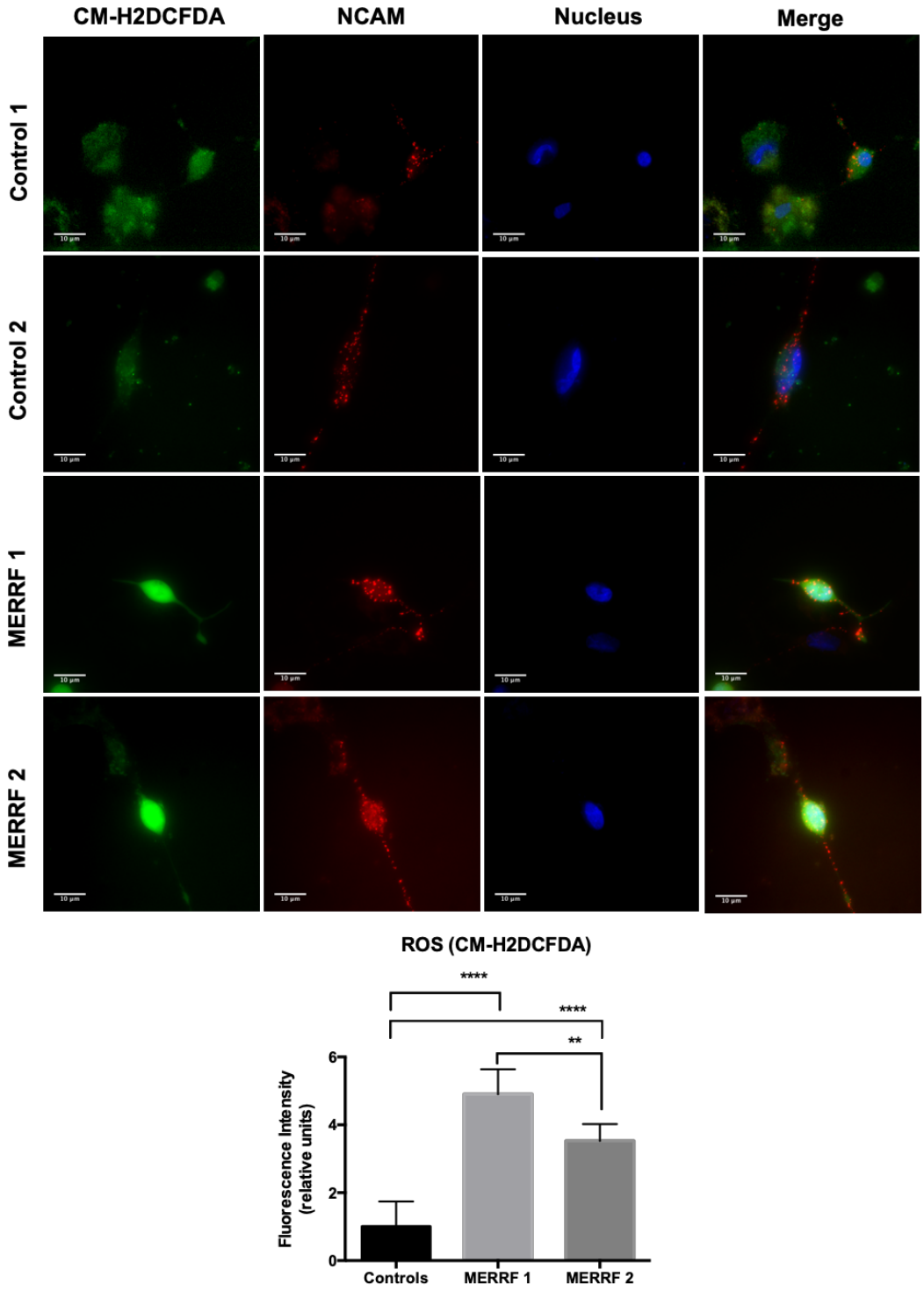

Figure R60. NCAM and CM-H_2DCFDA staining in controls and MERRF iNs.
Live cells were stained with the ROS-sensing fluorescent probe CM-H2DCFDA and with the neuron-specific anti-NCAM antibody. Merged images are shown in the righter panels, with the nuclei stained with Hoechst. [Scale bar = 10 µm]. The CM-H2DCFDA fluorescence signal from NCAM+ cells was quantified using Image J software and the data are shown in the plot as the mean ± SD of three independent experiments (at least 50 neurons for each condition and experiment were examined), **P<0.01 and ****P<0.0001.

Increased or disrupted autophagy has been observed in different cellular models of MERRF syndrome[202,219,629] and other mitochondrial diseases[201,203,204]. To evaluate autophagy in MERRF iNs, we performed immunofluorescence double staining with antibodies against LC3B (autophagosome marker) and Tau. Only the Tau+ cells were used to quantify the LC3B puncta.

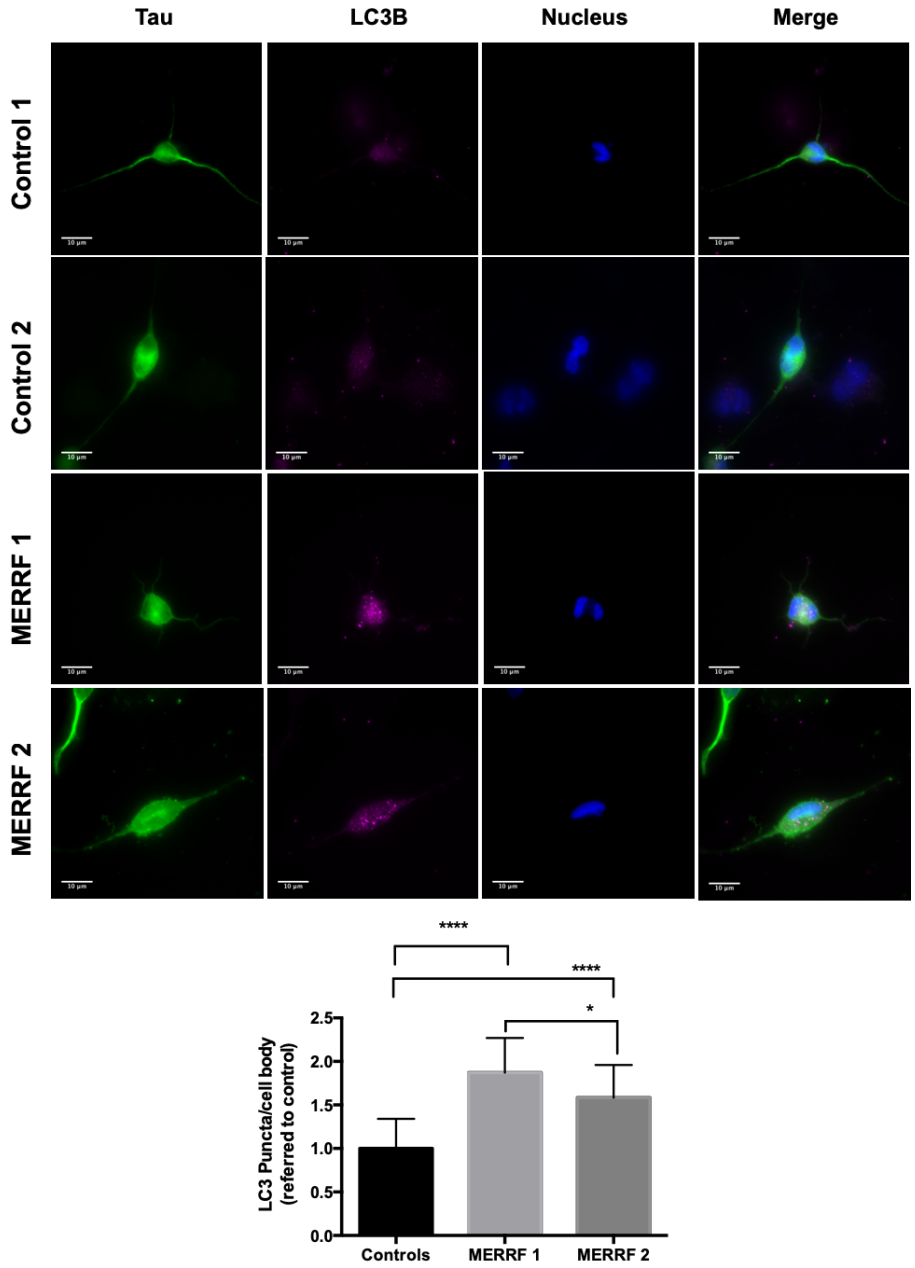

Figure R61. LC3B and Tau staining in controls and MERRF iNs.
Immunostaining of LC3B and Tau was performed to visualize LC3B puncta in control and MERRF iNs. To quantify the number of LC3B puncta/cell, Spot Counter ImageJ macro was used and the data are shown in the plot as the mean ± SD of three independent experiments (at least 50 neurons for each condition and experiment were examined), *P<0.05 and ****P<0.0001. [Scale bar = 10 µm].

LC3B staining was hardly detectable in controls iNs, whereas in both MERRF iNs we observed a significant increase in LC3B puncta per cell, suggesting autophagy activation (**Figure R61**).

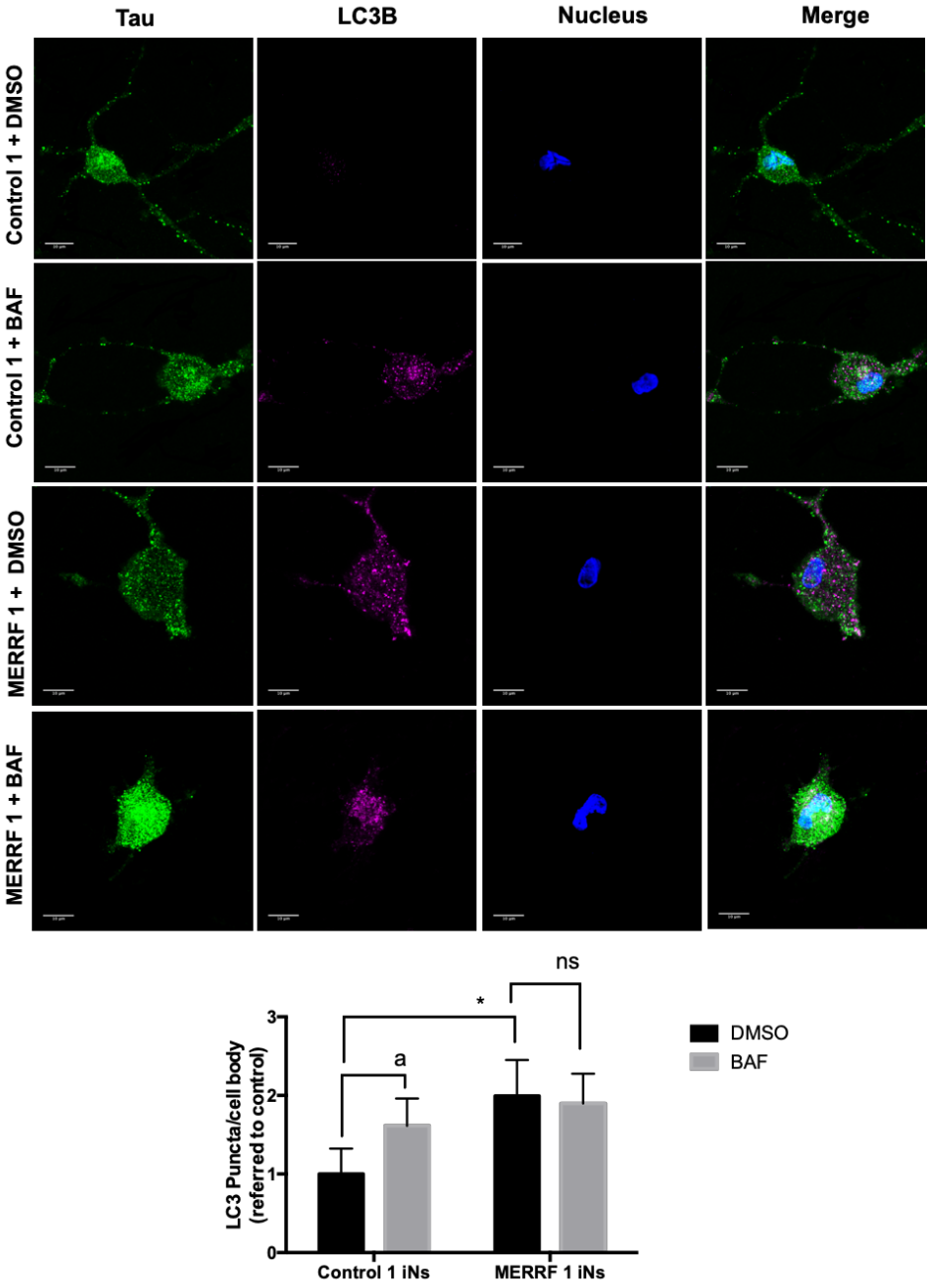

Figure R62. Autophagy flux in control 1 and MERRF 1 iNs.
Representative images of immunostaining of LC3B and Tau in control and MERRF iNs treated with DMSO (vehicle control) or Bafilomycin A1 (BAF). Quantification of LC3B puncta/cell was assessed by using Spot Counter ImageJ macro. Data are shown in the plot as the mean ± SD of three independent experiments (at least 20 neurons for each condition and experiment were examined), *P<0.05 (control versus MERRF), ^{a}P<0.05 (DMSO versus BAF) and ns = not statistically significant. [Scale bar=10 μm].

In order to evaluate if MERRF iNs showed increased or disrupted autophagy flux, we treated control 1 and MERRF 1 iNs with BAF.

After treatment with BAF, LC3B puncta per cell were markedly increased in control 1 iNs, indicating that the autophagy flux was not disrupted. On the other hand, BAF treatment had no effect on LC3B puncta in MERRF iNs, suggesting that autophagy flux was impaired in mutant cells (**Figure R62).**

To observe whether selective mitochondrial degradation or mitophagy was increased in MERRF iNs, we performed immunofluorescence double staining with antibodies against LC3B and Tau and with the fluorochrome MitoTracker™ Deep Red, which is independent of ΔΨm (**Figure R63)**.

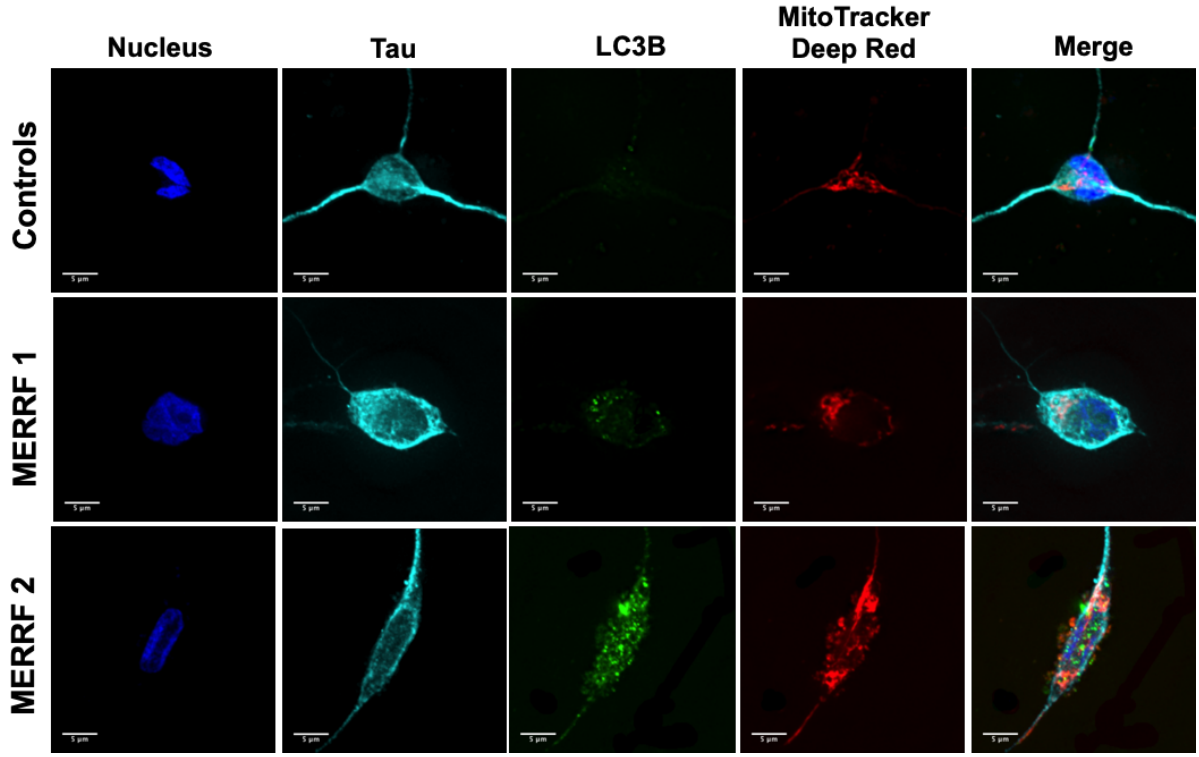

Figure R63. LC3B, Tau and MitoTracker™ Deep Red staining in controls and MERRF iNs.

Representative images of Immunostaining of MitoTracker™ Deep Red (mitochondrial marker), LC3B (autophagosome marker) and Tau (neuronal marker). This immunofluorescence triple staining was performed to visualize degrading mitochondria (puncta) in controls and MERRF iNs. [Scale bar = 5 μm].

Whereas in control iNs a rich tubular mitochondrial network negative for LC3B staining was observed, both MERRF 1 and MERRF 2 iNs showed a stronger LC3B

staining signal and more small, fragmented mitochondria, which were positive for LC3B (Pearson's coefficient of correlation, r>0.85). Quantification of MitoTracker™ Deep Red/LC3B colocalized puncta confirmed mitophagy activation in both MERRF iNs **(Figure R64**).

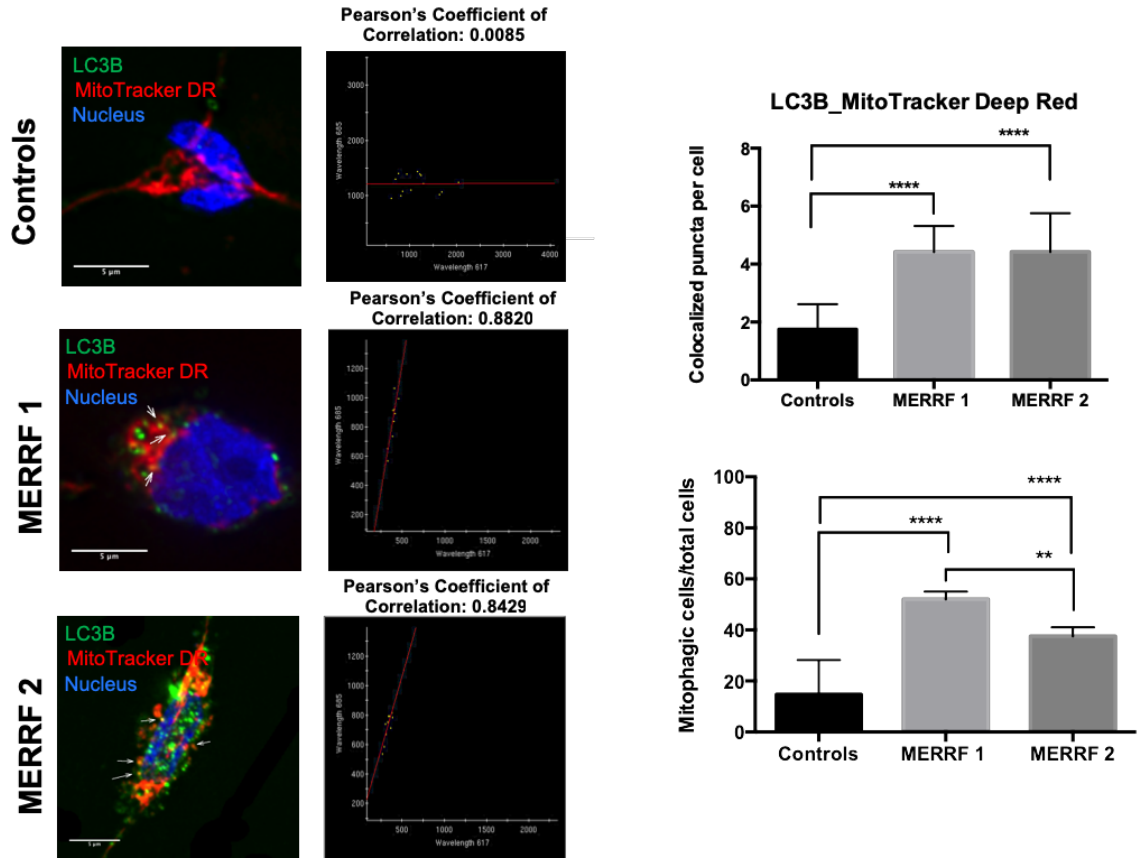

Figure R64. Mitophagy analysis in controls and MERRF iNs.
Magnified images of controls and MERRF iNs, stained with MitoTracker™ Deep Red (red, mitochondrial marker), LC3B (green, autophagosome marker) and DAPI (blue, nucleus) are shown. Controls iNs show tubular mitochondria with low MitoTracker™ Deep Red/LC3B colocalisation degree (Pearson's coefficient of correlation ~ 0.009). Both MERRF iNs show a smaller, rounded and fragmented population with high MitoTracker™ Deep Red/LC3B colocalisation degree (white arrows). Colocalisation analysis resulted in a high colocalisation (Pearson's coefficient of correlation ~ 0.85). [Scale bar = 5 µm]. To quantify mitophagy, MitoTracker™ Deep Red/LC3B colocalized puncta per cell were measured with the Red and Green puncta Colocalization ImageJ macro[563]. A positive mitophagic cell was scored when more than 5 puncta were observed per cell. Data are shown in the plot as the mean ± SD of three independent experiments (at least 50 neurons for each condition and experiment were examined), **P<0.01, ****P<0.0001, ns = not statistically significant.

It has been reported that m.8344A>G mutation can alter mitochondrial function in fibroblasts derived from patients with MERRF syndrome[219,349,350], and we have observed a failure in mitochondrial respiration in both MERRF fibroblasts and cybrids (subsections **RI** and **RIV**).

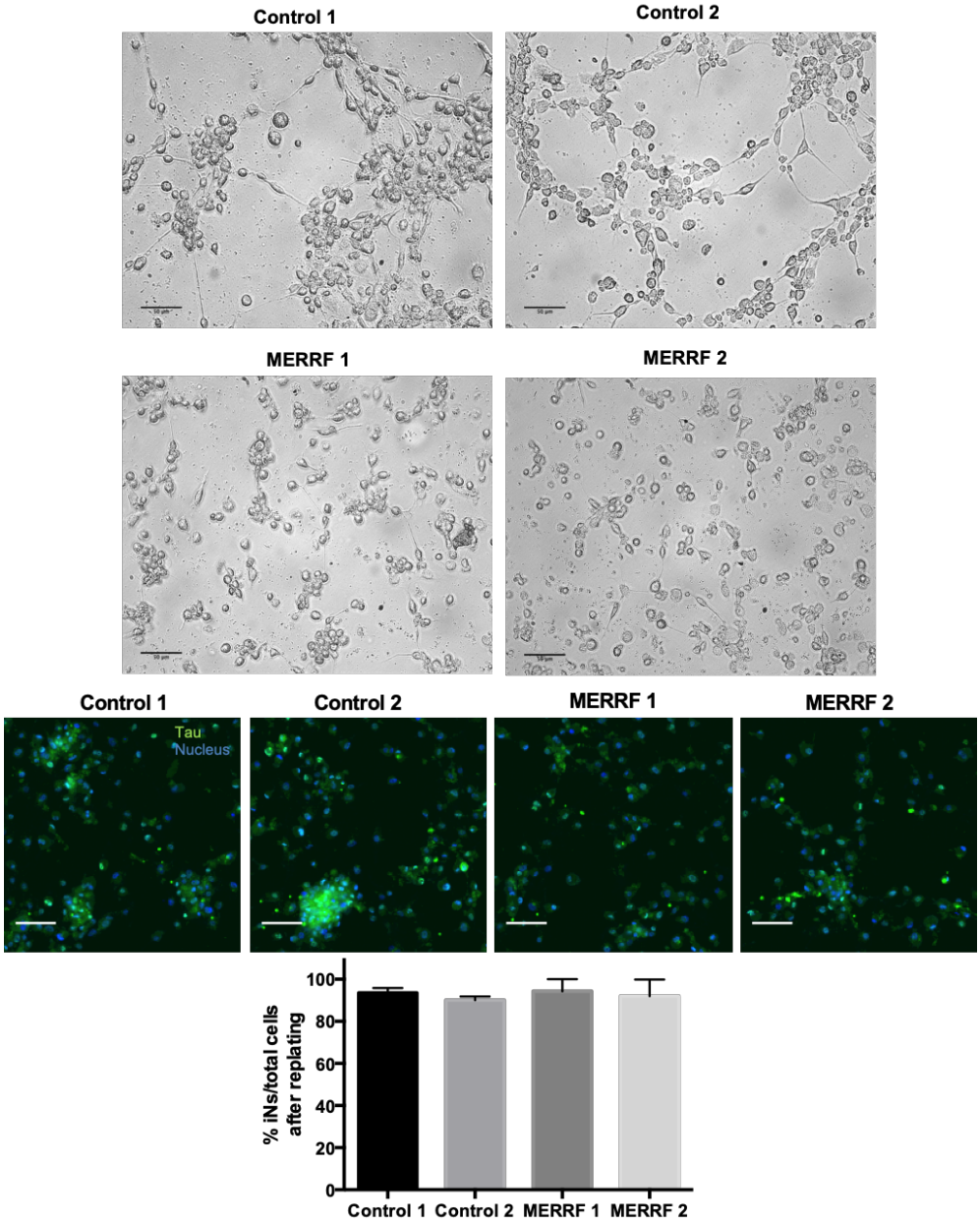

Figure R65. Enriched populations of controls and MERRF iNs for bioenergetic assays.

Representative brightfield images of the iNs morphology and connections after seeding them onto PFL-coated wells are shown [Scale bar = 50 µm]. Representative immunofluorescence images showing a high density of Tau+/DAPI+ cells in PFL-coated wells are shown [Scale bar = 50 µm]. The neuronal purity was calculated after seeding iNs onto PFL-coated Seahorse plates for bioenergetics assays.

Therefore, we used an extracellular flux analyzer to measure the OCR in order to evaluate the bioenergetic status of the controls and both MERRF iNs derived from dermal fibroblasts. All OCR measurements were normalized to cell number.

Controls and MERRF iNs were seeded on Seahorse XFe24 plates coated with PFL in order to enrich the population of neurons. Representative photographs of seeded controls and MERRF iNs can be observed in **Figure R65**.

To estimate the ETC function, we performed the Mito-stress test assay by the XFe24 extracellular flux analyzer (Seahorse Bioscience, Billerica, MA, USA). We sequentially added oligomycin A, FCCP as well as rotenone & antimycin A. When the experiment was finished, cell number and neuronal purity of each well was calculated by performing a double staining with Tau/DAPI. Neuronal purity of controls and MERRF iNs was higher than 90% (**Figure R65**).

The overall respiratory responses of controls and MERRF iNs are shown in **Figure R66**.

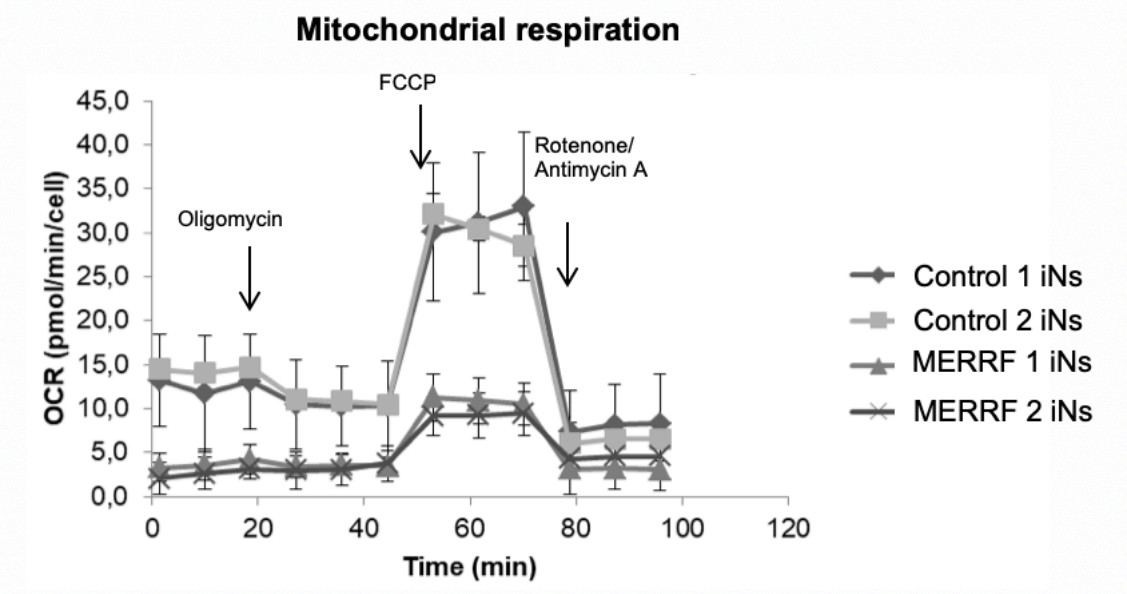

Figure R66. Representative respiratory flux profiles of controls and MERRF patients-derived iNs.

One representative of three independent experiments is shown. Addition of ATP synthase inhibitor oligomycin, electron transport chain uncoupler FCCP and complex I and III inhibitors rotenone and antimycin A are indicated. Control and MERRF iNs were seeded to 35,000 cells/well and incubated for 24 h. OCR was measured in XF base medium under basal conditions followed by the sequential addition of oligomycin (1 µM), FCCP (2 µM), as well as rotenone (1 µM) & antimycin A (2.5 µM), as indicated. Each data point represents an OCR measurement. Data are expressed as mean ± SD.

After carrying out Mito-stress test, different cellular bioenergetic parameters were calculated using the Seahorse XF Report Generator, a data analysis tool provided by Seahorse Bioscience.

A comparison of these parameters between controls and MERRF iNs showed significant differences. The basal respiration, maximal respiration and spare respiratory capacity of both MERRF 1 and MERRF 2 iNs were reduced compared to the controls iNs (**Figure R67**). Moreover, ATP production rate was reduced in MERRF 1 iNs (**Figure R67**). The extracellular flux analysis demonstrated that MERRF iNs exhibited decreased mitochondrial function parameters. These findings confirmed that the m.8344A>G mutation led to decreased mitochondrial respiration in iNs models of MERRF syndrome.

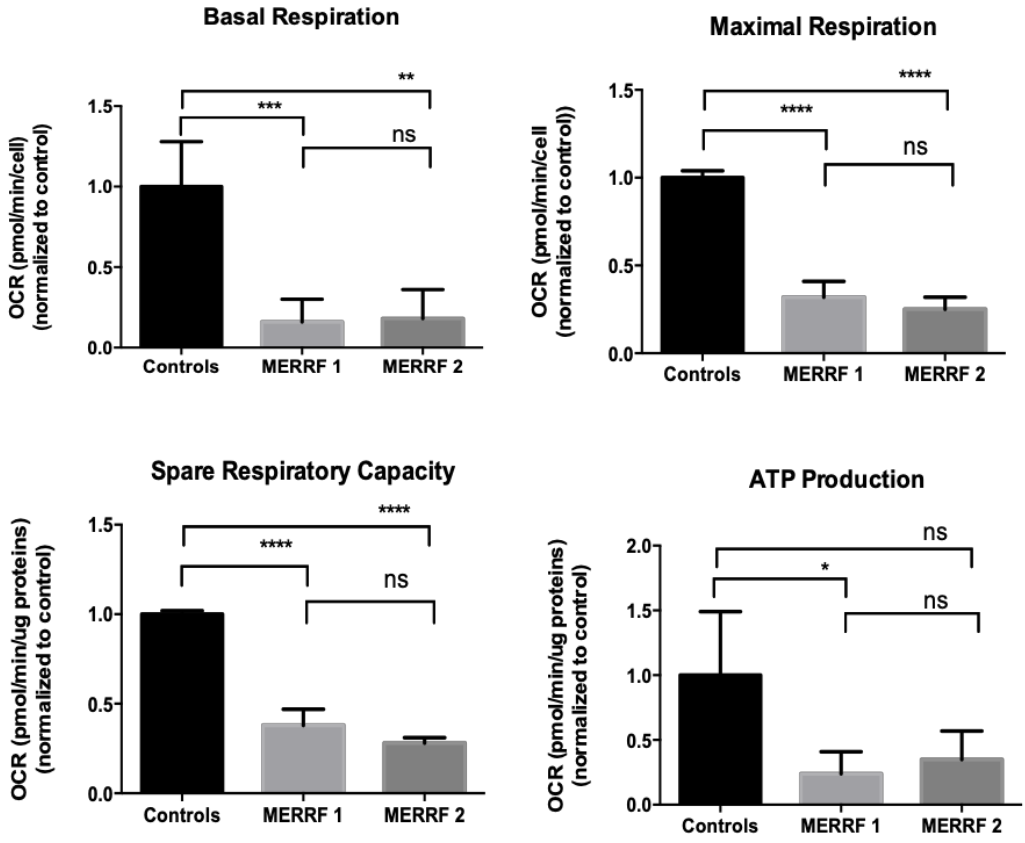

Figure R67. Parameters of mitochondrial respiratory function of controls and MERRF patients-derived iNs.

Basal mitochondrial respiration, Maximal respiration, Spare respiratory capacity and ATP-linked respiration are plotted. Results are expressed as mean ± SD. Statistical significance was evaluated by unpaired, two-tailed t-test. *P<0.05, **P<0.01, ***P<0.001, ****P<0.0001, ns = not statistically significant. All OCR readings were normalized to cell number as described in Materials & Methods section.

In conclusion, this study demonstrates that MERRF iNs harbouring the m.8344A>G mutation show mitochondrial dysfunction, decreased mitochondrial membrane potential and elevated ROS levels. Moreover, MERRF-derived iNs contain a fragmented mitochondrial network, autophagy flux disruption and mitophagy activation, demonstrating that this model is also useful to carry on functional analysis of autophagy and/or mitophagy pathways and to profoundly study the role of those mechanisms in MERRF iNs pathophysiology in the future.

R-VIII. MERRF iNs as a platform to validate the effectiveness of potential treatments for MERRF syndrome.

One of the most promising applications of iNs in the near future is the establishment of screening platforms to test the effects of potential therapeutic compounds or toxics in a neural cell model of different diseases, which is easier to generate and cheaper than other typical screening platforms, such as iPSCs[450].

So far, our investigations have generated a MERRF iNs model with the most common MERRF mutation that shows pathological characteristics in comparison to healthy volunteers-derived iNs.
One of our final goals was to check the suitability of the MERRF iNs to be used as a screening platform, since currently there are no effective treatments for MERRF syndrome or other mitochondrial diseases, due to the lack of clinical assays or inconsistencies in the previous results.
Along this work, we have demonstrated that MERRF iNs share common pathological characteristics with other models of MERRF diseases, such as patient-derived skin fibroblasts and cybrids, especially when mutational load is high. In this section, we propose the use of iNs generated from MERRF patient-derived skin fibroblasts with high heteroplasmy load for the evaluation of pre-screened selected drugs.
For that reason, we wanted to check the behavior of MERRF iNs after treatment with CoQ, since this molecule has demonstrated to be beneficial for different models of mitochondrial diseases[204,219,220,254] and we have confirmed that in the results presented in subsections **RI-RIV**.
In the case of iNs, we did not treat them with CoQ since the nature of the molecule forced us to solve it in ethanol, which seriously affected viability of iNs.
Consequently, instead of CoQ, we used a water-soluble stock solution of MSE 2001, Guttaquinon CoQ_{10} (hereinafter, GuttaQ), (MSE Pharmazeutika GmbH, Bad Homburg, Germany).

First, skin fibroblasts derived from one MERRF patient (MERRF 1, with the highest percentage of heteroplasmy, 65%) and skin fibroblasts from one healthy volunteer

were used for direct reprogramming. MERRF fibroblasts harboured the heteroplasmic m.8344A>G mutation.

Twenty-seven DPI, controls and MERRF iNs were seeded onto PFL-coated Seahorse XFe24 plates in order to enrich the population of neurons, reaching at least a 90% of neuronal purity (see Materials & Methods section) (**Figure R68**).

After incubating them for 24 hours, control and MERRF iNs were treated with 1 μM GuttaQ for 72 hours.

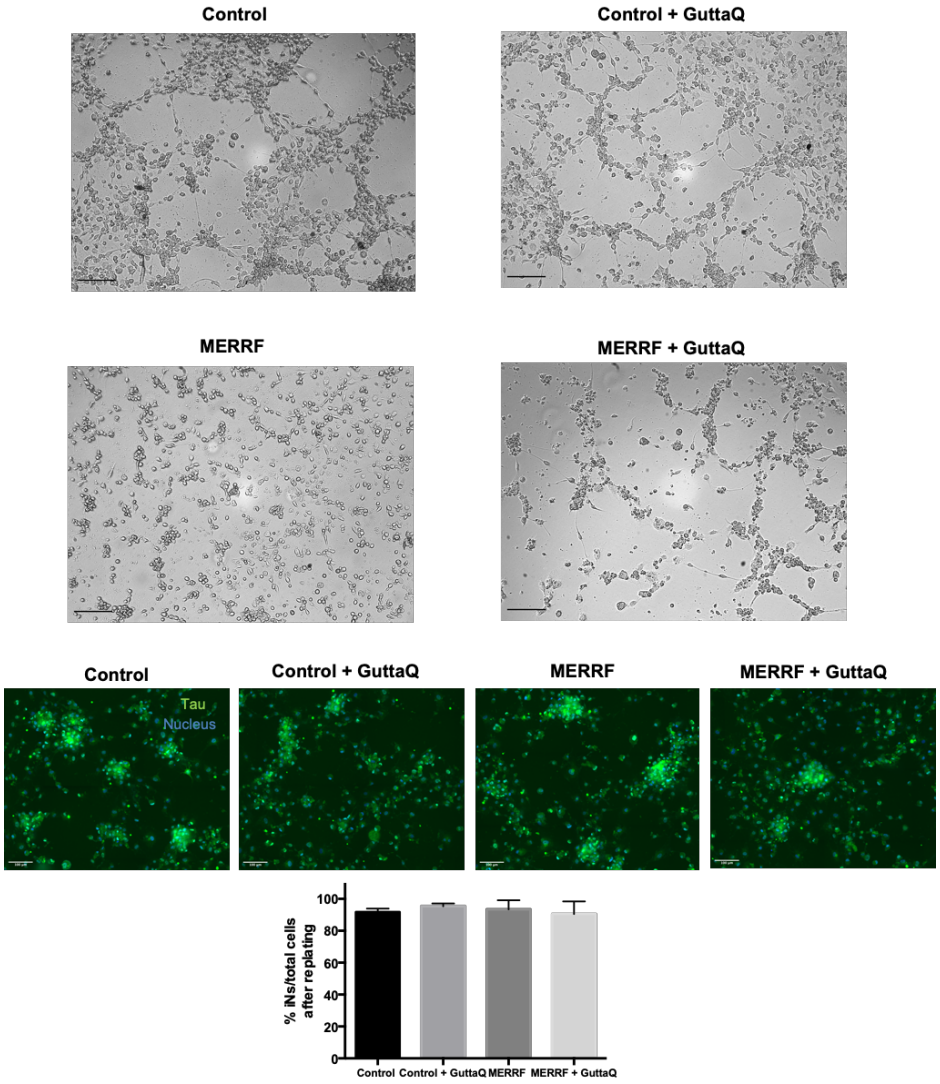

Figure R68. Untreated and GuttaQ-treated control and MERRF iNs purity after Mitostress test.

Representative brightfield images of the iNs morphology and connections after seeding them onto PFL-coated Seahorse XFe 24-well plates are shown. [Scale bar = 50 μm]. Representative immunofluorescence images showing a high density of Tau+/DAPI+ cells in PFL-coated wells are shown. [Scale bar = 50 μm]. The neuronal purity was calculated after seeding iNs onto PFL-coated Seahorse plates for bioenergetics assays.

Next, we used the Seahorse XFe24 extracellular flux analyzer to measure the OCR in order to evaluate the bioenergetic status of untreated and treated control and MERRF iNs derived from dermal fibroblasts. All OCR measurements were normalized to cell number.

To estimate the ETC function, we performed the Mito-stress test assay by the XFe24 extracellular flux analyzer (Seahorse Bioscience, Billerica, MA, USA). We added oligomycin A, FCCP as well as rotenone & antimycin A. When the experiment was finished, cell number and neuronal purity of each well was calculated by performing a double staining with Tau/DAPI (**Figure R68**).
The overall respiratory responses of untreated and GuttaQ-treated controls and MERRF iNs are shown in **Figure R69**.

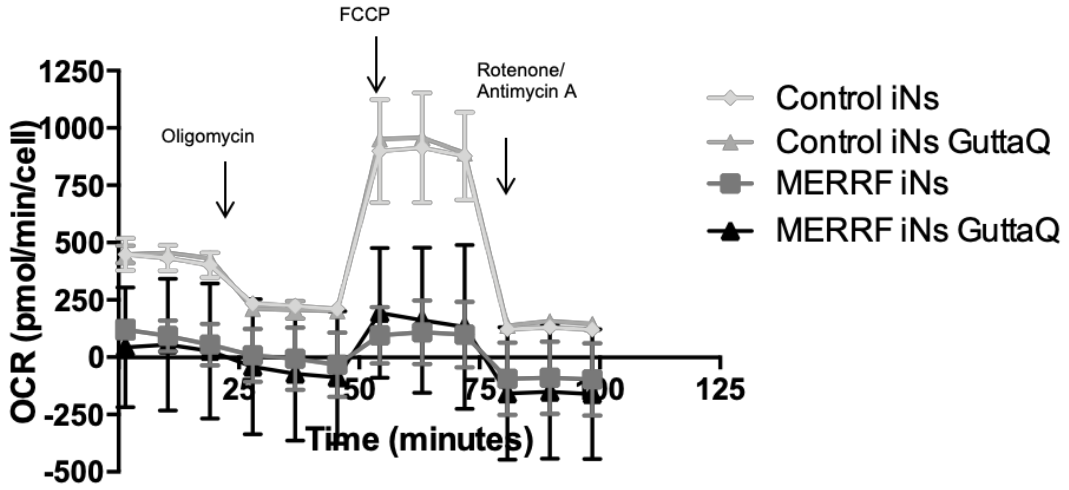

Figure R69. Representative respiratory flux profiles of untreated and GuttaQ-treated control and MERRF iNs.
One representative of three independent experiments is shown. Addition of ATP synthase inhibitor oligomycin, electron transport chain uncoupler FCCP and complex I and III inhibitors rotenone and antimycin A are indicated. Untreated and GuttaQ-treated control and MERRF iNs were seeded to 35,000 cells/well and incubated for 24 h. OCR was measured in XF base medium under basal conditions followed by the sequential addition of oligomycin (1 µM), FCCP (2 µM), as well as rotenone (1 µM) & antimycin A (2.5 µM), as indicated. Each data point represents an OCR measurement. Data are expressed as means ± SD.

After carrying out Mito-stress test, different cellular bioenergetic parameters were calculated using the Seahorse XF Report Generator, a data analysis tool provided by Seahorse Bioscience.

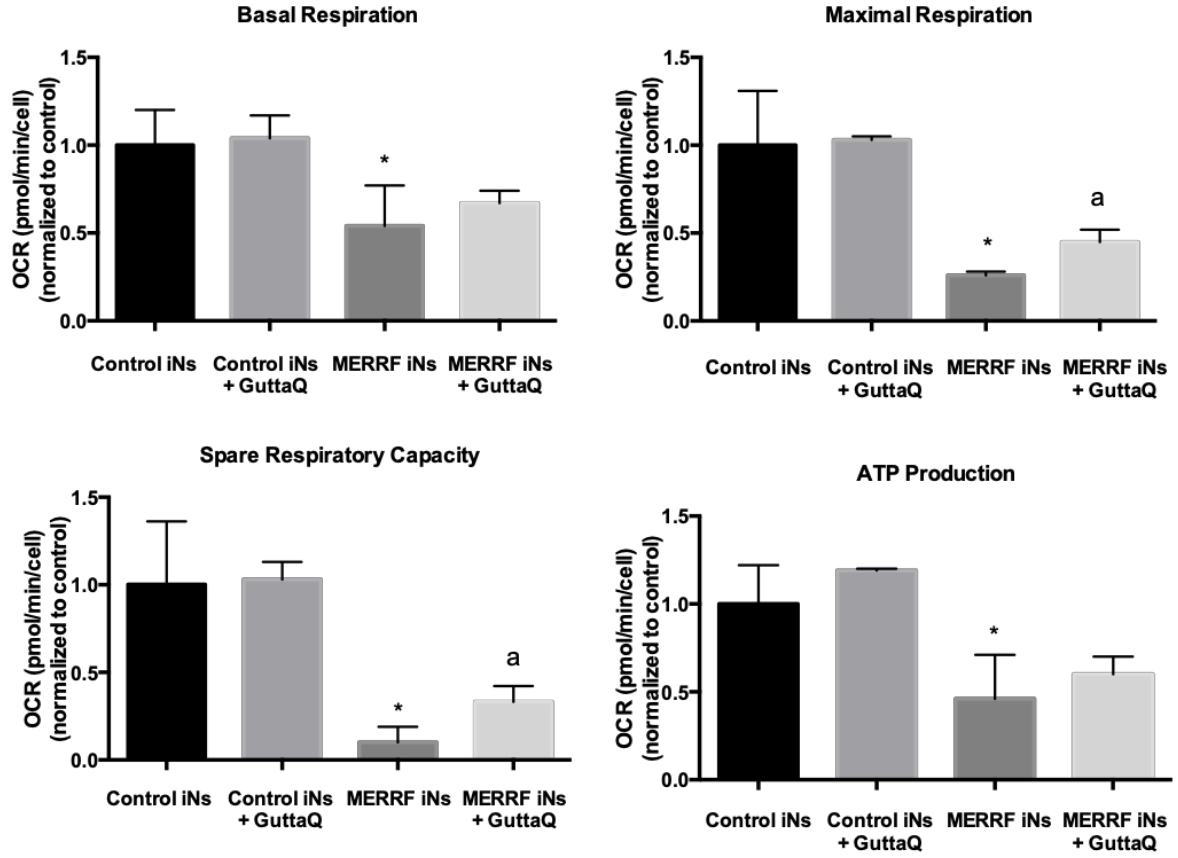

Figure R70. Parameters of mitochondrial respiratory function of untreated and GuttaQ-treated control and MERRF iNs.
Basal mitochondrial respiration, Maximal respiration, Spare respiratory capacity and ATP-linked respiration are plotted. Results are expressed as mean ± SD. Statistical significance was evaluated by unpaired, two-tailed t-test. Significance of MERRF respect to control iNs is represented as $^{*}P<0.05$. Significance between the presence and the absence of GuttaQ is represented as $^{a}P<0.05$. All OCR readings were normalized to cell number as described in Materials & Methods section.

A comparison of these parameters between untreated and GuttaQ-treated controls and MERRF iNs showed significant differences. The basal respiration, maximal respiration, spare respiratory capacity and ATP production rate of MERRF iNs were reduced compared to the controls iNs (**Figure R70**), confirming the results obtained in section **R-VII** and demonstrated that MERRF iNs exhibited decreased

mitochondrial function parameters. Moreover, excitingly, GuttaQ treatment was able to ameliorate some parameters of the mitochondrial function of MERRF iNs, such as the maximal respiration and the spare respiratory capacity, without affecting the mitochondrial function of the control iNs (**Figure R70**).

In conclusion, these results suggest that iNs derived from MERRF skin fibroblasts can be used as a new cellular screening platform, suitable for screening new drug candidates or validating pre-screened potential treatments for MERRF syndrome. In these assays, we observed that GuttaQ treatment significantly improved some mitochondrial respiration parameters of MERRF iNs, confirming our expectations since we have previously observed that CoQ ameliorates the pathophysiology of other cellular models of MERRF syndrome[219], (subsections **RI-RIV**) and this therapy is clinically used for the treatment of MERRF patients[360].
Therefore, iNs generated from MERRF patient-derived fibroblasts showing severe physiopathology and harbouring high heteroplasmy load seem to be appropriate models for testing the effects of potential treatments for MERRF patients.

DISCUSSION

DISCUSSION

MERRF syndrome is a rare, maternally inherited, multisystemic mitochondrial disease[318], which is associated in about 80% of cases with a mutation at position 8344 in the mitochondrial gene *MT-TK*, encoding mt-tRNA^{Lys} (m.8344A>G), although other mutations have also been described[321]. Like many mitochondrial diseases, there is no specific cure for MERRF syndrome and the treatments are primarily symptomatic. In the absence of proper clinical trials, it is difficult to evaluate the effect of proposed supportive treatments such as CoQ and its analogue idebenone, although both of them have been beneficial in some patients with mitochondrial diseases by increasing energy production[360].

In the first part of this thesis, we have studied the pathophysiology of the m.8344A>G mutation in two of the most commonly used MERRF cellular models: primary cultured skin fibroblasts derived from patients with MERRF syndrome and MERRF transmitochondrial cybrids harbouring the m.8344A>G mutation with an extremely high heteroplasmy load (90%). We were focused on the role of bulk autophagy and mitophagy as potential pathophysiological mechanisms of the disease, as well as the effect of CoQ supplementation in the correct flux of autophagy and mitophagy processes in MERRF cells.

First, our findings revealed that the skin fibroblasts derived from a MERRF patient showed clear pathophysiological alterations compared to control fibroblasts. We found significant differences in pathophysiological parameters such as proliferation rate, cell area, ΔΨm, mitochondrial ROS levels or carbonylated proteins levels. We observed that CoQ supplementation reversed these pathophysiological changes in MERRF fibroblasts. Increased ROS production and oxidative stress is a common consequence of mitochondrial dysfunction[204,221]. We identified a significant increase in ROS generation in MERRF fibroblasts, which had a clear connection with the raised amount of carbonylated proteins, one of the major targets of oxygen free radicals and other reactive species. Both mitochondrial ROS levels and increased carbonylated proteins in MERRF fibroblasts could be ameliorated by CoQ treatment. It has been proposed that excessive ROS levels can cause the opening of non-

specific high conductance PT pores in the IMM, inducing MPT[104] and leading to the simultaneous collapse of ΔΨm. The opening of PT pores causes mitochondria to become permeable to all solutes up to a molecular mass of about 1500 Da[630,631]. Moreover, a possible involvement of the PT in the induction of autophagy of altered mitochondria has been postulated. Thus, oxidative stress may play a prominent role in the induction of the mitochondrial damage, MPT and autophagy activation which we observed in MERRF fibroblasts, since an increased expression of autophagic proteins in cells harbouring the m.8344A>G mutation was detected.
In fact, autophagy machinery activation has been observed in different models of mitochondrial diseases[203] and neurodegenerative diseases that undergo mitochondrial dysfunction[212], and specifically in cellular models of MERRF syndrome[202].

CoQ treatment was able to decrease autophagic proteins levels in MERRF fibroblasts and cybrids. In light of this fact, we wondered whether CoQ treatment diminished autophagy activation or, on the other hand, accelerated the process, acting as an enhancer of autophagy flux. We will further discuss this question.

Autophagy activation in MERRF fibroblasts seems to be mediated by AMPK protein, which is phosphorylated in Thr172 in a high proportion in MERRF fibroblasts in comparison with control cells.
A few years ago, AMPK activation in skin fibroblasts derived from MERRF patients was reported[583]. In this work, the authors observed an increase of the expression of several proteins involved in the glycolytic pathways. The increase of ROS and reactive nitrogen species (RNS) in MERRF fibroblasts activated AMPK, leading to an increase of the glycolytic flux and an elevation of intracellular NADPH and glutathione (GSH) contents, due to the phosphorylation of the AMPK downstream target phosphofructokinase 2 (PFK2). This kinase promotes the oxidative branch of the pentose phosphate pathway.
Therefore, the authors concluded that AMPK activation mediated the metabolic shift from OXPHOS to glycolysis in MERRF cells, contributing to the adaptation of MERRF skin fibroblasts to oxidative stress and promoting mitochondrial biogenesis[584].

Actually, an induction of glycolytic genes has been observed in muscle biopsies of patients with other mitochondrial diseases such as MELAS, NARP and LHON[632].

We hypothesize that AMPK activation in MERRF fibroblasts is also involved in autophagy activation (**Figure D1**), since recently AMPK phosphorylation and subsequently activation have been observed in other models of mitochondrial diseases or mitochondrial dysfunctions that show autophagy and mitophagy enhancement, such as MELAS fibroblasts[220,633] and *CYTB*-/- cells[582], indicating that loss of mitochondrial respiration activates the AMPK signalling.

Moreover, AMPK is not only involved in autophagy but also in mitophagy activation. It has been demonstrated that cells with AMPK deficiency exhibit defective mitophagy[93]. Moreover, AMPK ameliorates mitochondrial fission *via* directly inhibiting DRP1 activity and/or phosphorylating MFN1 and MFN2 during autophagy induction[634]. Mitophagy shares the bulk autophagy machinery and some authors suggest that autophagy activation is necessary for mitophagy progression[222].
During the conduction of this thesis, we have observed both bulk autophagy and mitophagy activation in MERRF fibroblasts and cybrids. These phenomena have been previously detected in cellular models of MERRF syndrome[219] and in different models of mitochondrial diseases with primary and/or secondary CoQ deficiencies[204,220,221,254]. In those cases, disruption of mitophagy resulted in cell death by apoptosis. Furthermore, prevention of mitophagy in CoQ deficient cells by chemicals like 3-methyl adenine or wortmannin or by genetic knockdown of *ATG* genes caused apoptotic cell death[204,221].

The elimination of dysfunctional mitochondria could play a crucial role in protecting cells from the damage caused by perturbed mitochondrial function and the release of potentially proapoptotic molecules. Our finding that the autophagic protein LC3B colocalized with structurally abnormal mitochondria, but not with normal tubular mitochondria in MERRF fibroblasts, suggests that mitophagy specifically targets dysfunctional mitochondria in these cells. In this regard, it has been shown that VDAC1, a major component of the PT pore complex on the OMM, is more susceptible to oxidative damage in MERRF cybrids than in WT cybrids[353].

During this work, we have observed that CoQ treatment enhances activation of AMPK in MERRF cells by increasing phosphorylation of the Thr172 residue of the protein.
This effect has been previously observed in a fibroblasts model of MELAS syndrome[220], in 3T3-L1 preadipocytes[586], in endothelial progenitor cells[587] (EPCs), in human umbilical vein endothelial cells (HUVECs)[635] and in a senescence-accelerated mouse model[636].

However, the mechanism by which CoQ activates AMPK is still not fully understood. Currently, the main hypothesis is that CoQ treatment increases the levels of cAMP, an allosteric and direct activator of AMPK[636,637]. Moreover, it has been observed that CoQ induces an increase in cytoplasmic calcium concentrations, which may activate Ca^{2+}/calmodulin-dependent protein kinase-kinase (CaMKK), an upstream AMPK activator[586].
Interestingly, increasing the activity of AMPK has been observed to ameliorate the symptoms of mitochondrial diseases that course with dysfunctional mitophagy. For example, MELAS fibroblasts unable to activate AMPK ameliorated their severe phenotype by CoQ or AICAR treatment that activated AMPK pathway[220]. In accordance with these data, we have observed that stimulating AMPK pathway by CoQ supplementation ameliorated the pathophysiology of MERRF fibroblasts and cybrids.

In this work, one of our main interests was to characterize mitophagy in MERRF syndrome, because different types of selective degradation of mitochondria have been described for mammals' cells[130]. During the conduction of this thesis, we identified in MERRF cells the presence of necessary alterations for Parkin-mediated mitophagy to be initialize such as low $\Delta\Psi m$, high levels of ROS, bulk autophagy activation and high levels of Parkin and PINK1 proteins. Actually, the induction of the autophagy machinery in a background of low levels of Parkin protein did not promote mitophagy even in cellular models of mitochondrial diseases[222].
In fact, different authors suggest that all of these pathological characteristics have to be present in the cell to undergo Parkin-mediated mitophagy[222,223].

Besides all these features, we also found high levels of ubiquitinated proteins in MERRF fibroblasts, and interestingly, ubiquitin signal mostly colocalized with depolarized, fragmented mitochondria.

Considering the relationship between mitochondrial proteins ubiquitination and Parkin-mediated mitophagy[592,593], we hypothesized that mitophagy may be upregulated in MERRF cells.

Moreover, we detected aggresome-like structures with both ubiquitin and VDAC1 proteins in MERRF fibroblasts. This is in accordance with a study showed that Parkin-dependent ubiquitination of VDAC1 is a cardinal feature of mitophagy activation in a model of PD[106].

DRP1 protein levels were also increased in MERRF fibroblasts compared to controls. DRP1 is the main regulator of mitochondrial fission and several evidences have shown that mitochondrial fission coordinates with mitophagy in different mammalian cell types. Our data are in agreement with studies showing that DRP1-mediated mitochondrial fission must occur prior to mitophagy, dividing mitochondria into small ones susceptible to autophagosome engulfment[638-641].

As mitochondrial fission is crucial for the distribution of mitochondria throughout the cell, especially in neurons, DRP1 plays an essential role in the pathophysiology of several neurodegenerative diseases that undergo mitochondrial dysfunction[642], such as PD[643] or HD[644]. Interestingly, increased levels of DRP1 have been found in postmortem HD brains compared to HD-unaffected brains[645], suggesting an impairment in mitochondrial dynamics that could affect mitophagy flux.

Although more research is needed to understand the role of DRP1 in mitochondrial diseases, an excessive mitochondrial fission may be involved in the pathophysiology, at least in MERRF syndrome's. Currently, a great progress is being made in developing therapeutic molecules that can reduce excessive mitochondrial fission and at the same time maintain the fission–fusion balance in mitochondria.

M-divi[646-648], P110[649,650] and Dynasore[651] are the most promising mitochondrial fission inhibitors and it would be interesting to screen their effects in the pathophysiology of mitochondrial diseases in the near future.

We confirmed the presence of Parkin-mediated mitophagy in MERRF cells by finally detecting Parkin translocation from cytosol to mitochondria, an essential event for Parkin-mediated mitophagy activation.

Parkin-mediated mitophagy activation has been observed in cells carrying different mtDNA mutations[222,279] and other cellular and animal models of diseases that undergo mitochondrial dysfunction such as AD[652,653], kidney injury[654] or cardiac pathology[213].

Interestingly, high levels of Parkin accumulation in mitochondria were detectable in MERRF cells in basal conditions, even without autophagy blockers such as bafilomycin A1. This fact was interesting because bulk autophagy and mitophagy are fast processes when they function properly. Therefore, we hypothesized that a disruption and/or a slowdown of autophagy/mitophagy flux may be occurring in MERRF cells.

At this point of the thesis, we wanted to focus in the correct functioning of autophagy and mitophagy processes in MERRF syndrome. There are several studies about autophagy and mitophagy activation in MERRF cells and other mitochondrial diseases models, but there are almost no investigations about the state of the autophagy/mitophagy flux in these diseases.

By performing the bafilomycin assay, we checked that the increase of autophagic proteins that we observed in MERRF fibroblasts and cybrids was due to an impairment of the autophagy flux, which caused an accumulation of autophagosomes and the worsening of pathophysiology.

Moreover, by performing a mitophagy flux assay, we also checked that specifically mitophagy flux was impaired in MERRF fibroblasts.

But, if bulk autophagy and mitophagy are activated as a protective response against mitochondrial dysfunction, why is the flux impaired in MERRF cells? We hypothesize that the block of autophagy/mitophagy flux may be caused by a depletion of ATP levels, a characteristic of mitochondrial dysfunction which we had observed during the study of mitochondrial respiration using the extracellular flux analyzer. ATP is necessary to maintain lysosome function and sequester the cytosolic components[203,204].

This is in accordance with the observed beneficial effect of stimulating AMPK by CoQ in MERRF cells. Although AMPK is activated in MERRF patient-derived fibroblasts, the low levels of ATP in these cells could prevent the correct autophagy flux. Therefore, sustained activation of AMPK by external factors could stimulate

autophagy flux and reduce autophagolysosome accumulation, a possible cause of the worsening of the pathophysiology of the disease.

Moreover, the impairment of autophagy/mitophagy flux in cellular models with mitochondrial dysfunction could provide an explanation of why activation of autophagy or/and mitophagy is not enough to counteract the mitochondrial respiration dysfunction. Generally, both MERRF cells *in vitro* and patient cells *in vivo* tend to get worse and increase their heteroplasmy load[655-658].

During the conduction of this thesis, we observed that CoQ acts as an enhancer of bulk autophagy, in accordance with previous findings in different MELAS cellular models[220].

However, interestingly, for the first time we observed that CoQ specifically enhances mitophagy flux in MERRF cellular models, allowing the amelioration of the pathophysiology and preventing excessive Parkin translocation to mitochondria.

Under basal conditions, both MERRF cellular models, patient-derived fibroblasts and cybrids showed a reduced expression of mitochondrial proteins, in accordance with observations previously reported[349]. Interestingly, the expression levels of mitochondrial proteins increased after CoQ treatment.

But, if mitophagy flux is enhanced with CoQ, why did we observe an increase of mitochondrial mass in MERRF cells when treated with CoQ? As mentioned above, CoQ has a pleiotropic effect. Between its different action mechanisms, CoQ activates AMPK[586,587,635-637], and it is well known that AMPK activation is involved in mitochondrial biogenesis[165,166]. Therefore, CoQ treatment could enhance mitophagy flux and promote mitochondrial biogenesis at the same time. An ideal treatment with CoQ would permit a balance between mitophagy and mitochondrial biogenesis, ameliorating cell bioenergetics.

In fact, by carrying out the Mito-stress test by the XFe24 extracellular flux analyzer, we examined that MERRF fibroblasts harbouring a 57% of heteroplasmy load had decreased values of four of the most important parameters of mitochondrial function: basal respiration, maximal respiration, spare respiratory capacity and ATP production. CoQ treatment increased the values of all the parameters. This effect could be due to the antioxidant action, the enhancement of autophagy/mitophagy flux and/or the increase in mitochondrial biogenesis.

Therefore, these studies in cell cultures which harbour the m.8344A>G mutation provide robust experimental evidence that CoQ supplementation could be beneficial in the treatment of patients with MERRF.

Autophagy and Parkin-mediated mitophagy activation were also demonstrated in cybrids harbouring the m.8344A>G mutation, indicating that both processes arise as a consequence of this mutation, not of a concomitant nuclear mutation. In addition, CoQ treatment partially restored the pathophysiological alterations found in MERRF cybrids. Additionally, we noticed that the positive CoQ effect is affected by the heteroplasmy load, considering that CoQ treatment did not ameliorate neither the mitochondrial respiratory profile nor the mitochondrial bioenergetics parameters of MERRF cybrids harbouring an extremely high percentage of heteroplasmy load. Therefore, a major challenge in mitochondrial diseases is the mild effectiveness of the different pharmacological therapies, since it can vary depending on the concentration of the drug, the heteroplasmy load and the cell type.

Although there is no longer doubt about the importance of mitophagy in mitochondrial diseases, there is not a common consensus about if regulated degradation of mitochondria has a protective or pathological role during the course of these diseases.

To examine whether Parkin-mediated mitophagy is beneficial or harmful for the pathophysiology of MERRF cells, we used a MERRF cybrids cells model with a knockdown Parkin expression. By this way, we sought to establish the role of Parkin in MERRF syndrome and its impact on ROS levels and cells survival.

We found that knockdown of Parkin expression aggravated apoptosis levels and ROS production in MERRF cybrids, confirming that Parkin is involved in the removal of damaged mitochondria in MERRF cells and plays an important role in regulation of ROS production and MERRF cells survival.

There is strong evidence supporting the connection between mitochondrial redox homeostasis and Parkin-mediated mitophagy[659]. Mutations and/or deletions in the *PARK2* gene have been demonstrated to increase ROS production and susceptibility to oxidative conditions in *Drosophila*[660,661], mouse[662], zebrafish[663] and different cellular models[664].

Moreover, increased levels of superoxide dismutase proteins have been shown to rescue the pathological phenotype of Parkin mutant cellular and fly models[665].
Furthermore, in accordance with our data, the increase of mitochondria-induced ROS and apoptosis after knockdown of Parkin expression in nucleus pulposus (NP) cells has been recently published, suggesting a role of Parkin-mediated mitophagy in the pathogenesis of intervertebral disc degeneration (IDD)[666].

Therefore, our findings suggest that Parkin-mediated mitophagy may have a protective role in MERRF syndrome.
Mitophagy has shown to be a defense mechanism in different pathological situations. Experiments with *PINK1*−/− mice showed impaired mitochondrial respiration and an increase in large mitochondria, which can be related with the function of PINK1 to promote fission and mitophagy[667]. In addition, it has been demonstrated that alterations in mitophagy due to PINK1 silencing diminished cell resistance under hyperoxia situations and oxidative stress in the lung endothelium[206].
In addition, removal of aberrant mitochondria has been shown to play a protective role in age-related neurodegenerative disorders, such as PD. Specifically, Parkin, whose loss-of-function causes PD, is involved in this process. Since Parkin is essential for mitophagy, PD may be at least in part associated with the failure to eliminate dysfunctional mitochondria[668].
Interestingly, different mutations in some genes related to Parkin-mediated mitophagy, such as *OPTN*, *P62* and *TBK1* are linked to ALS, suggesting that the inefficient turnover of damaged mitochondria may contribute to neurodegeneration in this disease[669,670].
The first part of our study revealed that unbalanced autophagy and Parkin-mediated mitophagy are involved in the pathogenesis of MERRF syndrome and may serve as potential therapeutic targets for this and other mitochondrial diseases.
From our view, autophagy and Parkin-mediated mitophagy activation are mechanisms for MERRF cells to combat pathological conditions derived from the defective OXPHOS system, such as low membrane potential, high level of ROS and decreased ATP levels (**Figure D1**). However, possibly due to the low ATP levels, autophagy/mitophagy flux becomes impaired in MERRF cellular models, being the accumulation of defective mitochondria and/or autophagosomes one of the main causes of the worsening of the pathophysiology.

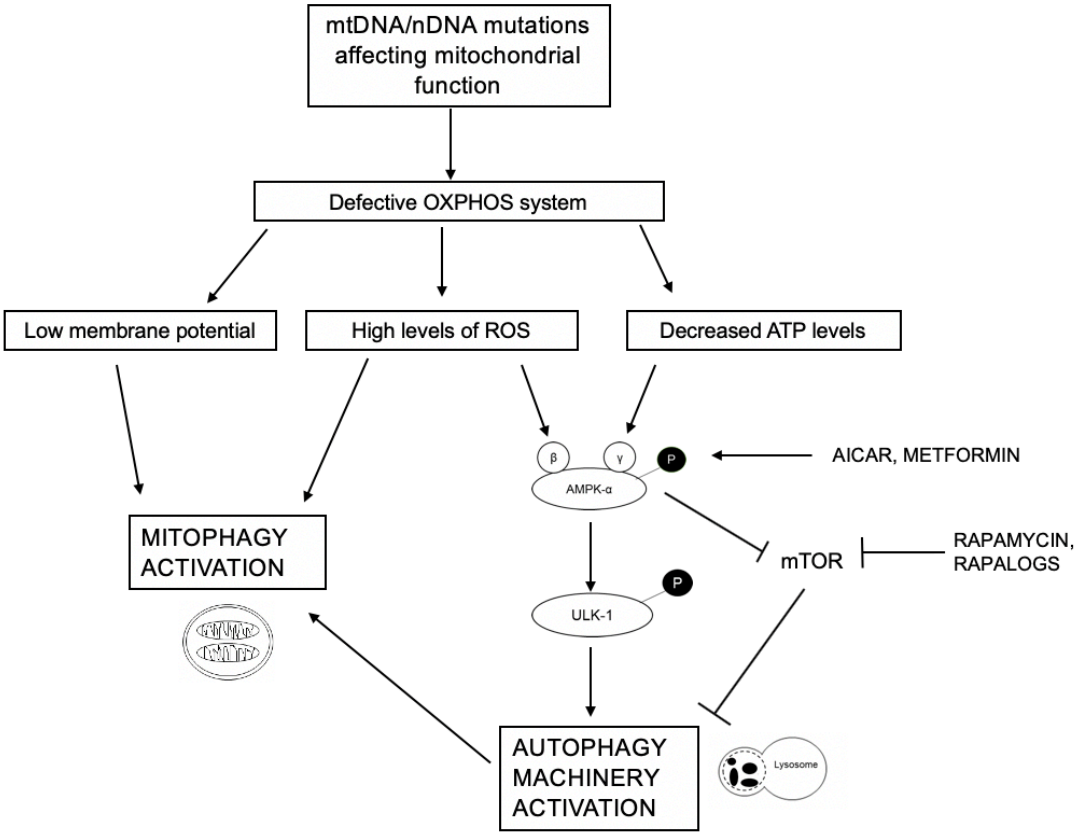

Figure D1. Mitochondrial dysfunction induces bulk autophagy machinery and mitophagy activation.
Adapted from Villanueva-Paz et al. (2016)[89].

Considering the disruption of autophagy/mitophagy flux of MERRF cells as one of the main causes of pathophysiological manifestations of the disease and the fact that CoQ treatment was not able to restore mitochondrial respiration parameters in a MERRF cybrids model with a 90% heteroplasmy load, bulk autophagy was stimulated by supplementation with rapamycin, one of the most studied autophagy inducers, and its effect on mitochondrial respiration of MERRF cells was evaluated.
We observed that rapamycin treatment increased the mitochondrial respiratory rate (basal and maximum), the spare respiratory capacity and the ATP production both in control and MERRF patient-derived fibroblasts, and this effect was sustainable in time. Interestingly, rapamycin-treated MERRF cybrids also showed an increased spare respiratory capacity and ATP production coupled to oxygen consumption, but neither basal nor maximal respiration rates ameliorated. These differences can be

due to the different percentage of heteroplasmy between MERRF fibroblasts (57%) and cybrids (90%) and the different metabolic rate of these cellular types.

These results were somewhat surprising, since mTORC1 activity has been described to exert a positive effect on mitochondrial function. In fact, rapamycin-mediated inhibition of this complex has been shown to decrease ΔΨm[671], mitochondrial respiration[671-673] and ATP production[671] in cultured cells.
However, it has been observed that the length of the rapamycin treatment has a crucial role on its effect on mitochondrial respiration. Short-term rapamycin treatment produced a decreased respiratory rate in mice, meanwhile long-term treated mice showed an increased respiratory rate[674].
Moreover, rapamycin treatment has been demonstrated to improve lifespan and survival and to attenuate the progression of the disease in cellular[675], mouse[314,676,677] and *Drosophila*[678] models of Leigh syndrome. Nevertheless, the mechanisms by which mTOR inhibition exerts these effects have not been identified yet.

In the same way, why rapamycin treatment ameliorates the defective mitochondrial respiratory profile of MERRF and other mitochondrial disease cellular models remains unknown.
A possible hypothesis is the activation of the mTORC2 complex due to the addition of rapamycin to the culture media. Although it is known that mTORC2 is inhibited by high concentrations of rapamycin (μM)[679], it has been shown that mTOR inhibition by rapamycin can trigger a feedback mechanism resulting in the activation of AKT pathway, and that this feedback activation of AKT is dependent on IGFs/IGF-1R signalling[680] and promotes cell survival and proliferation.

Moreover, some authors have observed an enhancement of ΔΨm and a reduction of ROS levels after the increase of autophagy flux due to rapamycin treatment in human fibroblasts[681].
Long-term rapamycin treatment at low doses diminished the number of depolarized mitochondria and cells maintained a more polarized mitochondrial network. The authors suggested that this fact could be due to the increase in the expression of proteins related to mitochondrial biogenesis such as NRF1, PGC1A y mtTFA, as well as the increase of autophagy/mitophagy flux. This link between mitochondrial

clearance and mitochondrial gene expression provoked by inhibition of mTOR has shown to be the interaction between P62 and KEAP1. This association promotes the accumulation of NRF2 in the nucleus and increases mitochondrial gene expression.

Furthermore, the authors observed that human fibroblasts grown in rapamycin-supplemented medium retained higher levels of both basal and ATP-coupled mitochondrial respiration when challenged with H_2O_2. In addition, rapamycin-treated cultures were resistant to mitochondrial depolarization from exogenous H_2O_2 exposure. This is in accordance with our results, since MERRF cells are exposed to a high intracellular stress due to mitochondrial ROS accumulation, and when treated with rapamycin, basal, maximal and ATP-coupled respiration are increased.

Very recently, the correction of the mitochondrial myopathy of a *Cox15*$^{sm/sm}$ mouse by rapamycin treatment has been published[682]. *Cox15*$^{sm/sm}$ mice lack the gene encoding Cox15 in skeletal muscle, suffering a serious COX deficiency[311,683].

Long-term rapamycin treatment improved motor endurance, corrected structural anomalies of muscle and increased COX activity of the diseased mice by restoring the disrupted autophagy/mitophagy flux and coordinately activating lysosomal biogenesis.

Therefore, we hypothesize that amelioration of mitochondrial respiration profile in MERRF cells after rapamycin treatment could be due to the attenuation of the endogenous stress associated with mitochondrial function. Rapamycin would improve mitochondrial homeostasis by altering P62 turnover and increasing turnover of dysfunctional mitochondrial components through mitophagy[106,278] (presumably Parkin-mediated[682]) (**Figure D1**), as well as increasing the expression of NRF2 target genes[684] and lysosomal biogenesis.

In light of all these data, we recommend to adjust rapamycin treatment for each cellular model and/or mitochondrial disease, since length of treatment and dosage can alter the effects of the drug on the mitochondrial function and cell pathophysiology.

According to our findings, we suggest a previous analysis of autophagy and mitophagy flux in MERRF and other mitochondrial disease cellular models, in order to perform a screening of autophagy/mitophagy flux modulators that could improve the mitochondrial pathophysiology.

In the second part of this thesis, the successful generation of disease-specific iNs by direct reprogramming from two different MERRF patient-derived fibroblasts harbouring the m.8344A>G mutation is described for the first time.

MERRF syndrome is one of the most frequent mitochondrial encephalomyopathies and its clinical phenotypes and pathological mechanisms have been extensively studied. However, the lack of animal models has hindered the understanding of the pathophysiology of the disease. Moreover, *in vitro* mitochondrial diseases modelling has been always challenging, since the most affected cell types in these diseases (such as neurons and/or muscle cells) are difficult to maintain in culture[685]. In the case of mitochondrial diseases caused by mtDNA mutations, such as MERRF syndrome, the understanding of the phenotypes is even more complicated due to the characteristic presence of heteroplasmy. For that reason, it is difficult to assess the effect of a particular mutation and to establish a threshold of heteroplasmy load sufficient to affect mitochondrial function[686]. Furthermore, the nDNA background can differentially modulate the disease progression in patients harbouring the same mutation at the same heteroplasmy level[687].

The discovery of hiPSCs, which are able to become any differentiated cell type, has been a major step forward in the field of disease modelling[452,688,689]. A further advance was achieved by obtaining iPSCs followed by their differentiation into particular cell types such as neurons[690]. By now, several diseases have been *in vitro* modelled using embryonic stem cells (ESCs) or iPSCs derivatives, with promising results[691]. More recently, iPSCs generation has also opened new doors in mitochondrial diseases modelling. Patient-derived iPSCs models have been established to study the pathophysiology of mitochondrial diseases caused by mutations in mtDNA such as MELAS and MERRF syndromes[692,693]. In a recent publication, cardiomyocyte-like cells (CMs) and NPCs differentiated from MERRF-iPSCs showed high ROS levels and upregulated antioxidant genes expression[438]. However, mitochondrial respiration dysfunction and high heteroplasmy levels strongly inhibited maturation and survival of MERRF iPSCs-derived neurons, suggesting that correct mitochondrial maturation actually contributes to cellular fate-determination processes[694].

One alternative approach to avoid the disadvantages of iPSCs generation and posterior differentiation is the direct somatic reprogramming into a particular cell type, bypassing an intermediate pluripotent state[695]. This approach is suitable for

different applications in disease modelling to shed light on the unknown disease pathogenesis, drug screening and drug toxicity testing.

Importantly, although it has been observed that high levels of heteroplasmic mtDNA mutation block cellular reprogramming to hiPSCs[696] and also hinder neuronal lineage commitment of hiPSCs[694], we have reached conversion efficiencies up to 70% using MERRF patient-derived fibroblasts harbouring high levels of heteroplasmy (65%) as starting cells to obtain iNs by direct reprogramming. Thus, at least in the case of this specific mtDNA mutation, moderate heteroplasmy loads did not compromise conversion efficiency of direct reprogramming of fibroblasts into iNs.

Reprogramming efficiency depends on several factors such as the conversion protocol, the starting cell type and the neural genes that are overexpressed[450]. For example, the order in which the conversion genes are placed in a lentiviral vector affects the level of expression. In addition, the age of donor cells, their passage number, etc. could restrict this parameter. In our studies, using the method developed by Drouin-Ouellet et al.[494], we obtained high conversion efficiencies which provided enough iNs to perform several assays. This fact is very valuable in the case of mitochondrial diseases due to the difficulty of obtaining a high number of starting cells.

Interestingly, in our study, we did not find significant differences in the conversion efficiency between controls and MERRF iNs. This is in accordance with the work of Drouin-Ouellet et al., in which the conversion efficiency of control, PD, HD and AD patient-derived fibroblasts into iNs was similar.

Another important parameter in direct reprogramming is the neuronal purity (the percentage of iNs in the final culture), which determines the homogeneity of the cell culture. Interestingly, in this work we obtained a higher neuronal purity in MERRF iNs cultures (67% in MERRF 1 iNs and 78% in MERRF 2 iNs) than in controls ones, being a 50%. A recent study performing direct reprogramming of mouse astroglial cells into neurons suggested that the metabolic state of the starter cell is important for conversion into another cell type, and that direct cell fate conversion from fibroblasts may require a metabolic switch from less to more OXPHOS, as occurs in endogenous neurogenesis[502].

In accordance with this idea, during the reprogramming process, we observed that MERRF patient-derived cells showed higher cell death rate compared to control cells. For that reason, we hypothesize that MERRF fibroblasts are more sensitive to

the metabolic switch needed to reach the conversion (they have a dysfunction of the OXPHOS) and most of them die during the process, but almost all the cells that survive to the process are converted. Meanwhile, control fibroblasts may be more resistant to the metabolic switch, being able to survive to the process although they are not fully converted.

Interestingly, after the reprogramming process, MERRF iNs maintained the original heteroplasmy load of the corresponding MERRF fibroblasts, indicating that the levels of heteroplasmy were not affected by the conversion protocol. The maintenance of heteroplasmy load after reprogramming is crucial whether iNs are going to be used to study pathophysiological alterations or as a screening platform for personalized medicine. Moreover, this fact establishes a huge difference between direct reprogramming and hiPSCs generation, since it has been demonstrated that, in the latter case, mtDNA segregation takes place due to an increase of mtDNA copy number. Thus, different cell populations with heteroplasmy loads close to homoplasmy are obtained[697]. In fact, in a recent study using MELAS fibroblasts with 77.7% of heteroplasmy load as starting cells, different MELAS-iPSCs clones with variable heteroplasmy loads (from 3.6 to 99.4%) were obtained[434].

In the present work, different indicators of neuronal maturation, such as bouton-like structures (swollen structures similar to presynaptic boutons, specialized areas within the axon of the presynaptic cells that contain neurotransmitters) or spine-like protrusions (structures similar to dendritic spines, which typically receive input from an axon at the synapse) were observed both in controls and MERRF iNs, suggesting that at 27 DPI mature iNs are generated. Moreover, electrophysiological recordings of 27 and 60-80 DPI-iNs showed that iNs generated by this method have functional properties.

However, one interesting observation from this research is that direct conversion of MERRF patient-derived fibroblasts into iNs led to neurons with smaller body area and shorter neurite outgrowth compared to controls iNs. This can be interpreted as the result of neuritic breakdown and degeneration in MERRF iNs, since small Tau+ neurite fragments were observed after reprogramming.

Most of neuropathological studies in MERRF syndrome have been performed by neuro-radiological imaging, MRI and immunohistochemical analysis of brain tissues.

These studies concluded that the neuropathology of MERRF syndrome is characterized by neuronal loss and atrophy, demyelination and astrocytosis. These processes mainly occur in the cerebral cortex, the superior cerebellar peduncle, the dentate nucleus and Purkinje cells of the cerebellum and inferior olive, red nuclei and substantia nigra of the brainstem[698-701]. However, the underlying molecular mechanism responsible for the neuron vulnerability in MERRF syndrome remains unknown, and there are no studies about the morphology and structural features of neurons derived from MERRF patients.

Currently, there are no antecedents of direct reprogramming of MERRF patients' fibroblasts into iNs, and only one work regarding NPCs derived from MERRF iPSCs has been published[438]. Nevertheless, in this work the characterization of morphology and maturation of MERRF NPCs was not performed. However, an increased ROS production and mitochondrial fragmentation were observed in MERRF NPCs compared to controls NPCs, as well as decreased values of mitochondrial parameters such as basal oxygen consumption, ATP production and maximal respiration. These findings support the results that we have obtained in MERRF iNs.

Moreover, there are some works in which direct reprogramming of patient-derived fibroblasts showed decreased neurite outgrowth and neuritic breakdown. For example, HD patients-derived iNs showed decreased neurite outgrowth and neuritic breakdown compared to control iNs, which is related to a progressive cell death of HD iNs[499]. Furthermore, in a recent study undergoing direct reprogramming of spinal muscular atrophy (SMA) patient-derived fibroblasts into iNs, SMA iNs exhibited a significantly reduced neurite outgrowth rate compared to controls iNs, and they also showed neuronal degeneration and neurite breakdown. In addition, the neurite length of SMA iNs was shorter in comparison to controls iNs[513]. Similarly, a reduction in outgrowth and branching has been shown in familial dysautonomia (FD) iNs compared to control-derived iNs[518].

Interestingly, a recent work of Yokota et al.[694] showed that iPSCs with high proportions of m.3243A>G (the most common mutation in MELAS syndrome, which is similar to MERRF disease) exhibited neuronal cell death and maturation defects, suggesting that mitochondrial respiratory dysfunction strongly inhibits maturation and survival of iPSCs-derived neurons.

Therefore, although we performed the morphology analysis of controls and MERRF iNs without any expectations or antecedents, our results are in accordance with what

is described in the literature about iNs derived from patients with other neurodegenerative diseases that undergo mitochondrial dysfunction.
However, further investigations are needed to understand the possible relationship between mitochondrial function and the trafficking of neurotrophic factors that may affect neuronal size and neurite outgrowth in MERRF iNs.

In this respect, MERRF iNs showed altered mitochondrial network and function accompanied by low ΔΨm and elevated ROS levels.
The ΔΨm is indispensable for ATP production and a crucial parameter to evaluate the functional state of mitochondria[702]. As we have mentioned above, in previous and the present studies, analyses of MERRF fibroblasts and cybrids have shown a dramatic decrease in ΔΨm[219,349,703]. In this work, MERRF iNs also showed mitochondrial depolarization, suggesting that both neuronal bioenergetics and mitochondrial protein import can be affected. Furthermore, mitochondrial membrane depolarization is a known stimulus for opening the MPT[704,705], which is thought to be one of the responsible processes of neuronal damage[706].
As well as loss of ΔΨm, we identified increased ROS levels in MERRF iNs. Commonly, mitochondrial dysfunction leads to increased ROS levels and oxidative stress[707]. In fact, previous and present works have described high levels of ROS in fibroblasts[219,353,427] and cybrids[219,422] harbouring the m.8344A>G mutation and also in iPSCs derived from MERRF fibroblasts[438].
It has been observed that ROS overproduction caused by nerve growth factor deprivation, or other stimuli such as starvation or addition of rapamycin, triggers bulk autophagy and mitophagy[117,581,708].
In the first part of this thesis, we described how autophagy flux is disrupted in MERRF fibroblasts and cybrids.
Interestingly, for the first time using a neural model, we have observed that MERRF iNs also showed an impaired autophagy flux compared to control iNs, accompanied with colocalisation of the autophagic protein LC3B with fragmented mitochondria, suggesting mitophagy activation. It is considered that disrupted autophagy flux plays a central role in the pathophysiology of numerous neurodegenerative diseases and episodes of brain injury since it contributes to neuronal cell death[212,709-711]. Thus, autophagy modulation has been proposed as a possible therapy for numerous diseases which present mitochondrial dysfunction[209,302,305]. In concrete, MERRF iNs

could be a potential model to study the role of autophagy in neurodegeneration and the therapeutic effectiveness of autophagy flux modulators[89].

Although it is clear that high ROS levels trigger bulk autophagy and mitophagy, it has been suggested that mitophagy acts as a negative regulatory feedback mechanism by eliminating dysfunctional mitochondria that overproduce ROS[712,713].

Elimination of damaged mitochondria depends on the relationship between mitophagy and mitochondrial dynamics, and it guarantees mitochondrial quality control. However, it is still unknown how dysfunctional mitochondria are distinguished from the healthy ones.

Changes in mitochondrial morphology are thought to have an essential role in this process. Damaged mitochondria suffer from the inactivation of the fusion factor OPA1, allowing their isolation due to the fragmentation of the mitochondrial network[714]. This process is thought to be a protective mechanism in order to restrain mitochondrial damage and it is crucial for the removal of damaged mitochondria from the cell[149,157,421]. Actually, it has been observed that mitochondrial fission blocking inhibits mitophagy[640,641]. These studies support the idea that mitochondrial dynamics and mitophagy are interconnected in order to ensure the correct mitochondrial function.

In the MERRF iNs model, both phenomena mitochondrial fragmentation accompanied with changes in mitochondrial morphology and mitophagy activation are clearly observed, which is in accordance with other studies performed in MERRF fibroblasts and cybrids[219]. MERRF iNs showed differences in several parameters related to mitochondrial morphology compared to control iNs, suggesting that MERRF iNs had a smaller and more fragmented mitochondrial network. Despite their importance, fission and mitochondrial fragmentation *per se* are not triggering mitophagy, for which complementary dysfunctions of the organelle such as mitochondrial depolarization are required[715]. In our work, we have observed in MERRF iNs that fragmented mitochondria are indeed depolarized.

In the particular case of mitochondrial diseases caused by point mutations in the mtDNA, we have shown during the conduction of this thesis that mitophagy may have an essential role in eliminating mitochondria harbouring the highest percentage of mutated mtDNA, which will presumably be the most dysfunctional mitochondria. In this sense, a specific characteristic of some cellular models of mitochondrial

dysfunctions is the decreased ΔΨm and high levels of ROS due to defects in the electron flux through the MRC[204,219,221,254].

Dysfunctional mitochondria not only increase ROS levels but also diminish mitochondrial respiratory parameters in affected cells. In our work, we found that mitochondrial respiration profile was decreased in MERRF iNs in comparison to controls iNs. In particular, patient-derived iNs showed considerably lower basal respiration, diminished ATP-coupled respiration, lower maximum respiration rate and a decreased spare respiratory capacity. This indicates a decreased electron flux through the MRC, which is coupled to depressed OXPHOS.

One important point of our work is the observation that pathological severity of MERRF iNs seems to depend on heteroplasmy load. We have worked with MERRF iNs generated from two MERRF patient-derived fibroblasts carrying different heteroplasmy load of m.8344A>G mutation (65%, MERRF 1 and 38%, MERRF 2). Both MERRF iNs show pathophysiological alterations compared to controls iNs; for example, a decreased mitochondrial respiration manifested in lower basal respiration, maximal respiration, spare respiratory capacity and ATP production. No difference was detected between the mitochondrial respiration profile in MERRF 1 iNs with 58% heteroplasmy and MERRF 2 iNs with 43% heteroplasmy. Therefore, these models, at least with these heteroplasmy loads, seem to behave in a similar way regarding to the pathophysiological parameters analyzed.

However, we have observed that pathological severity of MERRF 1 iNs is more pronounced, because MERRF 1 iNs showed decreased neural body area, more fragmented mitochondrial network, higher levels of ROS and a higher number of mitophagic cells compared to MERRF 2 iNs. Our findings also indicate that low heteroplasmy load (around 40%) is sufficient to cause pathophysiological alterations using iNs *in vitro.*

MERRF syndrome is associated with a wide range of clinical phenotypes: from patients with the whole spectrum of symptoms to asymptomatic individuals. The variations in phenotypes of MERRF syndrome seem to be the result of differences of heteroplasmy load in different tissues[196,219]. According to our findings, this phenotypic diversity in patients of MERRF syndrome was also manifested in iNs.

Other point mutations in mtDNA have been previously found to show correlation between heteroplasmy load and pathophysiology of mitochondrial disorders. For example, primary MELAS patients-derived fibroblasts carrying the m.3243A>G mutation with different heteroplasmy loads showed different pathophysiological severity according to the percentage of heteroplasmy[220]. Moreover, the heteroplasmy load of the m.3460G>A mutation is critical in the development of LHON (Leber's hereditary optic neuropathy)[716]. Therefore, maintenance of heteroplasmy load after direct reprogramming increases the suitability of iNs to be a useful tool for mitochondrial diseases modelling and drug screening.

A major challenge in MERRF syndrome is the lack of effective pharmacological therapies. For us, one of the most promising applications of mitochondrial disease's patients derived-iNs is the establishment of screening platforms to test the effect of potential therapeutic compounds or toxics in a neural cell model.
Along this work, we have demonstrated that iNs generated from MERRF patients-derived skin fibroblasts with high heteroplasmy load are suitable for the evaluation of pre-screened selected drugs, such as CoQ or its water-soluble analogue, GuttaQ. Moreover, we wanted to start the screening with this molecule since secondary CoQ deficiency has been previously identified in cellular models of MERRF syndrome[219].
There are several studies that suggest CoQ treatment protects from neuronal cell death due to its antioxidant action. For example, in kainic acid (KA) pre-treated hippocampal slice cultures, CoQ treatment reduced neuronal cell death through reduction of ROS formation[717]. Moreover, protective role of CoQ against ischemia-reperfusion[718] and ROS-induced damage[719] has been found in different neuronal models. However, studies about CoQ effect on neuronal mitochondria are scarce, although a decreased MRC activity and low ATP production due to neuronal CoQ deficiency have been observed[718].

Very recently, a novel CoQ analogue has been demonstrated to protect neuronal mitochondria from mitochondrial dysfunction caused by accumulation of oligomeric amyloid β (OAβ) in a neuronal model of AD[720].

This is in accordance with what we have observed in our work. Treatment of MERRF iNs with GuttaQ ameliorated both maximal respiration and spare respiratory capacity of MERRF iNs, two of the most important parameters of mitochondrial respiration.

This increment in the values of mitochondrial respiration parameters can be associated to an enhanced ETC. In fact, a correlation between CoQ concentration and mitochondrial respiratory rate has been reported, since physiological CoQ concentrations do not saturate the MRC[721]. Therefore, GuttaQ supplementation of MERRF iNs cultures was expected to induce an increase of mitochondrial respiration. Moreover, ROS accumulation in MERRF iNs suggests a MRC disruption and a leak of electrons that generates superoxide anion with the interaction with O_2[551]. We hypothesize that GuttaQ treatment acts as an "electron clamp" and enhances the electron transport between complexes I/II and III. This could explain the increased spare respiratory capacity and maximal respiration after GuttaQ treatment. On the other hand, the production of ROS in MERRF iNs could also be reduced by GuttaQ supplementation.

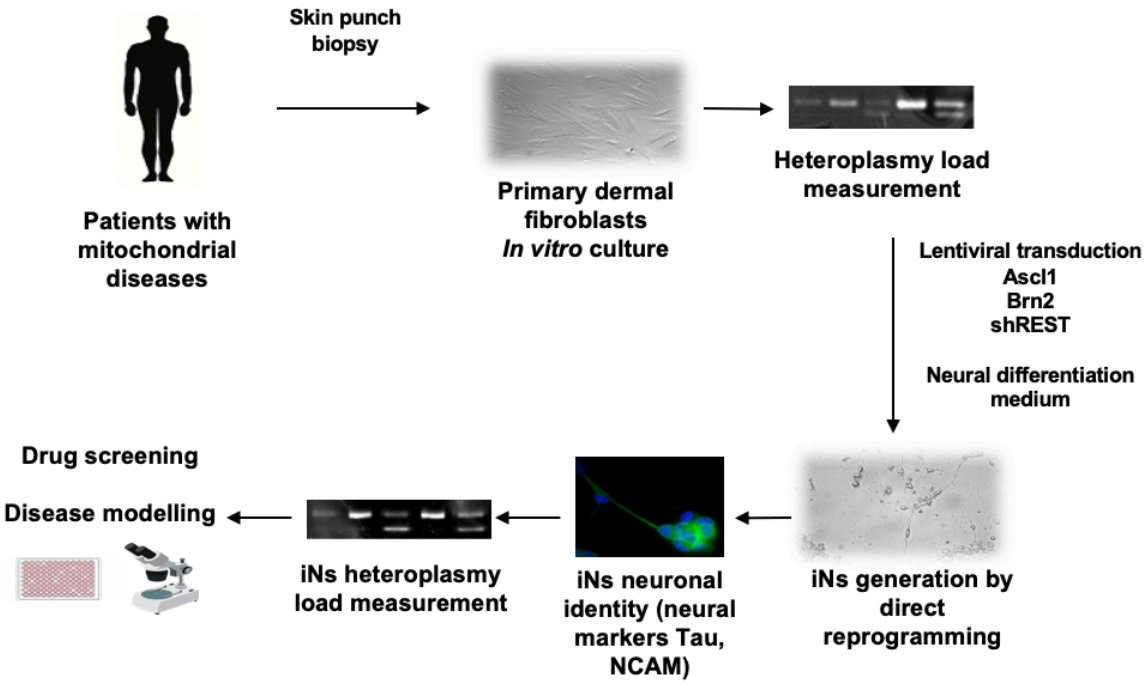

Figure D2. Experimental design for the generation of iNs from patient-derived dermal fibroblasts, molecular characterization and applications for disease modelling of mtDNA mutations.

In conclusion, patient-specific iNs generated from dermal fibroblasts by direct reprogramming can be used as a new cellular model to elucidate the mechanisms underlying MERRF syndrome. Moreover, patient-derived iNs can be used for testing the impact of a specific mtDNA mutation on neurons and to screen for drugs that correct the phenotype. Accordingly, we propose an experimental design (**Figure D2**) for the use of iNs as a new cellular model for the study of heteroplasmic mitochondrial diseases that can be used as a novel screening platform for potential treatments.

CONCLUSIONS

CONCLUSIONS

1. MERRF patient-derived skin fibroblasts and MERRF cybrids show disrupted autophagy flux.

2. MERRF patient-derived skin fibroblasts and MERRF cybrids show disrupted Parkin-mediated mitophagy.

3. Parkin-mediated mitophagy acts a cell survival mechanism in MERRF cybrids cell model.

4. Coenzyme Q_{10} acts as an enhancer of autophagy/mitophagy flux, improving cell pathophysiology.

5. Rapamycin, as an enhancer of autophagy flux, improves the mitochondrial function of both MERRF fibroblasts and cybrid cells models, with a sustainable effect.

6. Using direct reprogramming techniques, MERRF patient-derived fibroblasts can be successfully converted into induced neurons which show indicators of neuronal maturation.

7. MERRF iNs harbouring the m.8344A>G mutation show mitochondrial dysfunction and elevated ROS levels. Moreover, MERRF-derived iNs contain a fragmented mitochondrial network, autophagy flux disruption and mitophagy activation.

8. MERRF iNs constitute a suitable cellular model for the screening of potential treatments for MERRF syndrome or other mitochondrial diseases.

REFERENCES

REFERENCES

1 Schatz, G. The magic garden. *Annu Rev Biochem* **76**, 673-678, doi:10.1146/annurev.biochem.76.060806.091141 (2007).

2 Zimorski, V., Ku, C., Martin, W. F. & Gould, S. B. Endosymbiotic theory for organelle origins. *Curr Opin Microbiol* **22**, 38-48, doi:10.1016/j.mib.2014.09.008 (2014).

3 Margulis, L. & Bermudes, D. Symbiosis as a mechanism of evolution: status of cell symbiosis theory. *Symbiosis* **1**, 101-124 (1985).

4 Scheffler, I. E. in *Mitochondria* (ed I. E. Scheffler) (2007).

5 Alberts, B., Johnson, A., Lewis, J., Raff, M., Roberts, K., & Walter, P. in *Molecular Biology of the Cell* (ed New York: Garland Science) (2002).

6 Rappaport, L., Oliviero, P. & Samuel, J. L. Cytoskeleton and mitochondrial morphology and function. *Mol Cell Biochem* **184**, 101-105 (1998).

7 Vance, J. E. MAM (mitochondria-associated membranes) in mammalian cells: lipids and beyond. *Biochim Biophys Acta* **1841**, 595-609, doi:10.1016/j.bbalip.2013.11.014 (2014).

8 Area-Gomez, E. Assessing the function of mitochondria-associated ER membranes. *Methods Enzymol* **547**, 181-197, doi:10.1016/B978-0-12-801415-8.00011-4 (2014).

9 Ikon, N. & Ryan, R. O. Cardiolipin and mitochondrial cristae organization. *Biochim Biophys Acta Biomembr* **1859**, 1156-1163, doi:10.1016/j.bbamem.2017.03.013 (2017).

10 Truscott, K. N., Pfanner, N. & Voos, W. Transport of proteins into mitochondria. *Rev Physiol Biochem Pharmacol* **143**, 81-136 (2001).

11 Chaban, Y., Boekema, E. J. & Dudkina, N. V. Structures of mitochondrial oxidative phosphorylation supercomplexes and mechanisms for their stabilisation. *Biochim Biophys Acta* **1837**, 418-426, doi:10.1016/j.bbabio.2013.10.004 (2014).

12 Huttemann, M., Lee, I., Samavati, L., Yu, H. & Doan, J. W. Regulation of mitochondrial oxidative phosphorylation through cell signaling. *Biochim Biophys Acta* **1773**, 1701-1720 (2007).

13 Smith, R. A., Hartley, R. C., Cocheme, H. M. & Murphy, M. P. Mitochondrial pharmacology. *Trends Pharmacol Sci* **33**, 341-352, doi:10.1016/j.tips.2012.03.010 (2012).

14 Wallace, D. C., Fan, W. & Procaccio, V. Mitochondrial energetics and therapeutics. *Annu Rev Pathol* **5**, 297-348, doi:10.1146/annurev.pathol.4.110807.092314 (2010).

15 Milenkovic, D., Blaza, J. N., Larsson, N. G. & Hirst, J. The Enigma of the Respiratory Chain Supercomplex. *Cell Metab* **25**, 765-776, doi:10.1016/j.cmet.2017.03.009 (2017).

16 Schwartz, R. M. & Dayhoff, M. O. Origins of prokaryotes, eukaryotes, mitochondria, and chloroplasts. *Science* **199**, 395-403 (1978).

17 Anderson, S. *et al.* Sequence and organization of the human mitochondrial genome. *Nature* **290**, 457-465 (1981).

18 Chomyn, A. *et al.* URF6, last unidentified reading frame of human mtDNA, codes for an NADH dehydrogenase subunit. *Science* **234**, 614-618 (1986).

19 Chomyn, A. *et al.* Six unidentified reading frames of human mitochondrial DNA encode components of the respiratory-chain NADH dehydrogenase. *Nature* **314**, 592-597 (1985).

20 Attardi, G. & Schatz, G. Biogenesis of mitochondria. *Annu Rev Cell Biol* **4**, 289-333, doi:10.1146/annurev.cb.04.110188.001445 (1988).

21 Iborra, F. J., Kimura, H. & Cook, P. R. The functional organization of mitochondrial genomes in human cells. *BMC Biol* **2**, 9, doi:10.1186/1741-7007-2-9 (2004).

22 Wang, Y. & Bogenhagen, D. F. Human mitochondrial DNA nucleoids are linked to protein folding machinery and metabolic enzymes at the mitochondrial inner membrane. *J Biol Chem* **281**, 25791-25802, doi:10.1074/jbc.M604501200 (2006).

23 Gilkerson, R. W., Schon, E. A., Hernandez, E. & Davidson, M. M. Mitochondrial nucleoids maintain genetic autonomy but allow for functional complementation. *J Cell Biol* **181**, 1117-1128, doi:10.1083/jcb.200712101 (2008).

24 Calvo, S. E. & Mootha, V. K. The mitochondrial proteome and human disease. *Annu Rev Genomics Hum Genet* **11**, 25-44, doi:10.1146/annurev-genom-082509-141720 (2010).

25 Brandvain, Y. & Wade, M. J. The functional transfer of genes from the mitochondria to the nucleus: the effects of selection, mutation, population size and

rate of self-fertilization. *Genetics* **182**, 1129-1139, doi:10.1534/genetics.108.100024 (2009).

26 Pon, L. A., Vestweber, D., Yang, M. & Schatz, G. Interaction between mitochondria and the nucleus. *J Cell Sci Suppl* **11**, 1-11 (1989).

27 Diaz, F. & Moraes, C. T. Mitochondrial biogenesis and turnover. *Cell Calcium* **44**, 24-35, doi:10.1016/j.ceca.2007.12.004 (2008).

28 Spremulli, L. L., Coursey, A., Navratil, T. & Hunter, S. E. Initiation and elongation factors in mammalian mitochondrial protein biosynthesis. *Prog Nucleic Acid Res Mol Biol* **77**, 211-261, doi:10.1016/S0079-6603(04)77006-3 (2004).

29 Chang, D. D., Hauswirth, W. W. & Clayton, D. A. Replication priming and transcription initiate from precisely the same site in mouse mitochondrial DNA. *EMBO J* **4**, 1559-1567 (1985).

30 Holt, I. J. & Reyes, A. Human mitochondrial DNA replication. *Cold Spring Harb Perspect Biol* **4**, doi:10.1101/cshperspect.a012971 (2012).

31 Kasamatsu, H. & Vinograd, J. Unidirectionality of replication in mouse mitochondrial DNA. *Nat New Biol* **241**, 103-105 (1973).

32 Holt, I. J., Lorimer, H. E. & Jacobs, H. T. Coupled leading- and lagging-strand synthesis of mammalian mitochondrial DNA. *Cell* **100**, 515-524 (2000).

33 Kmiec, B., Woloszynska, M. & Janska, H. Heteroplasmy as a common state of mitochondrial genetic information in plants and animals. *Curr Genet* **50**, 149-159, doi:10.1007/s00294-006-0082-1 (2006).

34 Guo, Y. *et al.* Very low-level heteroplasmy mtDNA variations are inherited in humans. *J Genet Genomics* **40**, 607-615, doi:10.1016/j.jgg.2013.10.003 (2013).

35 Solignac, M., Monnerot, M. & Mounolou, J. C. Mitochondrial DNA heteroplasmy in Drosophila mauritiana. *Proc Natl Acad Sci U S A* **80**, 6942-6946 (1983).

36 Ye, K., Lu, J., Ma, F., Keinan, A. & Gu, Z. Extensive pathogenicity of mitochondrial heteroplasmy in healthy human individuals. *Proc Natl Acad Sci U S A* **111**, 10654-10659, doi:10.1073/pnas.1403521111 (2014).

37 Nachman, M. W., Brown, W. M., Stoneking, M. & Aquadro, C. F. Nonneutral mitochondrial DNA variation in humans and chimpanzees. *Genetics* **142**, 953-963 (1996).

38 Stewart, J. B. & Larsson, N. G. Keeping mtDNA in shape between generations. *PLoS Genet* **10**, e1004670, doi:10.1371/journal.pgen.1004670 (2014).

39 Lauri, A., Pompilio, G. & Capogrossi, M. C. The mitochondrial genome in aging and senescence. *Ageing Res Rev* **18**, 1-15, doi:10.1016/j.arr.2014.07.001 (2014).

40 Kennedy, S. R., Salk, J. J., Schmitt, M. W. & Loeb, L. A. Ultra-sensitive sequencing reveals an age-related increase in somatic mitochondrial mutations that are inconsistent with oxidative damage. *PLoS Genet* **9**, e1003794, doi:10.1371/journal.pgen.1003794 (2013).

41 Thyagarajan, B., Padua, R. A. & Campbell, C. Mammalian mitochondria possess homologous DNA recombination activity. *J Biol Chem* **271**, 27536-27543 (1996).

42 Kraytsberg, Y. *et al.* Recombination of human mitochondrial DNA. *Science* **304**, 981, doi:10.1126/science.1096342 (2004).

43 Zsurka, G. *et al.* Recombination of mitochondrial DNA in skeletal muscle of individuals with multiple mitochondrial DNA heteroplasmy. *Nat Genet* **37**, 873-877, doi:10.1038/ng1606 (2005).

44 Sato, M. & Sato, K. Maternal inheritance of mitochondrial DNA by diverse mechanisms to eliminate paternal mitochondrial DNA. *Biochim Biophys Acta* **1833**, 1979-1984, doi:10.1016/j.bbamcr.2013.03.010 (2013).

45 Morgan, J. A. *et al.* Hybridisation, paternal leakage and mitochondrial DNA linearization in three anomalous fish (Scombridae). *Mitochondrion* **13**, 852-861, doi:10.1016/j.mito.2013.06.002 (2013).

46 Aksyonova, E. *et al.* Heteroplasmy and paternally oriented shift of the organellar DNA composition in barley-wheat hybrids during backcrosses with wheat parents. *Genome* **48**, 761-769, doi:10.1139/g05-049 (2005).

47 Schwartz, M. & Vissing, J. Paternal inheritance of mitochondrial DNA. *N Engl J Med* **347**, 576-580, doi:10.1056/NEJMoa020350 (2002).

48 Fleming, T. P., Javed, Q. & Hay, M. Epithelial differentiation and intercellular junction formation in the mouse early embryo. *Dev Suppl*, 105-112 (1992).

49 Chinnery, P. F. Modulating heteroplasmy. *Trends Genet* **18**, 173-176 (2002).

50 Hanna, M. G., Nelson, I. P., Morgan-Hughes, J. A. & Harding, A. E. Impaired mitochondrial translation in human myoblasts harbouring the mitochondrial DNA tRNA lysine 8344 A-->G (MERRF) mutation: relationship to proportion of mutant mitochondrial DNA. *J Neurol Sci* **130**, 154-160 (1995).

51 Thorburn, D. R. & Dahl, H. H. Mitochondrial disorders: genetics, counseling, prenatal diagnosis and reproductive options. *Am J Med Genet* **106**, 102-114, doi:10.1002/ajmg.1380 (2001).

52 DiMauro, S. Mitochondrial DNA medicine. *Biosci Rep* **27**, 5-9, doi:10.1007/s10540-007-9032-5 (2007).

53 Wallace, D. C. & Chalkia, D. Mitochondrial DNA genetics and the heteroplasmy conundrum in evolution and disease. *Cold Spring Harb Perspect Biol* **5**, a021220, doi:10.1101/cshperspect.a021220 (2013).

54 Carelli, V. *et al.* Mitochondria: Biogenesis and mitophagy balance in segregation and clonal expansion of mitochondrial DNA mutations. *Int J Biochem Cell Biol* **63**, 21-24, doi:10.1016/j.biocel.2015.01.023 (2015).

55 Fischer, F., Hamann, A. & Osiewacz, H. D. Mitochondrial quality control: an integrated network of pathways. *Trends Biochem Sci* **37**, 284-292, doi:10.1016/j.tibs.2012.02.004 (2012).

56 Cox, A. G., Winterbourn, C. C. & Hampton, M. B. Mitochondrial peroxiredoxin involvement in antioxidant defence and redox signalling. *Biochem J* **425**, 313-325, doi:10.1042/BJ20091541 (2009).

57 Fourquet, S., Huang, M. E., D'Autreaux, B. & Toledano, M. B. The dual functions of thiol-based peroxidases in H2O2 scavenging and signaling. *Antioxid Redox Signal* **10**, 1565-1576, doi:10.1089/ars.2008.2049 (2008).

58 Croteau, D. L., Stierum, R. H. & Bohr, V. A. Mitochondrial DNA repair pathways. *Mutat Res* **434**, 137-148 (1999).

59 Haynes, C. M. & Ron, D. The mitochondrial UPR - protecting organelle protein homeostasis. *J Cell Sci* **123**, 3849-3855, doi:10.1242/jcs.075119 (2010).

60 Ugarte, N., Petropoulos, I. & Friguet, B. Oxidized mitochondrial protein degradation and repair in aging and oxidative stress. *Antioxid Redox Signal* **13**, 539-549, doi:10.1089/ars.2009.2998 (2010).

61 Hamon, M. P., Bulteau, A. L. & Friguet, B. Mitochondrial proteases and protein quality control in ageing and longevity. *Ageing Res Rev* **23**, 56-66, doi:10.1016/j.arr.2014.12.010 (2015).

62 Kotiadis, V. N., Duchen, M. R. & Osellame, L. D. Mitochondrial quality control and communications with the nucleus are important in maintaining mitochondrial function and cell health. *Biochim Biophys Acta* **1840**, 1254-1265, doi:10.1016/j.bbagen.2013.10.041 (2014).

63 Bayot, A. *et al.* Identification of novel oxidized protein substrates and physiological partners of the mitochondrial ATP-dependent Lon-like protease Pim1. *J Biol Chem* **285**, 11445-11457, doi:10.1074/jbc.M109.065425 (2010).

64 Wohlever, M. L., Baker, T. A. & Sauer, R. T. Roles of the N domain of the AAA+ Lon protease in substrate recognition, allosteric regulation and chaperone activity. *Mol Microbiol* **91**, 66-78, doi:10.1111/mmi.12444 (2014).

65 Levine, B. & Kroemer, G. Autophagy in the pathogenesis of disease. *Cell* **132**, 27-42, doi:10.1016/j.cell.2007.12.018 (2008).

66 Goldman, S. J., Taylor, R., Zhang, Y. & Jin, S. Autophagy and the degradation of mitochondria. *Mitochondrion* **10**, 309-315, doi:10.1016/j.mito.2010.01.005 (2010).

67 Galluzzi, L., Pietrocola, F., Levine, B. & Kroemer, G. Metabolic control of autophagy. *Cell* **159**, 1263-1276, doi:10.1016/j.cell.2014.11.006 (2014).

68 Li, W. W., Li, J. & Bao, J. K. Microautophagy: lesser-known self-eating. *Cell Mol Life Sci* **69**, 1125-1136, doi:10.1007/s00018-011-0865-5 (2012).

69 Cuervo, A. M. & Wong, E. Chaperone-mediated autophagy: roles in disease and aging. *Cell Res* **24**, 92-104, doi:10.1038/cr.2013.153 (2014).

70 Tsukada, M. & Ohsumi, Y. Isolation and characterization of autophagy-defective mutants of Saccharomyces cerevisiae. *FEBS Lett* **333**, 169-174 (1993).

71 Klionsky, D. J. *et al.* A unified nomenclature for yeast autophagy-related genes. *Dev Cell* **5**, 539-545 (2003).

72 Ravikumar, B. *et al.* Mammalian macroautophagy at a glance. *J Cell Sci* **122**, 1707-1711, doi:10.1242/jcs.031773 (2009).

73 Villanueva-Paz, M. *et al.* AMPK Regulation of Cell Growth, Apoptosis, Autophagy, and Bioenergetics. *EXS* **107**, 45-71, doi:10.1007/978-3-319-43589-3_3 (2016).

74 Green, D. R., Galluzzi, L. & Kroemer, G. Cell biology. Metabolic control of cell death. *Science* **345**, 1250256, doi:10.1126/science.1250256 (2014).

75 Yeh, L. A., Lee, K. H. & Kim, K. H. Regulation of rat liver acetyl-CoA carboxylase. Regulation of phosphorylation and inactivation of acetyl-CoA carboxylase by the adenylate energy charge. *J Biol Chem* **255**, 2308-2314 (1980).

76 Hardie, D. G. AMP-activated/SNF1 protein kinases: conserved guardians of cellular energy. *Nat Rev Mol Cell Biol* **8**, 774-785, doi:10.1038/nrm2249 (2007).

77 Mungai, P. T. *et al.* Hypoxia triggers AMPK activation through reactive oxygen species-mediated activation of calcium release-activated calcium channels. *Mol Cell Biol* **31**, 3531-3545, doi:10.1128/MCB.05124-11 (2011).

78 Emerling, B. M. *et al.* Hypoxic activation of AMPK is dependent on mitochondrial ROS but independent of an increase in AMP/ATP ratio. *Free Radic Biol Med* **46**, 1386-1391, doi:10.1016/j.freeradbiomed.2009.02.019 (2009).

79 Hwang, J. T. *et al.* AMP-activated protein kinase activity is required for vanadate-induced hypoxia-inducible factor 1alpha expression in DU145 cells. *Carcinogenesis* **25**, 2497-2507, doi:10.1093/carcin/bgh253 (2004).

80 Woods, A. *et al.* Ca2+/calmodulin-dependent protein kinase kinase-beta acts upstream of AMP-activated protein kinase in mammalian cells. *Cell Metab* **2**, 21-33, doi:10.1016/j.cmet.2005.06.005 (2005).

81 Hoyer-Hansen, M. *et al.* Control of macroautophagy by calcium, calmodulin-dependent kinase kinase-beta, and Bcl-2. *Mol Cell* **25**, 193-205, doi:10.1016/j.molcel.2006.12.009 (2007).

82 Hawley, S. A. *et al.* Calmodulin-dependent protein kinase kinase-beta is an alternative upstream kinase for AMP-activated protein kinase. *Cell Metab* **2**, 9-19, doi:10.1016/j.cmet.2005.05.009 (2005).

83 Jung, C. H. *et al.* ULK-Atg13-FIP200 complexes mediate mTOR signaling to the autophagy machinery. *Mol Biol Cell* **20**, 1992-2003, doi:10.1091/mbc.E08-12-1249 (2009).

84 Hosokawa, N. *et al.* Nutrient-dependent mTORC1 association with the ULK1-Atg13-FIP200 complex required for autophagy. *Mol Biol Cell* **20**, 1981-1991, doi:10.1091/mbc.E08-12-1248 (2009).

85 Wong, P. M., Puente, C., Ganley, I. G. & Jiang, X. The ULK1 complex: sensing nutrient signals for autophagy activation. *Autophagy* **9**, 124-137, doi:10.4161/auto.23323 (2013).

86 Kuroyanagi, H. *et al.* Human ULK1, a novel serine/threonine kinase related to UNC-51 kinase of Caenorhabditis elegans: cDNA cloning, expression, and chromosomal assignment. *Genomics* **51**, 76-85 (1998).

87 Chan, E. Y., Kir, S. & Tooze, S. A. siRNA screening of the kinome identifies ULK1 as a multidomain modulator of autophagy. *J Biol Chem* **282**, 25464-25474, doi:10.1074/jbc.M703663200 (2007).

88 Shang, L. & Wang, X. AMPK and mTOR coordinate the regulation of Ulk1 and mammalian autophagy initiation. *Autophagy* **7**, 924-926 (2011).

89 Villanueva Paz, M. *et al.* Targeting autophagy and mitophagy for mitochondrial diseases treatment. *Expert Opin Ther Targets* **20**, 487-500, doi:10.1517/14728222.2016.1101068 (2016).

90 Gwinn, D. M. *et al.* AMPK phosphorylation of raptor mediates a metabolic checkpoint. *Mol Cell* **30**, 214-226, doi:10.1016/j.molcel.2008.03.003 (2008).

91 Inoki, K., Zhu, T. & Guan, K. L. TSC2 mediates cellular energy response to control cell growth and survival. *Cell* **115**, 577-590 (2003).

92 Inoki, K., Li, Y., Zhu, T., Wu, J. & Guan, K. L. TSC2 is phosphorylated and inhibited by Akt and suppresses mTOR signalling. *Nat Cell Biol* **4**, 648-657, doi:10.1038/ncb839 (2002).

93 Egan, D. F. *et al.* Phosphorylation of ULK1 (hATG1) by AMP-activated protein kinase connects energy sensing to mitophagy. *Science* **331**, 456-461, doi:10.1126/science.1196371 (2011).

94 Kim, J., Kundu, M., Viollet, B. & Guan, K. L. AMPK and mTOR regulate autophagy through direct phosphorylation of Ulk1. *Nat Cell Biol* **13**, 132-141, doi:10.1038/ncb2152 (2011).

95 Alers, S., Loffler, A. S., Wesselborg, S. & Stork, B. Role of AMPK-mTOR-Ulk1/2 in the regulation of autophagy: cross talk, shortcuts, and feedbacks. *Mol Cell Biol* **32**, 2-11, doi:10.1128/MCB.06159-11 (2012).

96 Egan, D., Kim, J., Shaw, R. J. & Guan, K. L. The autophagy initiating kinase ULK1 is regulated via opposing phosphorylation by AMPK and mTOR. *Autophagy* **7**, 643-644 (2011).

97 Johansen, T. & Lamark, T. Selective autophagy mediated by autophagic adapter proteins. *Autophagy* **7**, 279-296 (2011).

98 Lemasters, J. J. Selective mitochondrial autophagy, or mitophagy, as a targeted defense against oxidative stress, mitochondrial dysfunction, and aging. *Rejuvenation Res* **8**, 3-5, doi:10.1089/rej.2005.8.3 (2005).

99 Liu, K. & Czaja, M. J. Regulation of lipid stores and metabolism by lipophagy. *Cell Death Differ* **20**, 3-11, doi:10.1038/cdd.2012.63 (2013).

100 Till, A., Lakhani, R., Burnett, S. F. & Subramani, S. Pexophagy: the selective degradation of peroxisomes. *Int J Cell Biol* **2012**, 512721, doi:10.1155/2012/512721 (2012).

101 Debnath, J., Baehrecke, E. H. & Kroemer, G. Does autophagy contribute to cell death? *Autophagy* **1**, 66-74 (2005).

102 Lambert, A. J. & Brand, M. D. Reactive oxygen species production by mitochondria. *Methods Mol Biol* **554**, 165-181, doi:10.1007/978-1-59745-521-3_11 (2009).

103 Lemasters, J. J., Theruvath, T. P., Zhong, Z. & Nieminen, A. L. Mitochondrial calcium and the permeability transition in cell death. *Biochim Biophys Acta* **1787**, 1395-1401, doi:10.1016/j.bbabio.2009.06.009 (2009).

104 Kim, I., Rodriguez-Enriquez, S. & Lemasters, J. J. Selective degradation of mitochondria by mitophagy. *Arch Biochem Biophys* **462**, 245-253, doi:10.1016/j.abb.2007.03.034 (2007).

105 Wang, Y., Nartiss, Y., Steipe, B., McQuibban, G. A. & Kim, P. K. ROS-induced mitochondrial depolarization initiates PARK2/PARKIN-dependent mitochondrial degradation by autophagy. *Autophagy* **8**, 1462-1476, doi:10.4161/auto.21211 (2012).

106 Geisler, S. *et al.* PINK1/Parkin-mediated mitophagy is dependent on VDAC1 and p62/SQSTM1. *Nat Cell Biol* **12**, 119-131, doi:10.1038/ncb2012 (2010).

107 Wirth, M., Joachim, J. & Tooze, S. A. Autophagosome formation--the role of ULK1 and Beclin1-PI3KC3 complexes in setting the stage. *Semin Cancer Biol* **23**, 301-309, doi:10.1016/j.semcancer.2013.05.007 (2013).

108 Mizushima, N. The role of the Atg1/ULK1 complex in autophagy regulation. *Curr Opin Cell Biol* **22**, 132-139, doi:10.1016/j.ceb.2009.12.004 (2010).

109 Itakura, E., Kishi-Itakura, C., Koyama-Honda, I. & Mizushima, N. Structures containing Atg9A and the ULK1 complex independently target depolarized mitochondria at initial stages of Parkin-mediated mitophagy. *J Cell Sci* **125**, 1488-1499, doi:10.1242/jcs.094110 (2012).

110 Kundu, M. *et al.* Ulk1 plays a critical role in the autophagic clearance of mitochondria and ribosomes during reticulocyte maturation. *Blood* **112**, 1493-1502, doi:10.1182/blood-2008-02-137398 (2008).

111 Wu, W. *et al.* ULK1 translocates to mitochondria and phosphorylates FUNDC1 to regulate mitophagy. *EMBO Rep* **15**, 566-575, doi:10.1002/embr.201438501 (2014).

112 Tian, W. *et al.* Phosphorylation of ULK1 by AMPK regulates translocation of ULK1 to mitochondria and mitophagy. *FEBS Lett* **589**, 1847-1854, doi:10.1016/j.febslet.2015.05.020 (2015).

113 Kanki, T. & Klionsky, D. J. Mitophagy in yeast occurs through a selective mechanism. *J Biol Chem* **283**, 32386-32393, doi:10.1074/jbc.M802403200 (2008).

114 Kanki, T. & Klionsky, D. J. The molecular mechanism of mitochondria autophagy in yeast. *Mol Microbiol* **75**, 795-800, doi:10.1111/j.1365-2958.2009.07035.x (2010).

115 Kanki, T., Wang, K., Cao, Y., Baba, M. & Klionsky, D. J. Atg32 is a mitochondrial protein that confers selectivity during mitophagy. *Dev Cell* **17**, 98-109, doi:10.1016/j.devcel.2009.06.014 (2009).

116 Okamoto, K., Kondo-Okamoto, N. & Ohsumi, Y. Mitochondria-anchored receptor Atg32 mediates degradation of mitochondria via selective autophagy. *Dev Cell* **17**, 87-97, doi:10.1016/j.devcel.2009.06.013 (2009).

117 Scherz-Shouval, R. *et al.* Reactive oxygen species are essential for autophagy and specifically regulate the activity of Atg4. *EMBO J* **26**, 1749-1760, doi:10.1038/sj.emboj.7601623 (2007).

118 Kelekar, A. Autophagy. *Ann N Y Acad Sci* **1066**, 259-271, doi:10.1196/annals.1363.015 (2005).

119 Mizushima, N., Ohsumi, Y. & Yoshimori, T. Autophagosome formation in mammalian cells. *Cell Struct Funct* **27**, 421-429 (2002).

120 Axe, E. L. *et al.* Autophagosome formation from membrane compartments enriched in phosphatidylinositol 3-phosphate and dynamically connected to the endoplasmic reticulum. *J Cell Biol* **182**, 685-701, doi:10.1083/jcb.200803137 (2008).

121 Hailey, D. W. *et al.* Mitochondria supply membranes for autophagosome biogenesis during starvation. *Cell* **141**, 656-667, doi:10.1016/j.cell.2010.04.009 (2010).

122 Ravikumar, B., Moreau, K., Jahreiss, L., Puri, C. & Rubinsztein, D. C. Plasma membrane contributes to the formation of pre-autophagosomal structures. *Nat Cell Biol* **12**, 747-757, doi:10.1038/ncb2078 (2010).

123 Rubinsztein, D. C., Shpilka, T. & Elazar, Z. Mechanisms of autophagosome biogenesis. *Curr Biol* **22**, R29-34, doi:10.1016/j.cub.2011.11.034 (2012).

124 Loos, B., du Toit, A. & Hofmeyr, J. H. Defining and measuring autophagosome flux-concept and reality. *Autophagy* **10**, 2087-2096, doi:10.4161/15548627.2014.973338 (2014).

125 Zhang, X. J., Chen, S., Huang, K. X. & Le, W. D. Why should autophagic flux be assessed? *Acta Pharmacol Sin* **34**, 595-599, doi:10.1038/aps.2012.184 (2013).

126 Klionsky, D. J. Guidelines for the use and interpretation of assays for monitoring autophagy (3rd edition). *Autophagy* **12**, 1-222, doi:10.1080/15548627.2015.1100356 (2016).

127 Yamamoto, A. *et al.* Bafilomycin A1 prevents maturation of autophagic vacuoles by inhibiting fusion between autophagosomes and lysosomes in rat hepatoma cell line, H-4-II-E cells. *Cell Struct Funct* **23**, 33-42 (1998).

128 Mauro-Lizcano, M. *et al.* New method to assess mitophagy flux by flow cytometry. *Autophagy* **11**, 833-843, doi:10.1080/15548627.2015.1034403 (2015).

129 García-Prat, L., Martínez-Vicente, M. & Muñoz-Cánoves, P. Methods for Mitochondria and Mitophagy Flux Analyses in Stem Cells of Resting and Regenerating Skeletal Muscle. **1460**, 223-240, doi:10.1007/978-1-4939-3810-0_16 (2016).

130 Youle, R. J. & Narendra, D. P. Mechanisms of mitophagy. *Nat Rev Mol Cell Biol* **12**, 9-14, doi:10.1038/nrm3028 (2011).

131 Novak, I. *et al.* Nix is a selective autophagy receptor for mitochondrial clearance. *EMBO Rep* **11**, 45-51, doi:10.1038/embor.2009.256 (2010).

132 Sandoval, H. *et al.* Essential role for Nix in autophagic maturation of erythroid cells. *Nature* **454**, 232-235, doi:10.1038/nature07006 (2008).

133 Allen, G. F., Toth, R., James, J. & Ganley, I. G. Loss of iron triggers PINK1/Parkin-independent mitophagy. *EMBO Rep* **14**, 1127-1135, doi:10.1038/embor.2013.168 (2013).

134 Narendra, D., Tanaka, A., Suen, D. F. & Youle, R. J. Parkin is recruited selectively to impaired mitochondria and promotes their autophagy. *J Cell Biol* **183**, 795-803, doi:10.1083/jcb.200809125 (2008).

135 Springer, W. & Kahle, P. J. Regulation of PINK1-Parkin-mediated mitophagy. *Autophagy* **7**, 266-278 (2011).

136 Deas, E. *et al.* PINK1 cleavage at position A103 by the mitochondrial protease PARL. *Hum Mol Genet* **20**, 867-879, doi:10.1093/hmg/ddq526 (2011).

137 Greene, A. W. *et al.* Mitochondrial processing peptidase regulates PINK1 processing, import and Parkin recruitment. *EMBO Rep* **13**, 378-385, doi:10.1038/embor.2012.14 (2012).

138 Meissner, C., Lorenz, H., Weihofen, A., Selkoe, D. J. & Lemberg, M. K. The mitochondrial intramembrane protease PARL cleaves human Pink1 to regulate Pink1 trafficking. *J Neurochem* **117**, 856-867, doi:10.1111/j.1471-4159.2011.07253.x (2011).

139 Matsuda, N. *et al.* PINK1 stabilized by mitochondrial depolarization recruits Parkin to damaged mitochondria and activates latent Parkin for mitophagy. *J Cell Biol* **189**, 211-221, doi:10.1083/jcb.200910140 (2010).

140 Kondapalli, C. *et al.* PINK1 is activated by mitochondrial membrane potential depolarization and stimulates Parkin E3 ligase activity by phosphorylating Serine 65. *Open Biol* **2**, 120080, doi:10.1098/rsob.120080 (2012).

141 Okatsu, K. *et al.* PINK1 autophosphorylation upon membrane potential dissipation is essential for Parkin recruitment to damaged mitochondria. *Nat Commun* **3**, 1016, doi:10.1038/ncomms2016 (2012).

142 Caulfield, T. R. *et al.* Phosphorylation by PINK1 releases the UBL domain and initializes the conformational opening of the E3 ubiquitin ligase Parkin. *PLoS Comput Biol* **10**, e1003935, doi:10.1371/journal.pcbi.1003935 (2014).

143 Kazlauskaite, A. *et al.* Phosphorylation of Parkin at Serine65 is essential for activation: elaboration of a Miro1 substrate-based assay of Parkin E3 ligase activity. *Open Biol* **4**, 130213, doi:10.1098/rsob.130213 (2014).

144 Kazlauskaite, A. *et al.* Parkin is activated by PINK1-dependent phosphorylation of ubiquitin at Ser65. *Biochem J* **460**, 127-139, doi:10.1042/BJ20140334 (2014).

145 Kazlauskaite, A. *et al.* Binding to serine 65-phosphorylated ubiquitin primes Parkin for optimal PINK1-dependent phosphorylation and activation. *EMBO Rep* **16**, 939-954, doi:10.15252/embr.201540352 (2015).

146 Sarraf, S. A. *et al.* Landscape of the PARKIN-dependent ubiquitylome in response to mitochondrial depolarization. *Nature* **496**, 372-376, doi:10.1038/nature12043 (2013).

147 Kirkin, V. *et al.* A role for NBR1 in autophagosomal degradation of ubiquitinated substrates. *Mol Cell* **33**, 505-516, doi:10.1016/j.molcel.2009.01.020 (2009).

148 Gegg, M. E. *et al.* Mitofusin 1 and mitofusin 2 are ubiquitinated in a PINK1/parkin-dependent manner upon induction of mitophagy. *Hum Mol Genet* **19**, 4861-4870, doi:10.1093/hmg/ddq419 (2010).

149 Twig, G. *et al.* Fission and selective fusion govern mitochondrial segregation and elimination by autophagy. *EMBO J* **27**, 433-446, doi:10.1038/sj.emboj.7601963 (2008).

150 Twig, G. & Shirihai, O. S. The interplay between mitochondrial dynamics and mitophagy. *Antioxid Redox Signal* **14**, 1939-1951, doi:10.1089/ars.2010.3779 (2011).

151 Youle, R. J. & van der Bliek, A. M. Mitochondrial fission, fusion, and stress. *Science* **337**, 1062-1065, doi:10.1126/science.1219855 (2012).

152 Suen, D. F., Norris, K. L. & Youle, R. J. Mitochondrial dynamics and apoptosis. *Genes Dev* **22**, 1577-1590, doi:10.1101/gad.1658508 (2008).

153 Amchenkova, A. A., Bakeeva, L. E., Chentsov, Y. S., Skulachev, V. P. & Zorov, D. B. Coupling membranes as energy-transmitting cables. I. Filamentous mitochondria in fibroblasts and mitochondrial clusters in cardiomyocytes. *J Cell Biol* **107**, 481-495 (1988).

154 Chen, H. *et al.* Mitofusins Mfn1 and Mfn2 coordinately regulate mitochondrial fusion and are essential for embryonic development. *J Cell Biol* **160**, 189-200, doi:10.1083/jcb.200211046 (2003).

155 Ni, H. M., Williams, J. A. & Ding, W. X. Mitochondrial dynamics and mitochondrial quality control. *Redox Biol* **4**, 6-13, doi:10.1016/j.redox.2014.11.006 (2015).

156 Zuchner, S. *et al.* Mutations in the mitochondrial GTPase mitofusin 2 cause Charcot-Marie-Tooth neuropathy type 2A. *Nat Genet* **36**, 449-451, doi:10.1038/ng1341 (2004).

157 Gomes, L. C. & Scorrano, L. High levels of Fis1, a pro-fission mitochondrial protein, trigger autophagy. *Biochim Biophys Acta* **1777**, 860-866, doi:10.1016/j.bbabio.2008.05.442 (2008).

158 Ding, W. X. & Yin, X. M. Mitophagy: mechanisms, pathophysiological roles, and analysis. *Biol Chem* **393**, 547-564, doi:10.1515/hsz-2012-0119 (2012).

159 Hollenbeck, P. J. & Saxton, W. M. The axonal transport of mitochondria. *J Cell Sci* **118**, 5411-5419, doi:10.1242/jcs.02745 (2005).

160 Liu, S. *et al.* Parkinson's disease-associated kinase PINK1 regulates Miro protein level and axonal transport of mitochondria. *PLoS Genet* **8**, e1002537, doi:10.1371/journal.pgen.1002537 (2012).

161 Wang, X. *et al.* PINK1 and Parkin target Miro for phosphorylation and degradation to arrest mitochondrial motility. *Cell* **147**, 893-906, doi:10.1016/j.cell.2011.10.018 (2011).

162 Crouser, E. D., Julian, M. W., Huff, J. E., Struck, J. & Cook, C. H. Carbamoyl phosphate synthase-1: a marker of mitochondrial damage and depletion in the liver during sepsis. *Crit Care Med* **34**, 2439-2446, doi:10.1097/01.CCM.0000230240.02216.21 (2006).

163 Rasbach, K. A. & Schnellmann, R. G. Signaling of mitochondrial biogenesis following oxidant injury. *J Biol Chem* **282**, 2355-2362, doi:10.1074/jbc.M608009200 (2007).

164 Hardie, D. G., Ross, F. A. & Hawley, S. A. AMPK: a nutrient and energy sensor that maintains energy homeostasis. *Nat Rev Mol Cell Biol* **13**, 251-262, doi:10.1038/nrm3311 (2012).

165 Jager, S., Handschin, C., St-Pierre, J. & Spiegelman, B. M. AMP-activated protein kinase (AMPK) action in skeletal muscle via direct phosphorylation of PGC-1alpha. *Proc Natl Acad Sci U S A* **104**, 12017-12022, doi:10.1073/pnas.0705070104 (2007).

166 Canto, C. *et al.* AMPK regulates energy expenditure by modulating NAD+ metabolism and SIRT1 activity. *Nature* **458**, 1056-1060, doi:10.1038/nature07813 (2009).

167 Palikaras, K. & Tavernarakis, N. Mitochondrial homeostasis: the interplay between mitophagy and mitochondrial biogenesis. *Exp Gerontol* **56**, 182-188, doi:10.1016/j.exger.2014.01.021 (2014).

168 Zhang, H. *et al.* Mitochondrial autophagy is an HIF-1-dependent adaptive metabolic response to hypoxia. *J Biol Chem* **283**, 10892-10903, doi:10.1074/jbc.M800102200 (2008).

169 Bellot, G. *et al.* Hypoxia-induced autophagy is mediated through hypoxia-inducible factor induction of BNIP3 and BNIP3L via their BH3 domains. *Mol Cell Biol* **29**, 2570-2581, doi:10.1128/MCB.00166-09 (2009).

170 Liu, L. *et al.* Mitochondrial outer-membrane protein FUNDC1 mediates hypoxia-induced mitophagy in mammalian cells. *Nat Cell Biol* **14**, 177-185, doi:10.1038/ncb2422 (2012).

171 Orvedahl, A. *et al.* Image-based genome-wide siRNA screen identifies selective autophagy factors. *Nature* **480**, 113-117, doi:10.1038/nature10546 (2011).

172 Lokireddy, S. *et al.* The ubiquitin ligase Mul1 induces mitophagy in skeletal muscle in response to muscle-wasting stimuli. *Cell Metab* **16**, 613-624, doi:10.1016/j.cmet.2012.10.005 (2012).

173 Ren, M., Phoon, C. K. & Schlame, M. Metabolism and function of mitochondrial cardiolipin. *Prog Lipid Res* **55**, 1-16, doi:10.1016/j.plipres.2014.04.001 (2014).

174 Ding, W. X. *et al.* Electron microscopic analysis of a spherical mitochondrial structure. *J Biol Chem* **287**, 42373-42378, doi:10.1074/jbc.M112.413674 (2012).

175 Ding, W. X. *et al.* Parkin and mitofusins reciprocally regulate mitophagy and mitochondrial spheroid formation. *J Biol Chem* **287**, 42379-42388, doi:10.1074/jbc.M112.413682 (2012).

176 Schaefer, A. M., Taylor, R. W., Turnbull, D. M. & Chinnery, P. F. The epidemiology of mitochondrial disorders--past, present and future. *Biochim Biophys Acta* **1659**, 115-120, doi:10.1016/j.bbabio.2004.09.005 (2004).

177 Bauer, M. F. *et al.* Mitochondrial disorders. A diagnostic challenge in clinical chemistry. *Clin Chem Lab Med* **37**, 855-876, doi:10.1515/CCLM.1999.129 (1999).

178 Wallace, D. C. Mitochondrial diseases in man and mouse. *Science* **283**, 1482-1488 (1999).

179 Davis, R. L., Liang, C. & Sue, C. M. Mitochondrial diseases. *Handb Clin Neurol* **147**, 125-141, doi:10.1016/B978-0-444-63233-3.00010-5 (2018).

180 Sproule, D. M. & Kaufmann, P. Mitochondrial encephalopathy, lactic acidosis, and strokelike episodes: basic concepts, clinical phenotype, and therapeutic management of MELAS syndrome. *Ann N Y Acad Sci* **1142**, 133-158, doi:10.1196/annals.1444.011 (2008).

181 Vasta, V., Merritt, J. L., 2nd, Saneto, R. P. & Hahn, S. H. Next-generation sequencing for mitochondrial diseases: a wide diagnostic spectrum. *Pediatr Int* **54**, 585-601, doi:10.1111/j.1442-200X.2012.03644.x (2012).

182 Taylor, R. W. *et al.* Use of whole-exome sequencing to determine the genetic basis of multiple mitochondrial respiratory chain complex deficiencies. *JAMA* **312**, 68-77, doi:10.1001/jama.2014.7184 (2014).

183 Carroll, C. J., Brilhante, V. & Suomalainen, A. Next-generation sequencing for mitochondrial disorders. *Br J Pharmacol* **171**, 1837-1853, doi:10.1111/bph.12469 (2014).

184 Angelini, C., Bello, L., Spinazzi, M. & Ferrati, C. Mitochondrial disorders of the nuclear genome. *Acta Myol* **28**, 16-23 (2009).

185 Lightowlers, R. N., Taylor, R. W. & Turnbull, D. M. Mutations causing mitochondrial disease: What is new and what challenges remain? *Science* **349**, 1494-1499, doi:10.1126/science.aac7516 (2015).

186 Tuppen, H. A., Blakely, E. L., Turnbull, D. M. & Taylor, R. W. Mitochondrial DNA mutations and human disease. *Biochim Biophys Acta* **1797**, 113-128, doi:10.1016/j.bbabio.2009.09.005 (2010).

187 Shoffner, J. M. *et al.* Myoclonic epilepsy and ragged-red fiber disease (MERRF) is associated with a mitochondrial DNA tRNA(Lys) mutation. *Cell* **61**, 931-937 (1990).

188 Goto, Y., Nonaka, I. & Horai, S. A mutation in the tRNA(Leu)(UUR) gene associated with the MELAS subgroup of mitochondrial encephalomyopathies. *Nature* **348**, 651-653, doi:10.1038/348651a0 (1990).

189 Howell, N. *et al.* Leber hereditary optic neuropathy: identification of the same mitochondrial ND1 mutation in six pedigrees. *Am J Hum Genet* **49**, 939-950 (1991).

190 Holt, I. J., Harding, A. E., Petty, R. K. & Morgan-Hughes, J. A. A new mitochondrial disease associated with mitochondrial DNA heteroplasmy. *Am J Hum Genet* **46**, 428-433 (1990).

191 Zeviani, M. *et al.* Deletions of mitochondrial DNA in Kearns-Sayre syndrome. *Neurology* **38**, 1339-1346 (1988).

192 Rotig, A. *et al.* Pearson's marrow-pancreas syndrome. A multisystem mitochondrial disorder in infancy. *J Clin Invest* **86**, 1601-1608, doi:10.1172/JCI114881 (1990).

193 Ruiz-Pesini, E. *et al.* An enhanced MITOMAP with a global mtDNA mutational phylogeny. *Nucleic Acids Res* **35**, D823-828, doi:10.1093/nar/gkl927 (2007).

194 Finsterer, J. Genetic, pathogenetic, and phenotypic implications of the mitochondrial A3243G tRNALeu(UUR) mutation. *Acta Neurol Scand* **116**, 1-14, doi:10.1111/j.1600-0404.2007.00836.x (2007).

195 Park, C. B. & Larsson, N. G. Mitochondrial DNA mutations in disease and aging. *J Cell Biol* **193**, 809-818, doi:10.1083/jcb.201010024 (2011).

196 Chinnery, P. F., Howell, N., Lightowlers, R. N. & Turnbull, D. M. Molecular pathology of MELAS and MERRF. The relationship between mutation load and clinical phenotypes. *Brain* **120 (Pt 10)**, 1713-1721 (1997).

197 Hofmann., S. & Bauer., M. F. in *eLS* (2006).

198 Taylor, R. W. & Turnbull, D. M. Mitochondrial DNA mutations in human disease. *Nat Rev Genet* **6**, 389-402, doi:10.1038/nrg1606 (2005).

199 DiMauro, S. & Hirano, M. Pathogenesis and treatment of mitochondrial disorders. *Adv Exp Med Biol* **652**, 139-170, doi:10.1007/978-90-481-2813-6_10 (2009).

200 Shepherd, R. K. *et al.* Measurement of ATP production in mitochondrial disorders. *J Inherit Metab Dis* **29**, 86-91, doi:10.1007/s10545-006-0148-8 (2006).

201 Tyynismaa, H. *et al.* Mutant mitochondrial helicase Twinkle causes multiple mtDNA deletions and a late-onset mitochondrial disease in mice. *Proc Natl Acad Sci U S A* **102**, 17687-17692, doi:10.1073/pnas.0505551102 (2005).

202 Yuan, J. H. *et al.* Mitochondrial myopathy with autophagic vacuoles in patients with the m.8344A>G mutation. *J Clin Pathol* **66**, 659-664, doi:10.1136/jclinpath-2012-201431 (2013).

203 Moran, M. *et al.* Bulk autophagy, but not mitophagy, is increased in cellular model of mitochondrial disease. *Biochim Biophys Acta* **1842**, 1059-1070, doi:10.1016/j.bbadis.2014.03.013 (2014).

204 Cotan, D. *et al.* Secondary coenzyme Q10 deficiency triggers mitochondria degradation by mitophagy in MELAS fibroblasts. *FASEB J* **25**, 2669-2687, doi:10.1096/fj.10-165340 (2011).

205 Jing, C. H. *et al.* Autophagy activation is associated with neuroprotection against apoptosis via a mitochondrial pathway in a rat model of subarachnoid hemorrhage. *Neuroscience* **213**, 144-153, doi:10.1016/j.neuroscience.2012.03.055 (2012).

206 Zhang, Y. *et al.* Endothelial PINK1 mediates the protective effects of NLRP3 deficiency during lethal oxidant injury. *J Immunol* **192**, 5296-5304, doi:10.4049/jimmunol.1400653 (2014).

207 Merenlender-Wagner, A. *et al.* New horizons in schizophrenia treatment: autophagy protection is coupled with behavioral improvements in a mouse model of schizophrenia. *Autophagy* **10**, 2324-2332, doi:10.4161/15548627.2014.984274 (2014).

208 Chen, N. & Debnath, J. Autophagy and tumorigenesis. *FEBS Lett* **584**, 1427-1435, doi:10.1016/j.febslet.2009.12.034 (2010).

209 Ryter, S. W. & Choi, A. M. Autophagy in lung disease pathogenesis and therapeutics. *Redox Biol* **4**, 215-225, doi:10.1016/j.redox.2014.12.010 (2015).

210 Peng, M. *et al.* Inhibiting cytosolic translation and autophagy improves health in mitochondrial disease. *Hum Mol Genet* **24**, 4829-4847, doi:10.1093/hmg/ddv207 (2015).

211 Lopez de Figueroa, P., Lotz, M. K., Blanco, F. J. & Carames, B. Autophagy activation and protection from mitochondrial dysfunction in human chondrocytes. *Arthritis Rheumatol* **67**, 966-976, doi:10.1002/art.39025 (2015).

212 Ghavami, S. *et al.* Autophagy and apoptosis dysfunction in neurodegenerative disorders. *Prog Neurobiol* **112**, 24-49, doi:10.1016/j.pneurobio.2013.10.004 (2014).

213 Piquereau, J. *et al.* Protective role of PARK2/Parkin in sepsis-induced cardiac contractile and mitochondrial dysfunction. *Autophagy* **9**, 1837-1851, doi:10.4161/auto.26502 (2013).

214 Yao, J. *et al.* Mitochondrial bioenergetic deficit precedes Alzheimer's pathology in female mouse model of Alzheimer's disease. *Proc Natl Acad Sci U S A* **106**, 14670-14675, doi:10.1073/pnas.0903563106 (2009).

215 Nunomura, A. *et al.* Oxidative damage is the earliest event in Alzheimer disease. *J Neuropathol Exp Neurol* **60**, 759-767 (2001).

216 Maurer, I., Zierz, S. & Moller, H. J. A selective defect of cytochrome c oxidase is present in brain of Alzheimer disease patients. *Neurobiol Aging* **21**, 455-462 (2000).

217 Moreira, P. I. *et al.* Increased autophagic degradation of mitochondria in Alzheimer disease. *Autophagy* **3**, 614-615 (2007).

218 Santos, R. X. *et al.* A synergistic dysfunction of mitochondrial fission/fusion dynamics and mitophagy in Alzheimer's disease. *J Alzheimers Dis* **20 Suppl 2**, S401-412, doi:10.3233/JAD-2010-100666 (2010).

219 De la Mata, M. *et al.* Recovery of MERRF fibroblasts and cybrids pathophysiology by coenzyme Q10. *Neurotherapeutics* **9**, 446-463, doi:10.1007/s13311-012-0103-3 (2012).

220 Garrido-Maraver, J. *et al.* Critical role of AMP-activated protein kinase in the balance between mitophagy and mitochondrial biogenesis in MELAS disease. *Biochim Biophys Acta* **1852**, 2535-2553, doi:10.1016/j.bbadis.2015.08.027 (2015).

221 Rodriguez-Hernandez, A. *et al.* Coenzyme Q deficiency triggers mitochondria degradation by mitophagy. *Autophagy* **5**, 19-32 (2009).

222 Gilkerson, R. W. *et al.* Mitochondrial autophagy in cells with mtDNA mutations results from synergistic loss of transmembrane potential and mTORC1 inhibition. *Hum Mol Genet* **21**, 978-990, doi:10.1093/hmg/ddr529 (2012).

223 Rakovic, A. *et al.* Phosphatase and tensin homolog (PTEN)-induced putative kinase 1 (PINK1)-dependent ubiquitination of endogenous Parkin attenuates mitophagy: study in human primary fibroblasts and induced pluripotent stem cell-derived neurons. *J Biol Chem* **288**, 2223-2237, doi:10.1074/jbc.M112.391680 (2013).

224 Quinzii, C. *et al.* A mutation in para-hydroxybenzoate-polyprenyl transferase (COQ2) causes primary coenzyme Q10 deficiency. *Am J Hum Genet* **78**, 345-349, doi:10.1086/500092 (2006).

225 Murphy, M. P. & Smith, R. A. Drug delivery to mitochondria: the key to mitochondrial medicine. *Adv Drug Deliv Rev* **41**, 235-250 (2000).

226 Kerr, D. S. Review of clinical trials for mitochondrial disorders: 1997-2012. *Neurotherapeutics* **10**, 307-319, doi:10.1007/s13311-013-0176-7 (2013).

227 Kanabus, M., Heales, S. J. & Rahman, S. Development of pharmacological strategies for mitochondrial disorders. *Br J Pharmacol* **171**, 1798-1817, doi:10.1111/bph.12456 (2014).

228 Hirano, M., Emmanuele, V. & Quinzii, C. M. Emerging therapies for mitochondrial diseases. *Essays Biochem* **62**, 467-481, doi:10.1042/EBC20170114 (2018).

229 Rodriguez, M. C. *et al.* Beneficial effects of creatine, CoQ10, and lipoic acid in mitochondrial disorders. *Muscle Nerve* **35**, 235-242, doi:10.1002/mus.20688 (2007).

230 Blanchet, L. *et al.* Quantifying small molecule phenotypic effects using mitochondrial morpho-functional fingerprinting and machine learning. *Sci Rep* **5**, 8035, doi:10.1038/srep08035 (2015).

231 Parikh, S. *et al.* A modern approach to the treatment of mitochondrial disease. *Curr Treat Options Neurol* **11**, 414-430 (2009).

232 Crane, F. L., Hatefi, Y., Lester, R. L. & Widmer, C. Isolation of a quinone from beef heart mitochondria. *Biochim Biophys Acta* **25**, 220-221 (1957).

233 Festenstein, G. N., Heaton, F. W., Lowe, J. S. & Morton, R. A. A constituent of the unsaponifiable portion of animal tissue lipids (lambda max. 272 m mu). *Biochem J* **59**, 558-566 (1955).

234 Wolf, D. E. *et al.* COENZYME Q. I. STRUCTURE STUDIES ON THE COENZYME Q GROUP. *Journal of the American Chemical Society* **80**
, doi:10.1021/ja01550a096 (1958).

235 Kagan, V. E. *et al.* Antioxidant action of ubiquinol homologues with different isoprenoid chain length in biomembranes. *Free Radic Biol Med* **9**, 117-126 (1990).

236 Quinzii, C. M. & Hirano, M. Coenzyme Q and mitochondrial disease. *Dev Disabil Res Rev* **16**, 183-188, doi:10.1002/ddrr.108 (2010).

237 Suarez-Rivero, J. M. *et al.* in
Coenzyme Q10: Uses, Health Effects and Role in Disease (ed Sabine Grigoryeva) 1-64 (Nova, 2018).

238 Navas, P., Villalba, J. M. & de Cabo, R. The importance of plasma membrane coenzyme Q in aging and stress responses. *Mitochondrion* **7 Suppl**, S34-40, doi:10.1016/j.mito.2007.02.010 (2007).

239 Fernandez-Ayala, D. J. *et al.* Coenzyme Q protects cells against serum withdrawal-induced apoptosis by inhibition of ceramide release and caspase-3 activation. *Antioxid Redox Signal* **2**, 263-275, doi:10.1089/ars.2000.2.2-263 (2000).

240 Navas, P. *et al.* Ceramide-dependent caspase 3 activation is prevented by coenzyme Q from plasma membrane in serum-deprived cells. *Free Radic Res* **36**, 369-374 (2002).

241 Papucci, L. *et al.* Coenzyme q10 prevents apoptosis by inhibiting mitochondrial depolarization independently of its free radical scavenging property. *J Biol Chem* **278**, 28220-28228, doi:10.1074/jbc.M302297200 (2003).

242 Sun, I. L., Sun, E. E. & Crane, F. L. Stimulation of serum-free cell proliferation by coenzyme Q. *Biochem Biophys Res Commun* **189**, 8-13 (1992).

243 Crane, F. L., Sun, I. L., Crowe, R. A., Alcain, F. J. & Low, H. Coenzyme Q10, plasma membrane oxidase and growth control. *Mol Aspects Med* **15 Suppl**, s1-11 (1994).

244 Schmelzer, C., Lindner, I., Vock, C., Fujii, K. & Doring, F. Functional connections and pathways of coenzyme Q10-inducible genes: an in-silico study. *IUBMB Life* **59**, 628-633, doi:10.1080/15216540701545991 (2007).

245 Cordero, M. D. *et al.* NLRP3 inflammasome is activated in fibromyalgia: the effect of coenzyme Q10. *Antioxid Redox Signal* **20**, 1169-1180, doi:10.1089/ars.2013.5198 (2014).

246 DePierre, J. W. & Ernster, L. Enzyme topology of intracellular membranes. *Annu Rev Biochem* **46**, 201-262, doi:10.1146/annurev.bi.46.070177.001221 (1977).

247 Molyneux, S. L. *et al.* Coenzyme Q10: an independent predictor of mortality in chronic heart failure. *J Am Coll Cardiol* **52**, 1435-1441, doi:10.1016/j.jacc.2008.07.044 (2008).

248 Mischley, L. K., Allen, J. & Bradley, R. Coenzyme Q10 deficiency in patients with Parkinson's disease. *J Neurol Sci* **318**, 72-75, doi:10.1016/j.jns.2012.03.023 (2012).

249 Quinzii, C. M., DiMauro, S. & Hirano, M. Human coenzyme Q10 deficiency. *Neurochem Res* **32**, 723-727, doi:10.1007/s11064-006-9190-z (2007).

250 Sohal, R. S. & Forster, M. J. Coenzyme Q, oxidative stress and aging. *Mitochondrion* **7 Suppl**, S103-111, doi:10.1016/j.mito.2007.03.006 (2007).

251 Ochoa, J. J., Quiles, J. L., Huertas, J. R. & Mataix, J. Coenzyme Q10 protects from aging-related oxidative stress and improves mitochondrial function in heart of rats fed a polyunsaturated fatty acid (PUFA)-rich diet. *J Gerontol A Biol Sci Med Sci* **60**, 970-975 (2005).

252 Ogasahara, S., Engel, A. G., Frens, D. & Mack, D. Muscle coenzyme Q deficiency in familial mitochondrial encephalomyopathy. *Proc Natl Acad Sci U S A* **86**, 2379-2382 (1989).

253 Gempel, K. *et al.* The myopathic form of coenzyme Q10 deficiency is caused by mutations in the electron-transferring-flavoprotein dehydrogenase (ETFDH) gene. *Brain* **130**, 2037-2044, doi:10.1093/brain/awm054 (2007).

254 Garrido-Maraver, J. *et al.* Screening of effective pharmacological treatments for MELAS syndrome using yeasts, fibroblasts and cybrid models of the disease. *Br J Pharmacol* **167**, 1311-1328, doi:10.1111/j.1476-5381.2012.02086.x (2012).

255 Zierz, S., Jahns, G. & Jerusalem, F. Coenzyme Q in serum and muscle of 5 patients with Kearns-Sayre syndrome and 12 patients with ophthalmoplegia plus. *J Neurol* **236**, 97-101 (1989).

256 Bresolin, N. *et al.* Clinical and biochemical correlations in mitochondrial myopathies treated with coenzyme Q10. *Neurology* **38**, 892-899 (1988).

257 Lekoubou, A. *et al.* Effect of long-term oral treatment with L-arginine and idebenone on the prevention of stroke-like episodes in an adult MELAS patient. *Rev Neurol (Paris)* **167**, 852-855, doi:10.1016/j.neurol.2011.02.038 (2011).

258 Napolitano, A. *et al.* Long-term treatment with idebenone and riboflavin in a patient with MELAS. *Neurol Sci* **21**, S981-982 (2000).

259 Glover, E. I. *et al.* A randomized trial of coenzyme Q10 in mitochondrial disorders. *Muscle Nerve* **42**, 739-748, doi:10.1002/mus.21758 (2010).

260 Berbel-Garcia, A. *et al.* Coenzyme Q 10 improves lactic acidosis, strokelike episodes, and epilepsy in a patient with MELAS (mitochondrial myopathy, encephalopathy, lactic acidosis, and strokelike episodes). *Clin Neuropharmacol* **27**, 187-191 (2004).

261 Ikejiri, Y. *et al.* Idebenone improves cerebral mitochondrial oxidative metabolism in a patient with MELAS. *Neurology* **47**, 583-585 (1996).

262 Taivassalo, T. *et al.* Endurance training and detraining in mitochondrial myopathies due to single large-scale mtDNA deletions. *Brain* **129**, 3391-3401, doi:10.1093/brain/awl282 (2006).

263 Tarnopolsky, M. A. Exercise as a therapeutic strategy for primary mitochondrial cytopathies. *J Child Neurol* **29**, 1225-1234, doi:10.1177/0883073814538512 (2014).

264 Voet, N. B. *et al.* Strength training and aerobic exercise training for muscle disease. *Cochrane Database Syst Rev*, CD003907, doi:10.1002/14651858.CD003907.pub4 (2013).

265 Viscomi, C. Toward a therapy for mitochondrial disease. *Biochem Soc Trans* **44**, 1483-1490, doi:10.1042/BST20160085 (2016).

266 Viscomi, C. *et al.* Combined treatment with oral metronidazole and N-acetylcysteine is effective in ethylmalonic encephalopathy. *Nat Med* **16**, 869-871, doi:10.1038/nm.2188 (2010).

267 Spinazzola, A. *et al.* Altered thymidine metabolism due to defects of thymidine phosphorylase. *J Biol Chem* **277**, 4128-4133, doi:10.1074/jbc.M111028200 (2002).

268 Taanman, J. W., Muddle, J. R. & Muntau, A. C. Mitochondrial DNA depletion can be prevented by dGMP and dAMP supplementation in a resting culture of deoxyguanosine kinase-deficient fibroblasts. *Hum Mol Genet* **12**, 1839-1845 (2003).

269 Lopez-Gomez, C. *et al.* Deoxycytidine and Deoxythymidine Treatment for Thymidine Kinase 2 Deficiency. *Ann Neurol* **81**, 641-652, doi:10.1002/ana.24922 (2017).

270 Bax, B. E. *et al.* Clinical and biochemical improvements in a patient with MNGIE following enzyme replacement. *Neurology* **81**, 1269-1271, doi:10.1212/WNL.0b013e3182a6cb4b (2013).

271 Halter, J. P. *et al.* Allogeneic haematopoietic stem cell transplantation for mitochondrial neurogastrointestinal encephalomyopathy. *Brain* **138**, 2847-2858, doi:10.1093/brain/awv226 (2015).

272 Dionisi-Vici, C. *et al.* Liver transplant in ethylmalonic encephalopathy: a new treatment for an otherwise fatal disease. *Brain* **139**, 1045-1051, doi:10.1093/brain/aww013 (2016).

273 Bouaita, A. *et al.* Downregulation of apoptosis-inducing factor in Harlequin mice induces progressive and severe optic atrophy which is durably prevented by AAV2-AIF1 gene therapy. *Brain* **135**, 35-52, doi:10.1093/brain/awr290 (2012).

274 Yu, H. *et al.* Gene delivery to mitochondria by targeting modified adenoassociated virus suppresses Leber's hereditary optic neuropathy in a mouse model. *Proc Natl Acad Sci U S A* **109**, E1238-1247, doi:10.1073/pnas.1119577109 (2012).

275 Guy, J. *et al.* Gene Therapy for Leber Hereditary Optic Neuropathy: Low- and Medium-Dose Visual Results. *Ophthalmology* **124**, 1621-1634, doi:10.1016/j.ophtha.2017.05.016 (2017).

276 Romero-Moya, D., Castano, J., Santos-Ocana, C., Navas, P. & Menendez, P. Generation, genome edition and characterization of iPSC lines from a patient with coenzyme Q10 deficiency harboring a heterozygous mutation in COQ4 gene. *Stem Cell Res* **24**, 144-147, doi:10.1016/j.scr.2016.09.007 (2017).

277 Suarez-Rivero, J. M. *et al.* in *Advances in Health and Disease* Vol. 3 (ed Lowell T. Duncan) (NOVA, 2017).

278 Dai, Y. *et al.* Rapamycin drives selection against a pathogenic heteroplasmic mitochondrial DNA mutation. *Hum Mol Genet* **23**, 637-647, doi:10.1093/hmg/ddt450 (2014).

279 Suen, D. F., Narendra, D. P., Tanaka, A., Manfredi, G. & Youle, R. J. Parkin overexpression selects against a deleterious mtDNA mutation in heteroplasmic cybrid cells. *Proc Natl Acad Sci U S A* **107**, 11835-11840, doi:10.1073/pnas.0914569107 (2010).

280 Valenci, I., Yonai, L., Bar-Yaacov, D., Mishmar, D. & Ben-Zvi, A. Parkin modulates heteroplasmy of truncated mtDNA in Caenorhabditis elegans. *Mitochondrion* **20**, 64-70, doi:10.1016/j.mito.2014.11.001 (2015).

281 Malena, A., Loro, E., Di Re, M., Holt, I. J. & Vergani, L. Inhibition of mitochondrial fission favours mutant over wild-type mitochondrial DNA. *Hum Mol Genet* **18**, 3407-3416, doi:10.1093/hmg/ddp281 (2009).

282 Bacman, S. R., Williams, S. L., Hernandez, D. & Moraes, C. T. Modulating mtDNA heteroplasmy by mitochondria-targeted restriction endonucleases in a 'differential multiple cleavage-site' model. *Gene Ther* **14**, 1309-1318, doi:10.1038/sj.gt.3302981 (2007).

283 Srivastava, S. & Moraes, C. T. Manipulating mitochondrial DNA heteroplasmy by a mitochondrially targeted restriction endonuclease. *Hum Mol Genet* **10**, 3093-3099 (2001).

284 Tanaka, M. *et al.* Gene therapy for mitochondrial disease by delivering restriction endonuclease SmaI into mitochondria. *J Biomed Sci* **9**, 534-541, doi:10.1159/000064726 (2002).

285 Hashimoto, M. *et al.* MitoTALEN: A General Approach to Reduce Mutant mtDNA Loads and Restore Oxidative Phosphorylation Function in Mitochondrial Diseases. *Mol Ther* **23**, 1592-1599, doi:10.1038/mt.2015.126 (2015).

286 Reddy, P. *et al.* Selective elimination of mitochondrial mutations in the germline by genome editing. *Cell* **161**, 459-469, doi:10.1016/j.cell.2015.03.051 (2015).

287 Papworth, M., Kolasinska, P. & Minczuk, M. Designer zinc-finger proteins and their applications. *Gene* **366**, 27-38, doi:10.1016/j.gene.2005.09.011 (2006).

288 Minczuk, M., Papworth, M. A., Kolasinska, P., Murphy, M. P. & Klug, A. Sequence-specific modification of mitochondrial DNA using a chimeric zinc finger methylase. *Proc Natl Acad Sci U S A* **103**, 19689-19694, doi:10.1073/pnas.0609502103 (2006).

289 Gammage, P. A., Rorbach, J., Vincent, A. I., Rebar, E. J. & Minczuk, M. Mitochondrially targeted ZFNs for selective degradation of pathogenic mitochondrial

genomes bearing large-scale deletions or point mutations. *EMBO molecular medicine* **6**, 458-466, doi:10.1002/emmm.201303672 (2014).

290 Wang, H. X. *et al.* CRISPR/Cas9-Based Genome Editing for Disease Modeling and Therapy: Challenges and Opportunities for Nonviral Delivery. *Chem Rev* **117**, 9874-9906, doi:10.1021/acs.chemrev.6b00799 (2017).

291 Jo, A. *et al.* Efficient Mitochondrial Genome Editing by CRISPR/Cas9. *Biomed Res Int* **2015**, 305716, doi:10.1155/2015/305716 (2015).

292 Li, R. & Guan, M. X. Human mitochondrial leucyl-tRNA synthetase corrects mitochondrial dysfunctions due to the tRNALeu(UUR) A3243G mutation, associated with mitochondrial encephalomyopathy, lactic acidosis, and stroke-like symptoms and diabetes. *Mol Cell Biol* **30**, 2147-2154, doi:10.1128/MCB.01614-09 (2010).

293 Perli, E. *et al.* The isolated carboxy-terminal domain of human mitochondrial leucyl-tRNA synthetase rescues the pathological phenotype of mitochondrial tRNA mutations in human cells. *EMBO molecular medicine* **6**, 169-182, doi:10.1002/emmm.201303198 (2014).

294 Giordano, C. *et al.* Efficient mitochondrial biogenesis drives incomplete penetrance in Leber's hereditary optic neuropathy. *Brain* **137**, 335-353, doi:10.1093/brain/awt343 (2014).

295 El-Hattab, A. W., Zarante, A. M., Almannai, M. & Scaglia, F. Therapies for mitochondrial diseases and current clinical trials. *Mol Genet Metab* **122**, 1-9, doi:10.1016/j.ymgme.2017.09.009 (2017).

296 Golubitzky, A. *et al.* Screening for active small molecules in mitochondrial complex I deficient patient's fibroblasts, reveals AICAR as the most beneficial compound. *PLoS One* **6**, e26883, doi:10.1371/journal.pone.0026883 (2011).

297 Komen, J. C. & Thorburn, D. R. Turn up the power - pharmacological activation of mitochondrial biogenesis in mouse models. *Br J Pharmacol* **171**, 1818-1836, doi:10.1111/bph.12413 (2014).

298 Dassa, E. P. *et al.* Expression of the alternative oxidase complements cytochrome c oxidase deficiency in human cells. *EMBO molecular medicine* **1**, 30-36, doi:10.1002/emmm.200900001 (2009).

299 Rai, P. K., Craven, L., Hoogewijs, K., Russell, O. M. & Lightowlers, R. N. Advances in methods for reducing mitochondrial DNA disease by replacing or manipulating the mitochondrial genome. *Essays Biochem* **62**, 455-465, doi:10.1042/EBC20170113 (2018).

300 Zhang, J. *et al.* Live birth derived from oocyte spindle transfer to prevent mitochondrial disease. *Reprod Biomed Online* **34**, 361-368, doi:10.1016/j.rbmo.2017.01.013 (2017).

301 Jain, I. H. *et al.* Hypoxia as a therapy for mitochondrial disease. *Science* **352**, 54-61, doi:10.1126/science.aad9642 (2016).

302 Sarkar, S. *et al.* A rational mechanism for combination treatment of Huntington's disease using lithium and rapamycin. *Hum Mol Genet* **17**, 170-178, doi:10.1093/hmg/ddm294 (2008).

303 Mita, M. M., Mita, A. & Rowinsky, E. K. The molecular target of rapamycin (mTOR) as a therapeutic target against cancer. *Cancer Biol Ther* **2**, S169-177 (2003).

304 Viscomi, C., Bottani, E. & Zeviani, M. Emerging concepts in the therapy of mitochondrial disease. *Biochim Biophys Acta* **1847**, 544-557, doi:10.1016/j.bbabio.2015.03.001 (2015).

305 Plantinga, T. S., Joosten, L. A., van der Meer, J. W. & Netea, M. G. Modulation of inflammation by autophagy: consequences for Crohn's disease. *Curr Opin Pharmacol* **12**, 497-502, doi:10.1016/j.coph.2012.01.017 (2012).

306 Marchetti, P. & Masini, M. Autophagy and the pancreatic beta-cell in human type 2 diabetes. *Autophagy* **5**, 1055-1056, doi:10.4161/auto.5.7.9511 (2009).

307 Rautou, P.-E. *et al.* Autophagy in liver diseases. *Journal of Hepatology* **53**, 1123-1134, doi:10.1016/j.jhep.2010.07.006 (2010).

308 Diot, A. *et al.* A novel quantitative assay of mitophagy: Combining high content fluorescence microscopy and mitochondrial DNA load to quantify mitophagy and identify novel pharmacological tools against pathogenic heteroplasmic mtDNA. *Pharmacol Res* **100**, 24-35, doi:10.1016/j.phrs.2015.07.014 (2015).

309 Khan, N. A. *et al.* Effective treatment of mitochondrial myopathy by nicotinamide riboside, a vitamin B3. *EMBO molecular medicine* **6**, 721-731, doi:10.1002/emmm.201403943 (2014).

310 Hardie, D. G. AMPK: a target for drugs and natural products with effects on both diabetes and cancer. *Diabetes* **62**, 2164-2172, doi:10.2337/db13-0368 (2013).

311 Viscomi, C. *et al.* In vivo correction of COX deficiency by activation of the AMPK/PGC-1alpha axis. *Cell Metab* **14**, 80-90, doi:10.1016/j.cmet.2011.04.011 (2011).

312 Li, Q. *et al.* Rapamycin attenuates mitochondrial dysfunction via activation of mitophagy in experimental ischemic stroke. *Biochem Biophys Res Commun* **444**, 182-188, doi:10.1016/j.bbrc.2014.01.032 (2014).

313 Pan, T. *et al.* Rapamycin protects against rotenone-induced apoptosis through autophagy induction. *Neuroscience* **164**, 541-551, doi:10.1016/j.neuroscience.2009.08.014 (2009).

314 Johnson, S. C. *et al.* mTOR inhibition alleviates mitochondrial disease in a mouse model of Leigh syndrome. *Science* **342**, 1524-1528, doi:10.1126/science.1244360 (2013).

315 Smirnova, E., Griparic, L., Shurland, D. L. & van der Bliek, A. M. Dynamin-related protein Drp1 is required for mitochondrial division in mammalian cells. *Mol Biol Cell* **12**, 2245-2256, doi:10.1091/mbc.12.8.2245 (2001).

316 Cassidy-Stone, A. *et al.* Chemical inhibition of the mitochondrial division dynamin reveals its role in Bax/Bak-dependent mitochondrial outer membrane permeabilization. *Dev Cell* **14**, 193-204, doi:10.1016/j.devcel.2007.11.019 (2008).

317 Cui, M., Tang, X., Christian, W. V., Yoon, Y. & Tieu, K. Perturbations in mitochondrial dynamics induced by human mutant PINK1 can be rescued by the mitochondrial division inhibitor mdivi-1. *J Biol Chem* **285**, 11740-11752, doi:10.1074/jbc.M109.066662 (2010).

318 Finsterer, J., Zarrouk-Mahjoub, S. & Shoffner, J. M. MERRF Classification: Implications for Diagnosis and Clinical Trials. *Pediatr Neurol* **80**, 8-23, doi:10.1016/j.pediatrneurol.2017.12.005 (2018).

319 Fukuhara, N., Tokiguchi, S., Shirakawa, K. & Tsubaki, T. Myoclonus epilepsy associated with ragged-red fibres (mitochondrial abnormalities): disease entity or a syndrome? Light-and electron-microscopic studies of two cases and review of literature. *J Neurol Sci* **47**, 117-133 (1980).

320 Couser, N. & Gucsavas-Calikoglu, M. in *Biomarkers in Inborn Errors of Metabolism* (eds Uttam Garg & Laurie D. Smith) 167-190 (Elsevier, 2017).

321 Lorenzoni, P. J., Scola, R. H., Kay, C. S., Silvado, C. E. & Werneck, L. C. When should MERRF (myoclonus epilepsy associated with ragged-red fibers) be the diagnosis? *Arq Neuropsiquiatr* **72**, 803-811 (2014).

322 Yoneda, M. *et al.* A common mitochondrial DNA mutation in the t-RNA(Lys) of patients with myoclonus epilepsy associated with ragged-red fibers. *Biochem Int* **21**, 789-796 (1990).

323 Cohen, B. H. in *Mitochondrial Case Studies* (eds Russell P. Saneto, Sumit Parikh, & Bruce H. Cohen) 31-36 (Academic Press, 2016).

324 Hammans, S. R. *et al.* The mitochondrial DNA transfer RNA(Lys)A-->G(8344) mutation and the syndrome of myoclonic epilepsy with ragged red fibres (MERRF). Relationship of clinical phenotype to proportion of mutant mitochondrial DNA. *Brain* **116 (Pt 3)**, 617-632 (1993).

325 Enriquez, J. A., Chomyn, A. & Attardi, G. MtDNA mutation in MERRF syndrome causes defective aminoacylation of tRNA(Lys) and premature translation termination. *Nat Genet* **10**, 47-55, doi:10.1038/ng0595-47 (1995).

326 Yasukawa, T. *et al.* Defect in modification at the anticodon wobble nucleotide of mitochondrial tRNA(Lys) with the MERRF encephalomyopathy pathogenic mutation. *FEBS Lett* **467**, 175-178 (2000).

327 Kirino, Y. & Suzuki, T. Human mitochondrial diseases associated with tRNA wobble modification deficiency. *RNA Biol* **2**, 41-44 (2005).

328 Silvestri, G., Moraes, C. T., Shanske, S., Oh, S. J. & DiMauro, S. A new mtDNA mutation in the tRNA(Lys) gene associated with myoclonic epilepsy and ragged-red fibers (MERRF). *Am J Hum Genet* **51**, 1213-1217 (1992).

329 Rossmanith, W. *et al.* The expanding mutational spectrum of MERRF substitution G8361A in the mitochondrial tRNALys gene. *Ann Neurol* **54**, 820-823, doi:10.1002/ana.10753 (2003).

330 Santorelli, F. M. *et al.* Maternally inherited cardiomyopathy and hearing loss associated with a novel mutation in the mitochondrial tRNA(Lys) gene (G8363A). *Am J Hum Genet* **58**, 933-939 (1996).

331 Mancuso, M. *et al.* A novel mitochondrial tRNAPhe mutation causes MERRF syndrome. *Neurology* **62**, 2119-2121 (2004).

332 Crimmins, D. *et al.* Mitochondrial encephalomyopathy: variable clinical expression within a single kindred. *J Neurol Neurosurg Psychiatry* **56**, 900-905 (1993).

333 Nishigaki, Y. *et al.* A novel mitochondrial tRNA(Leu(UUR)) mutation in a patient with features of MERRF and Kearns-Sayre syndrome. *Neuromuscul Disord* **13**, 334-340 (2003).

334 Emmanuele, V. *et al.* MERRF and Kearns-Sayre overlap syndrome due to the mitochondrial DNA m.3291T>C mutation. *Muscle Nerve* **44**, 448-451, doi:10.1002/mus.22149 (2011).

335 Zsurka, G. *et al.* Mutation in the mitochondrial tRNA(Ile) gene causes progressive myoclonus epilepsy. *Seizure* **22**, 483-486, doi:10.1016/j.seizure.2013.03.003 (2013).

336 Hahn, A. *et al.* MERRF-like phenotype associated with a rare mitochondrial trnaile mutation (m.4284 G>A). *Neuropediatrics* **42**, 148-151, doi:10.1055/s-0031-1283167 (2011).

337 Karppa, M., Kytovuori, L., Saari, M. & Majamaa, K. Mutation m.15923A>G in the MT-TT gene causes mild myopathy - case report of an adult-onset phenotype. *BMC Neurol* **18**, 149, doi:10.1186/s12883-018-1159-4 (2018).

338 del Mar O'Callaghan, M. *et al.* New mitochondrial DNA mutations in tRNA associated with three severe encephalopamyopathic phenotypes: neonatal, infantile, and childhood onset. *Neurogenetics* **13**, 245-250, doi:10.1007/s10048-012-0322-0 (2012).

339 Blakely, E. L. *et al.* A new mitochondrial transfer RNAPro gene mutation associated with myoclonic epilepsy with ragged-red fibers and other neurological features. *Arch Neurol* **66**, 399-402, doi:10.1001/archneurol.2008.576 (2009).

340 Herrero-Martin, M. D. *et al.* A MELAS/MERRF phenotype associated with the mitochondrial DNA 5521G>A mutation. *J Neurol Neurosurg Psychiatry* **81**, 471-472, doi:10.1136/jnnp.2009.173831 (2010).

341 Nakamura, M. *et al.* A novel point mutation in the mitochondrial tRNA(Ser(UCN)) gene detected in a family with MERRF/MELAS overlap syndrome. *Biochem Biophys Res Commun* **214**, 86-93, doi:10.1006/bbrc.1995.2260 (1995).

342 Melone, M. A. *et al.* Revelation of a new mitochondrial DNA mutation (G12147A) in a MELAS/MERFF phenotype. *Arch Neurol* **61**, 269-272, doi:10.1001/archneur.61.2.269 (2004).

343 Martin-Jimenez, R. *et al.* Clinical and cellular consequences of the mutation m.12300G>A in the mitochondrial tRNA(Leu(CUN)) gene. *Mitochondrion* **12**, 288-293, doi:10.1016/j.mito.2011.10.004 (2012).

344 Naini, A. B. *et al.* Novel mitochondrial DNA ND5 mutation in a patient with clinical features of MELAS and MERRF. *Arch Neurol* **62**, 473-476, doi:10.1001/archneur.62.3.473 (2005).

345 Blumenthal, D. T. *et al.* Myoclonus epilepsy with ragged red fibers and multiple mtDNA deletions. *Neurology* **50**, 524-525 (1998).

346 Van Goethem, G. *et al.* Patient homozygous for a recessive POLG mutation presents with features of MERRF. *Neurology* **61**, 1811-1813 (2003).

347 Park, S. Y., Kim, S. H. & Lee, Y. M. Molecular Diagnosis of Myoclonus Epilepsy Associated with Ragged-Red Fibers Syndrome in the Absence of Ragged Red Fibers. *Front Neurol* **8**, 520, doi:10.3389/fneur.2017.00520 (2017).

348 Jeppesen, T. D. *et al.* Mitochondrial DNA mutation load in a family with the m.8344A>G point mutation and lipomas: a case study. *Clin Case Rep* **5**, 2034-2039, doi:10.1002/ccr3.1096 (2017).

349 James, A. M., Wei, Y. H., Pang, C. Y. & Murphy, M. P. Altered mitochondrial function in fibroblasts containing MELAS or MERRF mitochondrial DNA mutations. *Biochem J* **318 (Pt 2)**, 401-407 (1996).

350 James, A. M., Sheard, P. W., Wei, Y. H. & Murphy, M. P. Decreased ATP synthesis is phenotypically expressed during increased energy demand in fibroblasts containing mitochondrial tRNA mutations. *Eur J Biochem* **259**, 462-469 (1999).

351 Boulet, L., Karpati, G. & Shoubridge, E. A. Distribution and threshold expression of the tRNA(Lys) mutation in skeletal muscle of patients with myoclonic epilepsy and ragged-red fibers (MERRF). *Am J Hum Genet* **51**, 1187-1200 (1992).

352 Chomyn, A. *et al.* In vitro genetic transfer of protein synthesis and respiration defects to mitochondrial DNA-less cells with myopathy-patient mitochondria. *Mol Cell Biol* **11**, 2236-2244 (1991).

353 Wu, S. B., Ma, Y. S., Wu, Y. T., Chen, Y. C. & Wei, Y. H. Mitochondrial DNA mutation-elicited oxidative stress, oxidative damage, and altered gene expression in cultured cells of patients with MERRF syndrome. *Mol Neurobiol* **41**, 256-266, doi:10.1007/s12035-010-8123-7 (2010).

354 Saneto, R. P. in *Advances in Genetics* Vol. 98 (ed Jay C. Dunlap Theodore Friedmann, Stephen F. Goodwin) 63-116 (Academic Press, 2017).

355 Wallace, D. C. *et al.* Familial mitochondrial encephalomyopathy (MERRF): genetic, pathophysiological, and biochemical characterization of a mitochondrial DNA disease. *Cell* **55**, 601-610 (1988).

356 Lamperti, C. & Zeviani, M. Myoclonus epilepsy in mitochondrial disorders. *Epileptic Disord* **18**, 94-102, doi:10.1684/epd.2016.0846 (2016).

357 Ozawa, M. *et al.* The 8,344 mutation in mitochondrial DNA: a comparison between the proportion of mutant DNA and clinico-pathologic findings. *Neuromuscul Disord* **5**, 483-488 (1995).

358 Molnar, M. J., Perenyi, J., Siska, E., Nemeth, G. & Nagy, Z. The typical MERRF (A8344G) mutation of the mitochondrial DNA associated with depressive mood disorders. *J Neurol* **256**, 264-265, doi:10.1007/s00415-009-0841-2 (2009).

359 Finsterer, J. Mitochondriopathies. *Eur J Neurol* **11**, 163-186 (2004).

360 DiMauro, S. & Hirano, M. in *GeneReviews® [Internet]* (ed Ardinger HH Adam MP, Pagon RA, et al.) (2003 Jun 3 [Updated 2015 Jan 29]).

361 Berkovic, S. F. *et al.* Myoclonus epilepsy and ragged-red fibres (MERRF). 1. A clinical, pathological, biochemical, magnetic resonance spectrographic and positron emission tomographic study. *Brain* **112 (Pt 5)**, 1231-1260 (1989).

362 DiMauro, S. *et al.* Clinical features and genetics of myoclonic epilepsy with ragged red fibers. *Adv Neurol* **89**, 217-229 (2002).

363 Crest, C., Dupont, S., Leguern, E., Adam, C. & Baulac, M. Levetiracetam in progressive myoclonic epilepsy: an exploratory study in 9 patients. *Neurology* **62**, 640-643 (2004).

364 Taivassalo, T. & Haller, R. G. Implications of exercise training in mtDNA defects--use it or lose it? *Biochim Biophys Acta* **1659**, 221-231, doi:10.1016/j.bbabio.2004.09.007 (2004).

365 Nakamaru-Ogiso, E. *et al.* The membrane subunit NuoL(ND5) is involved in the indirect proton pumping mechanism of Escherichia coli complex I. *J Biol Chem* **285**, 39070-39078, doi:10.1074/jbc.M110.157826 (2010).

366 Kao, M. C. *et al.* Characterization of the membrane domain subunit NuoJ (ND6) of the NADH-quinone oxidoreductase from Escherichia coli by chromosomal DNA manipulation. *Biochemistry* **44**, 3562-3571, doi:10.1021/bi0476477 (2005).

367 El Yacoubi, B., Bailly, M. & de Crecy-Lagard, V. Biosynthesis and function of posttranscriptional modifications of transfer RNAs. *Annu Rev Genet* **46**, 69-95, doi:10.1146/annurev-genet-110711-155641 (2012).

368 Armengod, M. E. *et al.* Modification of the wobble uridine in bacterial and mitochondrial tRNAs reading NNA/NNG triplets of 2-codon boxes. *RNA Biol* **11**, 1495-1507, doi:10.4161/15476286.2014.992269 (2014).

369 Armengod, M. E. *et al.* Enzymology of tRNA modification in the bacterial MnmEG pathway. *Biochimie* **94**, 1510-1520, doi:10.1016/j.biochi.2012.02.019 (2012).

370 Moukadiri, I. *et al.* Evolutionarily conserved proteins MnmE and GidA catalyze the formation of two methyluridine derivatives at tRNA wobble positions. *Nucleic Acids Res* **37**, 7177-7193, doi:10.1093/nar/gkp762 (2009).

371 Yim, L., Moukadiri, I., Bjork, G. R. & Armengod, M. E. Further insights into the tRNA modification process controlled by proteins MnmE and GidA of Escherichia coli. *Nucleic Acids Res* **34**, 5892-5905, doi:10.1093/nar/gkl752 (2006).

372 Atkins, J. F. & Bjork, G. R. A gripping tale of ribosomal frameshifting: extragenic suppressors of frameshift mutations spotlight P-site realignment. *Microbiol Mol Biol Rev* **73**, 178-210, doi:10.1128/MMBR.00010-08 (2009).

373 Bregeon, D., Colot, V., Radman, M. & Taddei, F. Translational misreading: a tRNA modification counteracts a +2 ribosomal frameshift. *Genes Dev* **15**, 2295-2306, doi:10.1101/gad.207701 (2001).

374 Elseviers, D., Petrullo, L. A. & Gallagher, P. J. Novel E. coli mutants deficient in biosynthesis of 5-methylaminomethyl-2-thiouridine. *Nucleic Acids Res* **12**, 3521-3534 (1984).

375 Baile, M. G. & Claypool, S. M. The power of yeast to model diseases of the powerhouse of the cell. *Front Biosci (Landmark Ed)* **18**, 241-278 (2013).

376 Montanari, A. *et al.* Yeast as a model of human mitochondrial tRNA base substitutions: investigation of the molecular basis of respiratory defects. *RNA* **14**, 275-283, doi:10.1261/rna.740108 (2008).

377 De Luca, C. *et al.* Can yeast be used to study mitochondrial diseases? Biolistic tRNA mutants for the analysis of mechanisms and suppressors. *Mitochondrion* **9**, 408-417, doi:10.1016/j.mito.2009.07.004 (2009).

378 Feuermann, M. *et al.* The yeast counterparts of human 'MELAS' mutations cause mitochondrial dysfunction that can be rescued by overexpression of the mitochondrial translation factor EF-Tu. *EMBO Rep* **4**, 53-58, doi:10.1038/sj.embor.embor713 (2003).

379 Umeda, N. *et al.* Mitochondria-specific RNA-modifying enzymes responsible for the biosynthesis of the wobble base in mitochondrial tRNAs. Implications for the molecular pathogenesis of human mitochondrial diseases. *J Biol Chem* **280**, 1613-1624, doi:10.1074/jbc.M409306200 (2005).

380 Rinaldi, T., Dallabona, C., Ferrero, I., Frontali, L. & Bolotin-Fukuhara, M. Mitochondrial diseases and the role of the yeast models. *FEMS Yeast Res* **10**, 1006-1022, doi:10.1111/j.1567-1364.2010.00685.x (2010).

381 Falk, M. J. *et al.* Subcomplex Ilambda specifically controls integrated mitochondrial functions in Caenorhabditis elegans. *PLoS One* **4**, e6607, doi:10.1371/journal.pone.0006607 (2009).

382 Tsang, W. Y., Sayles, L. C., Grad, L. I., Pilgrim, D. B. & Lemire, B. D. Mitochondrial respiratory chain deficiency in Caenorhabditis elegans results in developmental arrest and increased life span. *J Biol Chem* **276**, 32240-32246, doi:10.1074/jbc.M103999200 (2001).

383 Kayser, E. B., Morgan, P. G., Hoppel, C. L. & Sedensky, M. M. Mitochondrial expression and function of GAS-1 in Caenorhabditis elegans. *J Biol Chem* **276**, 20551-20558, doi:10.1074/jbc.M011066200 (2001).

384 Felkai, S. *et al.* CLK-1 controls respiration, behavior and aging in the nematode Caenorhabditis elegans. *EMBO J* **18**, 1783-1792, doi:10.1093/emboj/18.7.1783 (1999).

385 Ishii, N. *et al.* A mutation in succinate dehydrogenase cytochrome b causes oxidative stress and ageing in nematodes. *Nature* **394**, 694-697, doi:10.1038/29331 (1998).

386 Rea, S. L., Graham, B. H., Nakamaru-Ogiso, E., Kar, A. & Falk, M. J. Bacteria, yeast, worms, and flies: exploiting simple model organisms to investigate human mitochondrial diseases. *Dev Disabil Res Rev* **16**, 200-218, doi:10.1002/ddrr.114 (2010).

387 Grad, L. I. & Lemire, B. D. Riboflavin enhances the assembly of mitochondrial cytochrome c oxidase in C. elegans NADH-ubiquinone oxidoreductase mutants. *Biochim Biophys Acta* **1757**, 115-122, doi:10.1016/j.bbabio.2005.11.009 (2006).

388 Tsang, W. Y. & Lemire, B. D. The role of mitochondria in the life of the nematode, Caenorhabditis elegans. *Biochim Biophys Acta* **1638**, 91-105 (2003).

389 Jorgensen, E. M. & Mango, S. E. The art and design of genetic screens: caenorhabditis elegans. *Nat Rev Genet* **3**, 356-369, doi:10.1038/nrg794 (2002).

390 Ashburner, M., Golic, K. G. & Hawley, R. S. *Drosophila: A laboratory handbook*. 2 edn, (Cold Spring Harbor, 2005).

391 Al-Ramahi, I. *et al.* dAtaxin-2 mediates expanded Ataxin-1-induced neurodegeneration in a Drosophila model of SCA1. *PLoS Genet* **3**, e234, doi:10.1371/journal.pgen.0030234 (2007).

392 Tsuda, H. *et al.* The amyotrophic lateral sclerosis 8 protein VAPB is cleaved, secreted, and acts as a ligand for Eph receptors. *Cell* **133**, 963-977, doi:10.1016/j.cell.2008.04.039 (2008).

393 Park, J., Kim, Y. & Chung, J. Mitochondrial dysfunction and Parkinson's disease genes: insights from Drosophila. *Dis Model Mech* **2**, 336-340, doi:10.1242/dmm.003178 (2009).

394 Greene, J. C. *et al.* Mitochondrial pathology and apoptotic muscle degeneration in Drosophila parkin mutants. *Proc Natl Acad Sci U S A* **100**, 4078-4083, doi:10.1073/pnas.0737556100 (2003).

395 Clark, I. E. *et al.* Drosophila pink1 is required for mitochondrial function and interacts genetically with parkin. *Nature* **441**, 1162-1166, doi:10.1038/nature04779 (2006).

396 Mast, J. D., Tomalty, K. M., Vogel, H. & Clandinin, T. R. Reactive oxygen species act remotely to cause synapse loss in a Drosophila model of developmental mitochondrial encephalopathy. *Development* **135**, 2669-2679, doi:10.1242/dev.020644 (2008).

397 Liu, W. *et al.* Mutations in cytochrome c oxidase subunit VIa cause neurodegeneration and motor dysfunction in Drosophila. *Genetics* **176**, 937-946, doi:10.1534/genetics.107.071688 (2007).

398 Celotto, A. M. *et al.* Mitochondrial encephalomyopathy in Drosophila. *J Neurosci* **26**, 810-820, doi:10.1523/JNEUROSCI.4162-05.2006 (2006).

399 Kandul, N. P., Zhang, T., Hay, B. A. & Guo, M. Selective removal of deletion-bearing mitochondrial DNA in heteroplasmic Drosophila. *Nat Commun* **7**, 13100, doi:10.1038/ncomms13100 (2016).

400 Palladino, M. J. Modeling mitochondrial encephalomyopathy in Drosophila. *Neurobiol Dis* **40**, 40-45, doi:10.1016/j.nbd.2010.05.009 (2010).

401 Peralta, S., Torraco, A., Iommarini, L. & Diaz, F. Mitochondrial Diseases Part III: Therapeutic interventions in mouse models of OXPHOS deficiencies. *Mitochondrion* **23**, 71-80, doi:10.1016/j.mito.2015.01.007 (2015).

402 Iommarini, L., Peralta, S., Torraco, A. & Diaz, F. Mitochondrial Diseases Part II: Mouse models of OXPHOS deficiencies caused by defects in regulatory factors and other components required for mitochondrial function. *Mitochondrion* **22**, 96-118, doi:10.1016/j.mito.2015.01.008 (2015).

403 Torraco, A., Peralta, S., Iommarini, L. & Diaz, F. Mitochondrial Diseases Part I: mouse models of OXPHOS deficiencies caused by defects in respiratory complex subunits or assembly factors. *Mitochondrion* **21**, 76-91, doi:10.1016/j.mito.2015.01.009 (2015).

404 Tyynismaa, H. & Suomalainen, A. Mouse models of mitochondrial DNA defects and their relevance for human disease. *EMBO Rep* **10**, 137-143, doi:10.1038/embor.2008.242 (2009).

405 Battersby, B. J., Loredo-Osti, J. C. & Shoubridge, E. A. Nuclear genetic control of mitochondrial DNA segregation. *Nat Genet* **33**, 183-186, doi:10.1038/ng1073 (2003).

406 Fan, W. *et al.* A mouse model of mitochondrial disease reveals germline selection against severe mtDNA mutations. *Science* **319**, 958-962, doi:10.1126/science.1147786 (2008).

407 Inoue, K. *et al.* Generation of mice with mitochondrial dysfunction by introducing mouse mtDNA carrying a deletion into zygotes. *Nat Genet* **26**, 176-181, doi:10.1038/82826 (2000).

408 Nakada, K. *et al.* Accumulation of pathogenic DeltamtDNA induced deafness but not diabetic phenotypes in mito-mice. *Biochem Biophys Res Commun* **323**, 175-184, doi:10.1016/j.bbrc.2004.08.073 (2004).

409 Sligh, J. E. *et al.* Maternal germ-line transmission of mutant mtDNAs from embryonic stem cell-derived chimeric mice. *Proc Natl Acad Sci U S A* **97**, 14461-14466, doi:10.1073/pnas.250491597 (2000).

410 McGregor, A., Temperley, R., Chrzanowska-Lightowlers, Z. M. & Lightowlers, R. N. Absence of expression from RNA internalised into electroporated mammalian mitochondria. *Mol Genet Genomics* **265**, 721-729 (2001).

411 Houshmand, M., Lindberg, C., Moslemi, A. R., Oldfors, A. & Holme, E. A novel heteroplasmic point mutation in the mitochondrial tRNA(Lys) gene in a sporadic case of mitochondrial encephalomyopathy: de novo mutation and no transmission to the offspring. *Hum Mutat* **13**, 203-209, doi:10.1002/(SICI)1098-1004(1999)13:3<203::AID-HUMU4>3.0.CO;2-3 (1999).

412 Blakely, E. L. *et al.* Sporadic myopathy and exercise intolerance associated with the mitochondrial 8328G>A tRNALys mutation. *J Neurol* **254**, 1283-1285, doi:10.1007/s00415-006-0490-7 (2007).

413 Dieteren, C. E., Koopman, W. J. & Nijtmans, L. G. Chapter 7 Tracing human mitochondrial complex I assembly by use of GFP-tagged subunits. *Methods Enzymol* **456**, 133-151, doi:10.1016/S0076-6879(08)04407-8 (2009).

414 Lazarou, M., Smith, S. M., Thorburn, D. R., Ryan, M. T. & McKenzie, M. Assembly of nuclear DNA-encoded subunits into mitochondrial complex IV, and their preferential integration into supercomplex forms in patient mitochondria. *FEBS J* **276**, 6701-6713, doi:10.1111/j.1742-4658.2009.07384.x (2009).

415 Smeitink, J. A. *et al.* Distinct clinical phenotypes associated with a mutation in the mitochondrial translation elongation factor EFTs. *Am J Hum Genet* **79**, 869-877, doi:10.1086/508434 (2006).

416 Agier, V. *et al.* Defective mitochondrial fusion, altered respiratory function, and distorted cristae structure in skin fibroblasts with heterozygous OPA1 mutations. *Biochim Biophys Acta* **1822**, 1570-1580, doi:10.1016/j.bbadis.2012.07.002 (2012).

417 Gerards, M. *et al.* Riboflavin-responsive oxidative phosphorylation complex I deficiency caused by defective ACAD9: new function for an old gene. *Brain* **134**, 210-219, doi:10.1093/brain/awq273 (2011).

418 Ma, Y. S., Chen, Y. C., Lu, C. Y., Liu, C. Y. & Wei, Y. H. Upregulation of matrix metalloproteinase 1 and disruption of mitochondrial network in skin fibroblasts of patients with MERRF syndrome. *Ann N Y Acad Sci* **1042**, 55-63, doi:10.1196/annals.1338.006 (2005).

419 Wilkins, H. M., Carl, S. M. & Swerdlow, R. H. Cytoplasmic hybrid (cybrid) cell lines as a practical model for mitochondriopathies. *Redox Biol* **2**, 619-631, doi:10.1016/j.redox.2014.03.006 (2014).

420 Chang, J. C. *et al.* Functional recovery of human cells harbouring the mitochondrial DNA mutation MERRF A8344G via peptide-mediated mitochondrial delivery. *Neurosignals* **21**, 160-173, doi:10.1159/000341981 (2013).

421 Duvezin-Caubet, S. *et al.* Proteolytic processing of OPA1 links mitochondrial dysfunction to alterations in mitochondrial morphology. *J Biol Chem* **281**, 37972-37979, doi:10.1074/jbc.M606059200 (2006).

422 Chuang, Y. C. *et al.* Mitochondrial Transfer from Wharton's Jelly Mesenchymal Stem Cell to MERRF Cybrid Reduces Oxidative Stress and Improves Mitochondrial Bioenergetics. *Oxid Med Cell Longev* **2017**, 5691215, doi:10.1155/2017/5691215 (2017).

423 Rommelaere, G. *et al.* Hypersensitivity of A8344G MERRF mutated cybrid cells to staurosporine-induced cell death is mediated by calcium-dependent activation of calpains. *Int J Biochem Cell Biol* **44**, 139-149, doi:10.1016/j.biocel.2011.10.009 (2012).

424 Dunbar, D. R., Moonie, P. A., Jacobs, H. T. & Holt, I. J. Different cellular backgrounds confer a marked advantage to either mutant or wild-type mitochondrial genomes. *Proc Natl Acad Sci U S A* **92**, 6562-6566 (1995).

425 Bourgeron, T., Chretien, D., Rotig, A., Munnich, A. & Rustin, P. Isolation and characterization of mitochondria from human B lymphoblastoid cell lines. *Biochem Biophys Res Commun* **186**, 16-23 (1992).

426 Sie, L., Loong, S. & Tan, E. K. Utility of lymphoblastoid cell lines. *J Neurosci Res* **87**, 1953-1959, doi:10.1002/jnr.22000 (2009).

427 Chang, J. C. *et al.* Treatment of human cells derived from MERRF syndrome by peptide-mediated mitochondrial delivery. *Cytotherapy* **15**, 1580-1596, doi:10.1016/j.jcyt.2013.06.008 (2013).

428 Jiang, J., Lee, E. J. & Schmittgen, T. D. Increased expression of microRNA-155 in Epstein-Barr virus transformed lymphoblastoid cell lines. *Genes Chromosomes Cancer* **45**, 103-106, doi:10.1002/gcc.20264 (2006).

429 Trenz, K., Landgraf, J. & Speit, G. Mutagen sensitivity of human lymphoblastoid cells with a BRCA1 mutation. *Breast Cancer Res Treat* **78**, 69-79 (2003).

430 Sugimoto, M., Tahara, H., Ide, T. & Furuichi, Y. Steps involved in immortalization and tumorigenesis in human B-lymphoblastoid cell lines transformed by Epstein-Barr virus. *Cancer Res* **64**, 3361-3364, doi:10.1158/0008-5472.CAN-04-0079 (2004).

431 Rusanen, H., Majamaa, K. & Hassinen, I. E. Increased activities of antioxidant enzymes and decreased ATP concentration in cultured myoblasts with the 3243A-->G mutation in mitochondrial DNA. *Biochim Biophys Acta* **1500**, 10-16 (2000).

432 Sasarman, F., Karpati, G. & Shoubridge, E. A. Nuclear genetic control of mitochondrial translation in skeletal muscle revealed in patients with mitochondrial myopathy. *Hum Mol Genet* **11**, 1669-1681 (2002).

433 Takahashi, K. *et al.* Induction of pluripotent stem cells from adult human fibroblasts by defined factors. *Cell* **131**, 861-872, doi:10.1016/j.cell.2007.11.019 (2007).

434 Kodaira, M. *et al.* Impaired respiratory function in MELAS-induced pluripotent stem cells with high heteroplasmy levels. *FEBS Open Bio* **5**, 219-225, doi:10.1016/j.fob.2015.03.008 (2015).

435 Liang, D. *et al.* Generation of MERRF patient-derived induced pluripotent stem cell line iMERRF-C7. *Stem Cell Res* **17**, 616-618, doi:10.1016/j.scr.2016.11.008 (2016).

436 Wu, Y. T. *et al.* Generation of an induced pluripotent stem cell (iPSC) line from a 40-year-old patient with the A8344G mutation of mitochondrial DNA and MERRF (myoclonic epilepsy with ragged red fibers) syndrome. *Stem Cell Res* **27**, 10-14, doi:10.1016/j.scr.2017.12.013 (2018).

437 Chou, S. J. *et al.* Generation of two isogenic human induced pluripotent stem cell lines from a 15year-old female patient with MERRF syndrome and A8344G mutation of mitochondrial DNA. *Stem Cell Res* **30**, 201-205, doi:10.1016/j.scr.2018.05.011 (2018).

438 Chou, S. J. *et al.* Impaired ROS Scavenging System in Human Induced Pluripotent Stem Cells Generated from Patients with MERRF Syndrome. *Sci Rep* **6**, 23661, doi:10.1038/srep23661 (2016).

439 Suhr, S. T. *et al.* Mitochondrial rejuvenation after induced pluripotency. *PLoS One* **5**, e14095, doi:10.1371/journal.pone.0014095 (2010).

440 Van Haute, L., Spits, C., Geens, M., Seneca, S. & Sermon, K. Human embryonic stem cells commonly display large mitochondrial DNA deletions. *Nat Biotechnol* **31**, 20-23, doi:10.1038/nbt.2473 (2013).

441 Chal, J. *et al.* Differentiation of pluripotent stem cells to muscle fiber to model Duchenne muscular dystrophy. *Nat Biotechnol* **33**, 962-969, doi:10.1038/nbt.3297 (2015).

442 O'Callaghan, B., Hanna, M. G., Morgan, J., Houlden, H. & Madej, M. In vitro modelling of mitochondrial disease using human induced pluripotent stem cell (hIPSC) derived myotubes harbouring mtDNA mutations

. *Neuromuscular Disorders*

28, doi:10.1016/S0960-8966(18)30386-9 (2018).

443 Sanchez-Danes, A. *et al.* Efficient generation of A9 midbrain dopaminergic neurons by lentiviral delivery of LMX1A in human embryonic stem cells and induced pluripotent stem cells. *Hum Gene Ther* **23**, 56-69, doi:10.1089/hum.2011.054 (2012).

444 Silva, M. C. *et al.* Human iPSC-Derived Neuronal Model of Tau-A152T Frontotemporal Dementia Reveals Tau-Mediated Mechanisms of Neuronal Vulnerability. *Stem Cell Reports* **7**, 325-340, doi:10.1016/j.stemcr.2016.08.001 (2016).

445 Jones, V. C., Atkinson-Dell, R., Verkhratsky, A. & Mohamet, L. Aberrant iPSC-derived human astrocytes in Alzheimer's disease. *Cell Death Dis* **8**, e2696, doi:10.1038/cddis.2017.89 (2017).

446 Smith, C. *et al.* Efficient and allele-specific genome editing of disease loci in human iPSCs. *Mol Ther* **23**, 570-577, doi:10.1038/mt.2014.226 (2015).

447 Lorenz, C. *et al.* Human iPSC-Derived Neural Progenitors Are an Effective Drug Discovery Model for Neurological mtDNA Disorders. *Cell Stem Cell* **20**, 659-674 e659, doi:10.1016/j.stem.2016.12.013 (2017).

448 WADDINGTON, C. H. *The strategy of the genes. A discussion of some aspects of theoretical biology*. (George Allen & Unwin, Ltd., 1957).

449 Takahashi, K. & Yamanaka, S. Induction of pluripotent stem cells from mouse embryonic and adult fibroblast cultures by defined factors. *Cell* **126**, 663-676, doi:10.1016/j.cell.2006.07.024 (2006).

450 Ladewig, J., Koch, P. & Brustle, O. Leveling Waddington: the emergence of direct programming and the loss of cell fate hierarchies. *Nat Rev Mol Cell Biol* **14**, 225-236, doi:10.1038/nrm3543 (2013).

451 Sieweke, M. H. Waddington's valleys and Captain Cook's islands. *Cell Stem Cell* **16**, 7-8, doi:10.1016/j.stem.2014.12.009 (2015).

452 Davis, R. L., Weintraub, H. & Lassar, A. B. Expression of a single transfected cDNA converts fibroblasts to myoblasts. *Cell* **51**, 987-1000 (1987).

453 Choi, J. *et al.* MyoD converts primary dermal fibroblasts, chondroblasts, smooth muscle, and retinal pigmented epithelial cells into striated mononucleated myoblasts and multinucleated myotubes. *Proc Natl Acad Sci U S A* **87**, 7988-7992 (1990).

454 Weintraub, H. *et al.* Activation of muscle-specific genes in pigment, nerve, fat, liver, and fibroblast cell lines by forced expression of MyoD. *Proc Natl Acad Sci U S A* **86**, 5434-5438 (1989).

455 Feng, R. *et al.* PU.1 and C/EBPalpha/beta convert fibroblasts into macrophage-like cells. *Proc Natl Acad Sci U S A* **105**, 6057-6062, doi:10.1073/pnas.0711961105 (2008).

456 Xie, H., Ye, M., Feng, R. & Graf, T. Stepwise reprogramming of B cells into macrophages. *Cell* **117**, 663-676 (2004).

457 Kulessa, H., Frampton, J. & Graf, T. GATA-1 reprograms avian myelomonocytic cell lines into eosinophils, thromboblasts, and erythroblasts. *Genes Dev* **9**, 1250-1262 (1995).

458 Ieda, M. *et al.* Direct reprogramming of fibroblasts into functional cardiomyocytes by defined factors. *Cell* **142**, 375-386, doi:10.1016/j.cell.2010.07.002 (2010).

459 Qian, L. *et al.* In vivo reprogramming of murine cardiac fibroblasts into induced cardiomyocytes. *Nature* **485**, 593-598, doi:10.1038/nature11044 (2012).

460 Song, K. *et al.* Heart repair by reprogramming non-myocytes with cardiac transcription factors. *Nature* **485**, 599-604, doi:10.1038/nature11139 (2012).

461 Jayawardena, T. M. *et al.* MicroRNA-mediated in vitro and in vivo direct reprogramming of cardiac fibroblasts to cardiomyocytes. *Circ Res* **110**, 1465-1473, doi:10.1161/CIRCRESAHA.112.269035 (2012).

462 Sapir, T. *et al.* Cell-replacement therapy for diabetes: Generating functional insulin-producing tissue from adult human liver cells. *Proc Natl Acad Sci U S A* **102**, 7964-7969, doi:10.1073/pnas.0405277102 (2005).

463 Horb, M. E., Shen, C. N., Tosh, D. & Slack, J. M. Experimental conversion of liver to pancreas. *Curr Biol* **13**, 105-115 (2003).

464 Zhou, Q., Brown, J., Kanarek, A., Rajagopal, J. & Melton, D. A. In vivo reprogramming of adult pancreatic exocrine cells to beta-cells. *Nature* **455**, 627-632, doi:10.1038/nature07314 (2008).

465 Heinrich, C. *et al.* Directing astroglia from the cerebral cortex into subtype specific functional neurons. *PLoS Biol* **8**, e1000373, doi:10.1371/journal.pbio.1000373 (2010).

466 Heins, N. *et al.* Glial cells generate neurons: the role of the transcription factor Pax6. *Nat Neurosci* **5**, 308-315, doi:10.1038/nn828 (2002).

467 Berninger, B. *et al.* Functional properties of neurons derived from in vitro reprogrammed postnatal astroglia. *J Neurosci* **27**, 8654-8664, doi:10.1523/JNEUROSCI.1615-07.2007 (2007).

468 Sekiya, S. & Suzuki, A. Direct conversion of mouse fibroblasts to hepatocyte-like cells by defined factors. *Nature* **475**, 390-393, doi:10.1038/nature10263 (2011).

469 Huang, P. *et al.* Induction of functional hepatocyte-like cells from mouse fibroblasts by defined factors. *Nature* **475**, 386-389, doi:10.1038/nature10116 (2011).

470 Drouin-Ouellet, J., Pircs, K., Barker, R. A., Jakobsson, J. & Parmar, M. Direct Neuronal Reprogramming for Disease Modeling Studies Using Patient-Derived Neurons: What Have We Learned? *Front Neurosci* **11**, 530, doi:10.3389/fnins.2017.00530 (2017).

471 Vierbuchen, T. *et al.* Direct conversion of fibroblasts to functional neurons by defined factors. *Nature* **463**, 1035-1041, doi:10.1038/nature08797 (2010).

472 Pang, Z. P. *et al.* Induction of human neuronal cells by defined transcription factors. *Nature* **476**, 220-223, doi:10.1038/nature10202 (2011).

473 Passeri, E. *et al.* Enhanced conversion of induced neuronal cells (iN cells) from human fibroblasts: Utility in uncovering cellular deficits in mental illness-associated chromosomal abnormalities. *Neurosci Res* **101**, 57-61, doi:10.1016/j.neures.2015.07.011 (2015).

474 Pfisterer, U. *et al.* Efficient induction of functional neurons from adult human fibroblasts. *Cell Cycle* **10**, 3311-3316, doi:10.4161/cc.10.19.17584 (2011).

475 Caiazzo, M. *et al.* Direct generation of functional dopaminergic neurons from mouse and human fibroblasts. *Nature* **476**, 224-227, doi:10.1038/nature10284 (2011).

476 Yoo, A. S. *et al.* MicroRNA-mediated conversion of human fibroblasts to neurons. *Nature* **476**, 228-231, doi:10.1038/nature10323 (2011).

477 Richner, M., Victor, M. B., Liu, Y., Abernathy, D. & Yoo, A. S. MicroRNA-based conversion of human fibroblasts into striatal medium spiny neurons. *Nat Protoc* **10**, 1543-1555, doi:10.1038/nprot.2015.102 (2015).

478 Victor, M. B. *et al.* Generation of human striatal neurons by microRNA-dependent direct conversion of fibroblasts. *Neuron* **84**, 311-323, doi:10.1016/j.neuron.2014.10.016 (2014).

479 Xue, Y. *et al.* Direct conversion of fibroblasts to neurons by reprogramming PTB-regulated microRNA circuits. *Cell* **152**, 82-96, doi:10.1016/j.cell.2012.11.045 (2013).

480 Jorgensen, H. F. *et al.* REST selectively represses a subset of RE1-containing neuronal genes in mouse embryonic stem cells. *Development* **136**, 715-721, doi:10.1242/dev.028548 (2009).

481 Ladewig, J. *et al.* Small molecules enable highly efficient neuronal conversion of human fibroblasts. *Nat Methods* **9**, 575-578, doi:10.1038/nmeth.1972 (2012).

482 Hu, W. *et al.* Direct Conversion of Normal and Alzheimer's Disease Human Fibroblasts into Neuronal Cells by Small Molecules. *Cell Stem Cell* **17**, 204-212, doi:10.1016/j.stem.2015.07.006 (2015).

483 Liu, M. L. *et al.* Small molecules enable neurogenin 2 to efficiently convert human fibroblasts into cholinergic neurons. *Nat Commun* **4**, 2183, doi:10.1038/ncomms3183 (2013).

484 Wang, P. *et al.* Generation of patient-specific induced neuronal cells using a direct reprogramming strategy. *Stem Cells Dev* **23**, 16-23, doi:10.1089/scd.2013.0131 (2014).

485 Hsu, Y. C. *et al.* Signaling adaptor protein SH2B1 enhances neurite outgrowth and accelerates the maturation of human induced neurons. *Stem Cells Transl Med* **3**, 713-722, doi:10.5966/sctm.2013-0111 (2014).

486 Xu, Z. *et al.* Direct conversion of human fibroblasts to induced serotonergic neurons. *Mol Psychiatry* **21**, 62-70, doi:10.1038/mp.2015.101 (2016).

487 Chanda, S. *et al.* Generation of induced neuronal cells by the single reprogramming factor ASCL1. *Stem Cell Reports* **3**, 282-296, doi:10.1016/j.stemcr.2014.05.020 (2014).

488 Marro, S. *et al.* Direct lineage conversion of terminally differentiated hepatocytes to functional neurons. *Cell Stem Cell* **9**, 374-382, doi:10.1016/j.stem.2011.09.002 (2011).

489 Iovino, M. *et al.* The novel MAPT mutation K298E: mechanisms of mutant tau toxicity, brain pathology and tau expression in induced fibroblast-derived neurons. *Acta Neuropathol* **127**, 283-295, doi:10.1007/s00401-013-1219-1 (2014).

490 Passeri, E. *et al.* Infection and characterization of Toxoplasma gondii in human induced neurons from patients with brain disorders and healthy controls. *Microbes Infect* **18**, 153-158, doi:10.1016/j.micinf.2015.09.023 (2016).

491 Siegert, S. *et al.* The schizophrenia risk gene product miR-137 alters presynaptic plasticity. *Nat Neurosci* **18**, 1008-1016, doi:10.1038/nn.4023 (2015).

492 Bavamian, S. *et al.* Dysregulation of miR-34a links neuronal development to genetic risk factors for bipolar disorder. *Mol Psychiatry* **20**, 573-584, doi:10.1038/mp.2014.176 (2015).

493 Karow, M. *et al.* Reprogramming of pericyte-derived cells of the adult human brain into induced neuronal cells. *Cell Stem Cell* **11**, 471-476, doi:10.1016/j.stem.2012.07.007 (2012).

494 Drouin-Ouellet, J. *et al.* REST suppression mediates neural conversion of adult human fibroblasts via microRNA-dependent and -independent pathways. *EMBO molecular medicine* **9**, 1117-1131, doi:10.15252/emmm.201607471 (2017).

495 Ambasudhan, R. *et al.* Direct reprogramming of adult human fibroblasts to functional neurons under defined conditions. *Cell Stem Cell* **9**, 113-118, doi:10.1016/j.stem.2011.07.002 (2011).

496 Sun, C. K. *et al.* Senescence impairs direct conversion of human somatic cells to neurons. *Nat Commun* **5**, 4112, doi:10.1038/ncomms5112 (2014).

497 Fiesel, F. C. *et al.* (Patho-)physiological relevance of PINK1-dependent ubiquitin phosphorylation. *EMBO Rep* **16**, 1114-1130, doi:10.15252/embr.201540514 (2015).

498 Puschmann, A. *et al.* Heterozygous PINK1 p.G411S increases risk of Parkinson's disease via a dominant-negative mechanism. *Brain* **140**, 98-117, doi:10.1093/brain/aww261 (2017).

499 Liu, Y. *et al.* Direct reprogramming of Huntington's disease patient fibroblasts into neuron-like cells leads to abnormal neurite outgrowth, increased cell death, and aggregate formation. *PLoS One* **9**, e109621, doi:10.1371/journal.pone.0109621 (2014).

500 Lim, S. M. *et al.* Directly converted patient-specific induced neurons mirror the neuropathology of FUS with disrupted nuclear localization in amyotrophic lateral sclerosis. *Mol Neurodegener* **11**, 8, doi:10.1186/s13024-016-0075-6 (2016).

501 Su, Z. *et al.* Discovery of a biomarker and lead small molecules to target r(GGGGCC)-associated defects in c9FTD/ALS. *Neuron* **83**, 1043-1050, doi:10.1016/j.neuron.2014.07.041 (2014).

502 Gascon, S. *et al.* Identification and Successful Negotiation of a Metabolic Checkpoint in Direct Neuronal Reprogramming. *Cell Stem Cell* **18**, 396-409, doi: (2016).

503 Masserdotti, G. *et al.* Transcriptional Mechanisms of Proneural Factors and REST in Regulating Neuronal Reprogramming of Astrocytes. *Cell Stem Cell* **17**, 74-88, doi:10.1016/j.stem.2015.05.014 (2015).

504 Colasante, G. *et al.* Rapid Conversion of Fibroblasts into Functional Forebrain GABAergic Interneurons by Direct Genetic Reprogramming. *Cell Stem Cell* **17**, 719-734, doi:10.1016/j.stem.2015.09.002 (2015).

505 Santambrogio, P. *et al.* Mitochondrial iron and energetic dysfunction distinguish fibroblasts and induced neurons from pantothenate kinase-associated neurodegeneration patients. *Neurobiol Dis* **81**, 144-153, doi:10.1016/j.nbd.2015.02.030 (2015).

506 Kim, J. *et al.* Functional integration of dopaminergic neurons directly converted from mouse fibroblasts. *Cell Stem Cell* **9**, 413-419, doi:10.1016/j.stem.2011.09.011 (2011).

507 Pfisterer, U. *et al.* Direct conversion of human fibroblasts to dopaminergic neurons. *Proc Natl Acad Sci U S A* **108**, 10343-10348, doi:10.1073/pnas.1105135108 (2011).

508 Sheng, C. *et al.* Generation of dopaminergic neurons directly from mouse fibroblasts and fibroblast-derived neural progenitors. *Cell Res* **22**, 769-772, doi:10.1038/cr.2012.32 (2012).

509 Addis, R. C. *et al.* Efficient conversion of astrocytes to functional midbrain dopaminergic neurons using a single polycistronic vector. *PLoS One* **6**, e28719, doi:10.1371/journal.pone.0028719 (2011).

510 Dell'Anno, M. T. *et al.* Remote control of induced dopaminergic neurons in parkinsonian rats. *J Clin Invest* **124**, 3215-3229, doi:10.1172/JCI74664 (2014).

511 Son, E. Y. *et al.* Conversion of mouse and human fibroblasts into functional spinal motor neurons. *Cell Stem Cell* **9**, 205-218, doi:10.1016/j.stem.2011.07.014 (2011).

512 Qin, H., Zhao, A., Ma, K. & Fu, X. Chemical conversion of human and mouse fibroblasts into motor neurons. *Sci China Life Sci* **61**, 1151-1167, doi:10.1007/s11427-018-9359-8 (2018).

513 Zhang, Q. J. *et al.* Modeling the phenotype of spinal muscular atrophy by the direct conversion of human fibroblasts to motor neurons. *Oncotarget* **8**, 10945-10953, doi:10.18632/oncotarget.14641 (2017).

514 Liu, Y. *et al.* Ascl1 Converts Dorsal Midbrain Astrocytes into Functional Neurons In Vivo. *J Neurosci* **35**, 9336-9355, doi:10.1523/JNEUROSCI.3975-14.2015 (2015).

515 Guo, Z. *et al.* In vivo direct reprogramming of reactive glial cells into functional neurons after brain injury and in an Alzheimer's disease model. *Cell Stem Cell* **14**, 188-202, doi:10.1016/j.stem.2013.12.001 (2014).

516 Zhang, L. *et al.* Small Molecules Efficiently Reprogram Human Astroglial Cells into Functional Neurons. *Cell Stem Cell* **17**, 735-747, doi:10.1016/j.stem.2015.09.012 (2015).

517 Vadodaria, K. C. *et al.* Generation of functional human serotonergic neurons from fibroblasts. *Mol Psychiatry* **21**, 49-61, doi:10.1038/mp.2015.161 (2016).

518 Wainger, B. J. *et al.* Modeling pain in vitro using nociceptor neurons reprogrammed from fibroblasts. *Nat Neurosci* **18**, 17-24, doi:10.1038/nn.3886 (2015).

519 Blanchard, J. W. *et al.* Selective conversion of fibroblasts into peripheral sensory neurons. *Nat Neurosci* **18**, 25-35, doi:10.1038/nn.3887 (2015).

520 Xue, Y. *et al.* Sequential regulatory loops as key gatekeepers for neuronal reprogramming in human cells. *Nat Neurosci* **19**, 807-815, doi:10.1038/nn.4297 (2016).

521 Pfisterer, U. *et al.* Small molecules increase direct neural conversion of human fibroblasts. *Sci Rep* **6**, 38290, doi:10.1038/srep38290 (2016).

522 Shrigley, S., Pircs, K., Barker, R. A., Parmar, M. & Drouin-Ouellet, J. Simple Generation of a High Yield Culture of Induced Neurons from Human Adult Skin Fibroblasts. *J Vis Exp*, doi:10.3791/56904 (2018).

523 Schwab, A. J. & Ebert, A. D. Neurite Aggregation and Calcium Dysfunction in iPSC-Derived Sensory Neurons with Parkinson's Disease-Related LRRK2 G2019S Mutation. *Stem Cell Reports* **5**, 1039-1052, doi:10.1016/j.stemcr.2015.11.004 (2015).

524 Mertens, J. *et al.* Directly Reprogrammed Human Neurons Retain Aging-Associated Transcriptomic Signatures and Reveal Age-Related Nucleocytoplasmic Defects. *Cell Stem Cell* **17**, 705-718, doi:10.1016/j.stem.2015.09.001 (2015).

525 Huh, C. J. *et al.* Maintenance of age in human neurons generated by microRNA-based neuronal conversion of fibroblasts. *Elife* **5**, doi:10.7554/eLife.18648 (2016).

526 Liu, M. L., Zang, T. & Zhang, C. L. Direct Lineage Reprogramming Reveals Disease-Specific Phenotypes of Motor Neurons from Human ALS Patients. *Cell Rep* **14**, 115-128, doi:10.1016/j.celrep.2015.12.018 (2016).

527 Horvath, S. DNA methylation age of human tissues and cell types. *Genome Biol* **14**, R115, doi:10.1186/gb-2013-14-10-r115 (2013).

528 Miura, K. *et al.* Variation in the safety of induced pluripotent stem cell lines. *Nat Biotechnol* **27**, 743-745, doi:10.1038/nbt.1554 (2009).

529 Torper, O. *et al.* Generation of induced neurons via direct conversion in vivo. *Proc Natl Acad Sci U S A* **110**, 7038-7043, doi:10.1073/pnas.1303829110 (2013).

530 Guo, S. *et al.* Nonstochastic reprogramming from a privileged somatic cell state. *Cell* **156**, 649-662, doi:10.1016/j.cell.2014.01.020 (2014).

531 Li, Z. & Rana, T. M. A kinase inhibitor screen identifies small-molecule enhancers of reprogramming and iPS cell generation. *Nat Commun* **3**, 1085, doi:10.1038/ncomms2059 (2012).

532 Fishman, V. S. *et al.* Cell divisions are not essential for the direct conversion of fibroblasts into neuronal cells. *Cell Cycle* **14**, 1188-1196, doi:10.1080/15384101.2015.1012875 (2015).

533 Price, J. D. *et al.* The Ink4a/Arf locus is a barrier to direct neuronal transdifferentiation. *J Neurosci* **34**, 12560-12567, doi:10.1523/JNEUROSCI.3159-13.2014 (2014).

534 Xiao, D. *et al.* Direct reprogramming of fibroblasts into neural stem cells by single non-neural progenitor transcription factor Ptf1a. *Nat Commun* **9**, 2865, doi:10.1038/s41467-018-05209-1 (2018).

535 Barker, R. A., Barrett, J., Mason, S. L. & Bjorklund, A. Fetal dopaminergic transplantation trials and the future of neural grafting in Parkinson's disease. *Lancet Neurol* **12**, 84-91, doi:10.1016/S1474-4422(12)70295-8 (2013).

536 Kefalopoulou, Z. *et al.* Long-term clinical outcome of fetal cell transplantation for Parkinson disease: two case reports. *JAMA Neurol* **71**, 83-87, doi:10.1001/jamaneurol.2013.4749 (2014).

537 Torper, O. & Gotz, M. Brain repair from intrinsic cell sources: Turning reactive glia into neurons. *Prog Brain Res* **230**, 69-97, doi:10.1016/bs.pbr.2016.12.010 (2017).

538 Buffo, A. *et al.* Expression pattern of the transcription factor Olig2 in response to brain injuries: implications for neuronal repair. *Proc Natl Acad Sci U S A* **102**, 18183-18188, doi:10.1073/pnas.0506535102 (2005).

539 Gascon, S., Masserdotti, G., Russo, G. L. & Gotz, M. Direct Neuronal Reprogramming: Achievements, Hurdles, and New Roads to Success. *Cell Stem Cell* **21**, 18-34, doi:10.1016/j.stem.2017.06.011 (2017).

540 Niu, W. *et al.* In vivo reprogramming of astrocytes to neuroblasts in the adult brain. *Nat Cell Biol* **15**, 1164-1175, doi:10.1038/ncb2843 (2013).

541 Niu, W. *et al.* SOX2 reprograms resident astrocytes into neural progenitors in the adult brain. *Stem Cell Reports* **4**, 780-794, doi:10.1016/j.stemcr.2015.03.006 (2015).

542 Brulet, R. *et al.* NEUROD1 Instructs Neuronal Conversion in Non-Reactive Astrocytes. *Stem Cell Reports* **8**, 1506-1515, doi:10.1016/j.stemcr.2017.04.013 (2017).

543 Su, Z., Niu, W., Liu, M. L., Zou, Y. & Zhang, C. L. In vivo conversion of astrocytes to neurons in the injured adult spinal cord. *Nat Commun* **5**, 3338, doi:10.1038/ncomms4338 (2014).

544 Wang, L. L. *et al.* The p53 Pathway Controls SOX2-Mediated Reprogramming in the Adult Mouse Spinal Cord. *Cell Rep* **17**, 891-903, doi:10.1016/j.celrep.2016.09.038 (2016).

545 Heinrich, C. *et al.* Sox2-mediated conversion of NG2 glia into induced neurons in the injured adult cerebral cortex. *Stem Cell Reports* **3**, 1000-1014, doi:10.1016/j.stemcr.2014.10.007 (2014).

546 Grande, A. *et al.* Environmental impact on direct neuronal reprogramming in vivo in the adult brain. *Nat Commun* **4**, 2373, doi:10.1038/ncomms3373 (2013).

547 Rivetti di Val Cervo, P. *et al.* Induction of functional dopamine neurons from human astrocytes in vitro and mouse astrocytes in a Parkinson's disease model. *Nat Biotechnol* **35**, 444-452, doi:10.1038/nbt.3835 (2017).

548 King, M. P. & Attardi, G. Human cells lacking mtDNA: repopulation with exogenous mitochondria by complementation. *Science* **246**, 500-503 (1989).

549 Zufferey, R., Nagy, D., Mandel, R. J., Naldini, L. & Trono, D. Multiply attenuated lentiviral vector achieves efficient gene delivery in vivo. *Nat Biotechnol* **15**, 871-875, doi:10.1038/nbt0997-871 (1997).

550 Georgievska, B. *et al.* Regulated delivery of glial cell line-derived neurotrophic factor into rat striatum, using a tetracycline-dependent lentiviral vector. *Hum Gene Ther* **15**, 934-944, doi:10.1089/hum.2004.15.934 (2004).

551 Liu, Y., Fiskum, G. & Schubert, D. Generation of reactive oxygen species by the mitochondrial electron transport chain. *J Neurochem* **80**, 780-787 (2002).

552 Kudin, A. P., Bimpong-Buta, N. Y., Vielhaber, S., Elger, C. E. & Kunz, W. S. Characterization of superoxide-producing sites in isolated brain mitochondria. *J Biol Chem* **279**, 4127-4135, doi:10.1074/jbc.M310341200 (2004).

553 DiMauro, S. Pathogenesis and treatment of mitochondrial myopathies: recent advances. *Acta Myol* **29**, 333-338 (2010).

554 Brandt, R. & Keston, A. S. Synthesis of Diacetyldichlorofluorescin: A Stable Reagent for Fluorometric Analysis. *Anal Biochem* **11**, 6-9 (1965).

555 Cathcart, R., Schwiers, E. & Ames, B. N. Detection of picomole levels of hydroperoxides using a fluorescent dichlorofluorescein assay. *Anal Biochem* **134**, 111-116 (1983).

556 Jakubowski, W. & Bartosz, G. 2,7-dichlorofluorescin oxidation and reactive oxygen species: what does it measure? *Cell Biol Int* **24**, 757-760, doi:10.1006/cbir.2000.0556 (2000).

557 Vowells, S. J., Sekhsaria, S., Malech, H. L., Shalit, M. & Fleisher, T. A. Flow cytometric analysis of the granulocyte respiratory burst: a comparison study of fluorescent probes. *J Immunol Methods* **178**, 89-97 (1995).

558 Oksvold, M. P., Skarpen, E., Widerberg, J. & Huitfeldt, H. S. Fluorescent histochemical techniques for analysis of intracellular signaling. *J Histochem Cytochem* **50**, 289-303, doi:10.1177/002215540205000301 (2002).

559 Lowry, O. H., Rosebrough, N. J., Farr, A. L. & Randall, R. J. Protein measurement with the Folin phenol reagent. *J Biol Chem* **193**, 265-275 (1951).

560 Bowman, P. D., Meek, R. L. & Daniel, C. W. Aging of human fibroblasts in vitro. Correlations between DNA synthetic ability and cell size. *Exp Cell Res* **93**, 184-190 (1975).

561 Cottet-Rousselle, C., Ronot, X., Leverve, X. & Mayol, J. F. Cytometric assessment of mitochondria using fluorescent probes. *Cytometry A* **79**, 405-425, doi:10.1002/cyto.a.21061 (2011).

562 Leonard, A. P. *et al.* Quantitative analysis of mitochondrial morphology and membrane potential in living cells using high-content imaging, machine learning, and morphological binning. *Biochim Biophys Acta* **1853**, 348-360, doi:10.1016/j.bbamcr.2014.11.002 (2015).

563 Pampliega, O. *et al.* Functional interaction between autophagy and ciliogenesis. *Nature* **502**, 194-200, doi:10.1038/nature12639 (2013).

564 Davies, K. J., Delsignore, M. E. & Lin, S. W. Protein damage and degradation by oxygen radicals. II. Modification of amino acids. *J Biol Chem* **262**, 9902-9907 (1987).

565 Stadtman, E. R. Oxidation of free amino acids and amino acid residues in proteins by radiolysis and by metal-catalyzed reactions. *Annu Rev Biochem* **62**, 797-821, doi:10.1146/annurev.bi.62.070193.004053 (1993).

566 Levine, R. L. Oxidative modification of glutamine synthetase. I. Inactivation is due to loss of one histidine residue. *J Biol Chem* **258**, 11823-11827 (1983).

567 Farber, J. M. & Levine, R. L. Sequence of a peptide susceptible to mixed-function oxidation. Probable cation binding site in glutamine synthetase. *J Biol Chem* **261**, 4574-4578 (1986).

568 Oliver, C. N. Inactivation of enzymes and oxidative modification of proteins by stimulated neutrophils. *Arch Biochem Biophys* **253**, 62-72 (1987).

569 Pognonec, P., Kato, H. & Roeder, R. G. The helix-loop-helix/leucine repeat transcription factor USF can be functionally regulated in a redox-dependent manner. *J Biol Chem* **267**, 24563-24567 (1992).

570 Wolff, S. P. & Dean, R. T. Fragmentation of proteins by free radicals and its effect on their susceptibility to enzymic hydrolysis. *Biochem J* **234**, 399-403 (1986).

571 Rivett, A. J. Regulation of intracellular protein turnover: covalent modification as a mechanism of marking proteins for degradation. *Curr Top Cell Regul* **28**, 291-337 (1986).

572 Merrill, R. A., Flippo, K. H. & Strack, S. Measuring Mitochondrial Shape with ImageJ. **123**, 31-48, doi:10.1007/978-1-4939-6890-9_2 (2017).

573 Longair, M. H., Baker, D. A. & Armstrong, J. D. Simple Neurite Tracer: open source software for reconstruction, visualization and analysis of neuronal processes. *Bioinformatics* **27**, 2453-2454, doi:10.1093/bioinformatics/btr390 (2011).

574 Nicholls, D. G. *et al.* Bioenergetic profile experiment using C2C12 myoblast cells. *J Vis Exp*, doi:10.3791/2511 (2010).

575 Chen, R. S., Huang, C. C. & Chu, N. S. Coenzyme Q10 treatment in mitochondrial encephalomyopathies. Short-term double-blind, crossover study. *Eur Neurol* **37**, 212-218, doi:10.1159/000117445 (1997).

576 Bresolin, N. *et al.* Ubidecarenone in the treatment of mitochondrial myopathies: a multi-center double-blind trial. *J Neurol Sci* **100**, 70-78 (1990).

577 Vander Heiden, M. G., Chandel, N. S., Williamson, E. K., Schumacker, P. T. & Thompson, C. B. Bcl-xL regulates the membrane potential and volume homeostasis of mitochondria. *Cell* **91**, 627-637 (1997).

578 Mattiazzi, M. *et al.* The mtDNA T8993G (NARP) mutation results in an impairment of oxidative phosphorylation that can be improved by antioxidants. *Hum Mol Genet* **13**, 869-879, doi:10.1093/hmg/ddh103 (2004).

579 Szczepanowska, J., Malinska, D., Wieckowski, M. R. & Duszynski, J. Effect of mtDNA point mutations on cellular bioenergetics. *Biochim Biophys Acta* **1817**, 1740-1746, doi:10.1016/j.bbabio.2012.02.028 (2012).

580 Filomeni, G., De Zio, D. & Cecconi, F. Oxidative stress and autophagy: the clash between damage and metabolic needs. *Cell Death Differ* **22**, 377-388, doi:10.1038/cdd.2014.150 (2015).

581 Lee, J., Giordano, S. & Zhang, J. Autophagy, mitochondria and oxidative stress: cross-talk and redox signalling. *Biochem J* **441**, 523-540, doi:10.1042/BJ20111451 (2012).

582 Zhao, B. *et al.* Mitochondrial dysfunction activates the AMPK signaling and autophagy to promote cell survival. *Genes Dis* **3**, 82-87, doi:10.1016/j.gendis.2015.12.002 (2016).

583 Wu, S. B. & Wei, Y. H. AMPK-mediated increase of glycolysis as an adaptive response to oxidative stress in human cells: implication of the cell survival in mitochondrial diseases. *Biochim Biophys Acta* **1822**, 233-247, doi:10.1016/j.bbadis.2011.09.014 (2012).

584 Wu, S. B., Wu, Y. T., Wu, T. P. & Wei, Y. H. Role of AMPK-mediated adaptive responses in human cells with mitochondrial dysfunction to oxidative stress. *Biochim Biophys Acta* **1840**, 1331-1344, doi:10.1016/j.bbagen.2013.10.034 (2014).

585 Hawley, S. A. *et al.* Characterization of the AMP-activated protein kinase kinase from rat liver and identification of threonine 172 as the major site at which it phosphorylates AMP-activated protein kinase. *J Biol Chem* **271**, 27879-27887 (1996).

586 Lee, S. K. *et al.* Coenzyme Q10 increases the fatty acid oxidation through AMPK-mediated PPARalpha induction in 3T3-L1 preadipocytes. *Cell Signal* **24**, 2329-2336, doi:10.1016/j.cellsig.2012.07.022 (2012).

587 Tsai, H. Y. *et al.* Coenzyme Q10 Attenuates High Glucose-Induced Endothelial Progenitor Cell Dysfunction through AMP-Activated Protein Kinase Pathways. *J Diabetes Res* **2016**, 6384759, doi:10.1155/2016/6384759 (2016).

588 Narendra, D., Tanaka, A., Suen, D.-F. & Youle, R. J. Parkin is recruited selectively to impaired mitochondria and promotes their autophagy. *The Journal of Cell Biology* **183**, 795-803, doi:10.1083/jcb.200809125 (2008).

589 Hershko, A. & Ciechanover, A. The ubiquitin system. *Annu Rev Biochem* **67**, 425-479, doi:10.1146/annurev.biochem.67.1.425 (1998).

590 Segref, A. *et al.* Pathogenesis of human mitochondrial diseases is modulated by reduced activity of the ubiquitin/proteasome system. *Cell Metab* **19**, 642-652, doi:10.1016/j.cmet.2014.01.016 (2014).

591 Vilchez, D., Saez, I. & Dillin, A. The role of protein clearance mechanisms in organismal ageing and age-related diseases. *Nat Commun* **5**, 5659, doi:10.1038/ncomms6659 (2014).

592 Zhang, Y. *et al.* Parkin functions as an E2-dependent ubiquitin- protein ligase and promotes the degradation of the synaptic vesicle-associated protein, CDCrel-1. *Proc Natl Acad Sci U S A* **97**, 13354-13359, doi:10.1073/pnas.240347797 (2000).

593 Shimura, H. *et al.* Familial Parkinson disease gene product, parkin, is a ubiquitin-protein ligase. *Nat Genet* **25**, 302-305, doi:10.1038/77060 (2000).

594 Seranova, E. *et al.* Dysregulation of autophagy as a common mechanism in lysosomal storage diseases. *Essays Biochem* **61**, 733-749, doi:10.1042/EBC20170055 (2017).

595 Hsieh, C. W. *et al.* Impaired autophagic flux and its related inflammation in patients with adult-onset Still's disease. *Oncotarget* **9**, 110-121, doi:10.18632/oncotarget.23098 (2018).

596 Cuervo, A. M., Stefanis, L., Fredenburg, R., Lansbury, P. T. & Sulzer, D. Impaired degradation of mutant alpha-synuclein by chaperone-mediated autophagy. *Science* **305**, 1292-1295, doi:10.1126/science.1101738 (2004).

597 Bordi, M. *et al.* Autophagy flux in CA1 neurons of Alzheimer hippocampus: Increased induction overburdens failing lysosomes to propel neuritic dystrophy. *Autophagy* **12**, 2467-2483, doi:10.1080/15548627.2016.1239003 (2016).

598 Jang, M. *et al.* AMPK contributes to autophagosome maturation and lysosomal fusion. *Sci Rep* **8**, 12637, doi:10.1038/s41598-018-30977-7 (2018).

599 Dai, S. *et al.* Methyl-beta-cyclodextrin restores impaired autophagy flux in Niemann-Pick C1-deficient cells through activation of AMPK. *Autophagy* **13**, 1435-1451, doi:10.1080/15548627.2017.1329081 (2017).

600 Han, X. *et al.* AMPK activation protects cells from oxidative stress-induced senescence via autophagic flux restoration and intracellular NAD(+) elevation. *Aging Cell* **15**, 416-427, doi:10.1111/acel.12446 (2016).

601 Garrido-Maraver, J. *et al.* Coenzyme q10 therapy. *Mol Syndromol* **5**, 187-197, doi:10.1159/000360101 (2014).

602 Gewirtz, D. A. Autophagy and senescence in cancer therapy. *J Cell Physiol* **229**, 6-9, doi:10.1002/jcp.24420 (2014).

603 Mita, M. M., Mita, A. & Rowinsky, E. K. Mammalian target of rapamycin: a new molecular target for breast cancer. *Clin Breast Cancer* **4**, 126-137 (2003).

604 Oshiro, N. *et al.* Dissociation of raptor from mTOR is a mechanism of rapamycin-induced inhibition of mTOR function. *Genes Cells* **9**, 359-366, doi:10.1111/j.1356-9597.2004.00727.x (2004).

605 Sarbassov, D. D. *et al.* Prolonged rapamycin treatment inhibits mTORC2 assembly and Akt/PKB. *Mol Cell* **22**, 159-168, doi:10.1016/j.molcel.2006.03.029 (2006).

606 Faivre, S., Kroemer, G. & Raymond, E. Current development of mTOR inhibitors as anticancer agents. *Nat Rev Drug Discov* **5**, 671-688, doi:10.1038/nrd2062 (2006).

607 Zhou, H. Y. & Huang, S. L. Current development of the second generation of mTOR inhibitors as anticancer agents. *Chin J Cancer* **31**, 8-18, doi:10.5732/cjc.011.10281 (2012).

608 Petroulakis, E., Mamane, Y., Le Bacquer, O., Shahbazian, D. & Sonenberg, N. mTOR signaling: implications for cancer and anticancer therapy. *Br J Cancer* **96 Suppl**, R11-15 (2007).

609 Ye, X., Sun, X., Starovoytov, V. & Cai, Q. Parkin-mediated mitophagy in mutant hAPP neurons and Alzheimer's disease patient brains. *Hum Mol Genet* **24**, 2938-2951, doi:10.1093/hmg/ddv056 (2015).

610 Martin-Maestro, P., Gargini, R., Perry, G., Avila, J. & Garcia-Escudero, V. PARK2 enhancement is able to compensate mitophagy alterations found in sporadic Alzheimer's disease. *Hum Mol Genet* **25**, 792-806, doi:10.1093/hmg/ddv616 (2016).

611 Martinez-Vicente, M. *et al.* Cargo recognition failure is responsible for inefficient autophagy in Huntington's disease. *Nat Neurosci* **13**, 567-576, doi:10.1038/nn.2528 (2010).

612 Wong, Y. C. & Holzbaur, E. L. The regulation of autophagosome dynamics by huntingtin and HAP1 is disrupted by expression of mutant huntingtin, leading to defective cargo degradation. *J Neurosci* **34**, 1293-1305, doi:10.1523/JNEUROSCI.1870-13.2014 (2014).

613 Parikh, S. M. *et al.* Mitochondrial function and disturbances in the septic kidney. *Semin Nephrol* **35**, 108-119, doi:10.1016/j.semnephrol.2015.01.011 (2015).

614 Sinha, R. A. & Yen, P. M. Thyroid hormone-mediated autophagy and mitochondrial turnover in NAFLD. *Cell Biosci* **6**, 46, doi:10.1186/s13578-016-0113-7 (2016).

615 Smith, B. K. *et al.* Treatment of nonalcoholic fatty liver disease: role of AMPK. *Am J Physiol Endocrinol Metab* **311**, E730-E740, doi:10.1152/ajpendo.00225.2016 (2016).

616 Mizumura, K. *et al.* Mitophagy-dependent necroptosis contributes to the pathogenesis of COPD. *J Clin Invest* **124**, 3987-4003, doi:10.1172/JCI74985 (2014).

617 Cloonan, S. M. & Choi, A. M. Mitochondria in lung disease. *J Clin Invest* **126**, 809-820, doi:10.1172/JCI81113 (2016).

618 Bravo-San Pedro, J. M., Kroemer, G. & Galluzzi, L. Autophagy and Mitophagy in Cardiovascular Disease. *Circ Res* **120**, 1812-1824, doi:10.1161/CIRCRESAHA.117.311082 (2017).

619 Baines, C. P. *et al.* Loss of cyclophilin D reveals a critical role for mitochondrial permeability transition in cell death. *Nature* **434**, 658-662, doi:10.1038/nature03434 (2005).

620 Sanchez-Alcazar, J. A. *et al.* The apoptotic microtubule network preserves plasma membrane integrity during the execution phase of apoptosis. *Apoptosis* **12**, 1195-1208, doi:10.1007/s10495-006-0044-6 (2007).

621 Oropesa-Avila, M. *et al.* Apoptotic microtubules delimit an active caspase free area in the cellular cortex during the execution phase of apoptosis. *Cell Death Dis* **4**, e527, doi:10.1038/cddis.2013.58 (2013).

622 Alvarez-Cordoba, M. *et al.* Pantothenate Rescues Iron Accumulation in Pantothenate Kinase-Associated Neurodegeneration Depending on the Type of Mutation. *Mol Neurobiol*, doi:10.1007/s12035-018-1333-0 (2018).

623 Teves, J. M. Y. *et al.* Parkinson's Disease Skin Fibroblasts Display Signature Alterations in Growth, Redox Homeostasis, Mitochondrial Function, and Autophagy. *Front Neurosci* **11**, 737, doi:10.3389/fnins.2017.00737 (2017).

624 Gardiner, S. L. *et al.* Bioenergetics in fibroblasts of patients with Huntington disease are associated with age at onset. *Neurol Genet* **4**, e275, doi:10.1212/NXG.0000000000000275 (2018).

625 Perez, M. J., Ponce, D. P., Osorio-Fuentealba, C., Behrens, M. I. & Quintanilla, R. A. Mitochondrial Bioenergetics Is Altered in Fibroblasts from Patients with Sporadic Alzheimer's Disease. *Front Neurosci* **11**, 553, doi:10.3389/fnins.2017.00553 (2017).

626 Zhou, C., Huang, Y. & Przedborski, S. Oxidative stress in Parkinson's disease: a mechanism of pathogenic and therapeutic significance. *Ann N Y Acad Sci* **1147**, 93-104, doi:10.1196/annals.1427.023 (2008).

627 Wang, X. *et al.* Oxidative stress and mitochondrial dysfunction in Alzheimer's disease. *Biochim Biophys Acta* **1842**, 1240-1247, doi:10.1016/j.bbadis.2013.10.015 (2014).

628 Perez-Severiano, F. *et al.* Increased formation of reactive oxygen species, but no changes in glutathione peroxidase activity, in striata of mice transgenic for the Huntington's disease mutation. *Neurochem Res* **29**, 729-733 (2004).

629 Chen, C. Y. *et al.* Decreased heat shock protein 27 expression and altered autophagy in human cells harboring A8344G mitochondrial DNA mutation. *Mitochondrion* **11**, 739-749, doi:10.1016/j.mito.2011.05.014 (2011).

630 Forte, M. & Bernardi, P. Genetic dissection of the permeability transition pore. *J Bioenerg Biomembr* **37**, 121-128 (2005).

631 Zoratti, M. & Szabo, I. The mitochondrial permeability transition. *Biochimica et biophysica acta* **1241**, 139-176 (1995).

632 Heddi, A., Stepien, G., Benke, P. J. & Wallace, D. C. Coordinate induction of energy gene expression in tissues of mitochondrial disease patients. *J Biol Chem* **274**, 22968-22976 (1999).

633 Lin, D. S. *et al.* Inflexibility of AMPK-mediated metabolic reprogramming in mitochondrial disease. *Oncotarget* **8**, 73627-73639, doi:10.18632/oncotarget.20617 (2017).

634 Toyama, E. Q. *et al.* Metabolism. AMP-activated protein kinase mediates mitochondrial fission in response to energy stress. *Science* **351**, 275-281, doi:10.1126/science.aab4138 (2016).

635 Tsai, K. L. *et al.* Coenzyme Q10 suppresses oxLDL-induced endothelial oxidative injuries by the modulation of LOX-1-mediated ROS generation via the AMPK/PKC/NADPH oxidase signaling pathway. *Mol Nutr Food Res* **55 Suppl 2**, S227-240, doi:10.1002/mnfr.201100147 (2011).

636 Xu, Z. *et al.* Coenzyme Q10 Improves Lipid Metabolism and Ameliorates Obesity by Regulating CaMKII-Mediated PDE4 Inhibition. *Sci Rep* **7**, 8253, doi:10.1038/s41598-017-08899-7 (2017).

637 Tian, G. *et al.* Ubiquinol-10 supplementation activates mitochondria functions to decelerate senescence in senescence-accelerated mice. *Antioxid Redox Signal* **20**, 2606-2620, doi:10.1089/ars.2013.5406 (2014).

638 Zhao, C. *et al.* Drp1-dependent mitophagy protects against cisplatin-induced apoptosis of renal tubular epithelial cells by improving mitochondrial function. *Oncotarget* **8**, 20988-21000, doi:10.18632/oncotarget.15470 (2017).

639 Tanaka, A. *et al.* Proteasome and p97 mediate mitophagy and degradation of mitofusins induced by Parkin. *J Cell Biol* **191**, 1367-1380, doi:10.1083/jcb.201007013 (2010).

640 Gomes, L. C., Di Benedetto, G. & Scorrano, L. During autophagy mitochondria elongate, are spared from degradation and sustain cell viability. *Nat Cell Biol* **13**, 589-598, doi:10.1038/ncb2220 (2011).

641 Rambold, A. S., Kostelecky, B., Elia, N. & Lippincott-Schwartz, J. Tubular network formation protects mitochondria from autophagosomal degradation during nutrient starvation. *Proc Natl Acad Sci U S A* **108**, 10190-10195, doi:10.1073/pnas.1107402108 (2011).

642 Suarez-Rivero, J. M. *et al.* Mitochondrial Dynamics in Mitochondrial Diseases. *Diseases* **5**, doi:10.3390/diseases5010001 (2016).

643 Wang, H. *et al.* Parkin ubiquitinates Drp1 for proteasome-dependent degradation: implication of dysregulated mitochondrial dynamics in Parkinson disease. *J Biol Chem* **286**, 11649-11658, doi:10.1074/jbc.M110.144238 (2011).

644 Song, W. *et al.* Mutant huntingtin binds the mitochondrial fission GTPase dynamin-related protein-1 and increases its enzymatic activity. *Nat Med* **17**, 377-382, doi:10.1038/nm.2313 (2011).

645 Shirendeb, U. *et al.* Abnormal mitochondrial dynamics, mitochondrial loss and mutant huntingtin oligomers in Huntington's disease: implications for selective neuronal damage. *Hum Mol Genet* **20**, 1438-1455, doi:10.1093/hmg/ddr024 (2011).

646 Xie, N. *et al.* A selective inhibitor of Drp1, mdivi-1, protects against cell death of hippocampal neurons in pilocarpine-induced seizures in rats. *Neurosci Lett* **545**, 64-68, doi:10.1016/j.neulet.2013.04.026 (2013).

647 Zhang, N., Wang, S., Li, Y., Che, L. & Zhao, Q. A selective inhibitor of Drp1, mdivi-1, acts against cerebral ischemia/reperfusion injury via an anti-apoptotic pathway in rats. *Neurosci Lett* **535**, 104-109, doi:10.1016/j.neulet.2012.12.049 (2013).

648 Tang, W. X., Wu, W. H., Qiu, H. Y., Bo, H. & Huang, S. M. Amelioration of rhabdomyolysis-induced renal mitochondrial injury and apoptosis through suppression of Drp-1 translocation. *J Nephrol* **26**, 1073-1082, doi:10.5301/jn.5000268 (2013).

649 Qi, X., Qvit, N., Su, Y. C. & Mochly-Rosen, D. A novel Drp1 inhibitor diminishes aberrant mitochondrial fission and neurotoxicity. *J Cell Sci* **126**, 789-802, doi:10.1242/jcs.114439 (2013).

650 Guo, X. *et al.* Inhibition of mitochondrial fragmentation diminishes Huntington's disease-associated neurodegeneration. *J Clin Invest* **123**, 5371-5388, doi:10.1172/JCI70911 (2013).

651 Gao, D. *et al.* Dynasore protects mitochondria and improves cardiac lusitropy in Langendorff perfused mouse heart. *PLoS One* **8**, e60967, doi:10.1371/journal.pone.0060967 (2013).

652 Khandelwal, P. J., Herman, A. M., Hoe, H. S., Rebeck, G. W. & Moussa, C. E. Parkin mediates beclin-dependent autophagic clearance of defective mitochondria and ubiquitinated Abeta in AD models. *Hum Mol Genet* **20**, 2091-2102, doi:10.1093/hmg/ddr091 (2011).

653 Wang, L. *et al.* Synaptosomal Mitochondrial Dysfunction in 5xFAD Mouse Model of Alzheimer's Disease. *PLoS One* **11**, e0150441, doi:10.1371/journal.pone.0150441 (2016).

654 Wang, Y. *et al.* PINK1/Parkin-mediated mitophagy is activated in cisplatin nephrotoxicity to protect against kidney injury. *Cell Death Dis* **9**, 1113, doi:10.1038/s41419-018-1152-2 (2018).

655 Linnane, A. W., Marzuki, S., Ozawa, T. & Tanaka, M. Mitochondrial DNA mutations as an important contributor to ageing and degenerative diseases. *Lancet* **1**, 642-645 (1989).

656 Arnheim, N. & Cortopassi, G. Deleterious mitochondrial DNA mutations accumulate in aging human tissues. *Mutat Res* **275**, 157-167 (1992).

657 Li, M., Schroder, R., Ni, S., Madea, B. & Stoneking, M. Extensive tissue-related and allele-related mtDNA heteroplasmy suggests positive selection for somatic mutations. *Proc Natl Acad Sci U S A* **112**, 2491-2496, doi:10.1073/pnas.1419651112 (2015).

658 Ding, J. *et al.* Assessing Mitochondrial DNA Variation and Copy Number in Lymphocytes of ~2,000 Sardinians Using Tailored Sequencing Analysis Tools. *PLoS Genet* **11**, e1005306, doi:10.1371/journal.pgen.1005306 (2015).

659 Willems, P. H., Rossignol, R., Dieteren, C. E., Murphy, M. P. & Koopman, W. J. Redox Homeostasis and Mitochondrial Dynamics. *Cell Metab* **22**, 207-218, doi:10.1016/j.cmet.2015.06.006 (2015).

660 Greene, J. C., Whitworth, A. J., Andrews, L. A., Parker, T. J. & Pallanck, L. J. Genetic and genomic studies of Drosophila parkin mutants implicate oxidative stress and innate immune responses in pathogenesis. *Hum Mol Genet* **14**, 799-811, doi:10.1093/hmg/ddi074 (2005).

661 Pesah, Y. *et al.* Drosophila parkin mutants have decreased mass and cell size and increased sensitivity to oxygen radical stress. *Development* **131**, 2183-2194, doi:10.1242/dev.01095 (2004).

662 Palacino, J. J. *et al.* Mitochondrial dysfunction and oxidative damage in parkin-deficient mice. *J Biol Chem* **279**, 18614-18622, doi:10.1074/jbc.M401135200 (2004).

663 Flinn, L. *et al.* Complex I deficiency and dopaminergic neuronal cell loss in parkin-deficient zebrafish (Danio rerio). *Brain* **132**, 1613-1623, doi:10.1093/brain/awp108 (2009).

664 Mortiboys, H. *et al.* Mitochondrial function and morphology are impaired in parkin-mutant fibroblasts. *Ann Neurol* **64**, 555-565, doi:10.1002/ana.21492 (2008).

665 Biosa, A. *et al.* Superoxide dismutating molecules rescue the toxic effects of PINK1 and parkin loss. *Hum Mol Genet* **27**, 1618-1629, doi:10.1093/hmg/ddy069 (2018).

666 Zhang, Z. *et al.* Parkin-mediated mitophagy as a potential therapeutic target for intervertebral disc degeneration. *Cell Death Dis* **9**, 980, doi:10.1038/s41419-018-1024-9 (2018).

667 Gautier, C. A., Kitada, T. & Shen, J. Loss of PINK1 causes mitochondrial functional defects and increased sensitivity to oxidative stress. *Proc Natl Acad Sci U S A* **105**, 11364-11369, doi:10.1073/pnas.0802076105 (2008).

668 Vives-Bauza, C. & Przedborski, S. Mitophagy: the latest problem for Parkinson's disease. *Trends Mol Med* **17**, 158-165, doi:10.1016/j.molmed.2010.11.002 (2011).

669 Wong, Y. C. & Holzbaur, E. L. Optineurin is an autophagy receptor for damaged mitochondria in parkin-mediated mitophagy that is disrupted by an ALS-linked mutation. *Proc Natl Acad Sci U S A* **111**, E4439-4448, doi:10.1073/pnas.1405752111 (2014).

670 Moore, A. S. & Holzbaur, E. L. Dynamic recruitment and activation of ALS-associated TBK1 with its target optineurin are required for efficient mitophagy. *Proc Natl Acad Sci U S A* **113**, E3349-3358, doi:10.1073/pnas.1523810113 (2016).

671 Schieke, S. M. *et al.* The mammalian target of rapamycin (mTOR) pathway regulates mitochondrial oxygen consumption and oxidative capacity. *J Biol Chem* **281**, 27643-27652, doi:10.1074/jbc.M603536200 (2006).

672 Cunningham, J. T. *et al.* mTOR controls mitochondrial oxidative function through a YY1-PGC-1alpha transcriptional complex. *Nature* **450**, 736-740, doi:10.1038/nature06322 (2007).

673 Ramanathan, A. & Schreiber, S. L. Direct control of mitochondrial function by mTOR. *Proc Natl Acad Sci U S A* **106**, 22229-22232, doi:10.1073/pnas.0912074106 (2009).

674 Fang, Y. *et al.* Duration of rapamycin treatment has differential effects on metabolism in mice. *Cell Metab* **17**, 456-462, doi:10.1016/j.cmet.2013.02.008 (2013).

675 Zheng, X. *et al.* Alleviation of neuronal energy deficiency by mTOR inhibition as a treatment for mitochondria-related neurodegeneration. *Elife* **5**, doi:10.7554/eLife.13378 (2016).

676 Johnson, S. C. *et al.* Dose-dependent effects of mTOR inhibition on weight and mitochondrial disease in mice. *Front Genet* **6**, 247, doi:10.3389/fgene.2015.00247 (2015).

677 Felici, R. *et al.* Post onset, oral rapamycin treatment delays development of mitochondrial encephalopathy only at supramaximal doses. *Neuropharmacology* **117**, 74-84, doi:10.1016/j.neuropharm.2017.01.039 (2017).

678 Wang, A., Mouser, J., Pitt, J., Promislow, D. & Kaeberlein, M. Rapamycin enhances survival in a Drosophila model of mitochondrial disease. *Oncotarget* **7**, 80131-80139, doi:10.18632/oncotarget.12560 (2016).

679 Foster, D. A. & Toschi, A. Targeting mTOR with rapamycin: one dose does not fit all. *Cell Cycle* **8**, 1026-1029, doi:10.4161/cc.8.7.8044 (2009).

680 Wan, X., Harkavy, B., Shen, N., Grohar, P. & Helman, L. J. Rapamycin induces feedback activation of Akt signaling through an IGF-1R-dependent mechanism. *Oncogene* **26**, 1932-1940, doi:10.1038/sj.onc.1209990 (2007).

681 Lerner, C. *et al.* Reduced mammalian target of rapamycin activity facilitates mitochondrial retrograde signaling and increases life span in normal human fibroblasts. *Aging Cell* **12**, 966-977, doi:10.1111/acel.12122 (2013).

682 Civiletto, G. *et al.* Rapamycin rescues mitochondrial myopathy via coordinated activation of autophagy and lysosomal biogenesis. *EMBO molecular medicine* **10**, doi:10.15252/emmm.201708799 (2018).

683 Civiletto, G. *et al.* Opa1 overexpression ameliorates the phenotype of two mitochondrial disease mouse models. *Cell Metab* **21**, 845-854, doi:10.1016/j.cmet.2015.04.016 (2015).

684 Komatsu, M. *et al.* The selective autophagy substrate p62 activates the stress responsive transcription factor Nrf2 through inactivation of Keap1. *Nat Cell Biol* **12**, 213-223, doi:10.1038/ncb2021 (2010).

685 Zambelli, F. & Spits, C. A step forward in disease modelling for mitochondrial diseases. *Stem Cell Investig* **4**, 89, doi:10.21037/sci.2017.10.06 (2017).

686 Inak, G. *et al.* Concise Review: Induced Pluripotent Stem Cell-Based Drug Discovery for Mitochondrial Disease. *Stem Cells* **35**, 1655-1662, doi:10.1002/stem.2637 (2017).

687 Benit, P., El-Khoury, R., Schiff, M., Sainsard-Chanet, A. & Rustin, P. Genetic background influences mitochondrial function: modeling mitochondrial disease for therapeutic development. *Trends Mol Med* **16**, 210-217, doi:10.1016/j.molmed.2010.03.001 (2010).

688 Chambers, S. M. & Studer, L. Cell fate plug and play: direct reprogramming and induced pluripotency. *Cell* **145**, 827-830, doi:10.1016/j.cell.2011.05.036 (2011).

689 Park, I. H. *et al.* Disease-specific induced pluripotent stem cells. *Cell* **134**, 877-886, doi:10.1016/j.cell.2008.07.041 (2008).

690 Nityanandam, A. & Baldwin, K. K. Advances in reprogramming-based study of neurologic disorders. *Stem Cells Dev* **24**, 1265-1283, doi:10.1089/scd.2015.0044 (2015).

691 Kim, C. iPSC technology--Powerful hand for disease modeling and therapeutic screen. *BMB Rep* **48**, 256-265 (2015).

692 Hamalainen, R. H. Induced pluripotent stem cell-derived models for mtDNA diseases. *Methods Enzymol* **547**, 399-415, doi:10.1016/B978-0-12-801415-8.00019-9 (2014).

693 Hamalainen, R. H. Mitochondrial DNA mutations in iPS cells: mtDNA integrity as standard iPSC selection criteria? *EMBO J* **35**, 1960-1962, doi:10.15252/embj.201695185 (2016).

694 Yokota, M., Hatakeyama, H., Ono, Y., Kanazawa, M. & Goto, Y. I. Mitochondrial respiratory dysfunction disturbs neuronal and cardiac lineage commitment of human iPSCs. *Cell Death Dis* **8**, e2551, doi:10.1038/cddis.2016.484 (2017).

695 Kelaini, S., Cochrane, A. & Margariti, A. Direct reprogramming of adult cells: avoiding the pluripotent state. *Stem cells and cloning : advances and applications* **7**, 19-29, doi:10.2147/SCCAA.S38006 (2014).

696 Yokota, M., Hatakeyama, H., Okabe, S., Ono, Y. & Goto, Y. Mitochondrial respiratory dysfunction caused by a heteroplasmic mitochondrial DNA mutation blocks cellular reprogramming. *Hum Mol Genet* **24**, 4698-4709, doi:10.1093/hmg/ddv201 (2015).

697 Pickrell, A. M. & Youle, R. J. Mitochondrial disease: mtDNA and protein segregation mysteries in iPSCs. *Curr Biol* **23**, R1052-1054, doi:10.1016/j.cub.2013.10.048 (2013).

698 Huang, C. C. *et al.* Mitochondrial encephalomyopathies: CT and MRI findings and correlations with clinical features. *Eur Neurol* **35**, 199-205, doi:10.1159/000117128 (1995).

699 Ito, S., Shirai, W., Asahina, M. & Hattori, T. Clinical and brain MR imaging features focusing on the brain stem and cerebellum in patients with myoclonic epilepsy with ragged-red fibers due to mitochondrial A8344G mutation. *AJNR Am J Neuroradiol* **29**, 392-395, doi:10.3174/ajnr.A0865 (2008).

700 Erol, I., Alehan, F., Horvath, R., Schneiderat, P. & Talim, B. Demyelinating disease of central and peripheral nervous systems associated with a A8344G mutation in tRNALys. *Neuromuscul Disord* **19**, 275-278, doi:10.1016/j.nmd.2009.01.012 (2009).

701 Tanji, K., Kunimatsu, T., Vu, T. H. & Bonilla, E. Neuropathological features of mitochondrial disorders. *Semin Cell Dev Biol* **12**, 429-439, doi:10.1006/scdb.2001.0280 (2001).

702 Brand, M. D. & Nicholls, D. G. Assessing mitochondrial dysfunction in cells. *Biochem J* **435**, 297-312, doi:10.1042/BJ20110162 (2011).

703 Antonicka, H. *et al.* Defective kinetics of cytochrome c oxidase and alteration of mitochondrial membrane potential in fibroblasts and cytoplasmic hybrid cells with the mutation for myoclonus epilepsy with ragged-red fibres ('MERRF') at position 8344 nt. *Biochem J* **342 Pt 3**, 537-544 (1999).

704 Bernardi, P. Modulation of the mitochondrial cyclosporin A-sensitive permeability transition pore by the proton electrochemical gradient. Evidence that the pore can be opened by membrane depolarization. *J Biol Chem* **267**, 8834-8839 (1992).

705 Gogvadze, V., Orrenius, S. & Zhivotovsky, B. Analysis of mitochondrial dysfunction during cell death. *Current protocols in cell biology* **Chapter 18**, Unit 18 15, doi:10.1002/0471143030.cb1805s19 (2003).

706 Crompton, M. Mitochondria and aging: a role for the permeability transition? *Aging Cell* **3**, 3-6 (2004).

707 Hayashi, G. & Cortopassi, G. Oxidative stress in inherited mitochondrial diseases. *Free Radic Biol Med* **88**, 10-17, doi:10.1016/j.freeradbiomed.2015.05.039 (2015).

708 Scherz-Shouval, R. & Elazar, Z. ROS, mitochondria and the regulation of autophagy. *Trends Cell Biol* **17**, 422-427, doi:10.1016/j.tcb.2007.07.009 (2007).

709 Dehay, B. *et al.* Lysosomal impairment in Parkinson's disease. *Mov Disord* **28**, 725-732, doi:10.1002/mds.25462 (2013).

710 Sarkar, C. *et al.* Impaired autophagy flux is associated with neuronal cell death after traumatic brain injury. *Autophagy* **10**, 2208-2222, doi:10.4161/15548627.2014.981787 (2014).

711 Cui, D. *et al.* Impaired autophagosome clearance contributes to neuronal death in a piglet model of neonatal hypoxic-ischemic encephalopathy. *Cell Death Dis* **8**, e2919, doi:10.1038/cddis.2017.318 (2017).

712 Kurihara, Y. *et al.* Mitophagy plays an essential role in reducing mitochondrial production of reactive oxygen species and mutation of mitochondrial DNA by maintaining mitochondrial quantity and quality in yeast. *J Biol Chem* **287**, 3265-3272, doi:10.1074/jbc.M111.280156 (2012).

713 Scherz-Shouval, R. & Elazar, Z. Regulation of autophagy by ROS: physiology and pathology. *Trends Biochem Sci* **36**, 30-38, doi:10.1016/j.tibs.2010.07.007 (2011).

714 Bereiter-Hahn, J. & Voth, M. Dynamics of mitochondria in living cells: shape changes, dislocations, fusion, and fission of mitochondria. *Microsc Res Tech* **27**, 198-219, doi:10.1002/jemt.1070270303 (1994).

715 Gomes, L. C. & Scorrano, L. Mitochondrial morphology in mitophagy and macroautophagy. *Biochim Biophys Acta* **1833**, 205-212, doi:10.1016/j.bbamcr.2012.02.012 (2013).

716 Black, G. C., Morten, K., Laborde, A. & Poulton, J. Leber's hereditary optic neuropathy: heteroplasmy is likely to be significant in the expression of LHON in families with the 3460 ND1 mutation. *Br J Ophthalmol* **80**, 915-917 (1996).

717 Won, R., Lee, K. H. & Lee, B. H. Coenzyme Q10 protects neurons against neurotoxicity in hippocampal slice culture. *Neuroreport* **22**, 721-726, doi:10.1097/WNR.0b013e32834acb8d (2011).

718 Duberley, K. E. *et al.* Human neuronal coenzyme Q10 deficiency results in global loss of mitochondrial respiratory chain activity, increased mitochondrial oxidative stress and reversal of ATP synthase activity: implications for pathogenesis and treatment. *J Inherit Metab Dis* **36**, 63-73, doi:10.1007/s10545-012-9511-0 (2013).

719 Jing, L. *et al.* Coenzyme Q10 protects astrocytes from ROS-induced damage through inhibition of mitochondria-mediated cell death pathway. *Int J Biol Sci* **11**, 59-66, doi:10.7150/ijbs.10174 (2015).

720 Mastroeni, D. *et al.* Oligomeric amyloid beta preferentially targets neuronal and not glial mitochondrial-encoded mRNAs. *Alzheimers Dement* **14**, 775-786, doi:10.1016/j.jalz.2017.12.005 (2018).

721 Estornell, E. *et al.* Saturation kinetics of coenzyme Q in NADH and succinate oxidation in beef heart mitochondria. *FEBS Lett* **311**, 107-109 (1992).

APPENDIX

APPENDIX

A-I. List of figures and tables

Figures

Tables

A-II. Publications

- **M. Villanueva-Paz**, S. Povea-Cabello, I. Villalón-García, J.M Suarez-Rivero, M. Alvarez-Cordoba, M. de La Mata, M. Talaveron-Rey, S. Jackson and J.A. Sanchez-Alcazar, Pathophysiological characterization of MERRF patient-specific induced neurons generated by direct reprogramming, BBA Molecular Cell Research, 1866 (2019) 861-881. Article.
- **M. Villanueva Paz**, D. Cotan, J. Garrido-Maraver, M.D. Cordero, M. Oropesa-Avila, M. de La Mata, A. Delgado Pavon, I. de Lavera, E. Alcocer-Gomez, J.A. Sanchez-Alcazar, Targeting autophagy and mitophagy for mitochondrial diseases treatment, Expert Opin Ther Targets, 20 (2016) 487-500. Review.
- **M. Villanueva-Paz**, D. Cotan, J. Garrido-Maraver, M. Oropesa-Avila, M. de la Mata, A. Delgado-Pavon, I. de Lavera, E. Alcocer-Gomez, M. Alvarez-Cordoba, J.A. Sanchez-Alcazar, AMPK Regulation of Cell Growth, Apoptosis, Autophagy, and Bioenergetics, EXS, 107 (2016) 45-71. Book chapter.
- **M. Villanueva Paz**, D. Cotan, M. D. Cordero, J. Garrido-Maraver, M. Oropesa-Avila, M. de la Mata, A. Delgado-Pavon, E. Alcocer-Gomez, I. de Lavera, J.A. Sanchez-Alcazar, The Role of Autophagy and Mitophagy in Mitochondrial Diseases, Autophagy: Cancer, Other Pathologies, Inflammation, Immunity, Infection, and Aging (2016), 155-172. Book chapter.

A-III. Acknowledgments/Agradecimientos

Parecía que este momento no iba a llegar nunca, pero aquí estoy. Me dijeron que los agradecimientos de la tesis era una de las partes más difíciles de escribir. Sin embargo, tengo tanto que agradecer a tantas personas que lo difícil va a ser condensar en pocas palabras todo lo que he sentido estos últimos años. Porque sí, es cierto. Realizar una tesis te cambia en todos los aspectos.

En primer lugar, quería dar las gracias a mi director de tesis, el Dr. José Antonio Sánchez Alcázar. Gracias por la confianza que has depositado en mí durante todos estos años. Mucho antes de comenzar la tesis, desde que empecé como alumna interna en el laboratorio, siempre has intentado que dé lo mejor de mí, nunca quedarme a medias tintas, siempre ir más allá en la investigación.
Gracias contagiarme tu pasión por la ciencia y tu dedicación al trabajo. Me llevo tu optimismo en la vida, que llevas por bandera tanto en los buenos como en los malos momentos.

Durante los ocho años que he formado parte del Laboratorio 210, he conocido a muchas personas que, en mayor o menor medida, han contribuido a mi formación personal y profesional.
En las primeras etapas, muchas personas hicieron que me sintiera integrada en el mundo nuevo que era el CABD.
En primer lugar, gracias David. Tú fuiste el primero que me enseñó a trabajar en el laboratorio (aún me acuerdo de esa primera PCR sin nucleótidos), y me guiaste en el laberinto de la investigación. Gracias por todos los buenos ratos y por escuchar mis penas en momentos de crisis (que no eran pocos…).
Gracias, Mario y Manuel, por compartir vuestra experiencia y conocimientos, siempre dispuestos a echar una mano.
Gracias, Juan. Para mí fuiste un ejemplo de profesionalidad y de exigencia. No me olvido de los consejos que me diste en su día y de las conversaciones que, ahora que finalizo mi tesis, puedo entender.
Ale, gracias por tu sentido del humor, por tu actitud ante la vida (siempre luchando por tu objetivo) y los momentos de risas que compartimos.

Por supuesto, gracias a mis Supernenas, Isa e Ana. Dos supermujeres que he tenido la suerte de conocer en el laboratorio. Gracias por todos estos años de amistad, de confidencias y de apoyo. Seguiremos intentando salvar el (nuestro) mundo antes de irnos a la cama.
Tampoco me olvido de esas tardes de cervezas con José Carrascosa y José Luque, junto con el resto de "Herederos del 210" …Después de eso hemos compartido bodas y hasta nacimientos…se ve que nos hacemos mayores.

En los primeros años de la tesis hubo renovación del laboratorio…
Primero llegó Juanmi. Gracias por tu disposición para ayudar siempre y tu ilusión por la ciencia.
Y después llegaron poco a poco mis niñas del 210… Patri, Maripaz, Irene, Suleva, Aída y Salud (sí, vosotras también sois del 210). Agradeceros vuestro apoyo constante, vuestra preocupación sincera, las palabras de ánimo y los buenos ratos tanto dentro como fuera del CABD…Me hubiera gustado compartir más tiempo con vosotras en el laboratorio, lo echaré de menos.

Quiero dar las gracias especialmente a Suleva, por su apoyo y ayuda en la última etapa de esta tesis. Gracias por las incontables horas de discusión y revisión, por tu capacidad crítica y la búsqueda de perfección en el trabajo. Hemos formado un buen equipo, ¿no crees?

Por supuesto, gracias Mónica, nuestra "mami". Por cuidarnos a todas, por tu alegría, tu forma de ver las cosas que hacía que los problemas del laboratorio fueran mucho más llevaderos. Gracias por escucharme y compartir conmigo los éxitos y los fracasos. Aunque no lo creas, eres más mágica que Maléfica.

Gracias a Alejandra y Ángeles, las últimas en llegar, pero no por ello menos importantes. Os habéis preocupado por mi trabajo desde el primer momento. Seguid siempre con la ilusión y el compromiso que tenéis ahora.

También fuera del laboratorio del 210 he contado con muchas personas que han hecho más fácil esta etapa.

Gracias a los profesores doctores Antonio Arroyo, Manuel Ballesteros y Daniel Moreno, por haberme guiado en mi incursión en la docencia en la Universidad. Gracias por haberme tutorizado estos años y haberme involucrado en las tareas docentes como una más.

Mi corta estancia en la Universidad de Lund, Suecia, ha sido sin dudarlo una de las mejores experiencias que he vivido estos últimos años, tanto en lo personal como lo profesional.
Thanks to professor Malin Parmar for receiving me in her lab, those months that I spent there were very important to my thesis. I'm also very grateful to Janelle Drouin-Ouellet and to all the members of Malin's group and the Wallenberg Neuroscience Center in Lund, Sweden.

Quiero dar las gracias también a todo el personal del CABD por su excelente trabajo y predisposición para ayudar: Vanesa, Jose, Pachú. También al personal técnico de Cocinas y Limpieza, en especial a Natalia, Fati y Mª Ángeles, siempre dando los buenos días con una sonrisa.
Por supuesto, muchas gracias Kathy por tu inmensa ayuda en microscopía y tus palabras de apoyo.
Corín, gracias por tus consejos tanto científicos como no científicos, tu preocupación sincera, tu interés y nuestras charlas. Gracias por tu enorme labor poniendo a punto la sala que tan importante era para el desarrollo de los experimentos.

No quiero dejar pasar esta oportunidad para agradecer a las asociaciones de pacientes y familiares de pacientes con enfermedades raras la importante labor que realizan para que las investigaciones salgan adelante.
Quiero hacer una mención especial a la Asociación de Enfermos de Patología Mitocondrial (AEPMI) y la Asociación de pacientes con Enfermedades Neurodegenerativas por Acumulación Cerebral de Hierro (ENACH). Gracias por vuestro apoyo durante estos años. Ojalá todos tomemos conciencia del problema social de las enfermedades raras y la importancia de la investigación.

Por supuesto, hay muchas personas fuera del CABD que han contribuido a que hoy esté aquí, y por ello las quiero recordar ahora.

Gracias a mis niñas de Málaga: Paula, Marta, Patri y Laura. Por vuestro interés, por estar ahí siempre y escucharme, por vuestro apoyo cuando las fuerzas me faltaban, en los momentos de duda.

A mis amigas de universidad y ya de la vida, Irene M. Irene G. y Marta. Nuestras quedadas por Sevilla, Jerez, Rota… Han llenado de momentos inolvidables estos últimos años. Sois un ejemplo de fuerza y superación para mí.

Gracias Juan, mi Compañero en la vida. Has sido un sufridor de esta tesis, me has levantado cuando yo no tenía fuerzas para hacerlo, me has alegrado los días en los que parecía imposible sonreír y me has apoyado aun cuando sabías que me estaba chocando con una pared. Pero hemos continuado hasta que la hemos derribado. Ha sido bastante duro, pero…no nos van las cosas fáciles. Juntos podremos con todo lo que venga.

Finalmente, quiero agradecer a mi familia todo el esfuerzo que han realizado para que pueda finalizar esta etapa. Mi padres, Jesús y Lola, me han inculcado el valor del trabajo y el esfuerzo, y los veo cada día luchar por mí y por mi hermano con una fortaleza que no he visto en otra parte. Gracias por haberme apoyado en todo sin siquiera preguntar, respetar mis decisiones y no dejar que me viniese abajo. Ale, gracias por preocuparte por mí siempre, por ayudarme cada vez que lo he necesitado (no sé qué hubiera hecho sin tus conocimientos informáticos) y por animarme cada vez que me veías agobiada. Os quiero mucho.

Muchas gracias a todos.


UNIVERSIDAD
SEVILLA
AÑO 1997
PABLO DE OLAVIDE


UNIVERSIDAD
SEVILLA
AÑO 1997
PABLO DE OLAVIDE